Automating Power Quality Analysis

Emmanouil Styvaktakis

Department of Electric Power Engineering and Department of Signals and Systems
CHALMERS UNIVERSITY OF TECHNOLOGY
Göteborg, Sweden, 2002

Thesis for the degree of Doctor of Philosophy

Technical Report No. 423

Automating Power Quality Analysis

by

Emmanouil Styvaktakis

Department of Electric Power Engineering and Department of Signals and Systems
Chalmers University of Technology
412 96 Göteborg, Sweden

Göteborg 2002

Automating Power Quality Analysis
Emmanouil Styvaktakis
ISBN 91-7291-151-4

This thesis has been prepared using LaTeX.

Doktorsavhandlingar vid Chalmers Tekniska Högskola
Ny serie nr 1833
ISSN 0346-718X

Technical report No. 423
Signal Processing Group
Department of Signals and Systems
Chalmers University of Technology
412 96 Göteborg, Sweden.

Printed by Chalmers Reproservice.
Göteborg, May 2002

στους γονεὶς μου και στην Ξένια

Abstract

The increased requirements on supervision, control, and performance in modern power systems make power quality monitoring a common practise for utilities. Large databases are created and automatic processing of the data is required for fast and effective use of the available information.

Aim of the work presented in this thesis is the development of tools for automatic analysis of monitoring data and in particular measurements of voltage events. The main objective of the analysis is the identification of the event origin (event classification). It is shown that event classification can be achieved by considering the voltage magnitude of the three phases. In the group of events that cause a temporary decrease in voltage magnitude (voltage dips) three classes are found: fault-induced events, transformer saturation events and induction motor starting events. Measurements and simulations are used for the analysis of these events. Emphasis is given on fault-induced events that present different stages of magnitude (multistage dips) and transformer saturation dips.

Different aspects regarding voltage magnitude estimation are studied using Kalman filtering. Two segmentation algorithms are proposed to divide voltage waveforms into several possible events. Kalman filtering is also used for voltage dip detection.

An expert system is developed for automatic event classification and analysis. The expert system uses the voltage waveforms and distinguishes the different types of voltage dips as well as interruptions. A method for classification is used based on the proposed segmentation algorithms. The expert system is tested using over 900 measured voltage recordings. The results show that the expert system enables fast and accurate analysis of power quality measurements. One more method for automatic event classification is proposed. The method uses discrete rms voltage measurements. Discrete rms voltage measurements form a memory saving option that power quality monitors offer instead of saving the actual voltage waveforms. It is shown that classification is possible even with rms measurements using the segmentation-based approach.

Power system transients are also studied. Measurements and simulations are used for analysis of these events. Aspects related to the frequency contents of these events are discussed.

Overall, this thesis shows that automatic processing of power quality monitoring can be achieved by following a number of well-defined steps. Automatic classification can be applied to large databases and simplify the processing and analysis of monitoring data.

Keywords: power quality, power system monitoring, voltage dips, power system faults, induction motors, transformer saturation, short time Fourier transform, Kalman filtering, pattern classification, expert systems, power system transients.

Contents

Acknowledgements

First, I would to thank my supervisor and examiner, Math Bollen. I am grateful for all the help, ideas and encouragement he gave me.

I would like also to thank my second supervisor, Irene Gu for her help in signal processing, for interesting discussions and for her constant encouragement.

Thanks also goes to Professor Mats Viberg for his help and for making the Signal Processing Group an excellent working environment. Many thanks to all the people in the Signal Processing Group and Maxime Flament for helping me in different ways.

The research presented in this thesis has been funded through the Elektra program, which is jointly financed by Energimyndigheten, ABB Corporate Research and ABB Automation Products AB. The financial support is gratefully acknowledged. The project is a collaborated research between the Signal Processing group of the department of Signals and Systems and the department of Electric Power Engineering at Chalmers University of Technology.

Measurements were particularly important for this project. I would like to thank all the power companies, which have supplied me with data: Scottish Power, Göteborg Energi Nät AB and SINTEF Energy Research. Special thanks goes to Alastair Ferguson from Scottish Power, Christian Roxenius and Robert Olofsson from Göteborg Energi Nät AB, and Helge Seljeseth from SINTEF Energy Research.

Finally, I would like to thank the members of the steering group of this project for contributing in very useful meetings and commenting on this thesis: Murari Mohan Saha from ABB Automation Products AB, Helge Seljeseth from SINTEF Energy Research, Magnus Olofsson from STRI AB, Christian Roxenius from Göteborg Energi Nät AB and Robert Olofsson from Unipower AB.

Chapter 1

Introduction

1.1 Background

The increasing use of equipment sensitive to power system disturbances [1] and the related economic aspects [2], the increasing awareness of power quality issues and deregulation [3], have created a need for extensive monitoring of the power system operation. Customers with sensitive equipment like adjustable speed drives, power electronics or computers, use monitoring to locate the source of the problems that might occur. On the other side, utilities try to meet the demands of their customers: they monitor to prove that the quality of the offered power is within the pre-specified standards and to obtain the necessary information for solving problems. Finally, deregulation creates a challenging and competitive new environment, where power quality becomes a commodity and as such it must be monitored and measured.

1.1.1 Power quality and power system events

The term *power quality* refers to a wide variety of electromagnetic phenomena that characterise the voltage and current at a given time and at a given location on the power system [4].

A *power system event* is a recorded (or observed) current or voltage excursion outside the predetermined monitoring equipment thresholds . A *power disturbance* is a recorded (or observed) current or voltage excursion (event) which results in an undesirable reaction in the electrical environment or electronic equipment or systems. The term *power problem* refers to a set of disturbances or conditions that produce undesirable results for equipment, systems or a facility [5].

The term *event* is typically used to describe significant and sudden deviations of voltage or current from its normal or ideal waveform (like in Figure 1.1) unlike the term *variation* which is used to describe small deviations from the nominal values [6]. The monitoring of events is done using certain triggering thresholds. Voltage or current variations are obtained by continuous monitoring as shown in Figure 1.2.

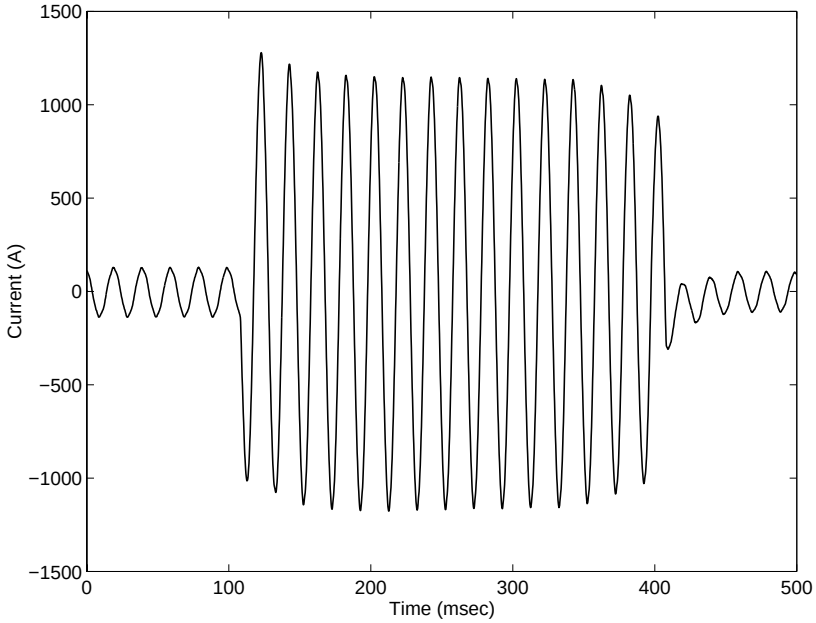

Figure 1.1: Measurement of current during a fault

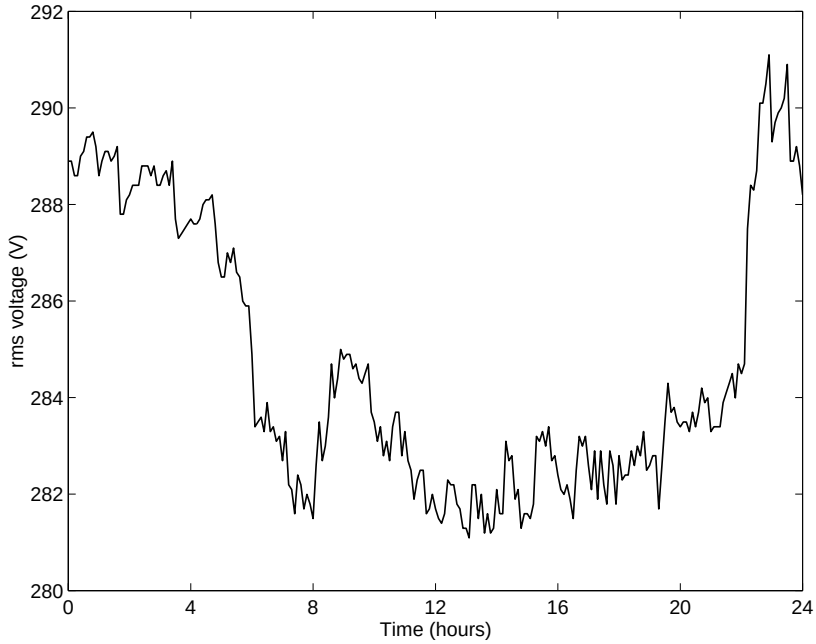

Figure 1.2: rms voltage measurement for one day

Table 1.1 gives the different categories of electromagnetic phenomena that may appear in a power system [4]. This categorisation is done in terms of the frequency components (spectral contents) which appear in the voltage signals during the phenomenon, the duration of the phenomenon and the typical voltage magnitude. These phenomena are mainly caused by:

- external to the power system factors. For example lightning strikes cause impulsive transients of large magnitude.
- switching actions in the system. A typical example is capacitor switching which causes oscillatory transients.
- faults which can be caused, for example, by lightning (on overhead lines) or insulation failure (in cables). Voltage dips and interruptions are phenomena related to faults.
- loads which use power electronics and introduce harmonics to the network.

For some of the events related to the classes in Table 1.1, protection operation is triggered. In the case of a fault the protection system will isolate the part of the network where the fault occurred. The protection system is designed to respond in short time and eliminate the risk for both the system and the customers (high currents caused by the fault are a threat for the elements of the system and the resulting voltage dips might cause problems to certain loads). In the case of high amplitude transients (caused by lightning or switching actions), overvoltage protection equipment (for example surge arresters) are employed to avoid damage in the elements of the system. However, for other events, protection operation is not expected. For example, the switching of large induction motor load might cause an increase in current and a voltage dip but normally no action is taken by the protection system.

1.2 Power quality monitoring objectives

The increased requirements on supervision, control, and performance in modern power systems make power quality monitoring a common practice for utilities. Power quality monitoring is necessary to characterise electromagnetic phenomena at a particular location of the network. The objective of monitoring can be [4]:

- the diagnosis of incompatibilities of the power system with the load.
- the evaluation of the electric environment at a part of the system in order to refine modelling techniques or to develop a power quality baseline.
- the prediction of future performance of load equipment or power quality mitigating devices.

For example, an important aspect of power quality monitoring is the collection of information regarding the performance of the system in terms of voltage dips

Table 1.1: Categorisation of electromagnetic phenomena [4]

Categories	**Typical spectral content**	**Typical duration**	**Typical voltage magnitude**
1.0 Transients			
1.1 Impulsive			
1.1.1 Nanosecond	5 nsec rise	$<$ 50 nsec	
1.1.2 Microsecond	1 μsec rise	50 nsec - 1 msec	
1.1.3 Millisecond	0.1 msec rise	$>$ 1 msec	
1.2 Oscillatory			
1.2.1 Low frequency	$<$ 5 kHz	0.3 -50 msec	0 - 4 pu
1.2.2 Medium frequency	5 - 500 kHz	20 μsec	0 - 8 pu
1.2.3 High frequency	0.5 - 5 MHz	5 μsec	0 - 4 pu
2.0 Short duration variations			
2.1 Instantaneous			
2.1.1 Interruption		0.5 - 30 cycles	$<$ 0.1 pu
2.1.2 Sag (dip)		0.5 - 30 cycles	0.1 - 0.9 pu
1.1 2.1.3 Swell		0.5 - 30 cycles	1.1 - 1.8 pu
2.2 Momentary			
2.2.1 Interruption		30 cycles - 3 sec	$<$ 0.1 pu
2.2.2 Sag (dip)		30 cycles - 3 sec	0.1 - 0.9 pu
2.2.3 Swell		30 cycles - 3 sec	1.1 - 1.4 pu
2.3 Temporary			
2.3.1 Interruption		3 sec - 1 min	$<$ 0.1 pu
2.3.2 Sag (dip)		3 sec - 1 min	0.1 - 0.9 pu
2.3.3 Swell		3 sec - 1 min	1.1 - 1.2 pu
3.0 Long duration variations			
3.1 Interruption sustained		$>$ 1 min	0.0 pu
3.2 Under-voltages		$>$ 1 min	0.8 - 0.9 pu
3.3 Overvoltages		$>$ 1 min	1.1 - 1.2 pu
4.0 Voltage unbalance		Steady state	0.5 - 2 %
5.0 Wave distortion			
5.1 dc offset		Steady state	0 - 0.1 %
5.2 Harmonics	0 - 100th harmonic	Steady state	0 - 20 %
5.3 Inter-harmonics	0-6 kHz	Steady state	0 - 2 %
5.4 Notching		Steady state	
5.5 Noise	Broadband	Steady state	0.1 %
6.0 Voltage fluctuations	$<$ 25 Hz	Intermittent	0.1 - 7 %
7.0 Power frequency variations		$<$ 10 sec	

and interruptions [6]. For voltage dips, the obtained information (magnitude and duration) are usually compared with the voltage tolerance curves of the loads (for example the CBEMA curve [6]) to evaluate the influence of these events.

Monitoring within a certain site (industrial, residential or domestic) can reveal the origin of problems and give the necessary information for their solution. In [7], two cases are described. In the first case, monitoring revealed that a pump control system was vulnerable to voltage dips and a constant voltage transformer was installed to support the voltage. In the second case, monitoring showed that plants in the same geographical area were experiencing voltage dips of relatively long duration. This long voltage dips were effecting the operation of a number of apparatuses. The problem was solved by speeding up the protection clearance times at certain points in the zone of influence of the plants. Fault analysis in general can be benefited by monitoring [8].

The collected waveforms of voltage and current can be also used to test protection and control algorithms [9].

1.3 Power quality monitoring equipment

Technological achievement in digital signal processing, microprocessors and storage devices made possible the development of monitoring systems with large capabilities. A wide variety of monitoring systems are available for different purposes (Figure 1.3).

These monitoring systems are designed to accept voltage and current quantities. Typical instrument input limits are 600 V rms for voltage and 5 A rms for current. Voltage transducers and current transformers are used to obtain usable signal levels [10].

Modern digital monitors utilise analog-to-digital (A/D) converters to convert the analogue signals (voltages or currents) into numeric values to be processed by the instrument. A/D converters of order up to 20 bits are available for increased resolution. Sampling rates up to 640 samples are today available thus increasing significantly the details on the variations in the waveform that can be captured. After the signals have been digitised, the processor of the monitor operates on the measurements to derive a number of power quality parameters. The measurements and the calculated parameters can be saved in the monitor or alternatively be transferred to a host computer. Intranet technologies are employed for the acquisition of the obtained information at the appropriate location [11]. The modems that are used for the transfer can reach a speed of 400 Mb/sec [10].

Typical power quality parameters obtained by most monitors are:

- rms values of voltage and current.
- harmonics of voltage and current.
- total harmonic distortion of voltage and current (THD).

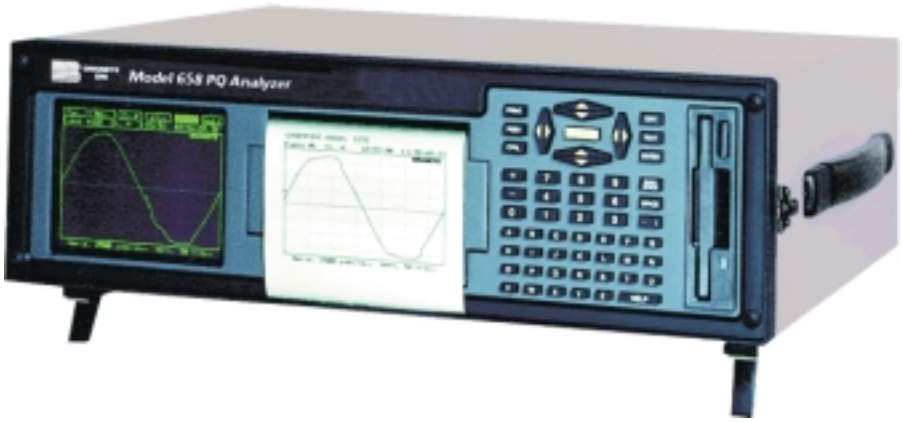

Figure 1.3: Power quality monitor

Typically, these attributes are calculated over a short period of time and then their averages are recorded by the monitor.

Probably the most important task of these monitors is to capture power system events without running out of memory while monitoring. For event capturing, a common method for triggering is on rms changes by setting thresholds. Typical thresholds are ±10 % of the nominal voltage. Comparison of each cycle with the previous cycle can also be used for capturing events that do not cause significant rms changes. Transients are captured with this type of triggering. Alternatively, the monitor can be set to capture events for which unbalance between the phases appears.

The choice of thresholds is important in order to avoid saturating the memory of the monitor with events of little importance. Adaptive thresholds can be utilised to regulate the rate of capture in case of high rate of incoming events [10]. A better solution is the monitor to analyse the event and then, based on the analysis results, decide whether to store it or not. Automatic processing tools are required in this case.

1.4 Data collection

The analysis presented in this thesis is on voltage measurements. Data presented and analysed come from:

- Göteborg Energi Nät AB. Göteborg Energi Nät AB is the electrical utility of the city of Göteborg, Sweden. The measurements were obtained by a small number of monitors placed at the sub-transmission and distribution network (132 kV, 10 kV and 400 V).

- SINTEF Energy Research. SINTEF is a norwegian research organisation. The measurements were obtained by monitors placed at medium and low voltage

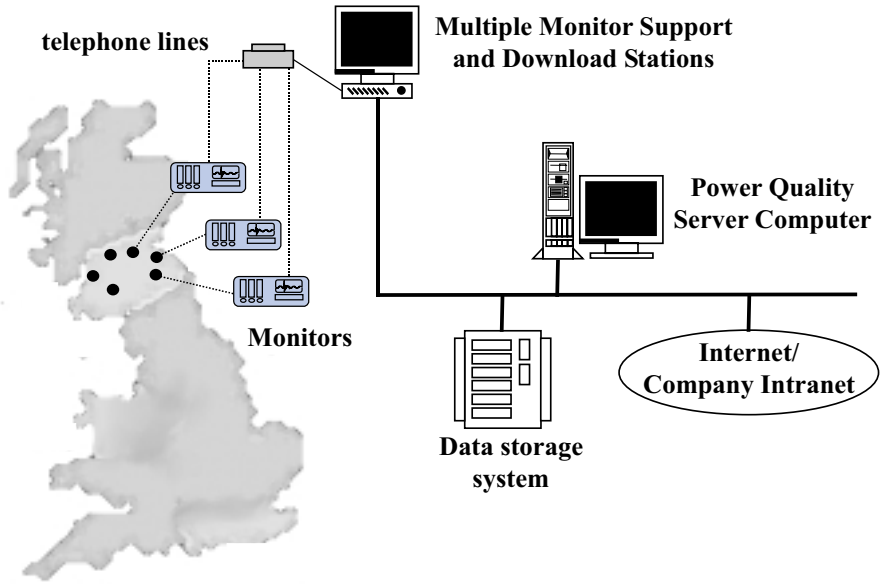

Figure 1.4: The Scottish Power monitoring program

networks during a power quality survey that was carried out for the norwegian utilities.

- Scottish Power (Scotland). More details about this monitoring program are given in the next section.

1.4.1 The Scottish Power monitoring program

Scottish Power, an electrical utility in Scotland, runs an extensive monitoring program in its distribution system for several years. Aim of the company is to provide monitored data for problem assessment, improve the communication with their customers and assist them with problem investigation.

The company serves over 1.7 million customers (domestic, commercial and industrial). The distribution system consists of 83,000 circuit kilometers of overhead lines and underground cables operating at 33 kV, 11 kV and 415/240 V with around 38,000 substations. About 70 % of the distribution network is underground.

A large number of fault recorders is installed: around 90 fault recorders were in operation in 1997 and over 150 at present [7]. The monitors are triggered by voltage or current excursions and are able to capture their waveforms. In two years of operation (1997-1999) over 20,000 events were captured. The recordings are transferred by modems in the main computer in the company's headquarters (Figure 1.4).

1.5 Motivation of the work

The most common practise in analysing the results of monitoring programs is to group the captured events in a number of classes. These classes are made using the minimum or maximum rms (voltage or current), or by comparing the captured waveforms with the ideal waveform. For example: if the minimum rms voltage is below a threshold for a certain period of the time then the captured event is classified as a voltage dip. Typical classes obtained like this are: voltage dips, voltage swells, interruptions and transients [12]. This classification is usually called *disturbance classification*.

Since individual inspection of all the waveshapes is not an option due to the large size of the databases, a small number of characteristics is extracted from the measurement: typically magnitude and duration for a voltage dip and maximum voltage for a transient. A more suitable solution would be to extract automatically all relevant information from the recordings.

The need for new characterisation methods and tools for optimal use of the available measurements is highlighted in a number of publications [10, 13, 14, 15, 16]. Commercial products are also available that provide functions for better visualisation and processing of the obtained measurements (for example: [13]) as well as extraction of useful information (for example: [14, 15]).

Towards the direction of intelligent power quality monitoring and the development of automatic classification and analysis tools, appropriate signal processing methods are required in order to extract information from the signals. Several signal processing methods have been proposed for feature extraction, like Fourier and wavelet transforms, combined with neural networks, fuzzy expert systems or pattern recognition methods [17, 18, 19, 20, 21, 22, 23, 24, 25].

Regarding the above mentioned trends and developments, the work in this thesis was carried out along the following three lines:

- the understanding of the phenomena captured by power quality monitors. This thesis focuses on voltage events (large and sudden deviations from the ideal voltage waveform) as measured in distribution networks.

- the use of appropriate signal processing tools for the extraction of the distinctive characteristics (features) of power system events. Feature extraction from the time-frequency components of voltage is important for in depth analysis and accurate characterisation. Signal processing methods can also be beneficial for diagnostics.

- the development of a knowledge-based system for automatic processing of measurements and event classification. *Event classification* is the analysis of the measurements not in terms of disturbances (voltage dip, interruption etc), but in terms of the underlying causes (fault, motor starting, load switching etc). Such a system can be used for the analysis of large databases and provide event statistics. Event statistics (instead of disturbance statistics) provide better understanding of the system's performance. This type of automatic processing

can be also implemented in the monitor. The results of the classification can be used to decide whether a captured event must be stored or whether an alarm must be sent to the system operator.

1.6 Outline of the thesis

Chapter 2

In this chapter several power system events are presented. Their common characteristic is that they present a distinctive signature in the fundamental frequency magnitude of voltage. The work presented in this chapter resulted from the analysis of measurements from different monitoring programs. Simulations and real voltage measurements are used to show the features of these phenomena. Emphasis is given on two types of events: transformer saturation and multistage voltage dips due to faults. Different types of overvoltages related with these events are also presented.

Chapter 3

Chapter 3 presents various aspects regarding the modelling and analysis of voltage disturbance signals. Kalman filtering is exploited for the extraction of the fundamental frequency magnitude of voltage signals. The characteristics of the estimated magnitude with respect to different modelling options are also presented. A segmentation algorithm is proposed for voltage disturbance signals. Additionally, the problem of voltage dip detection is presented and certain aspects of it are investigated.

Chapter 4

In this chapter an expert system is presented that is able to classify the power system events described in Chapter 2 and offer information in terms of power quality. The structure of the expert system and its components are described. The rules of the expert system, based on the features presented in Chapter 2, are given in detail. The classification strategy utilises the segmentation algorithm presented in Chapter 3. The expert system is tested using real measurements. Statistics on the frequency of the different events are presented as obtained using the expert system.

Chapter 5

In Chapter 5 a method is presented for automatic classification of power system events using only rms voltage measurements . The system is tested with real measurements. The limitations of this type of monitoring are also discussed.

Chapter 6

Chapter 6 deals with events that present high frequency characteristics and cannot be classified by the signature of the fundamental frequency magnitude. These events are mainly caused by switching actions. Simulations are used for the analysis of these events. Their characteristics are shown and signal processing methods are used for feature extraction.

Chapter 7

Conclusions and further work.

1.7 List of publications

[T1] E. Styvaktakis, M.H.J. Bollen and I.Y.H. Gu, "A fault location technique using high frequency fault clearing transients", *IEEE Power Engineering Review*, vol. 19, no. 5, pp. 58–60, May 1999.

[T2] E. Styvaktakis, M.H.J. Bollen and I.Y.H. Gu, "A fault location technique for two and three-terminal lines using high frequency fault clearing transients", *PowerTech Budapest 99*, pp. 255.

[T3] E. Styvaktakis, M.H.J. Bollen and I.Y.H. Gu, "Classification of power system transients: synchronised switching", *IEEE Power Engineering Society Winter Meeting*, vol. 4, pp. 2681–2686, 2000.

[T4] I.Y.H. Gu, M.H.J. Bollen and E. Styvaktakis, "The use of time-varying AR models for the characterization of voltage disturbances", *IEEE Power Engineering Society Winter Meeting*, vol. 4, pp. 2943–2948, 2000.

[T5] E. Styvaktakis, M.H.J. Bollen and I.Y.H. Gu, "Transformer saturation after a voltage dip", *IEEE Power Engineering Review*, vol. 20, no. 4, pp. 60–62, April 2000.

[T6] E. Styvaktakis, M.H.J. Bollen and I.Y.H. Gu, "Classification of power system events: Voltage dips", *9th International IEEE Conference on Harmonics and Quality of Power*, vol. 2, pp. 745–750, 2000. Also: *NORDAC 2000*, 22-23 May, 2000, Stjordal, Norway (invited paper).

[T7] M.H.J. Bollen and E. Styvaktakis, "Tutorial on voltage sag analysis", *9th International IEEE Conference on Harmonics and Quality of Power*, vol. 1, pp. 193–194, 2000.

[T8] M.H.J. Bollen and E. Styvaktakis, "Characterization of Three-Phase Unbalanced Dips (as easy as one-two-three?)", *9th International IEEE Conference on Harmonics and Quality of Power*, vol. 1, pp. 81–86, 2000. Also as panel session contribution at *IEEE Power Engineering Society Summer Meeting*, vol. 2, pp. 899–904, 2000.

[T9] E. M.H.J. Bollen, E. Styvaktakis and I.Y.H. Gu, "Analysis of voltage dips for event identification", *IEE Seminar on Power Quality: Monitoring and Solutions (Ref. No. 2000/136)*, pp. 4/1-4/4, 2000.

[T10] I.Y.H. Gu, E. Styvaktakis and M.H.J. Bollen, "Analysing power system disturbances using the residuals of AR models", *IEEE Power Engineering Review*, vol. 20, no. 4, pp. 60–62, April 2000.

[T11] E. Styvaktakis, M.H.J. Bollen and I.Y.H. Gu, "Expert system for voltage dip classification and analysis", *IEEE Power Engineering Society Summer Meeting*, vol. 1, pp. 671–676, 2001.

[T12] E. Styvaktakis, M.H.J. Bollen and I.Y.H. Gu, "Voltage dip detection and power system transients", *IEEE Power Engineering Society Summer Meeting*, vol. 1, pp. 683–688, 2001.

[T13] M.H.J. Bollen, A, Sannino, J. Svensson and E. Styvaktakis, "Testing of three-phase converters for voltage disturbances in the power system", *Proceedings of Nordic and Baltic workshop on Power Systems*, Tampere, Finland, 2002.

[T14] E. Styvaktakis, M.H.J. Bollen and I.Y.H. Gu, "Expert system for classification and analysis of power system events", *IEEE Transactions on Power Delivery*, vol. 17, no. 2, pp. 423–428, April 2002.

[T15] E. Styvaktakis, M.H.J. Bollen, "Signatures of voltage vips: transformer saturation and multistage dips", submitted to *IEEE Transactions on Power Delivery*.

[T16] M.H.J. Bollen, E. Styvaktakis and I.Y.H. Gu, "Voltage dip waveforms and characteristics in three-phase power systems", submitted to *IEE Power Engineering Journal*.

[T17] E. Styvaktakis, M.H.J. Bollen and I.Y.H. Gu, "Automatic classification of power system events using rms voltage measurements", accepted for presentation to *IEEE Power Engineering Society Summer Meeting 2002*.

Chapter 2

Power System Events

2.1 Introduction

In this chapter several types of power system events are presented in terms of voltage characteristics. Measurements from distribution systems as well as simulations are used for identifying the different classes of events. Emphasis is given on the characteristics of the fundamental frequency magnitude of voltage and its harmonic components as well as the relationship between the three phases. The events can be divided into two main categories:

- Fault-related events:
  - Voltage dips
  - Interruptions
- Switching-related events:
  - Induction motor starting
  - Transformer saturation
  - Energising
  - Load or other switching

The Electromagnetic Transients Program (EMTP) is used for simulations. The models for the important parts of the simulated systems can be found in Appendix A.

2.2 Short Time Fourier Transform

The Short Time Fourier Transform (STFT) is used for time-frequency analysis of non-stationary signals. STFT decomposes the time-varying signal into time-frequency domain components, thus it offers information on how the characteristics

of a signal component change in time [26]. For a signal $x(k)$, the discrete STFT for a frequency band n at time k is defined as:

$$X_k(e^{j\omega_n}) = \sum_m w(m)x(k-m)e^{-j\omega_n m} \tag{2.1}$$

where

ω_n	$= 2\pi n/N$, the frequency in radians
N	is the number of frequency bands
$w(m)$	is a selected symmetric window of size M

One way of interpreting the STFT, is as a set of bandpass filters (filter bank) which are centered at frequencies f_n given by [26]:

$$f_n = \frac{f_s n}{N}(\text{Hz}) \qquad n = 0, 1, \dots\ N-1 \tag{2.2}$$

where f_s is the sampling frequency at which the signal is sampled. All the bandpass filters have equal bandwidth determined by the selected window. The larger the window M, the smaller the bandwidth of the bandpass filter and the better the frequency resolution (it becomes easier to resolve two closely spaced frequency components). However, the improved frequency resolution is achieved at the expense of time resolution: a larger window cannot capture the fast changing characteristics of the signal)

The STFT can be used for the estimation of the unknown parameters of any signal (magnitude and phase at each frequency) by locating the bandpass filters at the required frequencies. For power systems where the voltage signal is a sinusoid with a frequency of 50 Hz (in Europe) or 60 Hz (in USA), the bandpass filters can be located at this frequency (fundamental frequency) and at its integer multiples (harmonics) i.e. 100 Hz, 150 Hz, etc. This way the fundamental frequency component as well as the harmonics of voltage can be extracted.

The fundamental frequency is almost constant; only small deviations are usually observed in the range of ± 1 %. This is also the deviation according to the standards [27]. The measurements analysed in this thesis do not present significant deviations in the fundamental frequency therefore the fundamental frequency is fixed to either 50 or 60 Hz in all the algorithms used in this thesis. However, large deviations from these values will effect the the accuracy of the estimating process.

The application of STFT transform for power quality measurements has been presented in a number of papers (for example: [26] and [28]). The STFT is used in this chapter for the estimation of:

- fundamental frequency magnitude of voltage in time
- voltage harmonics in time
- phase angle in time

using a rectangular window ($w(m) = 1$ for all m). The fundamental frequency of the systems where the measurements took place is 50 Hz. The segmentation of the

analysed signals is in overlapping windows of one 50 Hz cycle ($M = 1$ cycle). The number of frequency bands N is set equal to the number of samples per 50 Hz cycle. Using this N, the center frequencies of the bandpass filters are at integer multiples of the fundamental frequency. The signals that are analysed next are either sampled at a sampling frequency f_s, equal to 4800 Hz or 6400 Hz. For the 4800 Hz sampling frequency, the length of the window M is 96 samples and the positive frequency bands are $N/2 = 48$. For the 6400 Hz sampling frequency the window M is 128 samples and the positive frequency bands are 64.

With a window of one cycle, the magnitude of the fundamental frequency (50 Hz) component is:

$$A_1(k) = \frac{2|X_k(e^{j2\pi 50})|}{M} \tag{2.3}$$

and the phase:

$$\theta_1(k) = \arg(X_k(e^{j2\pi 50})) \tag{2.4}$$

2.3 Faults and voltage dips

Faults (or short circuits) are due to lightning and broken or faulty insulation. They cause a drop in voltage that propagates in the system. Faults are normally cleared by the protection system: a circuit breaker opens or a fuse is blown to isolate the faulty part of the network. Upon fault clearing, the voltage of the faulty part of the network goes to zero (interruption) and the voltage of the rest of the system recovers to its normal value. This temporary drop in voltage is called voltage dip.

Voltage dips due to faults can be severe and therefore are of major concern. They cause problems to a large number of customers as they propagate in the system [6].

2.3.1 Characteristics of fault-induced voltage dips

Voltage dip magnitude

The magnitude of fault-induced voltage dips at a certain point in the system depends mainly on the type and the resistance of the fault, the distance to the fault and the system configuration. The calculation of the dip magnitude for a fault somewhere within a radial distribution system requires the point of common coupling (PCC) between the fault and the load to be found. Figure 2.1 shows the voltage divider model, where Z_0 is the source impedance, Z_1 is the impedance between the PCC and the fault (including any fault impedance). For three-phase faults only positive sequence impedances are needed. For single faults the sum of positive, negative and zero sequence impedances is needed. The dip magnitude (%) at the load position equals the voltage (%) at the PCC (if we neglect all load currents):

$$V_{dip} = \frac{Z_1}{Z_0 + Z_1} E \tag{2.5}$$

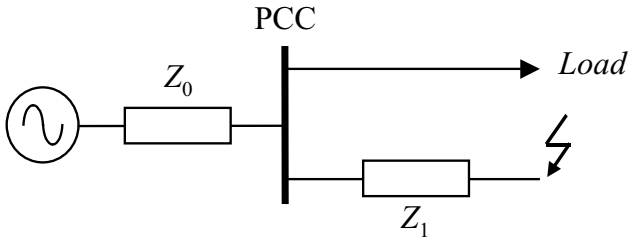

Figure 2.1: Voltage divider model for the calculation of voltage dip

where E is the source voltage. For faults closer to the PCC the sag becomes deeper (smaller Z_1). The dip becomes also deeper for weaker supplies (larger Z_0).

According to the type of the fault, there are two types of dips:

- symmetrical (for a three-phase or a three-phase-to-ground fault)
- asymmetrical (for a single-phase-to-ground or a two- phase or a two-phase-to-ground fault)

Figure 2.2 shows the voltage waveforms and the corresponding fundamental frequency magnitude for a dip that was measured in an 11 kV network. The dip was caused by a three-phase fault; all three phases present the same characteristics. Voltage returns to normal after fault clearing operation. The recovery of voltage is fast and it creates an almost rectangular shape for the fundamental frequency voltage magnitude. Figure 2.3 shows the voltage waveforms and the corresponding fundamental frequency magnitude for a dip caused by an asymmetrical fault. It must be noted here that the ratio of dip magnitude between the phases changes as the dip propagates in the system due to the different transformer connections between the fault point and the point where the voltage is measured. More about this are discussed in Section 2.4.3.

Voltage dip duration

The duration of voltage dips depends on the protection system. It is equal to the time required for the fault clearing device to operate after it receives a trip signal from the protection relays. The objective of the protection system is to isolate the part of the system where the fault occurs. Table 2.1 ([29]) contains the most common fault clearing devices, their typical operating times and the possible number of retries that can be executed. The option of retries (or reclosures) offers the possibility of short interruptions in the case of transient faults (faults which are removed after protection operation).

Figure 2.2 and Figure 2.3 show voltage dips of duration longer than 10 cycles (1 cycle=20 msec in a 50 Hz system). These were faults that were most likely

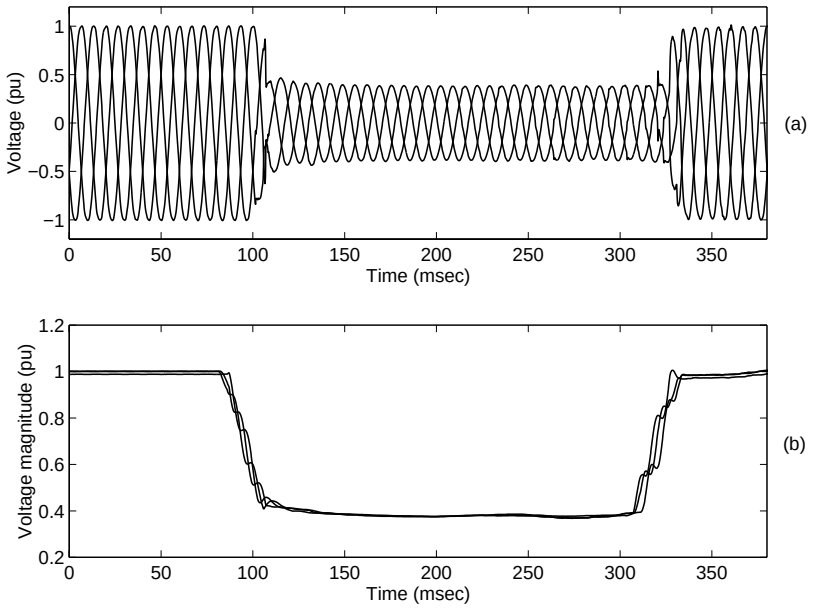

Figure 2.2: Voltage dip due to a symmetrical fault (a) Voltage waveforms (b) Voltage magnitude (measurement in an 11 kV network)

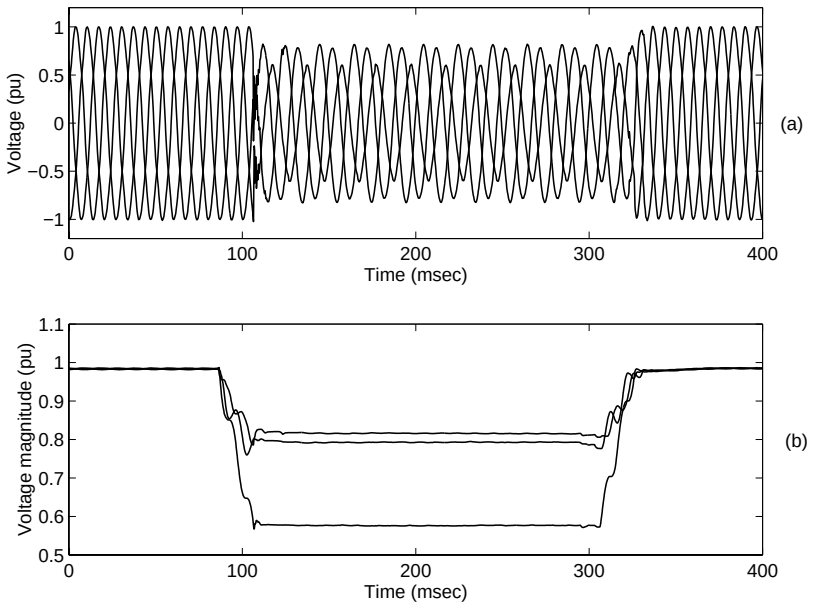

Figure 2.3: Voltage dip due to an asymmetrical fault (a) Voltage waveforms (b) Voltage magnitude (measurement in an 11 kV network)

Table 2.1: Fault clearing device operating time

Type of fault clearing device	**Minimum of clearing time in cycles**	**Typical time delay in cycles**	**Possible number of retries**
Expulsion Fuse	0.5	0.5 - 120	none
Current limiting fuse	< 0.25	0.25 - 6	none
Electronic recloser	3	1 - 30	0 - 4
Oil circuit breaker	5	1 - 60	0 - 4
SF6 or vacuum circuit breaker	2 - 3	1 - 60	0 - 4

cleared by circuit breaker opening. The voltage dip shown in Figure 2.4 recovers in less than 2 cycles (as it can be clearly seen in the voltage waveforms). This is probably due to a fault cleared by fuse operation. This is measurement from an 11 kV network.

Measurements of voltage during fuse-cleared faults are shown in [30]. Current limiting and expulsion fuses were used. The resulting voltage dips were of approximate duration 3/4 of a cycle for the expulsion fuses, and 1/4 of a cycle for the current limiting fuses.

Phase angle jump

Voltage dips lead to phase angle jumps. The single-phase voltage divider model of Figure 2.1 can be used again for the derivation of an expression for phase angle jumps [6]. Z_0 and Z_1 are complex quantities and can be written using the corresponding resistive and inductive components as $Z_0 = R_0 + jX_0$ and $Z_1 = R_1 + jX_1$. Then the phase angle jump can be found as:

$$\Delta\theta = \arctan(\frac{X_1}{R_1}) - \arctan(\frac{X_0 + X_1}{R_0 + R_1}) \tag{2.6}$$

If the X/R ratios of the source and the feeder are equal then the phase angle jump is zero. The phase angle jump occurs when the X/R ratios are not equal. As shown in [6] the phase angle jump appears to be large for faults on cables.

The phase angle jump is obtained with reference to the pre-event phase angle. The phase angle jump is typically calculated as [6]:

$$\Delta\theta(t_k) = \arg\left(\frac{V(t_k)}{V_0 e^{j\omega t_k}}\right) \tag{2.7}$$

where $V(t_k)$ is the complex fundamental voltage and V_0 the complex fundamental voltage at $t_k = 0$. Examples of phase angle jumps are given in Section 2.4.3. The complex fundamental voltage can be obtained using the STFT: after extracting the magnitude $A_1(t_k)$ and its phase $\theta_1(t_k)$, $V(t_k)$ can be written as:

$$V(t_k) = A_1(t_k) e^{j\theta_1(t_k)} \tag{2.8}$$

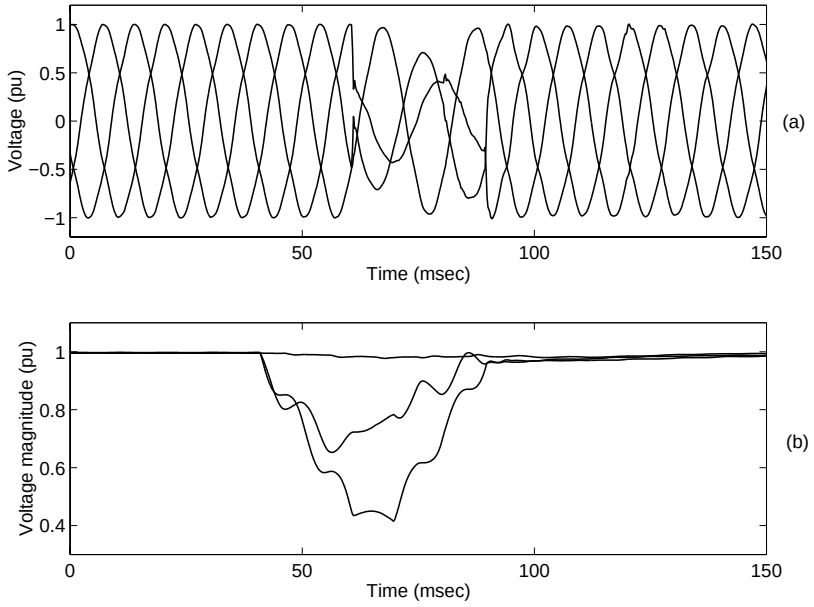

Figure 2.4: Short duration voltage dip (a) Voltage waveforms (b) Voltage magnitude (measurement in an 11 kV network)

Statistics on the phase angle jumps of rectangular voltage dips are given in Figure 2.5. The recordings were obtained from a medium voltage network (33 and 11 kV) over a one-month period. The statistics contain the phases that present a voltage dip of magnitude larger than 0.10 pu. It can be seen that there are more negative values than positive ones.

Summarising, voltage dips due to faults are:

- rectangular: voltage recovers fast after fault clearing operation.
- symmetrical or asymmetrical: depending on the type of fault that caused them.

2.3.2 Fault-related overvoltages

During an earth fault on an impedance-grounded or ungrounded system, the voltage of the phase that is shorted to ground is placed at ground potential and the remaining two phases are then subjected, with respect to earth, to the phase-to-phase voltage. This means that a sustained overvoltage (swell) appears on the healthy phases as long as the fault persists and disappears after fault clearing. The magnitude of this overvoltage depends on the grounding of the system. For a completely ungrounded system the overvoltage is equal to the phase-to-phase voltage of the system (that is an increase of 173 %). A measurement of a fault-induced overvoltage is given in Figure 2.6.

Fault initiation might cause transient overvoltage due to travelling waves that propagate in the system [31] or due to the nature of the fault (arcing) [32]. Fault

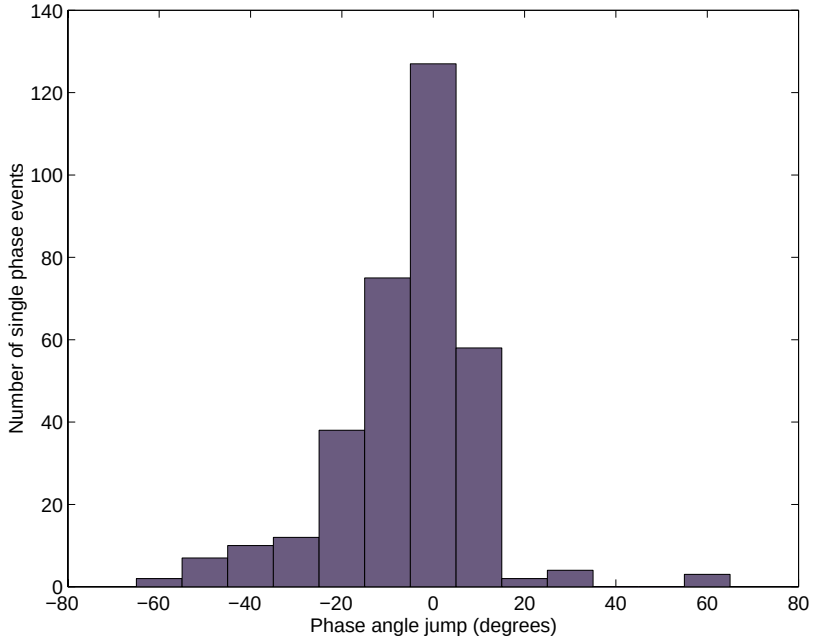

Figure 2.5: Statistics on phase angle jump for voltage dips due to faults

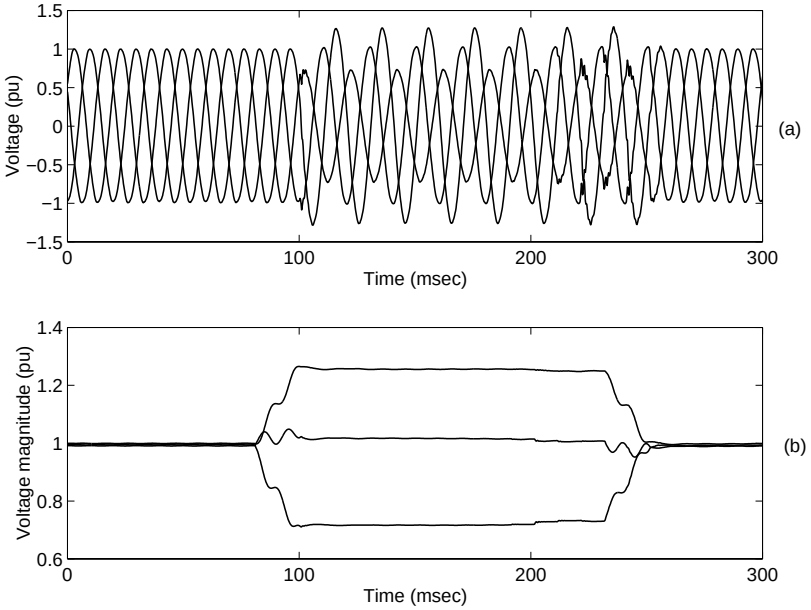

Figure 2.6: Overvoltage-swell due to a fault (a) Voltage waveforms (b) Voltage magnitude (measurement in an 11 kV network)

clearing might also cause transient overvoltages [31]. A special case is the overvoltage due to fuse clearing [30]. Examples of these types of overvoltages are given in Chapter 4.

2.3.3 Self-extinguishing faults

Earth faults might disappear before any protection operation, due to the self-extinction of the fault arc during the zero crossing of the fault current. This more likely to happen in reactance-grounded systems due to low fault current [33]. The event causes a short duration voltage dip, accompanied by an overvoltage for the healthy phases (as explained in Section 2.3.2), low fault current, slow voltage recovery and an oscillating zero-sequence voltage [34, 33]. The slow voltage recovery increases the possibility of the arc to extinguish itself [33].

Figure 2.7 shows the three voltage waveforms and their fundamental frequency magnitudes during a self-extinguishing fault. The measurement was performed in a 10 kV network. Voltage decreases for less than 2 cycles before it disappears without causing operation of the protection system. The healthy phases present an overvoltage and the faulty phase recovers slowly (approximately for one cycle) to normal voltage, after the fault is extinguished. For the measurement of Figure 2.7 the recovery of voltage starts 1-2 msec after fault initiation. However, according to measurements in distribution systems (20 kV) reported in [35], the average duration of self-extinguishing faults in the considered compensated networks was 540 msec and in the isolated networks was 440 msec.

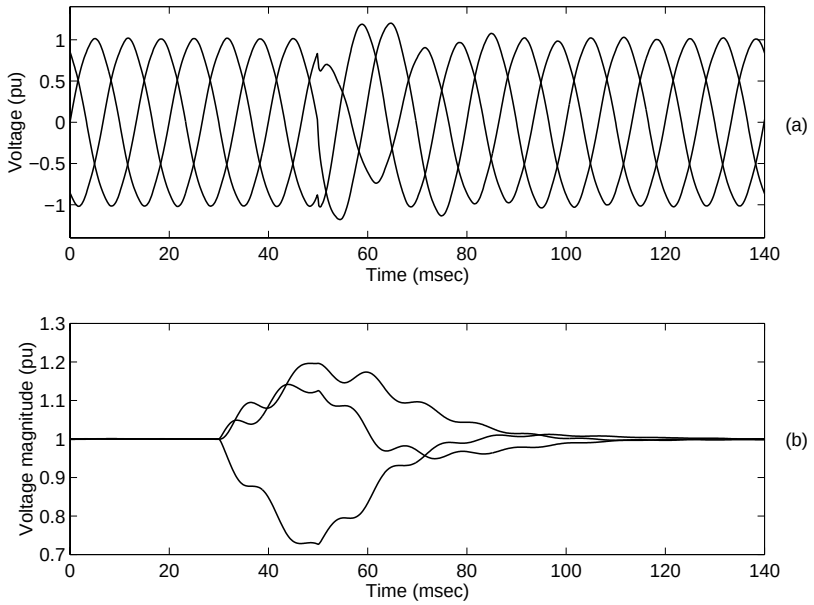

Figure 2.7: Self-extinguishing fault (a) Voltage waveforms (b) Voltage magnitude (measurement in a 10 kV network)

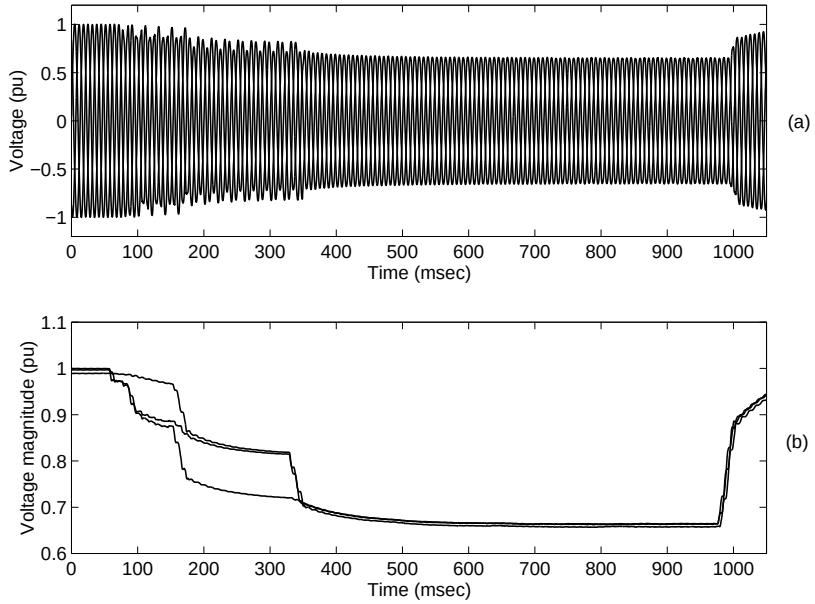

Figure 2.8: Multistage voltage dip measurement due to a cable fault (a) Voltage waveforms (b) Voltage magnitude (measurement in an 11 kV network)

2.4 Multistage voltage dips

Multistage dips are due to faults but they present different levels of magnitude before voltage returns back to normal. The case of multi-component dips has been reported before in the literature [36] but without further analysis.

It is shown in the following sections that these steps in the voltage dip magnitude can be due to either changes in the system configuration while the protection system tries to isolate the fault or changes in the nature of the fault itself (evolving faults).

The analysis of a large number of measurements showed that about 20 % of fault-induced voltage dips are multistage (Chapter 4).

2.4.1 Evolving faults

Figure 2.8 shows the voltage waveforms and the corresponding fundamental frequency magnitudes during a cable fault in an 11 kV network. The voltage magnitude presents three different stages of magnitude: it starts as a single-phase fault, becomes a two-phase fault and finally a three-phase fault. The phenomenon is probably related with the gradual failure of the cable insulation.

2.4.2 Multistage voltage dips due to changes in the system

A situation that leads to a multistage dip is a fault in the transmission system that is not cleared during the operation of zone-1 distance protection but only during the zone-2 operation. Consider the system shown in Figure 2.9a. Suppose that Z_1 and

Z_2 are the impedances between the source and the load bus and Z_0 is the source impedance. A fault occurs between the circuit breakers CB_1 and CB_2 at fraction p from the source. The voltage dip at the load bus (in p.u.) is given by:

$$V_{dip1} = \frac{p(1-p)Z_1^2}{Z_0(Z_1+Z_2)+pZ_1Z_2+p(1-p)Z_1^2} \tag{2.9}$$

If the fault is closer to CB_1, then CB_1 opens to clear the fault (Figure 2.9b) and the load bus will experience a voltage of magnitude:

$$V_{dip2} = \frac{(1-p)Z_1}{Z_0+Z_2+(1-p)Z_1} \tag{2.10}$$

By comparing the denominators of the above formulas it is easy to see that the opening of CB_1 will lead to an increase in voltage because $Z_0(Z_1+Z_2) > pZ_0Z_1$.

Similarly, if CB_2 opens first (Figure 2.9c), for a fault closer to CB_2, then the voltage dip magnitude will be:

$$V_{dip3} = \frac{pZ_1}{Z_0+pZ_1} \tag{2.11}$$

which is larger than V_{dip1}. Therefore, in both cases the voltage dip magnitude increases. The voltage dip at the load bus will recover completely only after both circuit breakers open.

2.4.3 Voltage dip characterisation method

Voltage dips propagate in the system and their characteristics change as they transfer through transformers. A characterisation method has been proposed in [37] for voltage dips due to faults that takes into account the different transformer connections. According to this method, the basic distinction of voltage dips is between types A, C and D:

- type A is an equal drop in the three phases.
- type C a drop in two phases.
- type D a large drop in one phase with a small drop in the other two phases.

For types C and D a further subdivision is needed to include the symmetrical phase (the phase with the large voltage drop for type D, the phase without voltage drop for type C). The resulting six types of three-phase unbalanced dips are shown in Figure 2.10. Type Db is a drop in phase b; type Cb a drop in phases a and c, etc. Alternatively, type Cb can be interpreted as a large drop in the ac voltage, etc. Examples of the three types of voltages dips (A, C and D) are given in Figure 2.11. These are measurements of single stage voltage dips in an 11 kV network. Both the

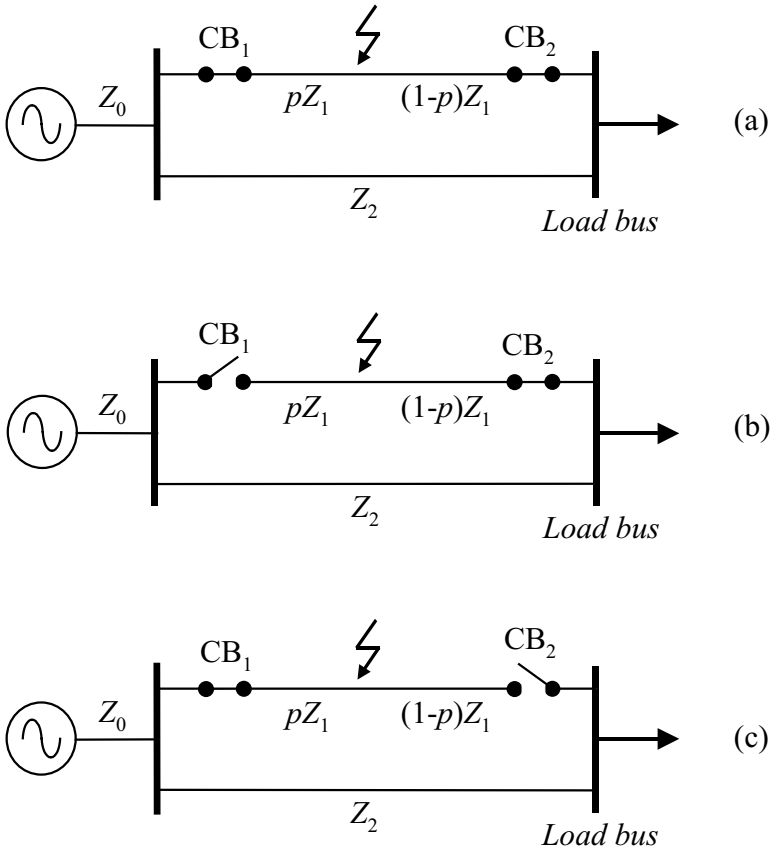

Figure 2.9: Equivalent circuits for faults in a loop (a) fault application in the loop (b) Circuit breaker CB1 opens to clear the fault (c) Circuit breaker CB2 opens to clear the fault

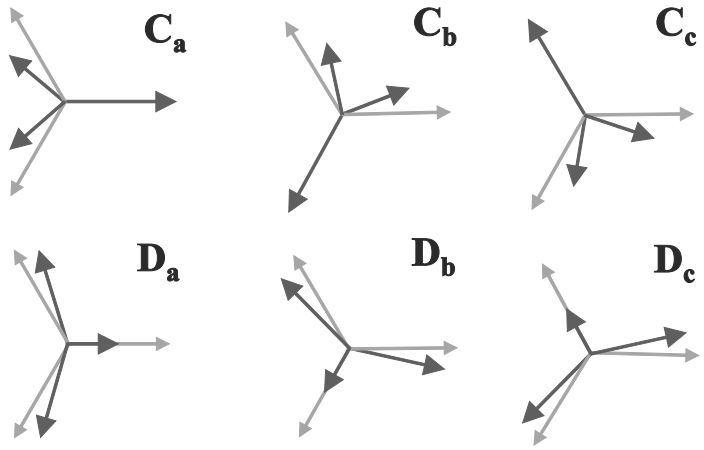

Figure 2.10: Six types of three-phase unbalanced voltage dips: grey arrows indicate normal voltages, black arrows voltages during the event

voltage magnitude and the phase angle are shown. The phase angle is plotted with reference to the pre-event phase angle.

Two-phase-to-ground faults can be included in the types C and D by adding a second characteristic. The two parameters quantifying the dip are the characteristic voltage V and the so-called PN factor F, both complex numbers. If the complex phase voltages are for each phase V_a, V_b, and V_c, then, for a type Ca dip:

$$\begin{aligned} V_{\mathrm{a}} &= F \\ V_b &= -\frac{1}{2}F - \frac{1}{2}jV\sqrt{3} \\ V_c &= -\frac{1}{2}F + \frac{1}{2}jV\sqrt{3} \end{aligned} \tag{2.12}$$

and for a type Da dip:

$$\begin{aligned} V_{\mathrm{a}} &= V \\ V_b &= -\frac{1}{2}V - \frac{1}{2}jF\sqrt{3} \\ V_c &= -\frac{1}{2}V + \frac{1}{2}jF\sqrt{3} \end{aligned} \tag{2.13}$$

The algorithm proposed in [37] determines the dip type from the positive sequence voltage V_1 and negative sequence voltage V_2, using the following transformation:

$$\begin{pmatrix} V_0 \\ V_1 \\ V_2 \end{pmatrix} = \frac{1}{3}\begin{pmatrix} 1 & 1 & 1 \\ 1 & \mathrm{a} & \mathrm{a}^2 \\ 1 & \mathrm{a}^2 & \mathrm{a} \end{pmatrix}\begin{pmatrix} V_{\mathrm{a}} \\ V_b \\ V_c \end{pmatrix} \tag{2.14}$$

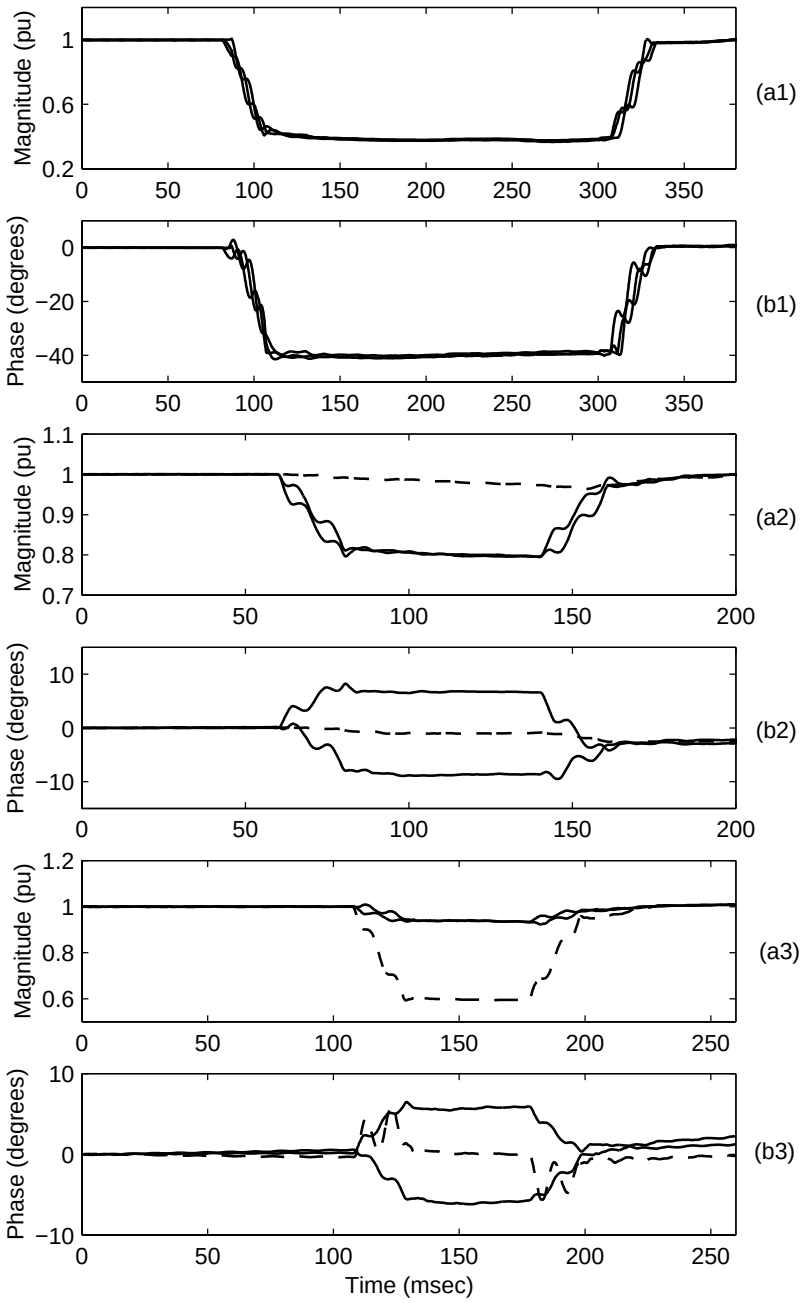

Figure 2.11: Voltages dip types: (a1) voltage magnitude and (b1) phase angle for a voltage dip of type A (a2) voltage magnitude and (b2) phase angle for a voltage dip of type Ca - phase a is the dashed line (a3) voltage magnitude and (b3) phase angle for a voltage dip of type Da - phase a is the dashed line

where $a = -\frac{1}{2} + j\frac{\sqrt{3}}{2}$.

It can be shown from (2.12), that for a type Ca dip, positive and negative sequence voltages are given by the following expressions:

$$V_1 = -\frac{1}{2}F - \frac{1}{2}V \tag{2.15}$$

$$V_2 = -\frac{1}{2}F + \frac{1}{2}V \tag{2.16}$$

For F =1 (the majority of events according to [37]) we obtain:

$$1 - V_1 = V_2 \tag{2.17}$$

i.e. the drop in positive sequence voltage is equal to the negative sequence voltage. For the other types, negative-sequence voltage and drop in positive sequence voltage are equal in absolute value but different in argument (angle).

The angle between the drop in positive sequence voltage and the negative sequence voltage provides the dip type (as explained in [37]), using:

$$T = \frac{1}{60^\circ} \arg \frac{V_2}{1 - V_1} \tag{2.18}$$

T is rounded to the nearest integer and the voltage dip type is given as follows:
if $T = 0$: type Ca
if $T = 1$: type Dc
if $T = 2$: type Cb
if $T = 3$: type Da
if $T = 4$: type Cc
if $T = 5$: type Db

The characteristic voltage V, and the PN factor F, can be calculated as:

$$V = V_1 - V_2' \tag{2.19}$$

$$F = V_1 + V_2' \tag{2.20}$$

where $V_2' = V_2 e^{-jT60^\circ}$.

F can be used to identify two-phase-to-ground faults [38]. The slow decay in F is a very common characteristic of voltage dips due to the presence of induction motors that slow down during the dip. However, a fast drop in F indicates a two-phase-to-ground fault.

2.4.4 Application of the characterisation method on measurements of multistage voltage dips

Considering the above described method, in a multistage dip:

- if the dip magnitude changes because of a change in the fault then the voltage dip type changes.

- if the dip magnitude changes because of a change in the system then the voltage dip type does not change.

The above characterisation method has been applied to several measurements of multistage dips. The results for four cases are shown here. The voltage magnitudes are shown in Figure 2.12. The results of the characterisation method are shown in Table 2.2. The results are obtained by applying the algorithm presented in the previous section at the different stages of the three phase voltages. Figure 2.13 shows F as calculated for two of the above cases.

The dip of case (a) is caused by a fault in a cable. By the changes in the voltage dip type we can conclude that the fault evolves from a single-phase fault to a two-phase-to-ground fault, to a three-phase fault. Inspection of Figure 2.13a shows a large drop in F at the second step of the dip, thus the fault for this stage is a two-phase-to-ground fault. During the first stage, F decreases slowly due to the presence of induction motor load (more about this phenomenon in Section 2.6.1). The same slow decrease can be seen in all the stages of the dip. During the three-phase fault, F is equal to the magnitude of the three voltages.

In case (b), the fault initially is a ground fault between phases b and c as indicated by the dip type and the drop in F, (Figure 2.13). In the second stage, the dip type indicates that the fault is cleared for phase b and it becomes a single-phase-to-ground fault (faulty phase is phase c) and F recovers to the pre-fault value. What happens in the system could be a partial self-extinguishing of the fault, or the fault being cleared by a fuse or single-phase breaker in just one phase.

Case (c) is a multistage voltage dip due to a three-phase fault. The change in the dip magnitude is due to a change in the system. In case (d) the dip magnitude changes but not the dip type. This indicates a change in the system as it tries to clear the fault that caused the dip.

Table 2.2: Results of voltage dip characterisation method

Case	Dip type
(a)	Cc to Db to A
(b)	Ca to Dc
(c)	A to A
(d)	Cb to Cb

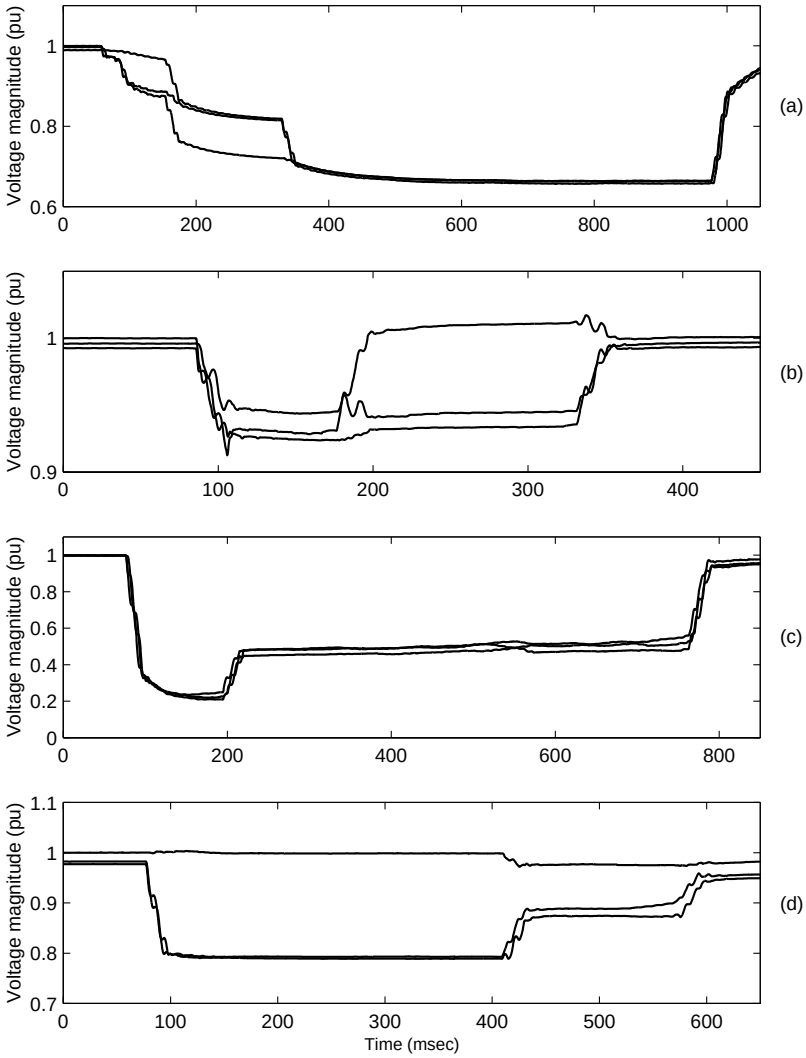

Figure 2.12: (a)-(d): Measurements of multistage voltage dips in an 11 kV distribution network

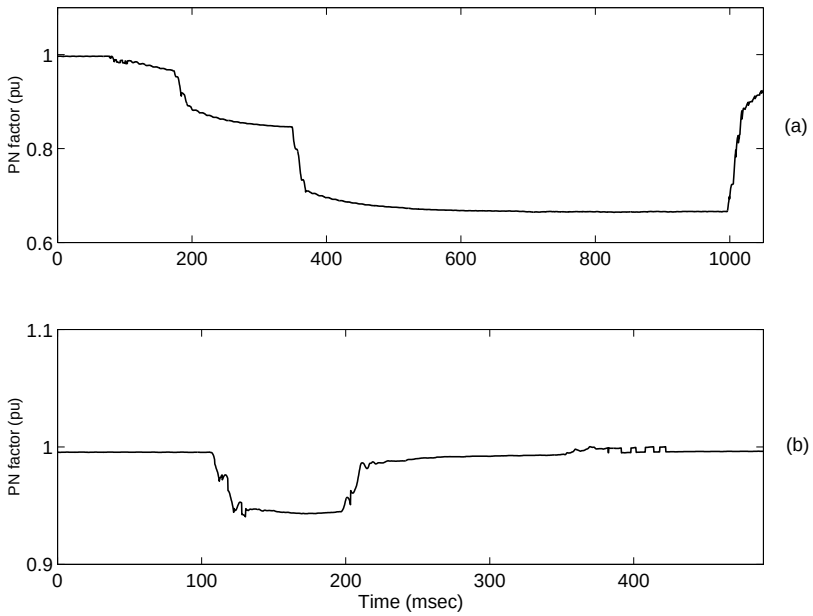

Figure 2.13: PN factor F for cases (a) and (b) of Figure 2.12

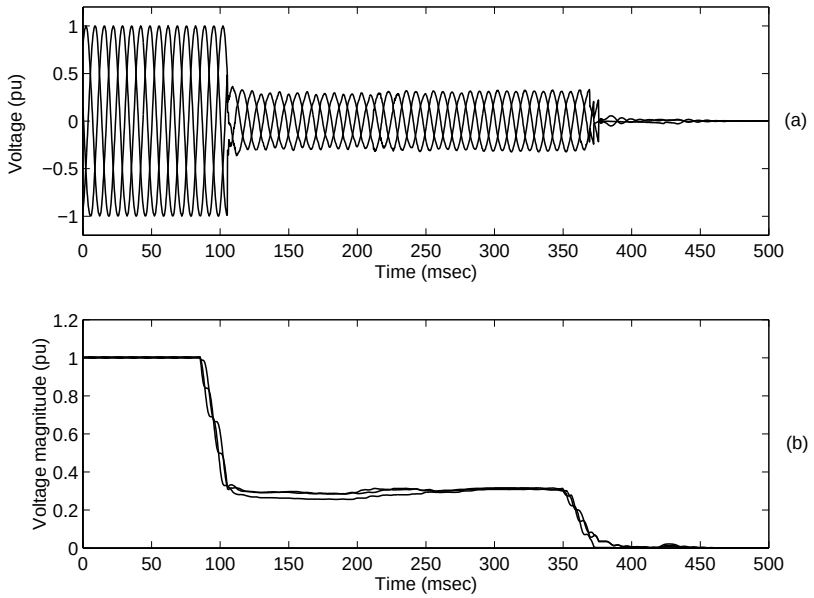

Figure 2.14: Fault interruption measurement (a) Voltage waveforms (b) voltage magnitude (measurement in an 11 kV network)

2.5 Faults and interruptions

As explained in the previous section, faults cause voltage dips that propagate in the system. These voltage dips present a rectangular shape due the fault clearing operation that isolates the part of the network where the fault is and voltage returns back to normal for the rest of the system. For the part of the system which is isolated by the protection system the voltage goes to zero causing an interruption.

Figure 2.14 shows a measurement of a fault-induced interruption in an 11 kV network. After fault initiation, voltage drops to approximately 0.30 pu and 250 msec later goes to zero due a fault clearing operation, most likely circuit breaker opening. The underlying fault is a three-phase fault (the three phases show similar characteristics) and the voltage magnitude during the fault is almost constant.

2.6 Induction motor starting

Starting of large induction motors is one more cause of voltage dips. It has been a concern for designers of industrial power systems [39, 6]. During start-up an induction motor takes current five to six times larger than normal. This current remains high until the motor reaches its nominal speed. This lasts between several seconds to one minute. The characteristics of the corresponding voltage dip depend on the characteristics of the induction motor (size, starting method, load, etc) and the strength of the system at the point where the motor is connected. The magnitude of the dip depends strongly on the system parameters. For the system in Figure

2.15, Z_0 is the source impedance and Z_M the motor impedance during starting. The voltage experienced at PCC is found from the voltage divider equation:

$$V_{dip} = \frac{Z_M}{Z_0 + Z_M} E \tag{2.21}$$

where E is the source voltage. The magnitude of voltage dips due to motor starting is rarely deeper than 0.85 pu [6].

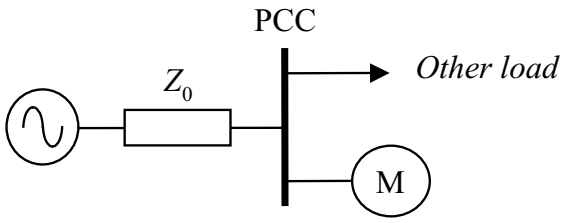

Figure 2.15: Voltage divider model for the calculation of voltage dip during motor starting

The duration of the voltage dip due to motor starting depends on a number of motor parameters. The most important of them is the motor inertia [6]. The duration of the dip is prolonged if other motor loads are connected to the same busbar, as they will further keep the voltage down.

Figure 2.16 shows the fundamental frequency magnitude of the three phases during the connection of a 500 HP induction motor on a 480 V bus as simulated in EMTP. The model of the induction motor used for this simulation can be found in Appendix A. The short circuit level of the busbar is 30 MVA. The initial drop in voltage is 0.09 pu and it takes approximately 400 msec for voltage to reach its steady state value. This voltage dip is symmetrical: all three phases drop equally and then recover gradually in a similar way because the starting current of the motor is the same for all three phases. A similar shape for the voltage magnitude during motor starting is shown in [4] and [40]. A measurement of a voltage dip due to induction motor starting is shown in Figure 2.17. The measurement comes from a low voltage network. The three phases present exactly the same characteristics. The voltage recovers within 7-8 cycles.

Summarising, voltage dips due to induction motor starting are:

- non-rectangular: voltage recovers gradually.
- symmetrical: all phases present the same behavior.

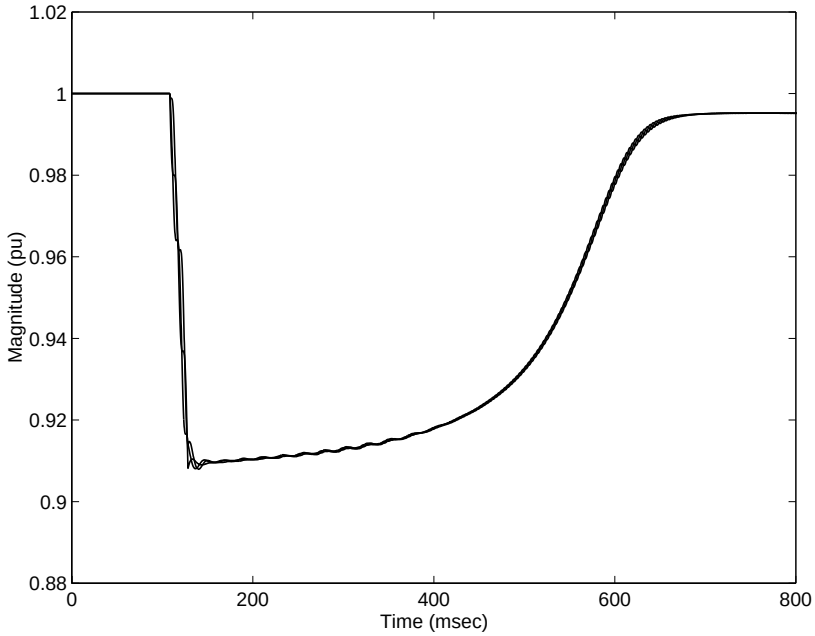

Figure 2.16: Voltage magnitude during induction motor starting (EMTP simulation-all three phases are shown)

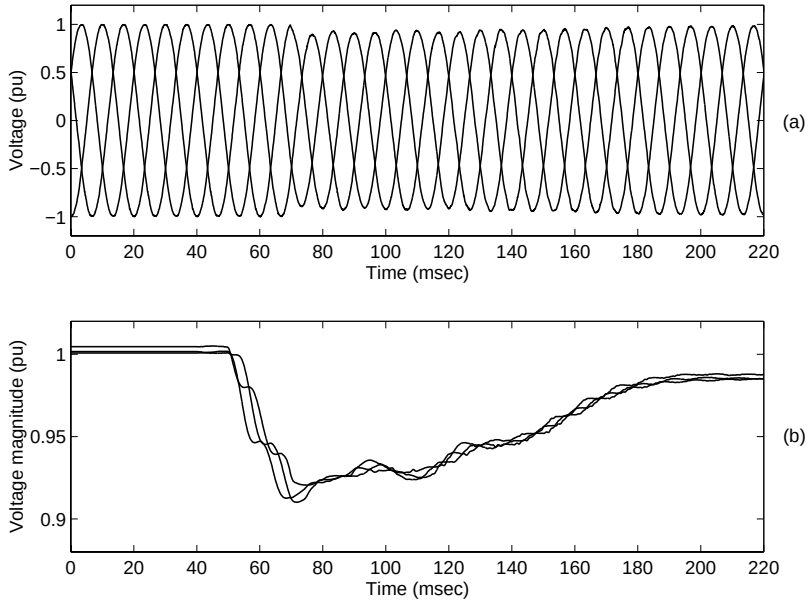

Figure 2.17: Induction motor starting (a) Voltage waveforms (b) Voltage magnitude (measurement in a 400 V network)

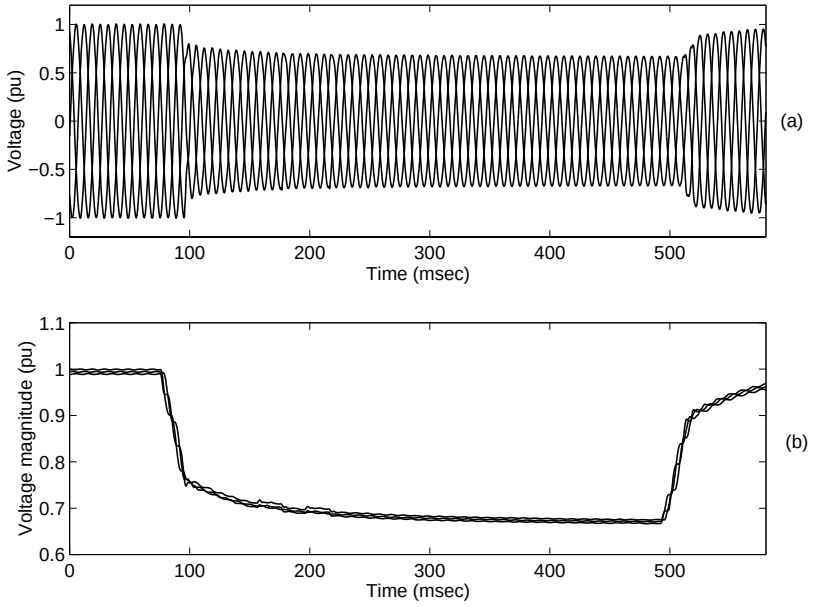

Figure 2.18: Influence of induction motor load during a fault (a) Voltage waveforms (b) Voltage magnitude (measurement in an 11 kV network)

2.6.1 Influence of induction motors on fault-induced voltage dips

Motors that experience a voltage drop, will typically slow down and draw more current from the supply. This shows up in the voltage recording as a slow decay in the voltage magnitude, during the fault. After fault clearing, motors re-accelerate delaying the full recovery of voltage and creating a post-fault dip as described in [41].

Figure 2.18 shows a voltage measurement in an 11 kV network of a voltage dip due to a three-phase fault. The influence of the motor load can be seen both during the fault and after fault clearing. Fault clearing causes a fast voltage increase to 0.90 pu and then the voltage increases gradually towards the normal voltage due to the motor load influence.

2.7 Transformer saturation

The fact that transformer saturation causes voltage dips is mentioned in the literature [42]. However, neither the frequency of appearance nor the characteristics of this event have been reported. The main attention has been given to the effects of the inrush current on the protection relays of the transformer itself [43]. As described in [42], the voltage dip that is caused by the magnetising inrush current can be long in duration and drive more transformers into saturation. The magnitude of the dip depends on a number of factors: the point on the wave where the switching

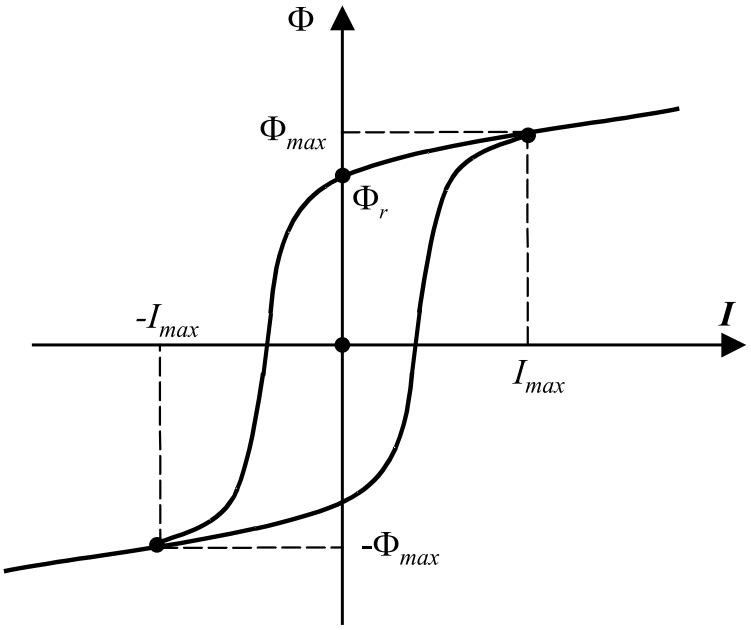

Figure 2.19: Magnetising curve and hysteresis loop of a transformer core

takes place, the strength of the source, the residual flux in the core and the damping of the network [32].

When a transformer is energised under a no-load condition, the magnetising current necessary to maintain the magnetic flux in the core is in general only few percent of the nominal rated load current. Figure 2.19 shows the magnetising curve and saturation loop. During steady state conditions the current oscillates between $\pm I_{max}$ as the flux Φ changes between $\pm\Phi_{max}$.

During transformer energising or a change of voltage in the transformer terminals, a transient occurs to change the flux in the core to the new steady state condition. In general this will cause the flux to go above the saturation value once each cycle until the average value of the flux (Φ) over a cycle has decayed to nearly zero. This temporary over-fluxing of the transformer core causes high values of the magnetising current, which is highly asymmetrical and decays exponentially. This phenomenon is known as magnetising inrush current and its magnitude depends on the point on the wave where the switching takes place and the core residual flux (Φ_r).

For a single-phase unloaded transformer which is to be switched onto an infinite busbar, the voltage $u(t)$ across the transformer's coil is given by:

$$u(t) = N\frac{d\Phi}{dt} \tag{2.22}$$

where $u(t) = \widehat{V}\sin(\omega t + \alpha)$, N is the number of turns of the energised coil and Φ is the flux associated with applied voltage. When a transformer has been switched off from the system, the transformer core is left with residual flux Φ_r. Integrating

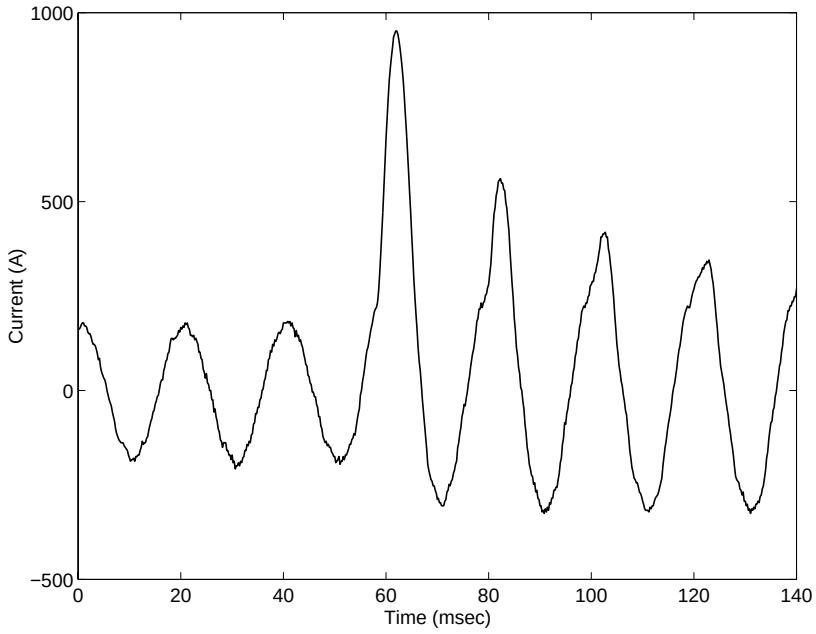

Figure 2.20: Current measurement during a reclosure after fault clearing (measurement in an 11 kV network)

(2.22) between 0 and t gives:

$$\Phi(t) - \Phi_r = -\frac{\widehat{V}}{\omega N}\{\cos(\omega t + \alpha) - cos\alpha\} \tag{2.23}$$

The value $\widehat{V}/\omega N$ represents the maximum flux value under the steady-state operation Φ_{max}. The flux at any instant t after switching can be obtained by:

$$\Phi(t) = \Phi_r + \Phi_{max}\cos(\alpha) - \Phi_{max}\cos(\omega t + \alpha) \tag{2.24}$$

Therefore, $\Phi(t)$ can reach the value of $\Phi_r + 2\Phi_{max}$, if the transformer is switched in at $\alpha = 0°$ and Φ_r has the same polarity as the peak value of voltage. If $\alpha = 90°$ then $\Phi(t)$ can reach a value of $\Phi_r + \Phi_{max}$.

As the core is forced into saturation the transformer draws a large current from the supplying network. When the voltage reverses its polarity in the next half cycle, then the maximum flux in the core is less than the maximum flux density Φ_{max} in the no-load situation. The transformer inrush current is therefore asymmetrical and contains a DC component, which takes, in same cases, seconds to disappear depending on the damping of the system [32]. Fig. 2.20 shows a current measurement in an 11 kV network during a reclosing operation (after fault clearing) that caused transformer saturation. It can be seen that the resulting current is asymmetrical.

2.7.1 Cases of transformer saturation

Apart from the case of transformer saturation during energising, the following cases of saturation have been reported in the literature:

- When another, nearby transformer is saturated. The phenomenon is called sympathetic interaction and it can cause prolonged temporary overvoltages [44].
- Due to lightning. Lightning can draw transformer into saturation due to the induced voltage impulse. In this case high inrush currents are produced that might blow fuses although this is not a fault situation [45].
- Load shedding. In [46], a real case is shown where high harmonic overvoltages are produced due to transformer saturation following load shedding depending on the resonances of the system.
- Geomagnetically induced currents [47].
- Fault application and fault clearing [48].
- Line opening [32].

2.7.2 Transformer saturation simulation

The energising of an unloaded transformer (14.4 kV/480 V, 500 kVA, wye-wye connected) was simulated in EMTP. The Type-96 non-linear element of EMTP is used in order to take into account the saturation effect. The transformer model can be found in Appendix A. Figure 2.21 shows the voltage waveforms and the corresponding fundamental frequency magnitudes during the energising of the transformer from a source with 7 MVA short circuit level. The voltage magnitude drops sharply and recovers gradually as the magnetising current decreases. The magnitude of the dip is not the same for all the phases because the degree of saturation is different for each phase (different switching angle for each phase).

Figure 2.22 shows the minimum voltage dip during energising of the above mentioned transformer from sources with different short circuit level. It can be seen that as the source becomes stronger the voltage dip becomes less severe.

2.7.3 Transformer saturation measurements

Analysis of measurements from different distribution systems showed that transformer saturation dips are common and might take place during energising of transformers or due to reclosing actions after a fault clearing operation. The measurements exhibit the same characteristics as the simulation shown in the previous section.

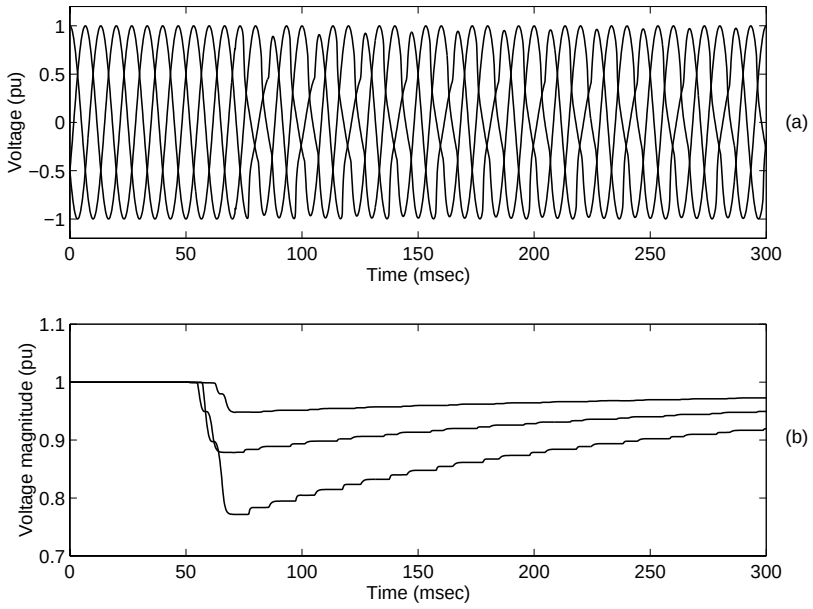

Figure 2.21: Transformer energising (a) Voltage waveforms (b) Voltage magnitude (EMTP simulation)

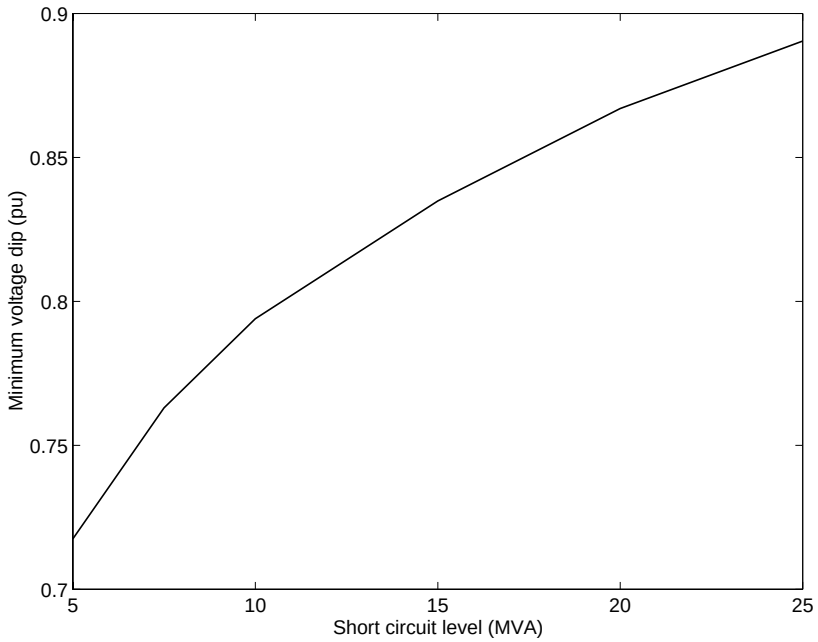

Figure 2.22: Minimum voltage dip for different source strength

Figure 2.23 shows the voltage waveforms as well as their fundamental frequency magnitude of a measurement in a 11 kV network. An asymmetrical gradually recovering voltage dip can be observed. The largest drop is 0.15 pu for one of the phases and the distortion in the waveforms is visible even 200 msec after the beginning of the event.The measurements showed that the voltage recovery is almost exponential, following the exponential decay of the magnetising current. However, one time constant is not enough to describe the phenomenon because the involved inductance is non-linear [32].

Additionally, the voltage presents temporary harmonic distortion as can be seen in Figure 2.24 and described in a number of papers (for example [44]). The STFT has been used for the estimation of the harmonics (from 2^{nd} to 5^{th}) of the voltage of one of the phases of Figure 2.23. The 2^{nd} harmonic is contributing the most.

Summarising, voltage dips due to transformer saturation are:

- non-rectangular: voltage recovers gradually as the inrush current decays.
- non-symmetrical: each phase presents a different degree of saturation.
- rich in harmonics: due to the asymmetry of the inrush current.

2.7.4 Harmonic overvoltages due to transformer saturation

Another phenomenon related to transformer saturation is the so-called harmonic overvoltages [48]. The harmonics that are produced by the saturation might coincide with the resonances of the system and overvoltages are built up. Cable systems and capacitor banks might create such resonances at relatively low frequencies.

Figure 2.25 shows the voltage waveforms as well as their fundamental frequency magnitude of a measurement in an 11 kV network of such a phenomenon. The overvoltage is around 1.2 pu. Although the voltage waveforms are very distorted and the peaks of each cycle are exceeding the pre-event peaks, the magnitude of voltage is similar to the voltage magnitude of the cases presented above. This shows that the event is the result of transformer saturation. The magnitude of the fundamental component is significantly lower than the maximum value of the voltage waveform due to the nature of the phenomenon (harmonic distortion).

Harmonics from 2^{nd} to 5^{th} of the phase voltage that presents the most severe voltage dip are shown in Figure 2.26. The 2^{nd} harmonic dominates at the beginning of the event. However, at the end of the recording all the harmonics are equally high. Comparing Figure 2.24 and Figure 2.26, the harmonic contents of the two cases are of the same order of magnitude. This shows that the harmonic overvoltage depends significantly on the phase of the harmonics with respect to the fundamental component.

An EMTP simulation is carried out for transformer energising with a capacitor bank connected to the same bus as shown in Figure 2.27. The same transformer and source are used for the simulation as in Section 2.7.2. The resonance of the system

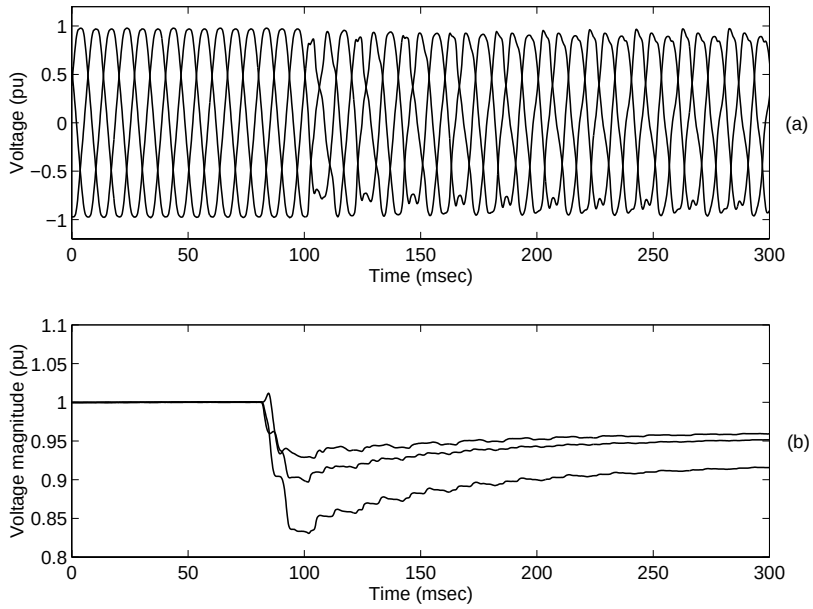

Figure 2.23: Transformer saturation (a) Voltage waveforms (b) Voltage magnitude (measurement in an 11 kV network)

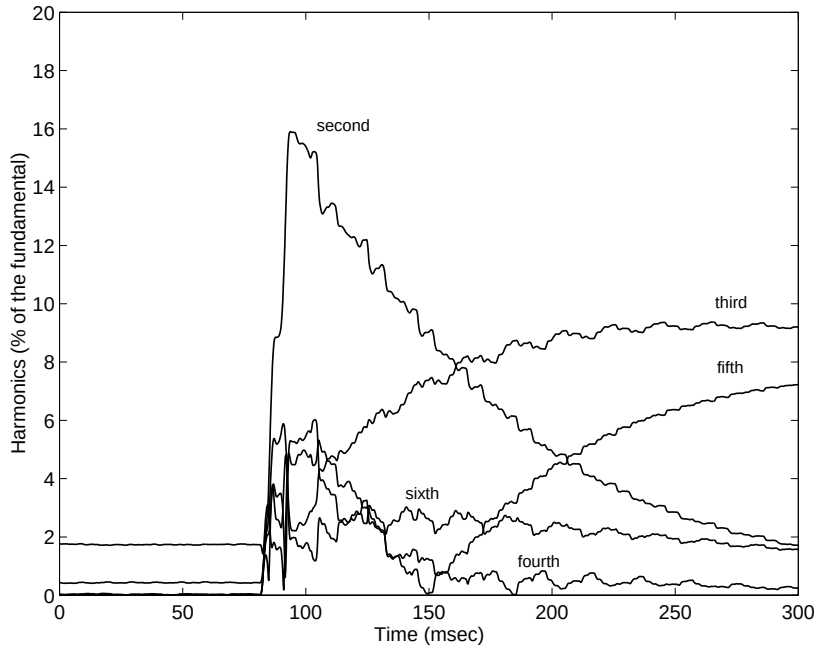

Figure 2.24: Harmonics in time of voltage during transformer saturation

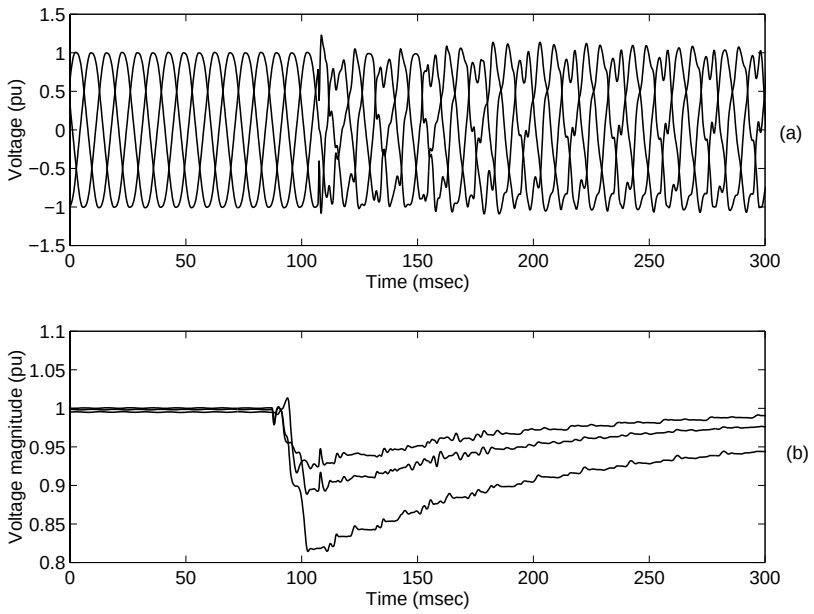

Figure 2.25: Harmonic overvoltage measurement (a) Voltage waveforms (b) Voltage magnitude (measurement in an 11 kV network)

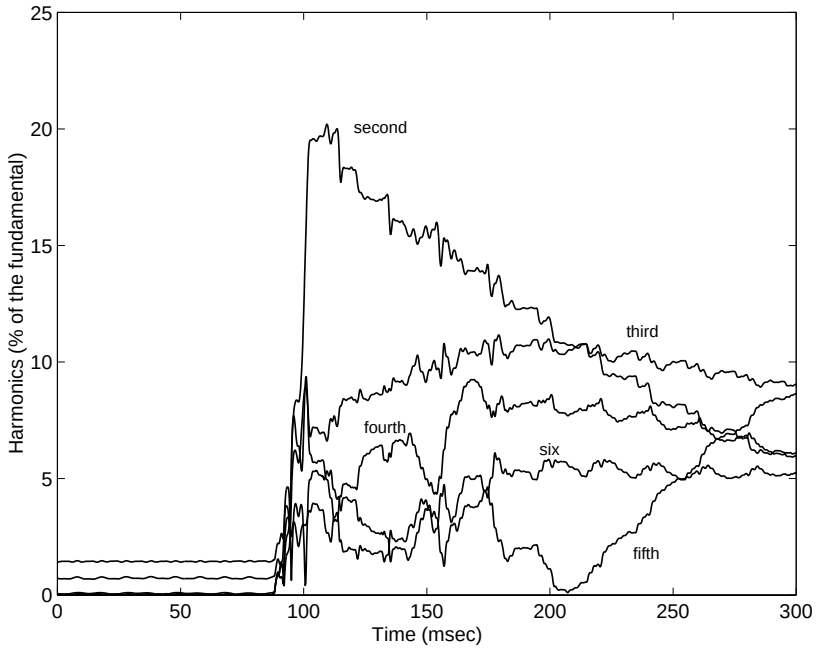

Figure 2.26: Harmonics of voltage during harmonic overvoltage

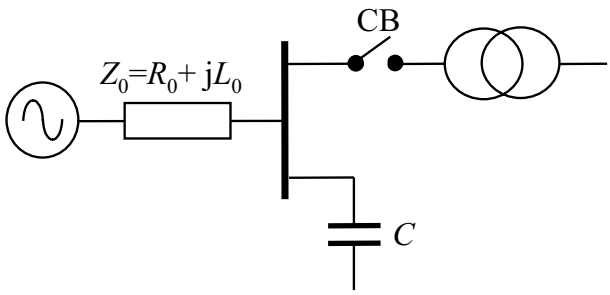

Figure 2.27: System for simulating harmonic overvoltages during transformer energising

is at the 3^{rd} harmonic:

$$\frac{1}{2\pi\sqrt{L_0 C}} = 150 \text{ Hz} \tag{2.25}$$

As shown in Figure 2.28, the voltage presents the characteristics of transformer saturation as in the case of Figure 2.25. The produced overvoltage is around 1.2 pu. The harmonics analysis (shown in Figure 2.29) presents similar features with the one in Figure 2.26: the 2^{nd} and the 4^{th} harmonics dominate. The 3^{rd} harmonic (where the resonance of the system is) is significant at the beginning of the event. Although, the magnitude of the harmonic components is twice as high as in the measurement of Figure 2.26, the resulting overvoltage is almost the same. As mentioned above, the resulting harmonic overvoltage depends significantly on the phase on the harmonics. Compared to the energising case without a capacitor bank (Figure 2.21) the voltage dip of Figure 2.28 is considerably larger.

2.7.5 Transformer saturation: calculation of rms voltage using one-cycle window and half-cycle window

Typically, the magnitude of dips is represented by the minimum value of the rms voltage of the recording. The rms voltage can be calculated over a window of two or one or half-cycle as:

$$u_{rms} = \sqrt{\frac{1}{M}\sum_{i=1}^{M} u(i)^2} \tag{2.26}$$

where M is the size of the window and $u(i)$ the ith sample of the voltage waveform. The rms voltage shown in the next figures is calculated in overlapping windows of one cycle or half cycle (M =1 or 0.5 cycle).

Figure 2.30 shows the rms voltage of one of the phases of the measurement in Figure 2.23 calculated using one-cycle and half-cycle windows. The rms voltage

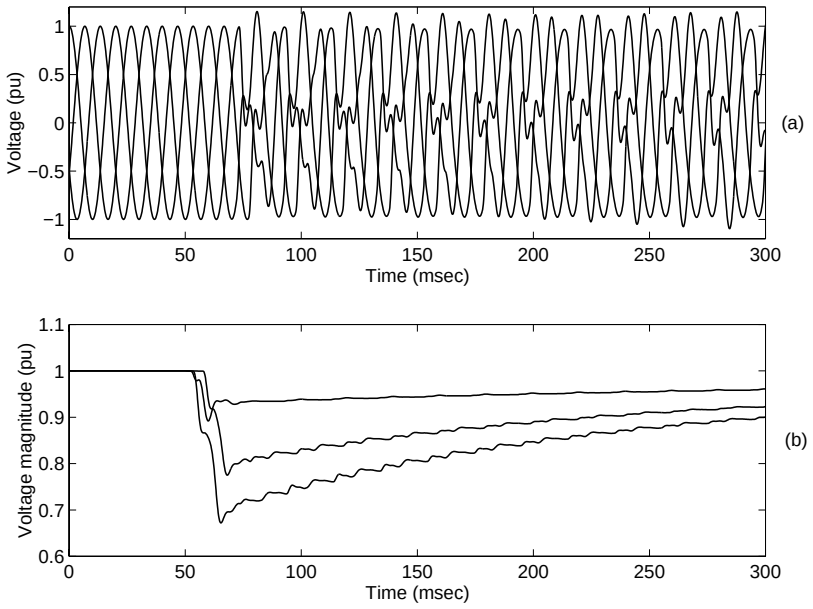

Figure 2.28: Harmonic overvoltage due to transformer energising (a) Voltage waveforms (b) Voltage magnitude (EMTP simulation)

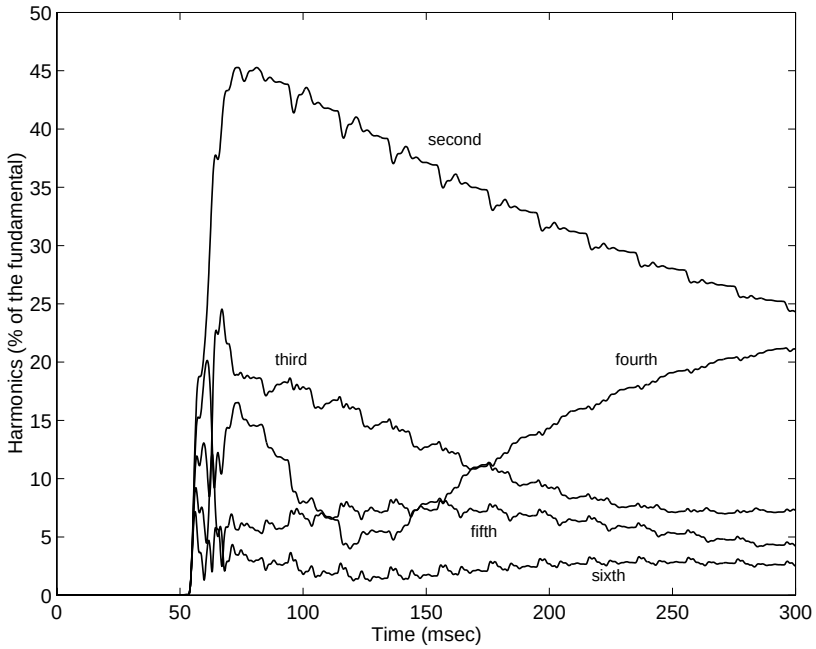

Figure 2.29: Harmonics of voltage during transformer energising

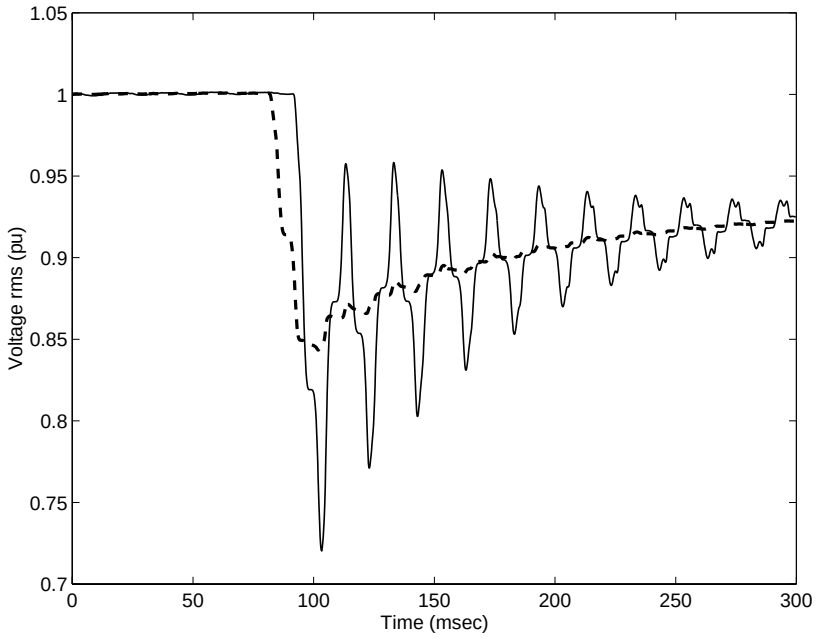

Figure 2.30: rms magnitude of voltage versus time during transformer saturation calculated over a one-cycle window (dashed line) and a half-cycle window (solid line)

obtained using a one-cycle window does not differ noticeably from the voltage magnitude as obtained using the STFT.

Calculation of the rms voltage over a half-cycle window shows how transformer saturation leads to variations of voltage magnitude between two consecutive half-cycles. As the transformer magnetising current is only present during part of the cycle, the voltage disturbance becomes a succession of sub-cycle voltage dips. It can be noticed that the minimum rms voltage as calculated over a half-cycle window is significantly lower than the one calculated over a one-cycle window. The difference in the estimated rms between the two windows lies in the fact that during transformer saturation the voltage magnitude changes fast therefore the long window (one cycle) is not able to capture these changes.

For a total of 109 measurements of voltage dips due to transformer energising (obtained over a two-month period in a distribution system of 33 and 11 kV) the lowest rms voltage has been obtained for each phase separately. The results are shown in Figure 2.31 for the rms voltage calculated over a one-cycle window. In that case 11 events show an rms voltage lower than 0.90 pu (that is the rms voltage exceeds the 0.90 pu threshold for at least one phase). The results in Figure 2.32 show the rms voltage calculated over a half-cycle window: 76 events show an rms voltage less than 0.90 pu. Table 2.3 contains the most important information as obtained from the measurements. Transformer saturation events are 13 % of the total number of measured dips below the 0.95 pu threshold as shown in Chapter 4.

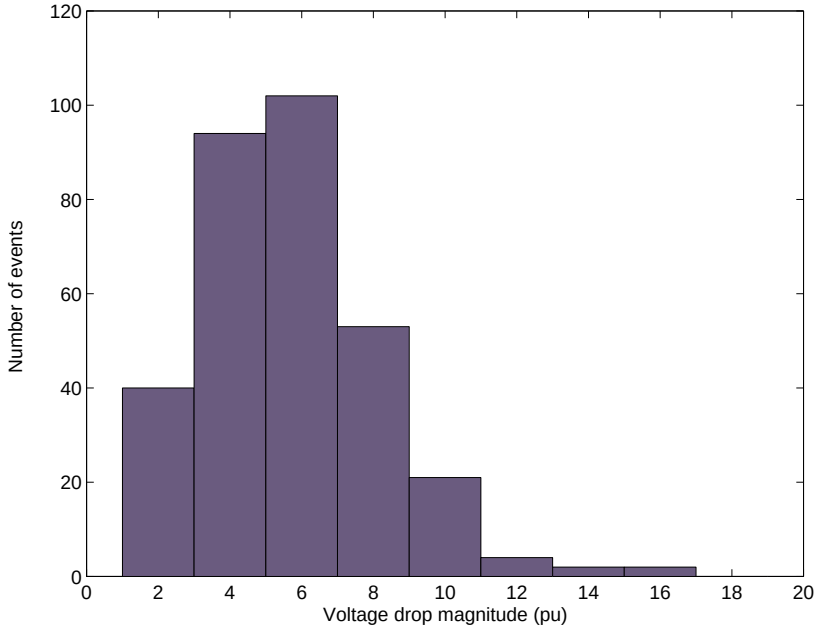

Figure 2.31: Transformer saturation minimum rms magnitude using one-cycle window

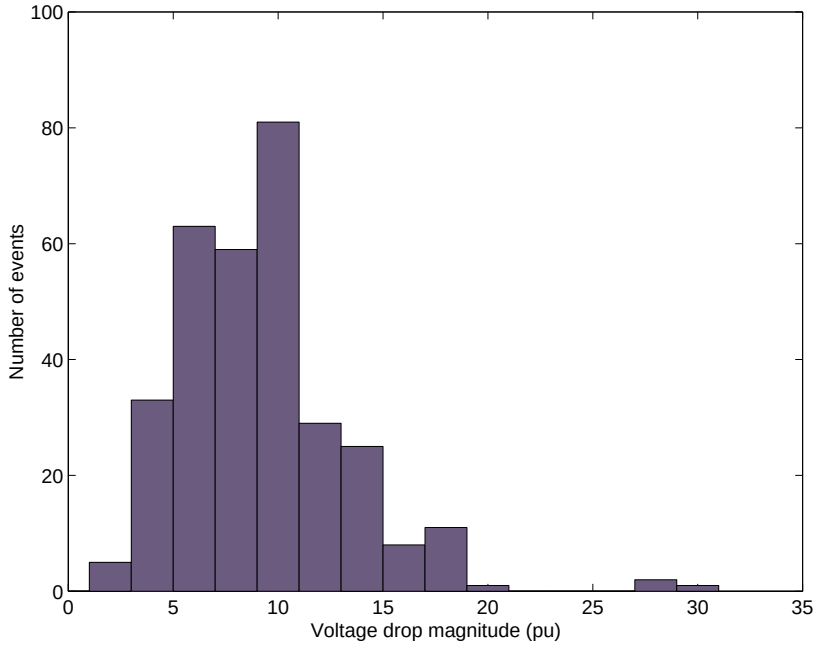

Figure 2.32: Transformer saturation minimum rms magnitude using half-cycle window

Table 2.3: Statistics on transformer saturation measurements

Monitoring period	2 months
Number of transformer saturation events	109
Maximum voltage drop (1 cycle rms)	0.17 pu
Maximum voltage drop (half cycle rms)	0.32 pu
Number of events with a voltage drop above 0.10 pu (one-cycle rms)	11
Number of events with a voltage drop above 0.10 pu (half-cycle rms)	76

2.7.6 Transformer saturation on fault application and on fault clearing

Fault application and fault clearing can lead to transformer saturation [48, 49] and the half-cycle rms calculation can be used to identify the event in measurements of voltage dips.

Figure 2.33 shows the rms voltage during a fault induced dip measured at an 11 kV network. The rms voltage is calculated using a half-cycle window. Figure 2.34 shows the rms voltage using a one-cycle window, for the same measurement. The following can be observed:

- the signature of repeating voltage dips of decreasing magnitude that can be seen after fault clearing is characteristic of transformer saturation.
- the one-cycle rms voltage presents a prolonged slowly recovering voltage dip after fault clearing similar to the one that is caused by the re-acceleration of motor load (Section 2.6.1).
- the initial slow decay at the beginning of the dip (which can be seen with both the half and one-cycle rms) is due the influence of the induction motor load of the network (as explained in Section 2.6.1). Therefore the prolonged dip after fault clearing is a combination of the effect of transformer saturation and the re-acceleration of the motor load of the network.

Figure 2.35 shows the rms voltages of a measurement where transformer saturation takes place during the fault. The signature of repeating voltage dips due to transformer saturation can be seen in all phases but the variation in the magnitude is higher for the phase that seems to be non-faulted. In this measurement the phenomenon of saturation (variations in the rms magnitude) is over before fault clearing.

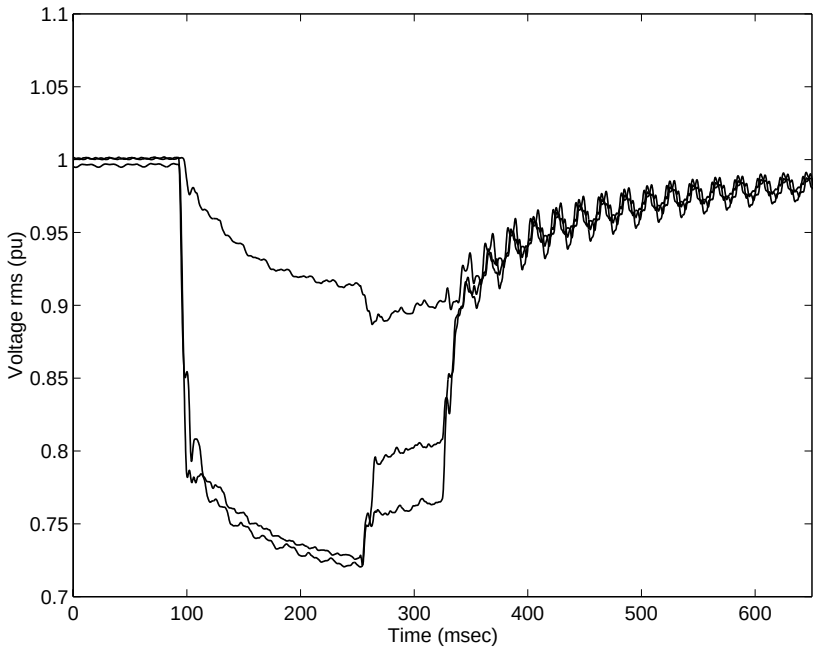

Figure 2.33: Voltage dip due to fault followed by transformer saturation: rms voltage calculated using a half-cycle window (measurement in an 11 kV network)

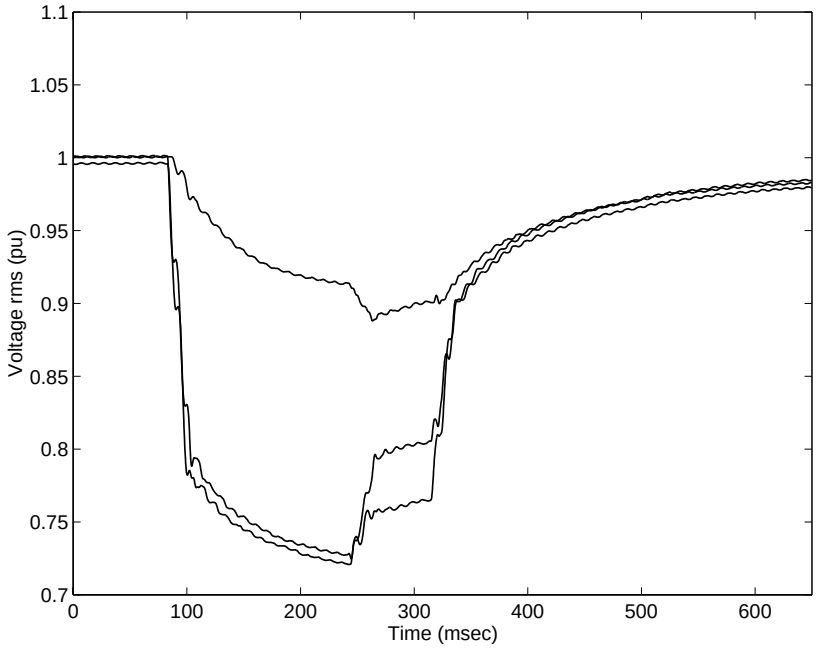

Figure 2.34: Voltage dip due to fault followed by transformer saturation: rms voltage calculated using a one-cycle window (measurement at 11 kV)

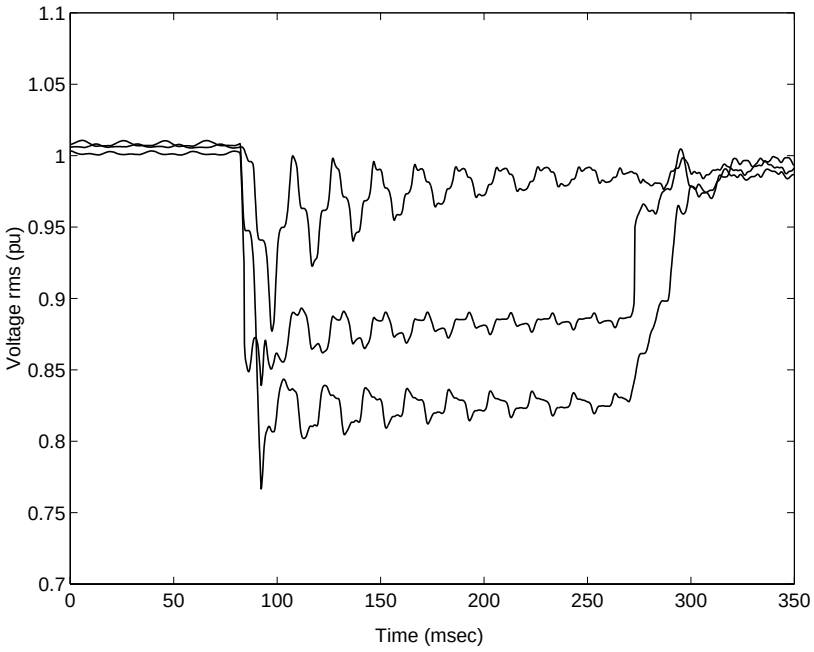

Figure 2.35: Voltage dip due to fault associated by transformer saturation: rms voltage calculated using a half-cycle window (measurement at 11 kV)

2.7.7 STFT-extracted and rms voltage magnitude

The STFT used as described in Section 2.2, provides an estimate of the fundamental frequency magnitude that does not differ significantly from the calculated rms value using a one-cycle window; the difference is zero for an ideal sinusoid (no harmonics).

However, in the presence of strong harmonics the difference could be noticeable. Figure 2.36 shows the STFT-estimated fundamental frequency of voltage and the calculated rms for the case of harmonic overvoltages due to transformer saturation. It can be seen that one of the phases shows a dip when the STFT is used but the rms shows an increase. The difference in magnitude is less than 0.05 pu but it is important in terms of characterising-classifying the event.

A half-cycle window can be used with the STFT for better time resolution. In this case the bandpass filters that correspond to the filter bank realisation of the STFT, must be located at the fundamental (50 Hz) and the multiples of it frequencies (Section 2.2). In the case of transformer saturation, the STFT with these settings will provide similar results as those obtained using the half-cycle rms.

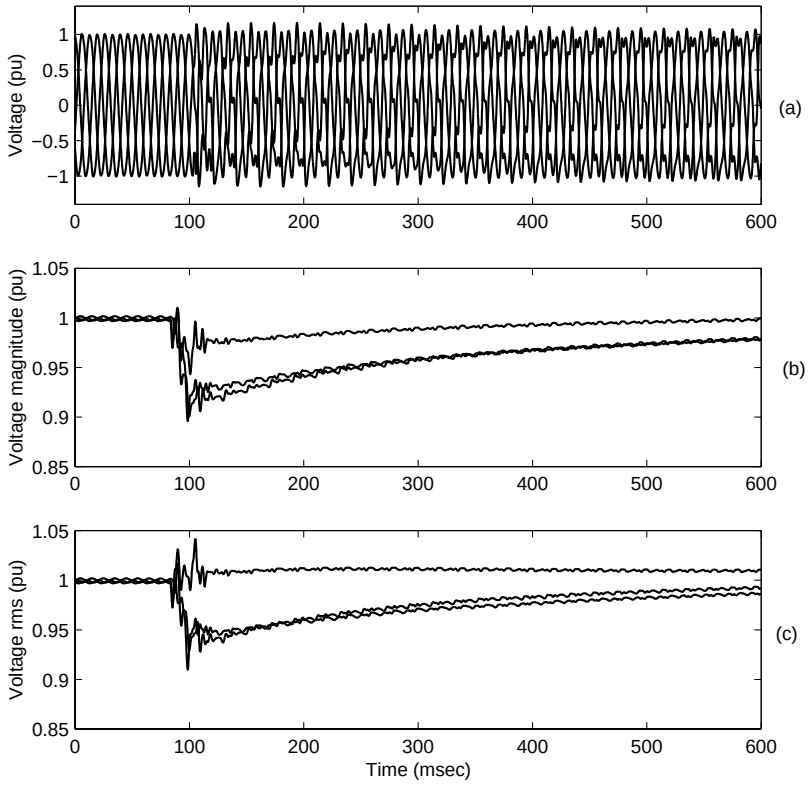

Figure 2.36: Transformer saturation measurement (a) Voltage waveforms (b) Voltage magnitude using STFT (c) rms voltage magnitude

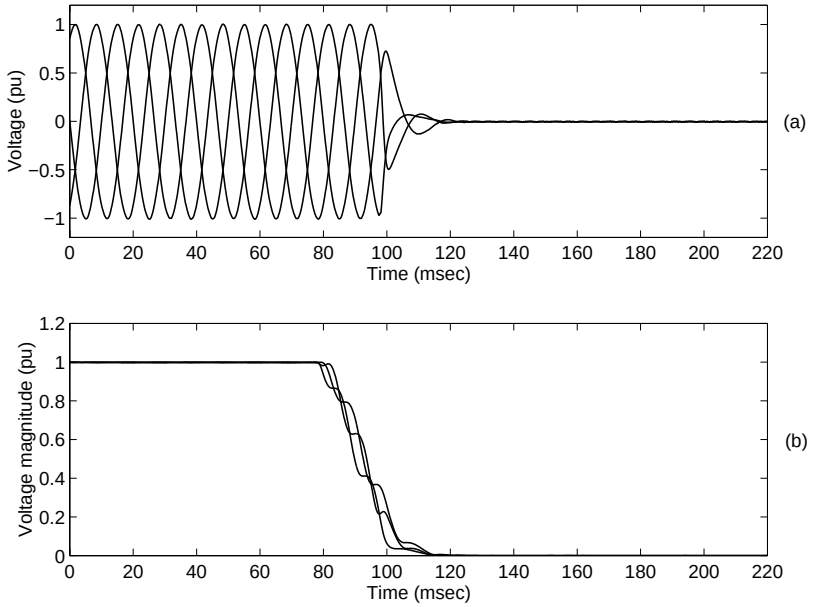

Figure 2.37: Non-fault interruption measurement (a) Voltage waveforms (b) Voltage magnitude (measurement in an 11 kV network)

2.8 Non-fault interruption

Disconnection of lines for maintenance causes interruptions. Unlike the fault-induced interruptions presented in Section 2.5, interruptions due to manual operations do not present a stage between the normal and zero voltage. An example of such an event is given in Figure 2.37. The measurement took place in an 11 kV network.

2.8.1 Overvoltages during interruptions

There are two cases of overvoltages during interruptions:

Transformer saturation

In a case where a line is opened with a transformer attached to it, the line charge has a path through which it is discharged. About half cycle after the switching operation, the transformer saturates, creating another path and its impedance quickly drops allowing a rapid discharge from the line. As the current approaches maximum, the voltage polarity reverses, creating a new cycle. On this reverse cycle, the core again saturates and the phenomenon is repeated. The process continues until the line is discharged and it results in a square-shape diminishing voltage waveform that lasts a few cycles [32]. An example of such an event is given in Figure 2.38. Only one phase is shown: the one with the highest overvoltage. The other two phases present similar characteristics. The measurement took place in an 11 kV network.

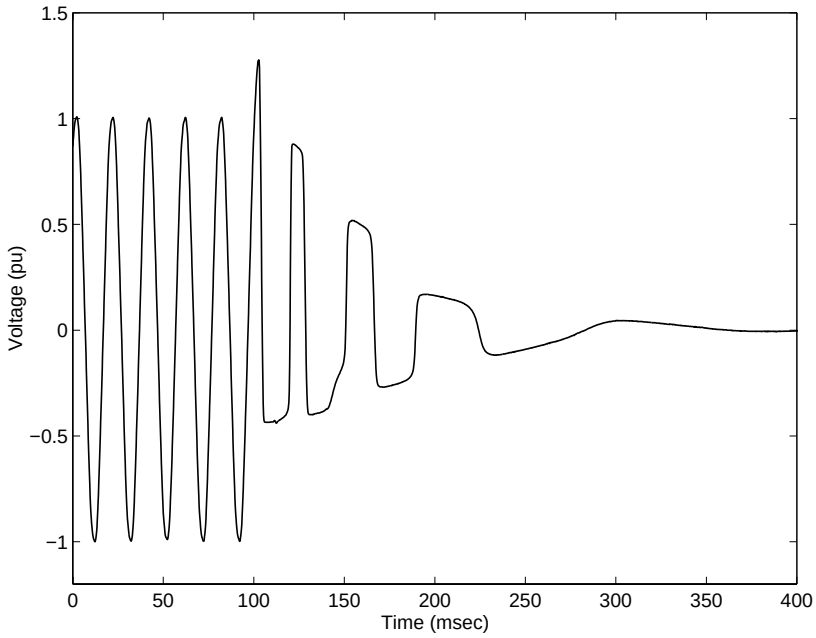

Figure 2.38: Voltage waveform during transformer saturation caused by interruption (measurement in an 11 kV network)

Current chopping

Current chopping occurs when the current is prematurely forced to zero by the aggressive interrupting action of the circuit breaker. When opening a breaker, the current can be interrupted before it reaches its natural zero point due to the instabilities in the arc. The energy present at that moment in the inductive load will oscillate via the present capacitance and an overvoltage is caused of a value which depends on this energy.

The phenomenon is often observed when the no-load current of a transformer is being switched or when a shunt reactor is disconnected [32]. In the case of the unloaded transformer the interrupted current is the magnetising current. An overvoltage can be generated, neglecting damping of magnitude [32]:

$$V = I_0 \sqrt{\frac{L_m}{C}} \tag{2.27}$$

where I_0 is the value of the current at the time the chop occurs, L_m is the magnetising inductance of the transformer and C the capacitance of the system that is primarily the transformer winding capacitance. An example of such an event is given in Figure 2.39. The measurement took place in an 11 kV network and the maximum voltage is approximately 3.1 pu. Similar voltage waveforms are shown in [50].

Both events (transformer saturation and current chopping) take place at the line side or the transformer side of the circuit breaker that opens. The measurements that are shown in this section are from monitors that are placed at these points

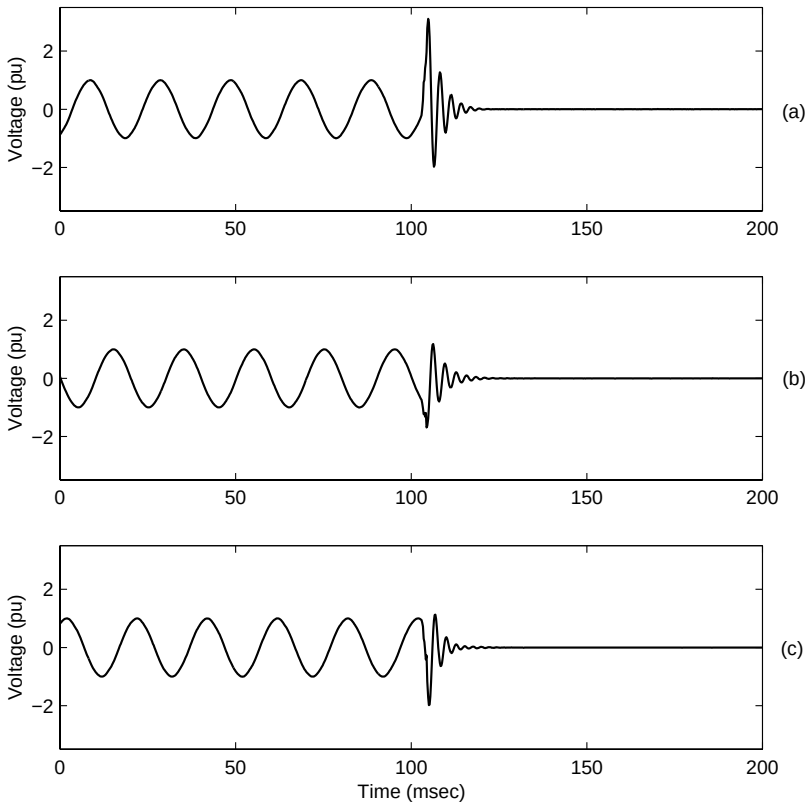

Figure 2.39: Voltage waveforms during current chopping (a) phase a (b) phase b (c) phase c (measurement in an 11 kV network)

and not at the source side. Monitors placed at the source side do not capture these events.

Regarding the classification of interruptions into non-fault and fault-related, the overvoltages described above occur mainly on the non-fault case. During a fault-related interruption transformer saturation is possible but current chopping is not. Current chopping happens typically during the interruption of low currents and during a fault the current is high.

2.9 Other switching actions

The following types of events are described in this section,

- Energising
- Load switching
- Reactive power compensation switching

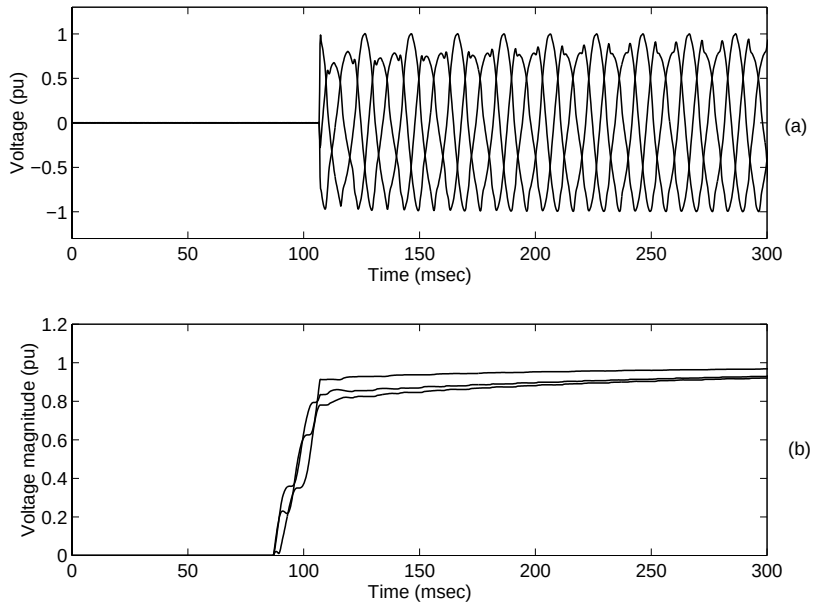

Figure 2.40: Energising measurement (a) Voltage waveforms (b) Voltage magnitude (measurement in an 11 kV network)

These events correspond to fast (step) changes in voltage magnitude. Figure 2.40 shows the voltage waveforms and the corresponding fundamental frequency voltage magnitude of a measurement in an 11 kV network during an energising process. The voltage increases fast to a value close to nominal, around 0.80 pu (Figure 2.40b). From that point onwards the voltage magnitude increases gradually. The gradual increase is due to transformer saturation and the asymmetry in the voltage waveforms (Figure 2.40a) verifies that, as explained in Section 2.7.

Figure 2.41 shows the voltage waveforms and the corresponding fundamental frequency voltage magnitude of a measurement in an 11 kV network during the switching of a large load. The voltage drops fast approximately 0.10 pu and remains at its new value.

Similar signatures are produced by switching actions for reactive power compensation. These events are treated in more detail in Chapter 6. Figure 2.42 shows the voltage waveforms and the corresponding fundamental frequency voltage magnitude of a measurement in a 10 kV network during the energising of a capacitor bank. The voltage increases fast, approximately 0.04 pu for all the phases and remains at its new value. Capacitor banks are usually used for this particular purpose: support of voltage. Switching of shunt reactors will give similar voltage events.

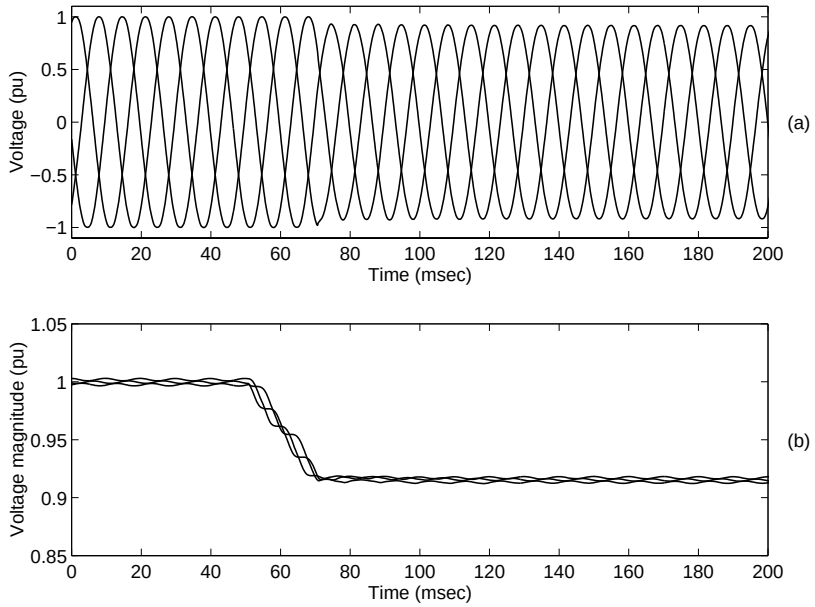

Figure 2.41: Step change measurement: load switching (a) Voltage waveforms (b) Voltage magnitude (measurement in an 11 kV network)

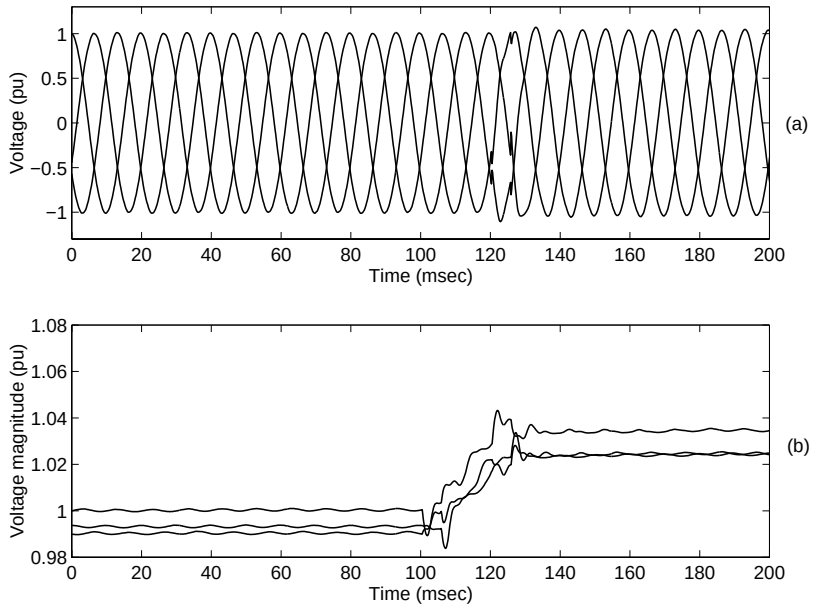

Figure 2.42: Step change measurement. capacitor energising (a) Voltage waveforms (b) Voltage magnitude (measurement in a 10 kV network)

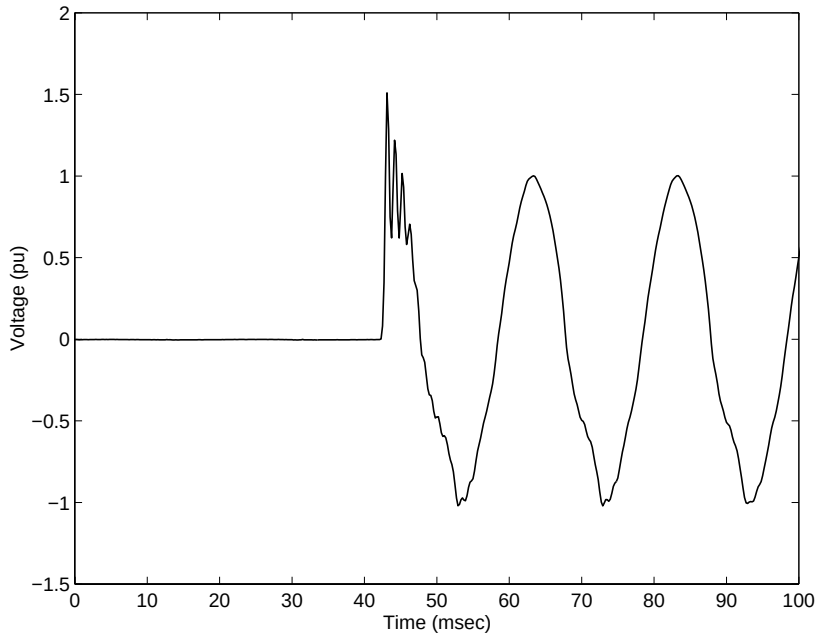

Figure 2.43: Voltage waveform during energising (measurement in an 11 kV network)

2.9.1 Overvoltages during energising

Travelling waves are initiated by the switching of a line that could cause transient overvoltages [31]. An example of such an event is shown in Figure 2.43. The measurement took place in an 11 kV network.

2.10 Conclusions

A number of power system events were presented in this chapter. Measurements and simulations were used to extract the characteristics of these events in terms of voltage.

The analysis presented in this chapter offers the means for event classification instead of disturbance classification, i.e. classification of the measurements in terms of the underlying event (fault, saturation, motor starting) and not only in terms of the identified disturbance (voltage dip, interruption, swell). As shown, different events cause similar disturbances (for example voltage dips) and more thorough analysis is needed to reveal the origin of a measurement.

Faults form probably the most important class of power system events because they cause significant problems (interruptions, voltage dips). Their characteristics were presented using measurements from distribution systems. Fault-induced dips are rectangular (voltage recovers fast after fault clearing). Fault-induced interruptions are also presented. Furthermore, self-extinguishing faults are considered; these are faults that disappear before any protection operation.

A new subclass of fault-induced events was added: multistage dips. The different stages in the dip magnitude are either due to changes in the system as it tries to isolate the fault or due to changes in the nature of the fault. A characterisation method for fault induced dips can be used for the analysis of such dips. The method is applied to measurements from a distribution network and the results show that the method can be used for better understanding of the measurements. Multistage dips form a significant part of the fault-induced events captured by power quality monitors (as shown in Chapter 4).

Induction motor starting is another class of power system events presented in this chapter. They also cause voltage dips which are non-rectangular (voltage recovers gradually) and symmetrical (all phases present the same characteristics). Simulations and measurements from low voltage networks are used for extracting their features.

For the class of transformer saturation events it is found that they cause dips which are non-rectangular and asymmetrical (each phase has different voltage dip magnitude due to the different degree of saturation of each phase). This class of events is also a large part of the monitoring data (as shown in Chapter 4).

Transformer saturation dips are in general shallow. The worst case in the available measurements is an rms drop 0.17 pu when a one-cycle window is used. If a half-cycle window is used then the drop becomes larger (0.32 pu). Finally, the rms voltage calculated over a half-cycle window gives a distinctive signature of repeating short duration voltage dips.

The phenomenon of transformer saturation is important for the protection relays of the transformer itself however transformer events are found to be of interest for other reasons also. As described in [51], transformer energising might cause commutation failure of a HVDC converter bridge. Furthermore, transformer events trigger fast voltage dip detection algorithms and cause unnecessary operations of voltage dip protection schemes [52]. This is explained in more detail in Chapter 3.

Other switching actions are also included in the analysis: non-fault interruptions, energising, step changes. The results of the analysis of all the above mentioned events are summarised in Figure 2.44.

Considering all the different types of voltage dips and the way that voltage recovers, there are:

- non-rectangular dips (transformers and induction motor dips)
- rectangular dips (fault-induced dips)

Considering the relationship between the phases there are:

- symmetrical dips (induction motor dips and dips due to three-phase faults)
- asymmetrical dips (transformer dips and dips due to asymmetrical faults).

These features are used for a knowledge-based system for automatic classification of power system events which is presented in Chapter 4.

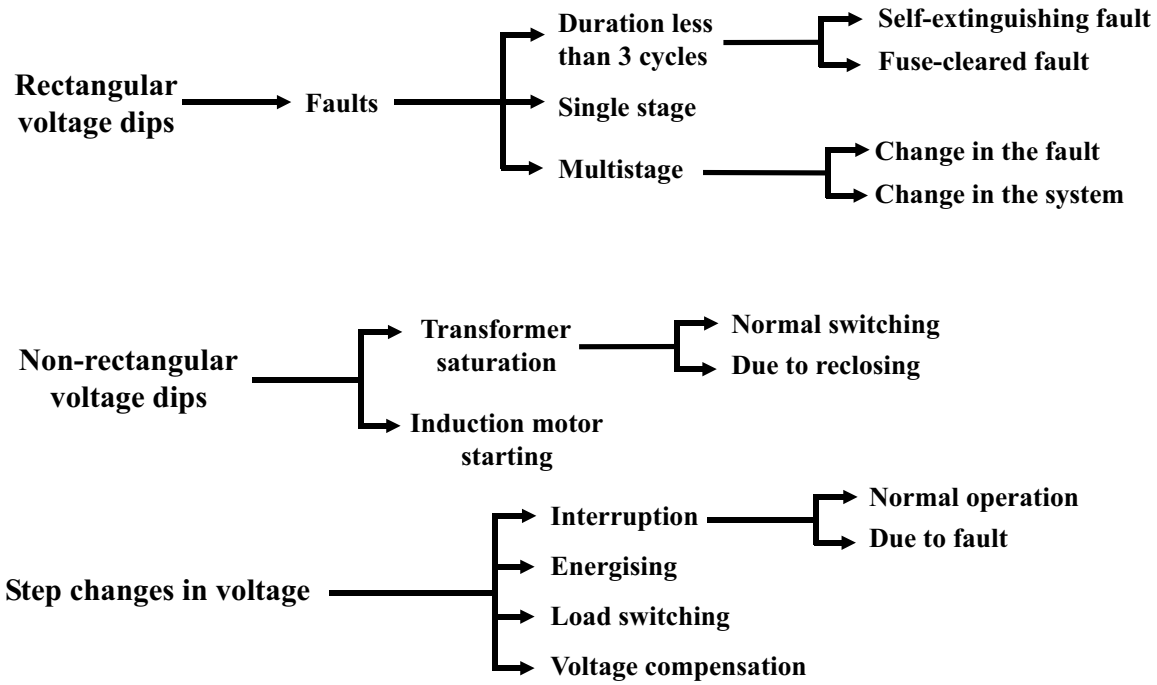

Figure 2.44: From disturbance classification to event classification

Chapter 3

Voltage magnitude estimation for power system event analysis

3.1 Introduction

A number of power system events was presented in Chapter 2, and it was shown that classification of these events is possible by examining the fundamental frequency magnitude of the three phase voltages. The fundamental frequency voltage magnitude was extracted using the Short Time Fourier Transform (STFT).

In this Chapter, the Kalman filter is used for the extraction of the fundamental frequency magnitude because:

- it can be designed to provide the same signatures as the STFT.
- it offers, as an inherent part of its structure, a measure of how well the estimation of the voltage signal parameters is. This feature can be used for the detection of changes.

The subjects that are treated using Kalman filtering are:

- voltage magnitude estimation and its limitations in the presence of harmonics and short duration events.
- segmentation of voltage disturbance recordings.
- the problem of voltage dip detection.

These issues are discussed regarding the characteristics of the power system events presented in the previous chapter. A segmentation algorithm is proposed for analysis of the voltage disturbance signals and its properties are presented. Finally, the

voltage dip detection problem is presented with respect to different types of events and the parameters of the model used for voltage magnitude estimation.

3.2 Kalman filtering

Kalman filtering is a method of state-space modelling and parameter estimation [53]. Kalman filtering has been used for a number of applications in power systems: for the continuous real-time tracking of harmonics [54, 55], the estimation of voltage and current parameters for protection systems [56, 57] or the estimation of the parameters of transients [58].

Kalman filtering provides the means for estimating the parameters of time-varying signals. In the case of voltage signals a natural choice for the model is the one that consists of the fundamental frequency component and a certain number of harmonics N:

$$z(t) = \sum_{n=1}^{N} A_n(t) \cos(n\omega_o t + \theta_n(t)) \tag{3.1}$$

where $\omega_o = 2\pi f_o$ (f_o is the system frequency or fundamental frequency: 50 or 60 Hz). The unknown parameters of the model in (3.1) are the magnitude A_n and phase θ_n for each harmonic component.

Consider the signal:

$$z_1(t_k) = A_1 \cos(\omega_o t_k + \theta_1) \tag{3.2}$$

If we define $A_{1,r}(t_k)$ and $A_{1,i}(t_k)$ as:

$$A_{1,r}(t_k) = A_1 \cos(\omega_o t_k + \theta_1) \tag{3.3}$$

and

$$A_{1,i}(t_k) = A_1 \sin(\omega_o t_k + \theta_1) \tag{3.4}$$

then at time $t_{k+1} = \Delta t + t_k$ [59]:

$$\begin{aligned} A_{1,r}(t_{k+1}) &= A_1 \cos(\omega_o t_k + \omega_o \Delta t + \theta_1) \\ &= A_{1,r}(t_k) \cos(\omega_o \Delta t) - A_{1,i}(t_k) \sin(\omega_o \Delta t) \end{aligned}$$

and

$$\begin{aligned} A_{1,i}(t_{k+1}) &= A_1 \sin(\omega_o t_k + \omega_o \Delta t + \theta_1) \\ &= A_{1,r}(t_k) \sin(\omega_o \Delta t) + A_{1,i}(t_k) \cos(\omega_o \Delta t) \end{aligned}$$

Considering the variables $A_{n,r}(t_k)$ and $A_{n,i}(t_k)$ for each n ($n = 1, \ldots, N$), the discrete system to be estimated is described at the time instant t_k by the state and measurement equations. The state equation is:

$$x(t_{k+1}) = \Phi_k x(t_k) + w(t_k) \tag{3.5}$$

where $t_k = k\Delta t$ and Δt is the sampling period. For $z(t_k)$ the sampled measurement of $z(t)$ at time instant t_k, the measurement equation is:

$$z(t_k) = H_k x(t_k) + v(t_k) \tag{3.6}$$

In (3.5), $x(t_k)$ is the state variable vector of size $2N$:

$$x(t_k) = \begin{bmatrix} A_{1,r}(t_k) & A_{1,i}(t_k) & \dots & A_{N,r}(t_k) & A_{N,i}(t_k) \end{bmatrix}^T \tag{3.7}$$

and $w(t_k)$ is the modelling noise, assumed to be zero mean white with a covariance matrix:

$$Q_k = E\Big[w(t_k)w(t_k)^T\Big] = \sigma_q^2 \mathrm{I} \tag{3.8}$$

The transition matrix, Φ_k in (3.5) is a diagonal matrix of size $2N$, defined as:

$$\Phi_k = diag[M_1 \quad \dots \quad M_N] \tag{3.9}$$

with

$$M_n = \begin{pmatrix} \cos(n\omega_o\Delta t) & -\sin(n\omega_o\Delta t) \\ \sin(n\omega_o\Delta t) & \cos(n\omega_o\Delta t) \end{pmatrix} \tag{3.10}$$

where

$$\Delta t = \frac{1}{f_s} \tag{3.11}$$

and f_s is the sampling frequency.

The matrix H_k that connects the measurement $z(t_k)$ with the state vector $x(t_k)$ is:

$$H_k = \begin{bmatrix} 1 & 0 & \dots & 1 & 0 \end{bmatrix}^T \tag{3.12}$$

and $v(t_k)$ is the measurement noise assumed to be a zero mean white sequence with known covariance σ_v^2 and uncorrelated with $w(t_k)$.

For the estimation procedure, $\widehat{x}(t_k|t_k)$ denotes the estimate of the state $x(t_k)$ at time t_k given the observation $z(i)$ for $i = 1, 2, \dots, t_k$ and $\widehat{x}(t_k|t_k - 1)$ denotes the estimate given observation up to time $t_k - 1$. The corresponding state estimation errors $\varepsilon(t_k|t_k)$ and $\varepsilon(t_k|t_k - 1)$ are:

$$\varepsilon(t_k|t_k) = x(t_k) - \widehat{x}(t_k|t_k) \tag{3.13}$$

$$\varepsilon(t_k|t_k - 1) = x(t_k) - \widehat{x}(t_k|t_k - 1) \tag{3.14}$$

and $P(t_k|t_k)$ and $P(t_k|t_k - 1)$ are the error covariance matrices:

$$P(t_k|t_k) = \Big[\varepsilon(t_k|t_k))\varepsilon(t_k|t_k))^T\Big] \tag{3.15}$$

$$P(t_k|t_k-1) = \Big[\varepsilon(t_k|t_k-1))\varepsilon(t_k|t_k-1))^T\Big] \tag{3.16}$$

The estimator procedure starts by setting estimate $\widehat{x}(0|0)$ of the state vector x and the error covariance matrix for this estimate $P(0|0)$. Then the predicted values of the state $\widehat{x}(t_k|t_k-1)$ and the error covariance matrix $P(t_k|t_k-1)$ at the next time instant are found by:

$$\widehat{x}(t_k|t_k-1) = \Phi_k\widehat{x}(t_k-1|t_k-1) \tag{3.17}$$

$$P(t_k|t_k-1) = \Phi_k P(t_k-1|t_k-1)\Phi_k^T + Q_k \tag{3.18}$$

The blending factor (or Kalman gain) K is calculated as:

$$K(t_k) = P(t_k|t_k-1)H_k\Big[H_k^T P(t_k|t_k-1)H_k + \sigma_v^2\Big]^{-1} \tag{3.19}$$

The updated estimate of $x(t_k)$, $\widehat{x}(t_k|t_k)$ is given by:

$$\widehat{x}(t_k|t_k) = \widehat{x}(t_k|t_k-1) + K(t_k)\Big[z(t_k) - H_k^T\widehat{x}(t_k|t_k-1)\Big] \tag{3.20}$$

The error covariance matrix associated with the updated estimate is also updated:

$$P(t_k|t_k) = (\mathrm{I} - K(t_k)H_k^T)P(t_k|t_k-1) \tag{3.21}$$

and the procedure starts over from (3.17). The expression $H_k^T\widehat{x}(t_k|t_k-1)$ is the estimated value of $z(t_k)$, $\widehat{z}(t_k)$. The amplitude of the fundamental frequency component is given by:

$$A_1(t_k) = \sqrt{A_{1,r}(t_k)^2 + A_{1,i}(t_k)^2} \tag{3.22}$$

The modelling noise (w) and measurement noise (v) are user-defined parameters. The tracking ability of the Kalman filter is dependent on the modelling noise σ_q^2. A small σ_q^2 will reduce the reaction speed of the filter to sudden changes however with more accurate estimates [55, 60]. The frequency response of the Kalman filter and its ability to accommodate harmonic elements depends on the selected noise values as shown in [55, 61, 62].

For the following examples, a large σ_q^2 is selected ($\sigma_q^2 = 0.4$) for faster response to changes. The measurement noise is set to $\sigma_v^2 = 10^{-5}$.

The estimated magnitude of voltage using the STFT is similar to the estimated voltage magnitude using a Kalman filter with the model of (3.1) where the order N is set equal to the number of frequency bands used in STFT. The STFT can be seen as a signal modelling method where the underlying model is a sum of sinusoids like the model described in (3.1). The relationship between the Kalman filter and the STFT is discussed in [62].

Figure 3.1 shows the estimated magnitude of a voltage dip measurement using the two methods where the STFT parameters are set as in Chapter 2, and the model

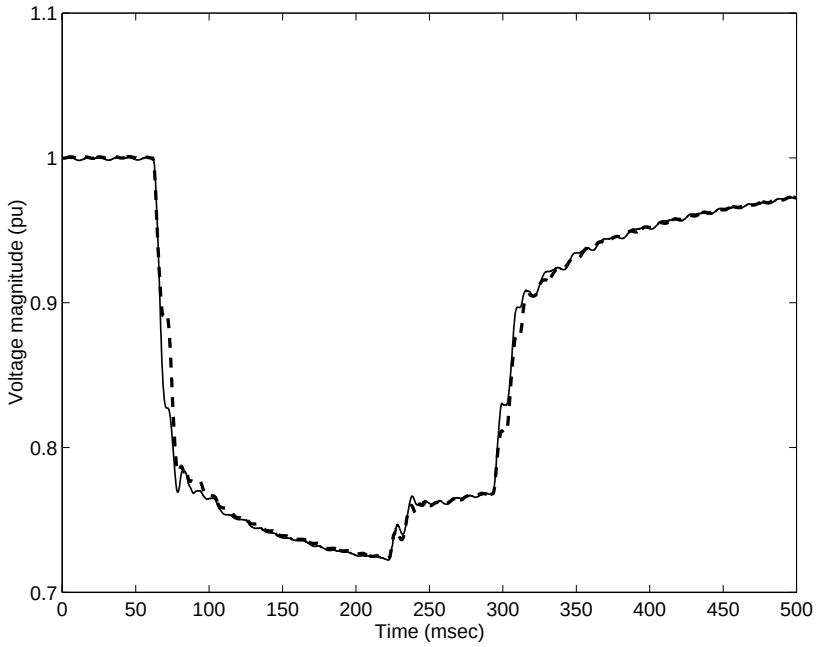

Figure 3.1: Magnitude estimation for a voltage dip measurement using a Kalman filter of order 20 (solid line) and STFT (dashed line)

order N of the Kalman filter is set to be equal to 20. The sampling frequency is 4800 Hz so the number of positive frequency bands for the STFT is 48. Thus the frequencies from 1000 Hz to 2400 Hz are not covered by the Kalman filter of order 20. Nevertheless, the differences between the two estimates are minor. This is due to the fact that the spectral content of this voltage signal in the above mentioned region is low. Typically, higher frequency components appear at the beginning or the end of an event (fault clearing, fault initiation, capacitor switching etc). We will later see that the fact that the Kalman filter of order-20 does not cover these frequencies is beneficial from a detection point of view (Section 3.4.7).

3.3 Kalman filter for power quality analysis

3.3.1 Kalman filter model order

For power quality analysis, it is important to estimate the parameters of the signals (voltages and currents) as they change in time. Furthermore, the characteristics of these signals must be taken into account in order to adjust the parameters of the estimation method (design parameters). For the voltage signals that correspond to the events in Chapter 2, the estimation of the magnitude of the fundamental frequency component is of great importance. Two aspects must be taken into account:

- Estimation of the magnitude of the fundamental frequency component must be done in the presence of harmonic distortion. Components whose frequencies

are different than the fundamental exist in the voltage signals. They are due to non-linear loads or other phenomena (for example: transformer saturation).

- Changes in the magnitude might be close in time. The estimation method must have appropriate tracking ability in order to resolve two or more successive changes of magnitude.

It is explained above that the modelling noise (w) and the measurement noise (v) must be set by the user. Additionally, the order of the model in (3.1) can be selected by the user. Two options are available. The first one is to use a model that only describes the fundamental frequency component. The second option is to use a higher order model (by adding harmonic components to the fundamental frequency component). The advantages and the drawbacks of each choice are shown using three examples.

Example 1: step change

Figure 3.2 shows a synthetic voltage waveform with a step change in magnitude and the estimated magnitude using a Kalman filter of order $N = 1$ and $N = 20$ respectively. The order-one filter is faster in tracking the change than the order-20 filter. The reduction in tracking speed is due to the fact that the energy of the sudden change in the amplitude is spread over all frequencies in the high order model case. For the order-20 Kalman filter it takes approximately one cycle before the estimated magnitude converges to the correct value. Approximately half of this time is required for the order-1 Kalman filter.

Example 2: short duration dip

The importance of the convergence speed becomes more obvious in the example of Figure 3.3. The synthetic voltage waveform contains a short duration (0.60 cycle) dip. The magnitude estimated by the order-1 Kalman filter is closer to the actual magnitude during the event. The order-20 filter inaccurately estimates the magnitude: its minimum value is higher than the actual magnitude minimum and the duration of the dip appears longer that it actually is. Both effects are due to the slower response of this filter to changes.

Example 3: step change and harmonic distortion

Figure 3.4 shows the synthetic voltage waveform of a step change in magnitude and the corresponding estimated magnitudes when a 3^{rd} harmonic of 0.05 pu magnitude is superimposed to the fundamental component. The order-1 Kalman filter estimation is effected by the presence of the harmonic element unlike the order-20 filter that gives the correct magnitude. Although the performance of the order-1 filter is better in terms of time resolution it cannot reject harmonic components different than the fundamental. Unless these components are modelled the estimated magnitude of the voltage is distorted.

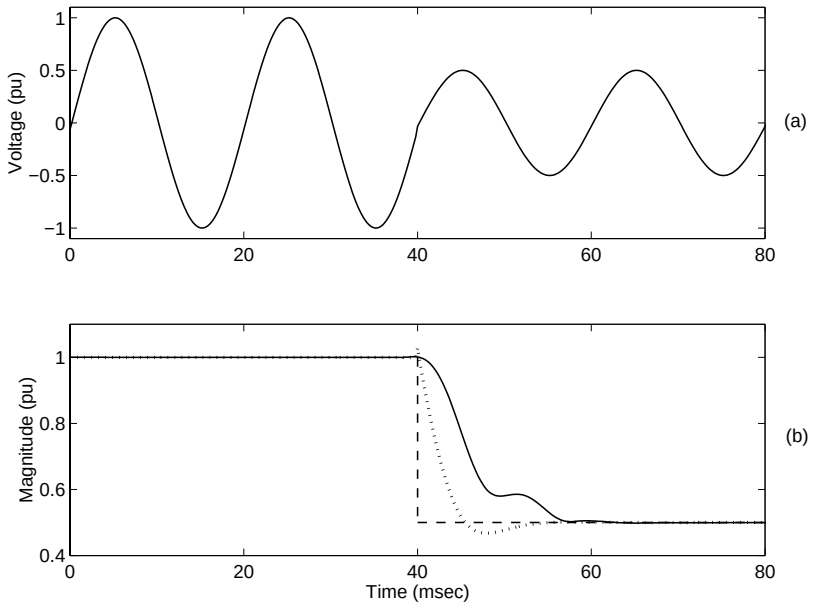

Figure 3.2: (a) Voltage waveform of a step change in magnitude (synthetic signal)(b) Estimated magnitude using Kalman filter of order 20 (solid line) and order 1 (dotted line). Real magnitude: dashed line

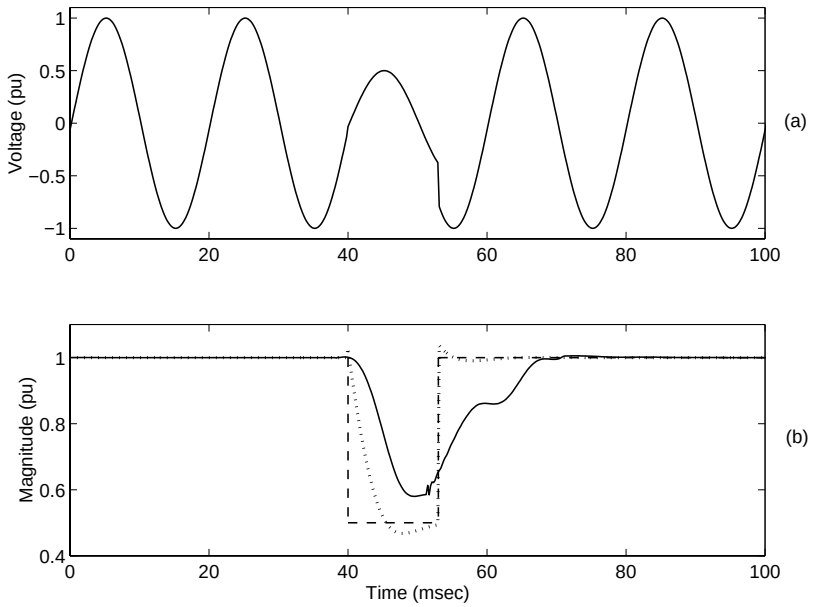

Figure 3.3: (a) Voltage waveform of a short duration dip (b) Estimated magnitude using Kalman filter of order 20 (solid line) and order 1 (dotted line). Real magnitude: dashed line

The order-1 filter can be tuned (with the values of the noise) to be less effected by non-fundamental frequency elements. However, by changing the frequency response of the filter to be less sensitive to these components, its response become slower [61]. This can be also shown if, instead of tuning the filter parameters, a low-pass filter is applied to the estimated magnitude in order to remove the distortion caused by the presence of harmonics.

The selection of the low-pass filter and its cut-off frequency are important. The filter's impulse response must short to achieve minimum delay. Its cut-off frequency must be sufficiently high (to ensure the tracking speed) but not too high (to be able to attenuate high frequency transients). A problem imposed by the requirement of short length is that the low-pass filter has a wide transition bandwidth within which, frequency components cannot be adequately attenuated.

Figure 3.4 shows the result of such an operation. The estimated magnitude obtained by the order-1 Kalman filter is filtered with a low-pass Butterworth filter of order 1 with a cut-off frequency of 50 Hz. The z-transform of this filter is:

$$H(z) = \frac{0.031699 + 0.031699z^{-1}}{1 - 0.9366z^{-1}} \tag{3.23}$$

The filtered magnitude is less distorted but its response to the change is slower and closer to the response of the Kalman filter of order 20. However, the improvement that is achieved by using the order-1 Kalman and the low-pass filter can be beneficial for analysing short duration events as it is explained in later sections.

In order to entirely remove the influence of harmonics on the estimated magnitude a higher order filter is required. By increasing the order of the filter, higher frequencies are better attenuated as shown in Figure 3.5. However, a higher order filter introduce a longer response times. Figure 3.6 shows the effect of the filter order on the estimation speed. In Figure 3.6a the increase in the filter order introduces a clearly observed delay. Similarly, the increase in the filter cut-off frequency leads to a faster response. However, this gain in time is not important (Figure 3.6b).

3.3.2 Types of changes in voltage magnitude

Regarding the speed of change of the events presented in Chapter 2, there are three types of voltage magnitude changes:

1. Fast changes: voltage magnitude increases or decreases to a new value within a short period of time (less than half-cycle).

2. Slow changes: voltage magnitude increases or decreases gradually for a long period of time (from one cycle to several cycles).

3. Fast repeating changes: voltage magnitude decreases and then increases (or vice-versa) within a short period of time (less than one cycle).

Fast changes in voltage magnitude are mainly due to:

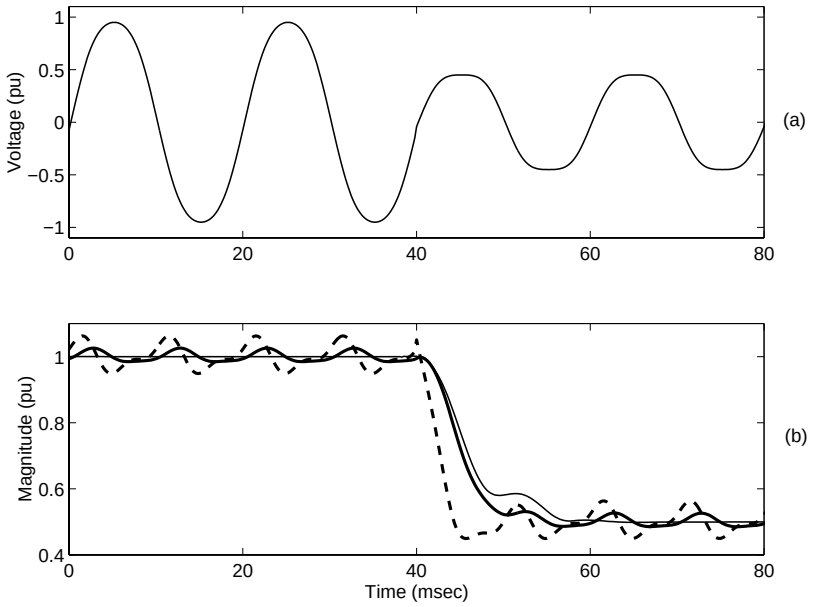

Figure 3.4: (a) Voltage waveform of a step change in the presence of harmonic distortion (synthetic signal) (b) Estimated magnitude using Kalman filter of order 20 (solid line), order 1 (dashed line) and order 1 with a low-pass filter (thicker solid line)

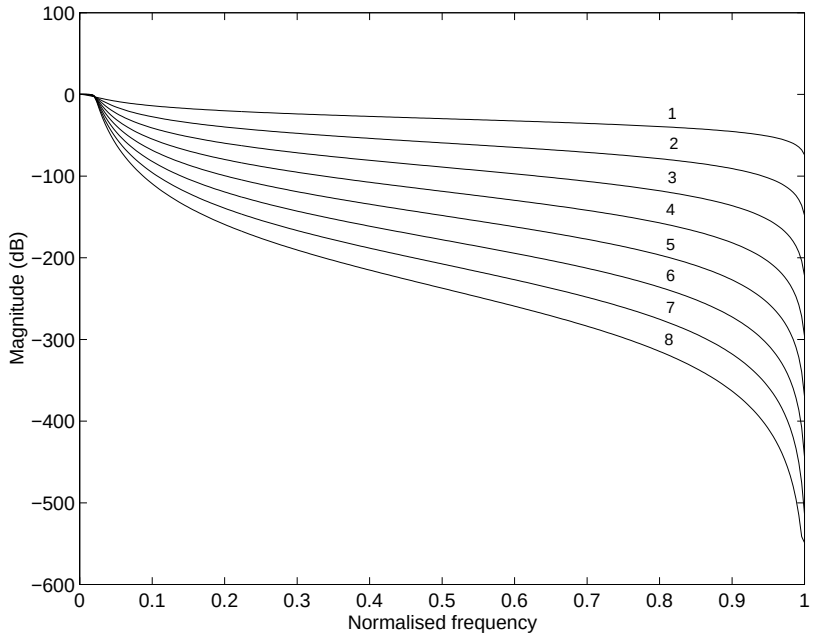

Figure 3.5: Magnitude of low-pass Butterworth filter for different order

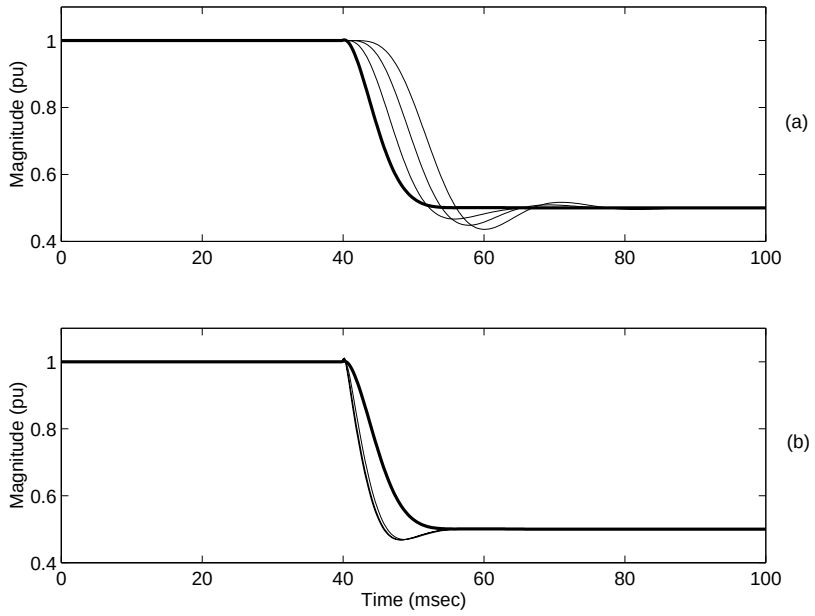

Figure 3.6: Voltage magnitude of a step change in magnitude using a Kalman filter of order 1 and Butterworth filters (a) of different order (1, 2,3 and 4) and cut-off frequency of 50 Hz and (b) of different cut-off frequency (50, 250, 450 and 650 Hz) and order 1 (thicker line: Butterworth filter of order 1 and cut-off frequency of 50 Hz)

- Fault initiation: on fault application the voltage magnitude of the faulted phases decreases suddenly and obtains a new value. By observing measurements it was found that this transition is usually completed in less than half cycle, however, evolving faults present longer transitions.
- Fault clearing: protection system operation in the occasion of a fault will in general cause a fast change in the voltage magnitude towards its normal value. In the case of circuit breaker operation, the transition is influenced by the fact that phases are cleared at different time instances (at current zero). The effect of the circuit breaker opening in one phase induces transients to the other phases so the fault clearing transition appears longer.
- Load switching: in general, the connection (or the disconnection) of a load causes a fast change in the voltage magnitude. A typical example is the connection of motor load which causes a sudden drop in voltage magnitude.
- Capacitor switching: the connection (or the disconnection) of a capacitor bank causes a fast increase (or decrease) in voltage magnitude.

Slow changes in magnitude are mainly due to:

- Motor load influence: as described in Chapter 2, the presence of motor load close to the fault location effects the voltage magnitude during the fault (slow decay) as well as after fault clearing (slow increase). In both cases, the effect is present for several cycles.
- Recovery of voltage after motor starting: the increase in voltage following the initial drop upon the connection of motor load is gradual and might last for long periods of time (up to 1 sec), as explained in Chapter 2.
- Recovery after a self-extinguishing fault as explained in Chapter 2: in the example shown in Chapter 2, it takes approximately one cycle for the voltage to return to its normal value upon fault clearing.

Fast successive changes in voltage magnitude are mainly due to:

- Transformer saturation: as shown in Chapter 2, transformer saturation leads to variations of voltage magnitude between two consecutive half-cycles. As the transformer magnetising current is only present during part of the cycle, the voltage disturbance becomes a succession of sub-cycle voltage dips. Transformer saturation can be due to the energising of the transformer, due to the voltage change at fault initiation and fault clearing, or due to other reasons.
- Arcing faults: these are faults that exhibit heavy current arcs with non-linear voltage-current characteristics. The non-linear arc voltage-current characteristics manifest themselves by producing high frequency components which in turn distort the arc voltage into a near square wave [63]. After fault clearing the arc disappears so it is safe to reclose. In distribution systems, downed

conductors cause low current faults that cannot be detected therefore are dangerous [64]. The developed arc of the fault results also to harmonic distortion.

Table 3.1: Types of voltage magnitude change

Fast	**Slow**	**Fast repeating**
Fault initiation	Motor load influence	Transformer saturation
Fault clearing	a. During a fault	a. Energising
Load switching	b. After a fault	b. During a fault
Capacitor switching	After motor connection	c. After a fault
	After self-extinguishing fault	Arcing fault

The different types of changes are summarised in Table 3.1. Considering fast changes, the ones due to fault related events can be large in magnitude. On the other hand, changes due to load switching are in general of small magnitude. The measurement of motor load starting (shown in Chapter 2), shows a drop in magnitude of about 0.10 pu. Capacitor switching causes changes that do not exceed 0.05 pu. Transformer saturation statistics (presented in Chapter 2) show that the magnitude of change can be significant.

As shown in the previous section, the changes in the voltage magnitude are not immediately captured by the magnitude estimator. The estimated magnitude reaches the new value of voltage with a delay. This delay depends on the type of the method used and its settings. For a fast step change, an order-20 Kalman filter requires approximately one cycle to reach the new value and the order-1 Kalman filter about half of this time. Three examples are given below considering the different types of changes and the properties of the estimators.

Voltage dip

Figure 3.7 shows the estimated magnitude of voltage during a fault. This is a measurement from an 11 kV network. The order-1 and order-20 Kalman filters are used. Two fast changes of large magnitude can both be seen in the estimated magnitudes: one due to fault initiation (around 100 msec) and one due to fault clearing (at 300 msec). A fast change of low magnitude can be seen between 200 and 300 msec. This is probably due to a change in the system. This change is better seen when the order-20 Kalman filter is used because the estimated magnitude is not distorted as that in the order-1 Kalman filter. The influence of the motor load is obvious both in the during-the-fault stage of voltage and the post-fault-stage. The voltage magnitude changes slowly in both cases.

Harmonic distortion during a fault

Figure 3.8 shows the estimated magnitude of voltage during a fault that exhibits high distortion probably due to arcing. This is a measurement in an 11 kV network.

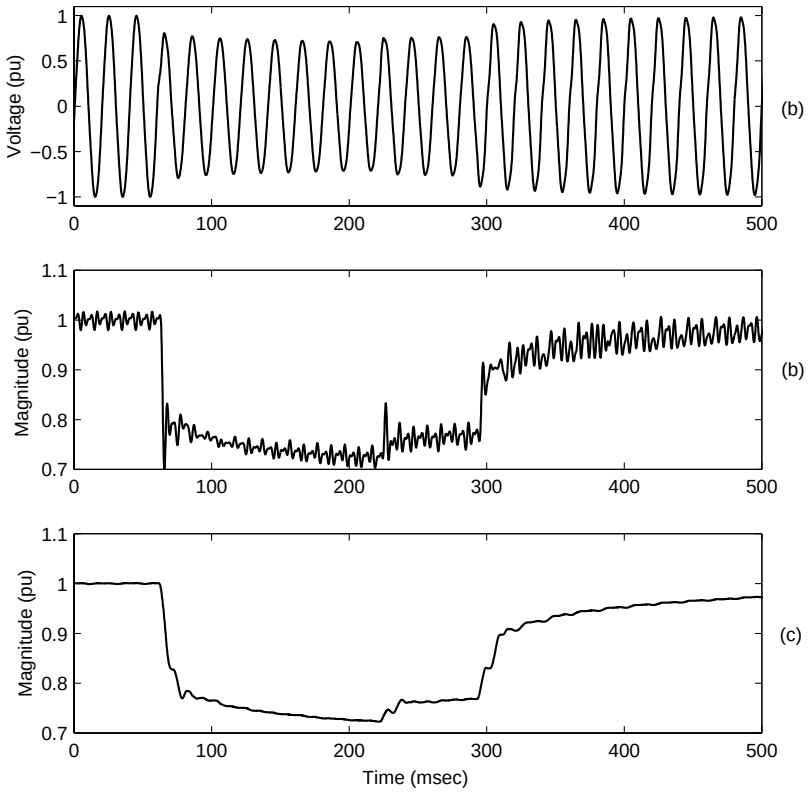

Figure 3.7: (a) Voltage waveform during a fault (b) Estimated magnitude using Kalman filter of order 1 (c) Kalman filter of order 20

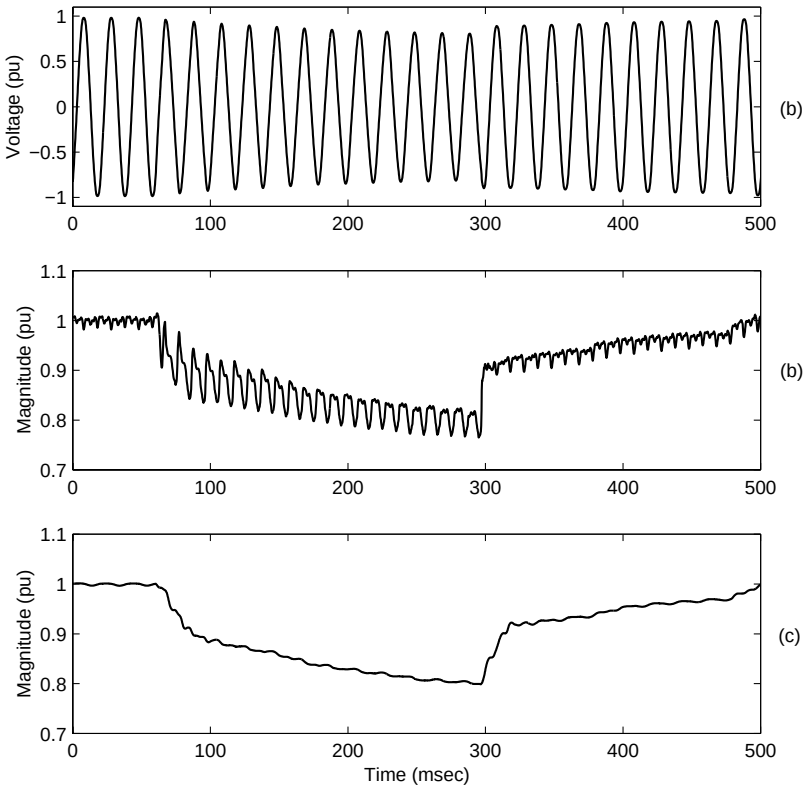

Figure 3.8: Harmonic distortion during a fault (a) Voltage waveform (b) Estimated magnitude using Kalman filter of order 1 (c) Kalman filter of order 20

According to the utility that provided the measurements the event originated in the 275 kV network. Several monitors in the 11 kV network captured this event. The pattern of the voltage distortion can be seen in the magnitude estimated by the order-1 Kalman filter. The magnitude estimated by the order-20 Kalman filter is smoother because the distortion of voltage is accommodated by the higher frequency components of the state equation. The slow change of the dip magnitude can be also seen. So, during the fault two types of changes take place: fast successive changes probably due to arcing and a slow change probably due to motor influence.

Transformer saturation

Figure 3.9 shows the estimated magnitude of voltage during transformer saturation. This is a measurement from an 11 kV network. The fast successive changes caused by saturation can be seen in the estimated magnitude by the order-1 Kalman filter. The magnitude of these successive voltage dips is decreasing slowly. In the order-20 Kalman filter estimation, the magnitude recovers slowly back to normal and a much smoother voltage magnitude signature is obtained.

Summarising, an order-1 Kalman filter or a higher order Kalman filter can be used for the extraction of voltage magnitude. Comparing the two types of estimators

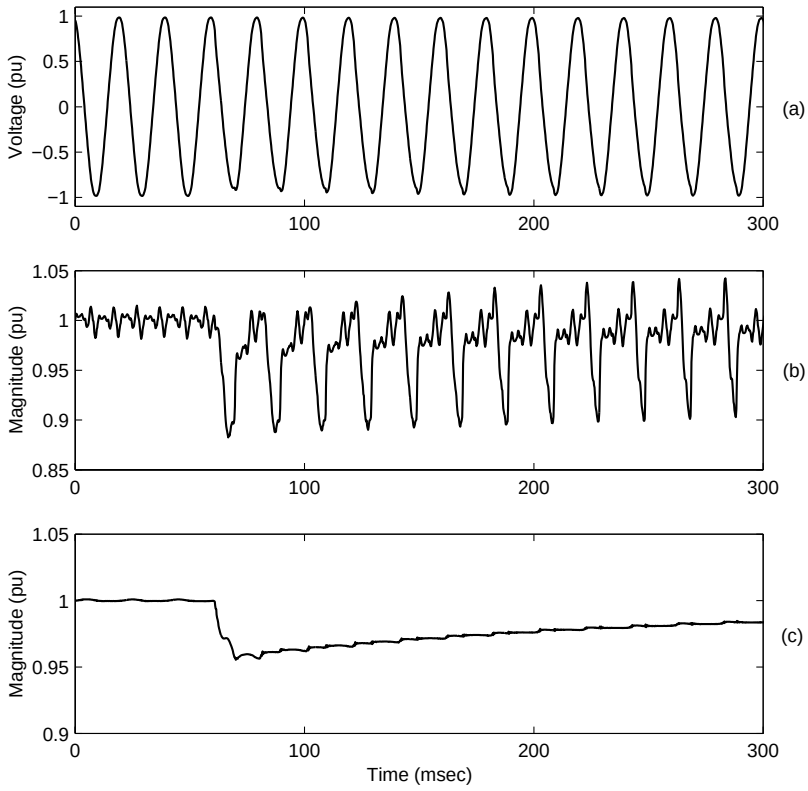

Figure 3.9: (a) Voltage waveform during transform saturation (b) Estimated magnitude using Kalman filter of order 1 (c) Kalman filter of order 20

the former one has faster convergence speed to sudden changes but the estimated magnitude is very distorted either due to harmonic distortion caused by loads or fast successive changes caused by the nature of the event. Due to distortion, it becomes difficult to extract simple information relative to the magnitude (for example the trend).

A high order estimator has a slower response to changes, however the characteristics of the magnitude are easily extracted. When using an order-1 estimator it becomes difficult to observe fast changes in the magnitude because of the distortion (for example the fault clearing instant in the presence of harmonic distortion). The advantage of fast tracking speed of an order-one estimator becomes important for short duration events. Therefore, a higher order estimator is appropriate for events where changes are well apart in time. The order-1 estimator can be used for short duration events as it shown in Section 3.4.5.

3.4 Segmentation of voltage disturbance recordings

3.4.1 The segmentation problem

Segmentation is the process of splitting a recorded voltage waveform in a number of segments along the time direction. Segmentation as the means for further analysis or classification of non-stationary signals has been employed in many other fields of engineering such as speech signal processing [65] and biomedical signal processing [66]. Segmentation can be considered as a detection problem where the limits of each different stage in the signal must accurately be found [67].

In the case of voltage disturbances an important characteristic is the way that magnitude changes. Distinctive signatures are produced by considering the behavior of voltage magnitude for different types of power system events. As shown in the previous section, there are three types of changes in voltage magnitude (fast, slow and fast repeating) and in general, two options in estimating the magnitude: fast or slow estimator. For classification purposes it is important to detect when the changes of magnitude occur and process the different parts of the signal as they are defined by these changes. Fast changes are more important to be detected because they correspond to phenomena such as fault initiation, fault clearing or changes in the system configuration, and uniquely characterise the voltage recordings. So, the segmentation of voltage disturbance signals described next is based on the detection of fast changes in voltage magnitude.

According to the above, a typical recording of a voltage dip due to a fault may be split in three segments: before the fault, during the fault and after the fault. The divisions between the segments correspond to fault initiation and fault clearing. For a dip due to motor starting, the recording may be split in only two segments: before and after the starting instant. The starting current (and thus the voltage drop) decays gradually and smoothly towards the new steady state. For a motor with a star-delta switching the recording may be split in three segments, etc.

In general, for segmentation purposes, a detector is constructed to monitor one or more characteristics of the signal in question and provides an alarm in case of changes. Several options can be followed for the construction of the detector. Some of these options are:

- Detection based on the voltage magnitude values or their changes.
- Detection based on the high frequency parts of the voltage signals.
- Model-based detection: monitoring of how well the model fits the data by setting an appropriate measure and detection of changes based on this measure.

The first option seems to be the most natural. However, unlike classical detection problems where every event is well identified in its time and frequency contents, voltage disturbance characteristics vary significantly for different system and operational conditions. Therefore, it is very difficult to incorporate a priori knowledge on the parameters of the hypotheses that correspond to the various states to be detected. The detection of sudden changes also suffers from the fact that it is difficult to set a threshold to detect them. The magnitude of the change is not a priori known and the voltage magnitude might be changing slowly. A detector that would trace sudden changes in the voltage magnitude should be immune to slow variations. Therefore it would not be possible to be sensitive enough to trace sudden changes of small magnitude.

The use of the high frequency part of the voltage signals for the detection of the beginning and the end of a dip has been proposed in the literature [68, 69]. Filter banks are used to extract information from different frequency levels of the signal because the beginning and the end of a dip is expected to give high values in the higher frequency levels. The use of such a method is restricted by the fact that high frequency elements might be present (for example due to arcing faults or transformer saturation) in the signal additionally to the ones produced by the fault initiation and clearing.

3.4.2 A segmentation algorithm for voltage disturbances

The proposed algorithm utilises a model-based detection scheme that monitors how well the model fits the data. A measure of how well the model fits the data is the residue $\varepsilon(t_k)$, calculated as

$$\varepsilon(t_k) = z(t_k) - \widehat{z}(t_k) \tag{3.24}$$

where $\widehat{z}(t_k)$ is the estimated value of the signal $z(t_k)$. The calculation of the residue is an inherent part of the Kalman filter equation as shown in Section 3.2. Figure 3.10 shows the residues of the transformer saturation measurement of Figure 3.9 for the two Kalman filters (order-1 and order-20). The residues of the order-20 model are of lower magnitude and present only high frequency characteristics because lower frequencies are accommodated by the model.

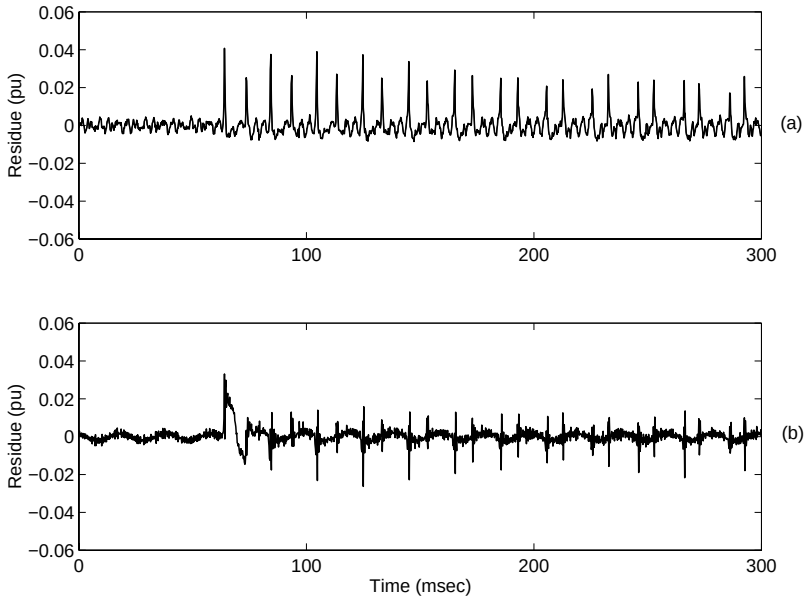

Figure 3.10: The residues in the estimation of the parameters of a transformer saturation dip using (a) order-1 Kalman filter and (b) order-20 Kalman filter

The method proposed here for segmentation of voltage disturbance recordings is based on monitoring the residuals of the model obtained by the Kalman filter. The residues of the model, being a measure of how well the recorded data fit the underlying model (in our case: (3.1)), can be used to detect changes in the signal. An increase in the residues is due to a transition of the voltage from one state to another and this can be used for segmentation purposes.

For monitoring the residues, the detection index di is designed:

$$di(t_k) = \left[\frac{1}{l}\sum_{i=t_k}^{t_k+l}\varepsilon(i)\right]^2 = \left[\frac{1}{l}\sum_{i=t_k}^{t_k+l}(z(i)-\widehat{z}(i))\right]^2 \qquad t_k = l,\ldots,L-l \qquad (3.25)$$

where

$\widehat{z}(i)$ the estimated value of the signal $z(i)$

l the length of the sliding window in which the residue ε is calculated

L the length of the signal

The detection index di, gives the squared mean of the residues thus it is a measure of the changes in the voltage waveform over the window with length l. The detection of sudden changes in the voltage waveform is done by comparing di, with a threshold δ for each time instant. Two different hypotheses are tested:

- H_0(no change is present): $di < \delta$
- H_1(a change is present): $di \geq \delta$

The segmentation scheme is summarised in Figure 3.11.

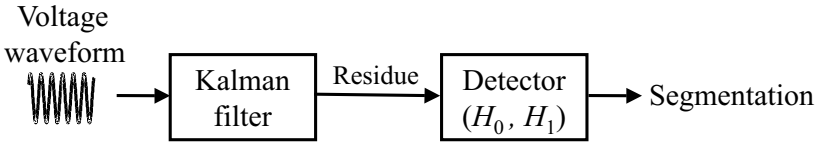

Figure 3.11: The structure of the segmentation scheme

Considering the nature of the phenomena that could appear during the events under consideration, the order of the model in (3.1) must be set high enough so that:

- transformer saturation or arcing would not influence the segmentation process. The example of Figure 3.10 shows that a high order filter produces lower residues in the case of transformer saturation.
- the estimated voltage magnitude can be easily characterised as explained in the previous section.

Two types of segments are defined according to the detection index:

- *Event segments* (E_m): the detection index is low.
- *Transition segments* (T_m): the detection index is high.

Transition segments are the ones that correspond to fast changes due to fault initiation, fault clearing, motor starting etc. Event segments correspond to parts of the voltage signals where the characteristics of voltage are constant or slowly varying. Normally, a recording starts and ends with an event segment. Consequently, the original signal can be represented as a sequence of event and transition segments. When the detection index, that is calculated over a window of size (l), exceeds the threshold δ the start point of a transition is defined. The end point of the transition is found when the detection index is below the threshold for a certain number of samples (l_e).

3.4.3 Application of the segmentation algorithm

The settings of the algorithm are given in Table 3.2. The model order is set to 20, i.e. the state equation covers the frequency range 50 to 1000 Hz in steps of 50 Hz. From the tests it was found that this model order is adequate for accommodating the frequency components produced by transformer saturation or arcing. The sampling frequency for most of the available measurements is 4800 Hz. Therefore, the model order can be increased to cover frequencies up to 2400 Hz. However, the consequent increase in the computational burden of the algorithm is not necessary.

The modelling noise σ_q^2 is set high to ensure fast responses when a change in the signal occurs.

Table 3.2: Settings for the segmentation algorithm

Kalman filter settings	
Model order (N)	20
Modelling noise (σ_q^2)	0.4
Measurement noise (σ_v^2)	10^{-5}
Detector settings	
window size (l)	half-cycle
window size (l_e)	half-cycle
Threshold (δ)	$0.2 \cdot 10^{-4}$

The size of the window l is set to one half-cycle. This window is used to obtain a detection index with less fluctuations than the residuals at the point of a change. A larger window would smooth even more the detection index, but the time resolution of the scheme would be reduced. The size of the window l_e used to find the boundaries of a transition segment is also set to one half-cycle. This is to ensure that fluctuations in the detection index due to evolving events do not lead to incorrect detection of the transition segment boundaries.

Figure 3.12 shows the residuals and the corresponding detection index as obtained for a synthetic voltage signal that presents a fast magnitude drop of 0.10 pu. The above mentioned settings are used. The detection index smooths the fluctuations that appear in the residues. Note that for di, the time indices correspond to the first sample of the window with size l.

The most important class of power system events as presented in Chapter 2 is formed by voltage dips due to faults. These events are characterised by two or more fast changes that correspond to fault initiation, fault clearing operations, or changes in the type of the fault. The segmentation algorithm is tuned for this class of events. Tests show that the algorithm with these settings performs well for all the other classes of events. Figure 3.13 shows the maximum of the detection index for a 0.05 pu drop in voltage magnitude for different points on the wave of synthetic signals. The threshold δ is set as to detect a 0.05 pu drop in voltage magnitude. A lower threshold would make the detection scheme more sensitive to changes in magnitude but would also lead to incorrect detection of the transition segment boundaries when the event segments present harmonic distortion. The properties of the segmentation scheme are shown in Section 3.4.7.

To demonstrate the efficiency of the scheme two examples are given below.

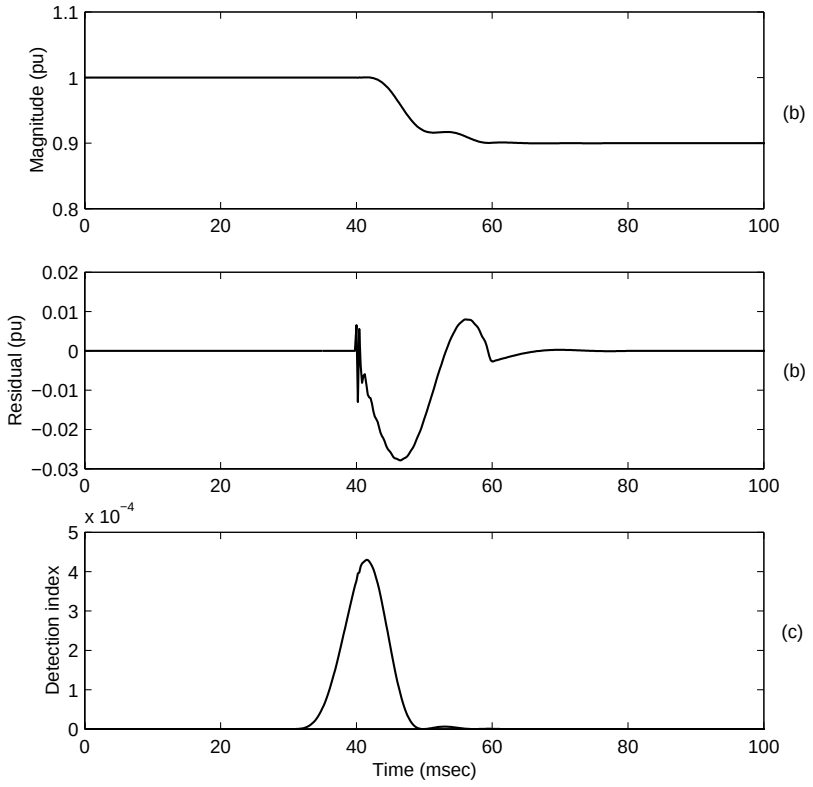

Figure 3.12: (a) Estimated magnitude for 0.10 pu voltage drop using an order-20 Kalman filter (b) The corresponding residues (c) The corresponding detection index

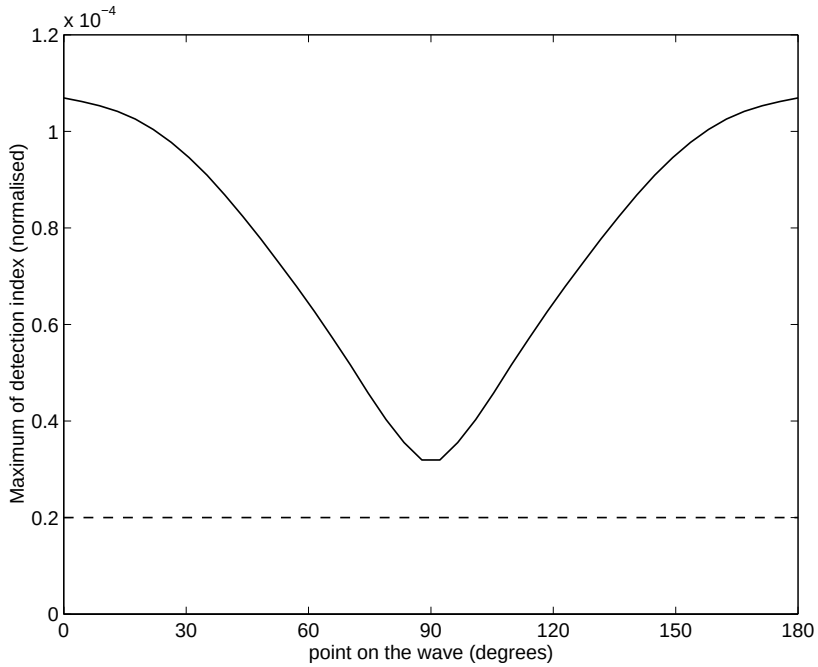

Figure 3.13: Detection index maximum for a 0.05 pu voltage drop for varying point on the wave. Dashed line: threshold δ

Evolving fault

Figure 3.14 shows the voltage waveform, the output of a high-pass filter which is applied to the original voltage waveform (Butterworth filter of order 8, cut-off frequency 150 Hz), the estimated magnitude of the fundamental frequency voltage, the detection index di, and the segmentation results. The output of the high-pass filter is given as a measure of the harmonic contents of the signal. The detection index is normalised with the threshold δ.

This is a measurement of an evolving fault in an 11 kV system. The voltage waveform presents an initial gradual small drop that becomes larger after a few cycles (Figure 3.14a). The high frequency part of the signal exhibits high energy between 40 and 140 msec but no more information can be drawn from it (Figure 3.14b). The estimated magnitude shows initially a slow change around 50 msec and a more obvious change at 150 msec (Figure 3.14c).

The detection index and the segmentation scheme are able to extract both changes in the voltage despite the fact that they are close in time and the first one is gradual. The voltage decays slowly after the initial changes due to the presence of induction motor load. It recovers back to normal when a circuit breaker operates to clear the fault (not shown in Figure 3.14).

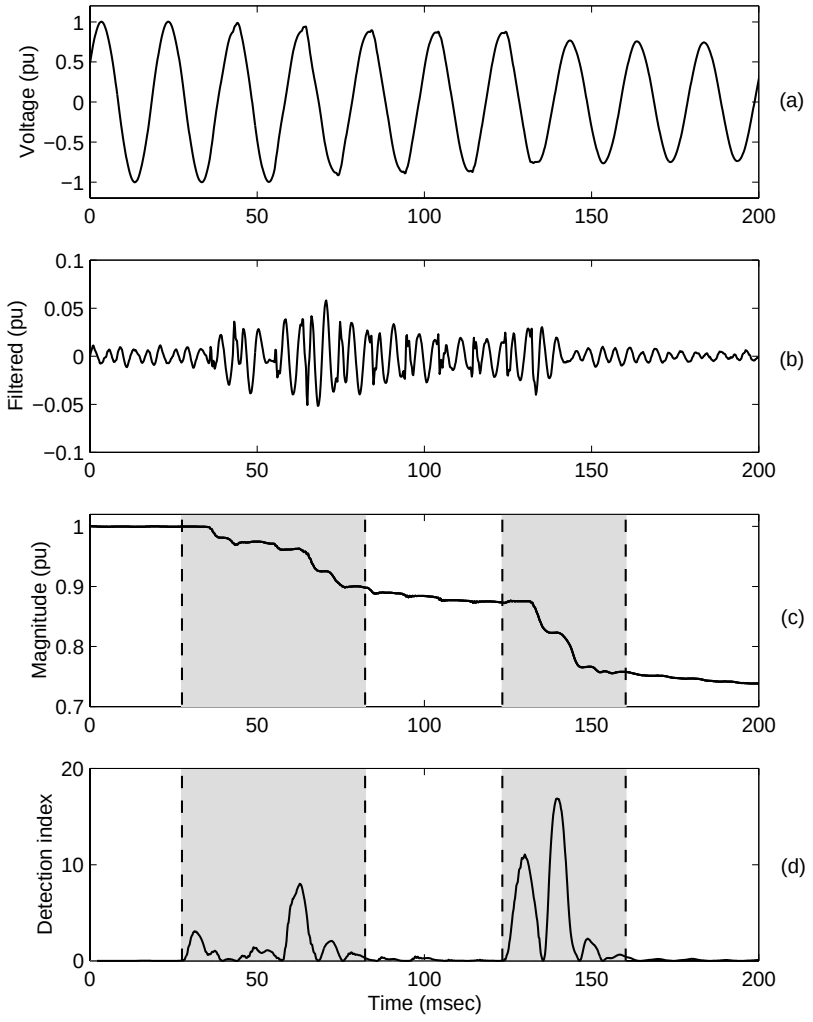

Figure 3.14: (a) Voltages waveform (b) high-pass filtered signal (c) fundamental frequency voltage magnitude and segmentation results (d) detection index (normalised) and the segmentation results (shadowed parts: transition segments)

Transformer saturation

Figure 3.15 shows the case of transformer saturation probably due to transformer energising. The same features are plotted as before. The voltage waveform presents an initial drop followed by a gradual recovery. The event is accompanied by temporary harmonic distortion. Harmonics close to the fundamental increase and then decay slowly as the voltage magnitude returns to normal. The harmonic distortion is obvious in Figure 3.15b. The detection index is able to extract the initial drop in voltage magnitude and remains low despite the presence of harmonics. The Kalman filter models adequately the harmonic distortion caused by the saturation of the transformer.

3.4.4 Segmentation considering the three phases

For classification purposes not only the phases must be segmented but also the corresponding segments between the phases must be compared. In order to achieve the best possible match between the phases, the segmentation algorithm is modified to cope with 3 phases. A change in any of the three phases points to a change in the underlying event or in the system which may also effect the other two phases. The detection scheme is applied to all three phases and the detection index is created for each one $(di^{\mathrm{a}}, di^{b}, di^{c})$. Then, a detection index di is obtained by taking the maximum of the three indices at each time instant:

$$di(t_k) = max(di^{\mathrm{a}}(t_k), di^{b}(t_k), di^{c}(t_k)) \quad t_k = 1, \ldots, L - l \tag{3.26}$$

Figure 3.16 shows the fundamental magnitude of the three phase voltages of the multistage dip that is partly shown in Figure 3.14. The detection index as obtained by (3.26) and the segmentation results are also shown. It becomes clear that the dip is caused by a short-circuit that evolves to a three-phase fault. The segmentation results as obtained by considering all the phases and by considering only one phase are almost the same for this case.

3.4.5 Segmentation of voltage recordings of short duration events

Regarding the segmentation algorithm presented above, time resolution problems might occur when two or more transitions occur close in time. The detection index di, is high for a period of time after a transition. This period of time is found to be approximately one cycle for a fast change (see Figure 3.13). If the increase in the detection index due to the first transition is not over before the second one starts then the two transitions will not be resolved. Recall that a half cycle window is used to decide whether a transition is over, i.e. the detection index must be below the threshold for at least one half-cycle. There are recordings which present fast-changing characteristics during the whole disturbance and the detection index is continuously high thus the stages of the signal cannot be identified.

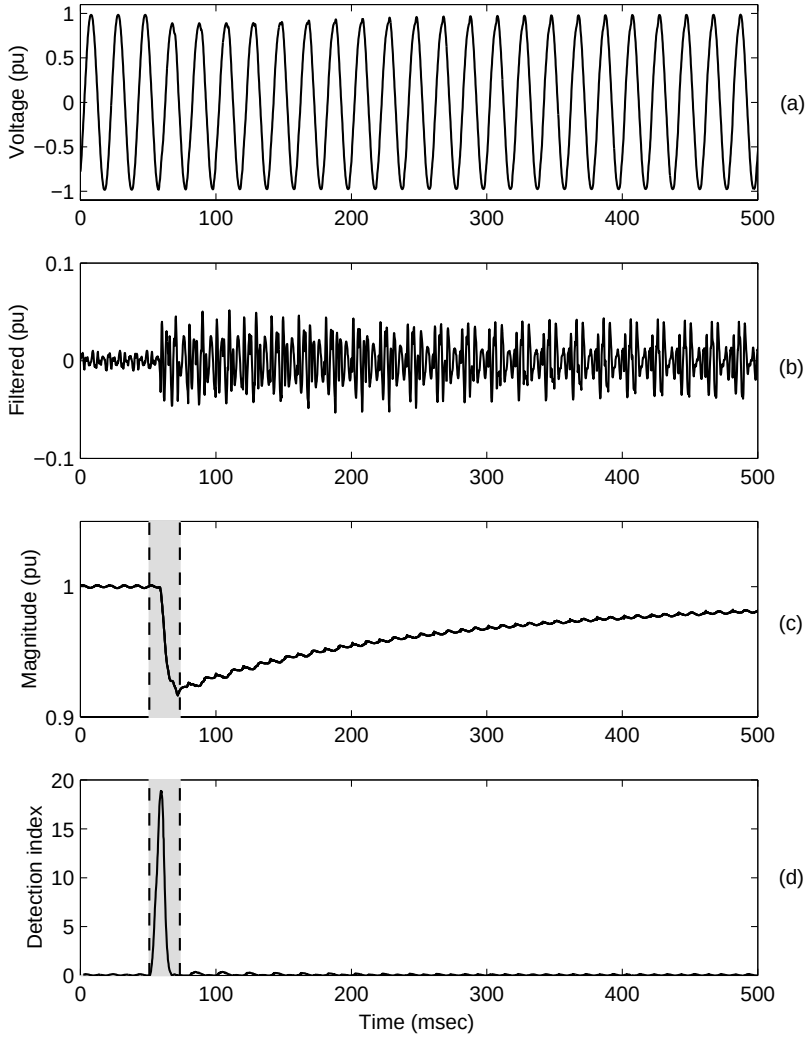

Figure 3.15: (a) Voltages waveform (b) high-pass filtered signal (c) fundamental frequency voltage magnitude and the segmentation results (d) detection index (normalised) and segmentation results (shadowed parts: transition segments)

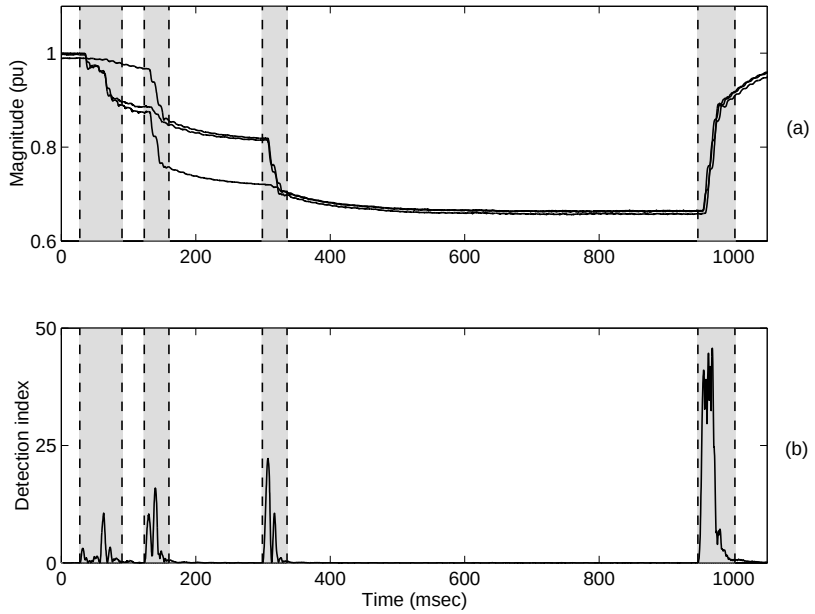

Figure 3.16: Fundamental frequency voltage magnitude (b) detection index (normalised) and segmentation results (shadowed parts: the transition segments)

Additionally, when two changes are close in time not only they cannot be resolved but also the estimated magnitude might not be correct. An example is a short duration dip where the voltage recovery starts before the estimated magnitude reaches the real dip magnitude.

Therefore, if the time interval between two fast transitions is:

1. shorter than one and a half cycles, the detection index will not be below the threshold (δ) for the required time (half cycle) and the transitions will not be resolved.

2. shorter than one cycle the estimated magnitude will not be correct.

One class of short duration events of interest is formed by fuse-cleared faults. As shown in Chapter 2, these produce voltage dips of short duration. Several measurements from distribution networks were found that present voltage dips of duration shorter than 3 cycles probably due to fuse-clearing operations (3 cycles is the minimum time for a circuit breaker to clear a fault). Other events that are of short duration are dips caused by self-extinguishing faults. In the case of self-extinguishing faults, the available measurements showed that the fault extinguishes within 1-2 msec.

3.4.6 The stage detection algorithm

For short duration events the order-1 Kalman filter is a better way for estimating the voltage magnitude. The estimated magnitude is of high variance due to the

presence of load-generated harmonics and high frequency transients, however, the variance of the magnitude can be reduced with a low-order low-pass filter as shown in Section 3.3.

The residuals of the order-1 Kalman filter cannot be used for segmentation purposes because they are of high magnitude due to the presence of harmonics. However, for short duration events, segmentation can be done by identifying the fault stage (between fault initiation and fault clearing) which is of almost constant magnitude as a number of measurements showed. A stage detection algorithm is described below. The algorithm consists of the following steps:

1. First w is set equal to w_0.

2. For the time instant t_k, the standard deviation $s(t_k)$ of the estimated magnitude of the fundamental frequency voltage (A_1) is calculated for the window of size w:

$$s(t_k) = \Big[\frac{1}{w}\sum_{k=t_k}^{t_{k+w}}(A_1(k) - m_k)^2\Big]^{\frac{1}{2}} \tag{3.27}$$

$$m_k = \frac{1}{w}\sum_{k=t_k}^{t_{k+w}}(A_1(k)) \tag{3.28}$$

3. An alarm is produced, indicating the starting point of an event segment if:

$$s(t_k) < h \tag{3.29}$$

4. Then the window size w is increased by one sample ($w = w + \Delta t$) and steps 2 and 3 are repeated until (3.29) is not true.

5. Then an alarm is produced indicating the end point of an event segment and the algorithm starts from step 1 with $t_k = t_{k+w}$.

Parts of the signal where (3.29) is not satisfied are transition segments. The whole scheme is summarised in Figure 3.17. For the test shown next, the window size w is set to be half cycle and h equals to 0.02. The size of the window w_0 is set to be half cycle because that is approximately the time it takes for the order-1 Kalman filter (with the above mentioned settings) to respond to a fast change.

Figure 3.18a shows a voltage disturbance of short duration. It is already obvious in Figure 3.18a that the recording contains a voltage dip of duration approximately one and a half cycles. The voltage reduction is captured by the order-20 Kalman filter (Figure 3.18b). However, the convergence speed of the estimated voltage magnitude is slow and the obtained middle stage of voltage is significantly shorter than the actual one. The detection index and the segmentation results as obtained from the algorithm in Section 3.4.3 are shown in Figure 3.18c. The recorded event is

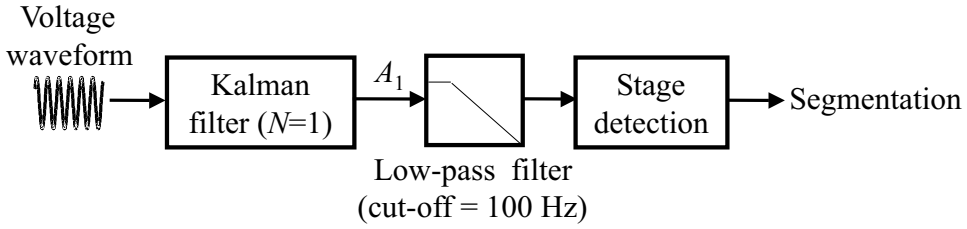

Figure 3.17: The structure of the segmentation scheme

a voltage dip due to a fault. The fault initiation and the fault clearing instants are close in time. The detection index increases at both instants however the time interval between the two events is not adequate for the scheme to decide whether the first transition is over before the second one starts. Therefore the middle stage is not revealed.

Figure 3.18d shows the estimated magnitude using a Kalman filter of order 1. The changes in voltage are faster than that in Figure 3.18b, however the variance of the estimation is higher for all stages (before, during and after the dip). Fault clearing causes an overshoot in the estimated voltage that is not observed in the actual voltage waveform.

Figure 3.18e shows the filtered voltage magnitude and the results of the segmentation algorithm described above. There are two transition segments found (shadowed parts) and between them there is an event segment corresponding to the voltage dip. The method detects the new stage in voltage and its boundaries are found.

3.4.7 Properties of the detection index

In this section, the properties of the detection index are presented. Synthetic signals (sinusoids of 50 Hz frequency) are used that contain fast changes in magnitude. Variations in the point on the wave where the change occurs and the phase angle jump are considered. A sampling frequency of 4800 Hz is used.

Figure 3.19 shows the maximum value that the detection index obtains for different magnitude changes (decrease). The maximum value of the detection index is normalised with the threshold δ. Both the dependence of the detection index on the point on the wave and the magnitude of the change can be seen. The detection index is low for points on the wave closer to the voltage peak and high for larger changes.

Figure 3.20 shows the maximum value that the detection index obtains for a 0.10 pu decrease accompanied by a positive phase angle jump. The detection index increases significantly for large phase angle jumps. The detection index also increases for negative phase angle jump (Figure 3.21). The increased detection index in the presence of phase angle jumps is beneficial to the segmentation scheme because fault-induced dips present this phenomenon, as explained in Chapter 2.

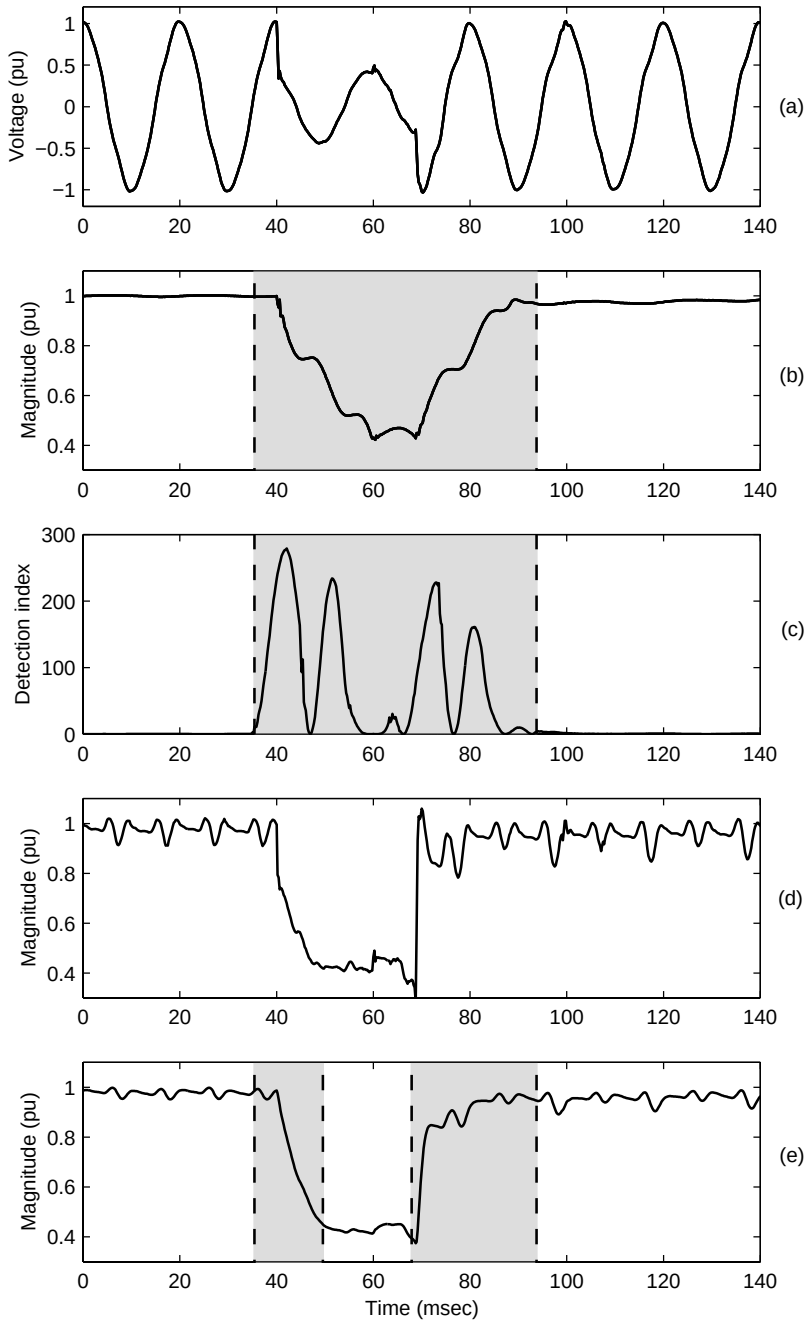

Figure 3.18: (a) Voltage waveform (b) Estimated magnitude - Kalman filter of order 20 (c) detection index (normalised) and segmentation results using the first algorithm (d) Estimated magnitude - Kalman filter of order 1 (e) Filtered magnitude and segmentation results (transition segments: shadowed parts).

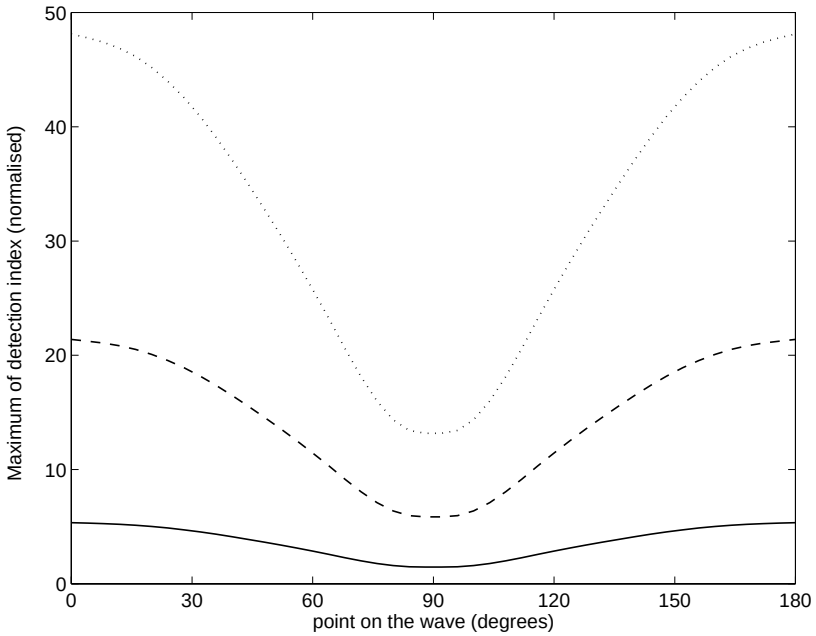

Figure 3.19: Maximum of detection index for step decrease of 0.05 pu (solid line), 0.10 pu (dashed line) and 0.15 pu (dotted line)

The influence of high frequency transients on the detection index is shown using a synthetic signal of a 0.05 pu drop added to a signal $u_{sup}(t_k)$ which is an exponentially damped sinusoid of frequency f_n given by the following formula:

$$u_{sup}(t_k) = Be^{-\alpha t_k} \cos(2\pi f_n t_k) \tag{3.30}$$

where α is the constant that defines the decaying rate of the exponential. A value is chosen so the transient decays to zero within one cycle. Two cases are considered for the frequency f_n of the superimposed transient. The first case is f_n to be within the range of frequencies modelled by the Kalman filter (0-1000 Hz) and the second case is to be higher (1000-2400 Hz for a 4800 Hz sampling frequency).

Figure 3.22 shows the maximum of the detection index for different values of B for frequencies ranging from 100 Hz to 1000 Hz for a 0.05 pu drop in magnitude. The range of frequencies corresponds to that modelled by the order-20 Kalman filter. The detection index obtains higher values for increasing B. The influence of the transients is significant for lower frequencies close to the fundamental. For higher frequencies the value of the detection index is not influenced by the frequency of the transient.

If the frequency of the transient is outside the frequency range modelled by the Kalman filter then the influence of the frequency of the transient is significant. Figure 3.23 shows the maximum of the detection index for different B values, for frequencies ranging from 1000 Hz to 2400 Hz, and for a 0.05 pu drop in magnitude. As the frequency of the transient increases the detection index increases significantly.

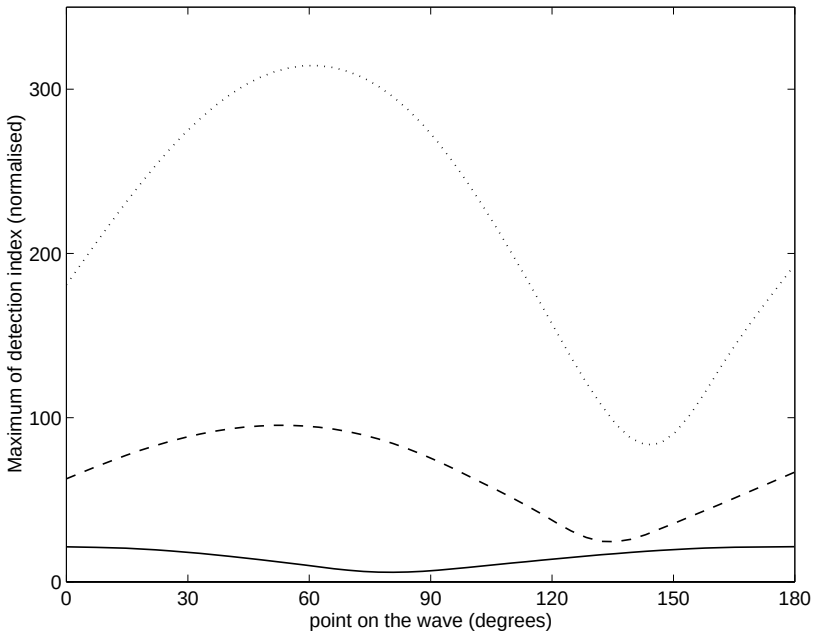

Figure 3.20: Maximum of detection index for step decrease of 0.10 pu and phase angle jump of 0° (solid line), 10° (dashed line) and 20° (dotted line)

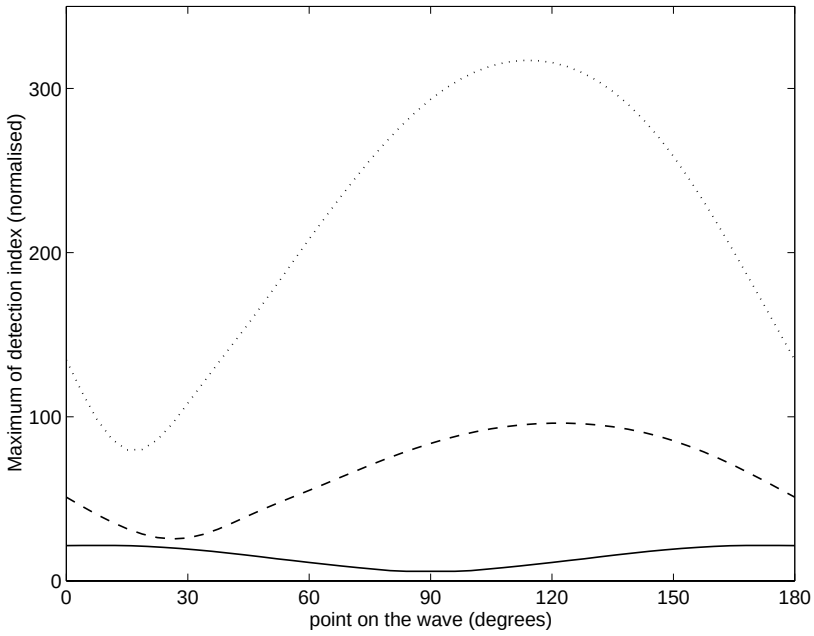

Figure 3.21: Maximum of detection index for step decrease of 0.10 pu and phase angle jump of 0° (solid line), −10° (dashed line) and −20° (dotted line)

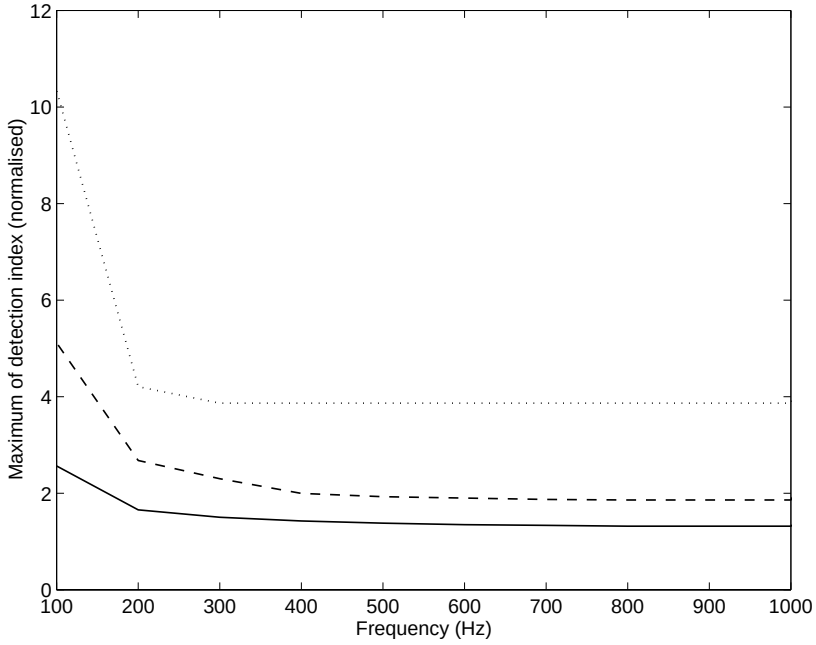

Figure 3.22: Maximum of detection index for step decrease of 0.05 pu and a superimposed exponentially decaying sinusoid of amplitude B equal to 0.20 pu (solid line), 0.40 pu (dashed line) and 0.60 pu (dotted line) for frequencies up to 1000 Hz

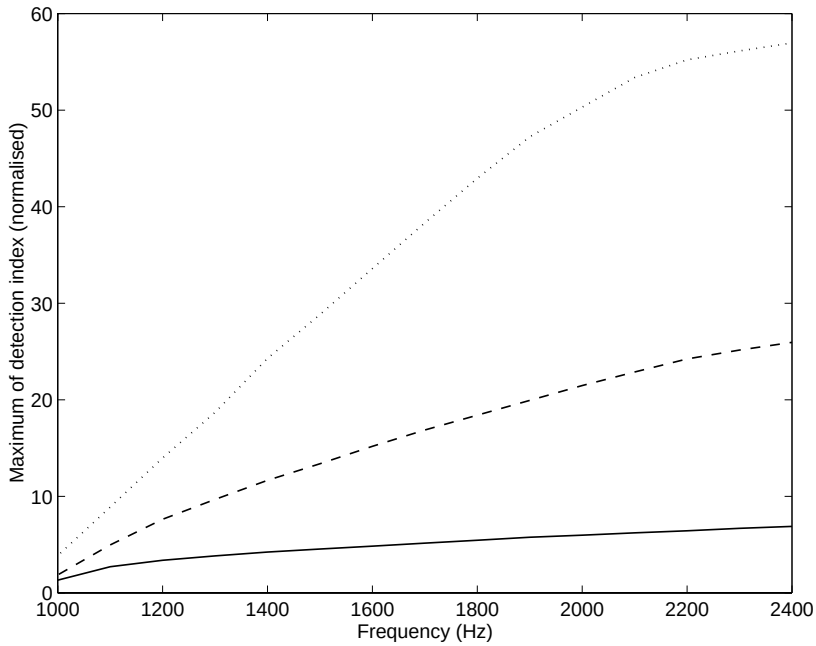

Figure 3.23: Maximum of detection index for step decrease of 0.05 pu and a superimposed exponentially decaying sinusoid of amplitude B equal to 0.20 pu (solid line), 0.40 pu (dashed line) and 0.60 pu (dotted line) for frequencies higher than 1000 Hz

The increase of the detection index in the presence of frequencies not modelled by the Kalman filter is beneficial for the segmentation scheme because higher frequencies are expected at the transition points, during fault initiation, fault clearing or capacitor energising.

3.5 Voltage dip detection

The problem of voltage dip detection is considered in a number of publications [70, 71] mainly for voltage dip mitigation equipment such as static transfer switches. In [52] the proposed detection scheme uses three settings: fast setting 1/8 cycle, slow setting 1/4 cycle and a one-cycle rms setting at 0.90 pu. In one year of operation the system was used 47 times as shown in Table 3.3. Only for 9 cases the operation was needed according to the authors (four of the dips and all five outages). The other 38 operations were due to capacitor switching, transformer energising, shallow voltage dips and other unidentified disturbances. It is not mentioned which setting was used. However, the scheme does not have the ability of distinguishing voltage dips from other disturbances.

Table 3.3: Static transfer switch transfers during one year of operation (from [52])

Disturbance cause	**Number of transfers**
Voltage dip	13
Outage	5
Capacitor switching	8
Substation transformer energising	9
Unknown	12

Figure 3.24 shows a measured voltage waveform when a fault starts and the corresponding estimated magnitude using an order-1 Kalman filter, an order-20 Kalman filter and an order-1 Kalman filter cascaded with a low-pass filter as described in Section 3.3 (Butterworth low-pass filter of order 1 and cut-off frequency of 50 Hz). The estimation speed of the latter is a compromise between accuracy and speed. This filter also removes the initial overshoot in the order-1 Kalman filter. Furthermore, the variance of the estimated magnitude has been reduced due to the filtering operation.

As explained before, if model-based methods are used for voltage amplitude estimation then two options can be adopted. The first option is to use a model that describes only the fundamental frequency component. In this case a change in the voltage waveform is quickly traced by the method. The main drawback of this approach is that in the case of a disturbance the initial estimation of voltage amplitude might be quite different from the actual value. The second option is to use a higher order model. This way the detection speed becomes much slower but the estimation is more reliable. The initial estimated amplitude is not overestimated or

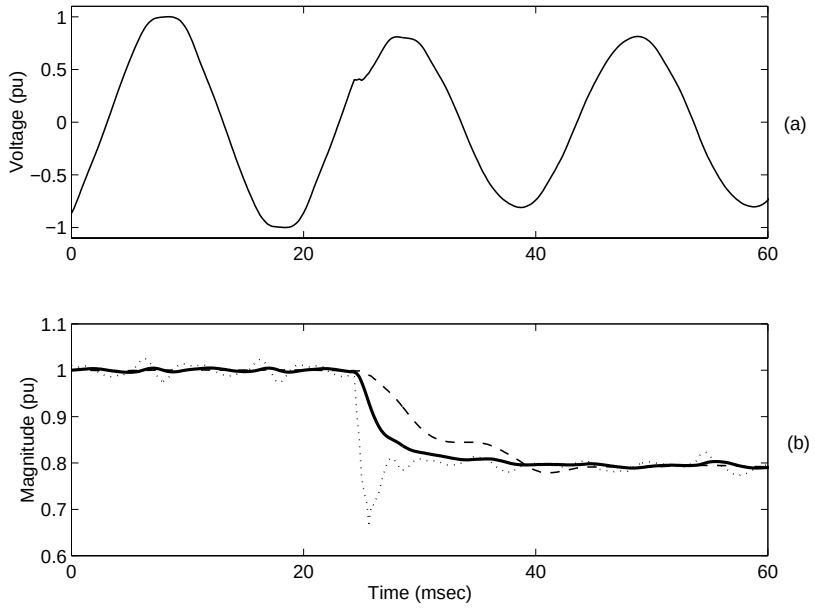

Figure 3.24: (a) Voltage waveform (b) Estimated magnitude using Kalman filter of order 1 (dotted line), Kalman filter of order 20 (dashed line) and Kalman filter order 1 with a low-pass filter (solid line)

underestimated and high frequency transients or harmonics that might exist are accommodated by the model and do not cause changes in the fundamental component amplitude. A compromise between the two options is to use a model that contains only the fundamental frequency and then for detection purposes apply a low-pass filter to the estimated amplitude as described in previous sections.

The performance of these estimators is shown below using simulations with synthetic rectangular voltage dips. The characteristics of such dips (due to faults) considered in Chapter 2 are summarised in Figure 3.25.

3.5.1 Detection of rectangular dips

Four methods are considered here for voltage dip detection. Their performance in speed is presented in terms of the time that it takes for the estimated magnitude to go below 0.90 pu of the normal voltage. The methods are:

1. rms calculated over one-cycle overlapping windows
2. rms calculated over half-cycle overlapping windows
3. Kalman filter of order 20
4. Kalman filter order 1 cascaded with a low-pass filter

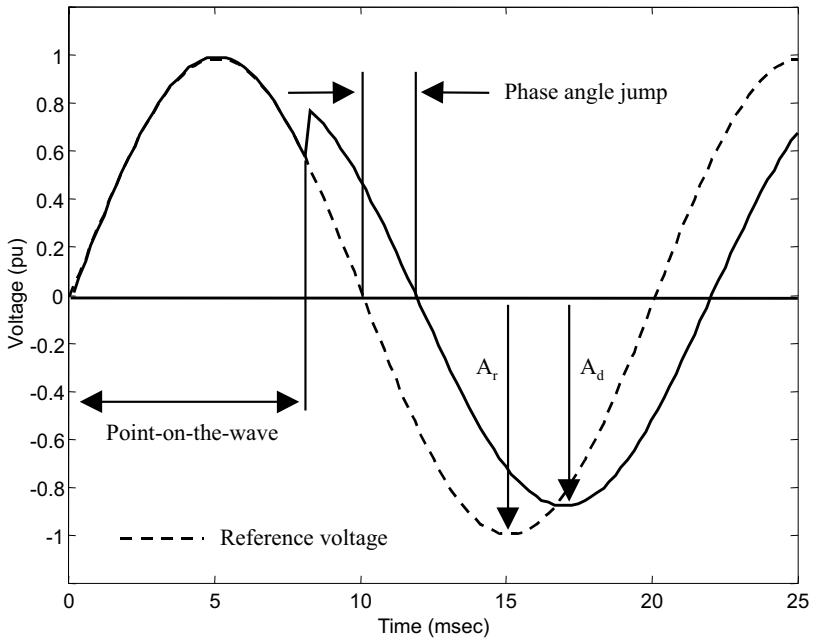

Figure 3.25: Rectangular voltage dip characteristics

Figure 3.26a shows the performance of these methods in estimating the voltage magnitude of synthetic rectangular voltage dips with a magnitude drop of 0.15 pu for different points on the wave. Figure 3.26b shows the calculated speed when the voltage drop is 0.30 pu. The order-1 Kalman filter with the low-pass filter is faster than both the one-cycle rms and the Kalman filter of high order, and slightly faster than the half-cycle rms.

As the voltage drop increases, the speed of the detection increases as expected and the differences between the different estimators become less significant. For very large voltage drops the changes in the estimators are minor in terms of how fast the estimated voltage magnitude exceeds the 0.90 pu threshold. However the differences are significant in terms of how fast this magnitude reaches its new value, as shown in Section 3.3.

The dependence of the estimation speed on the phase angle jump is shown in Figure 3.27a for the order-1 Kalman filter with a low-pass filter and voltage dips of magnitude 0.15 pu. A negative phase angle jump can delay or speed up significantly the estimation. On the other hand the effect of a positive phase angle jump causes either a small delay or a significant improvement. For voltage dips of larger magnitude the influence of the phase is less significant, as can be seen in Figure 3.27b.

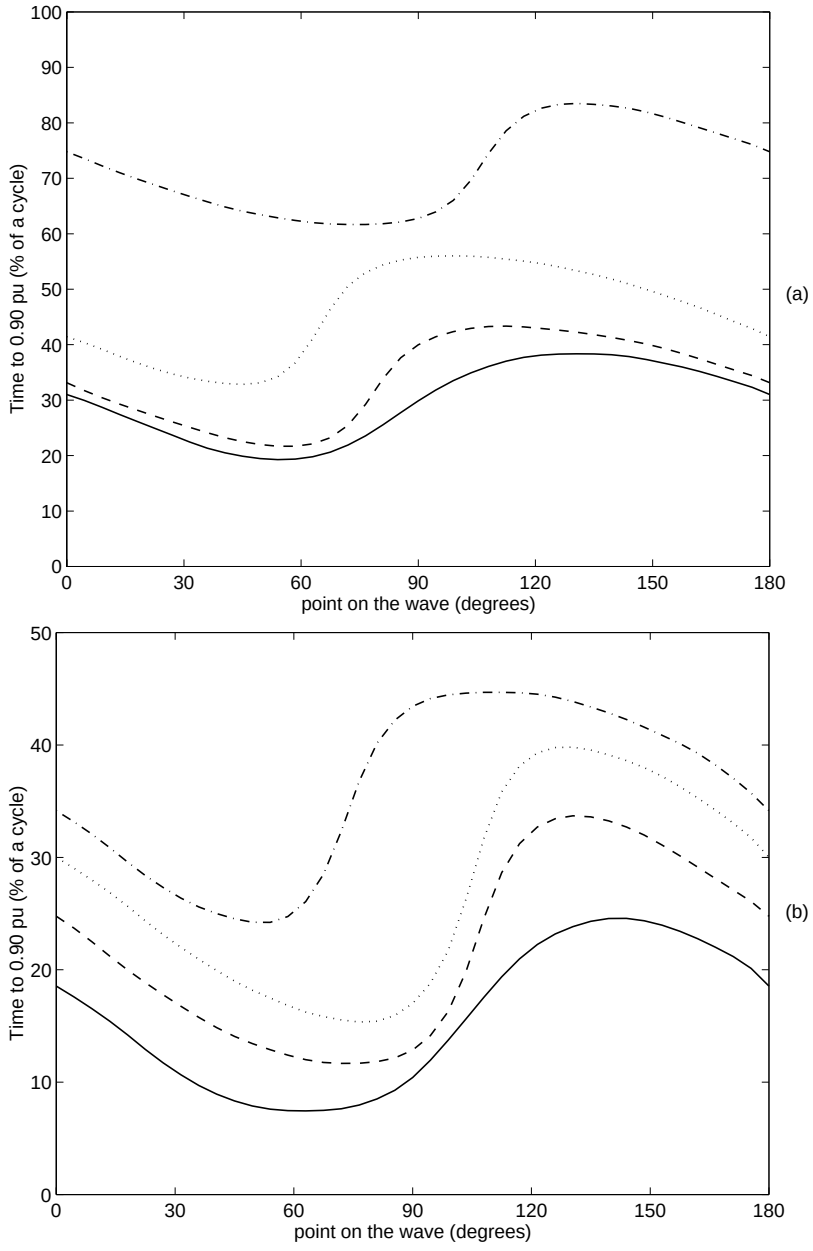

Figure 3.26: Speed of voltage dip detection using Kalman filter order 1 with a low-pass filter (solid line) , half-cycle rms (dashed line), order 20 Kalman filter (dotted line) and one-cycle rms (dash-dotted line) for (a) a 0.15 pu voltage drop (b) a 0.30 pu voltage drop

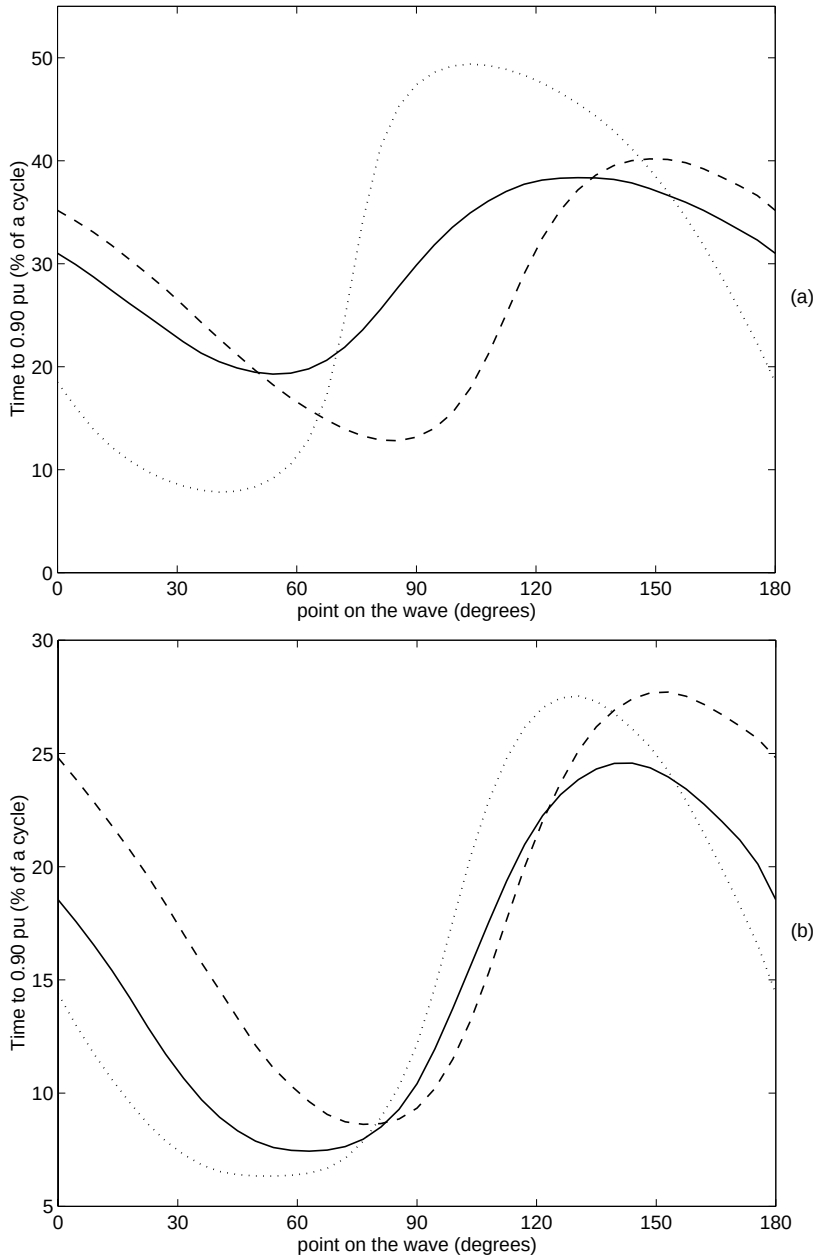

Figure 3.27: Speed of voltage dip detection using Kalman filter order 1 with a low-pass filter. (a) Voltage drop 0.15 pu (b) Voltage drop 0.30 pu. Phase angle jump of 0° (solid line), 20° (dashed line), −20° (dotted line)

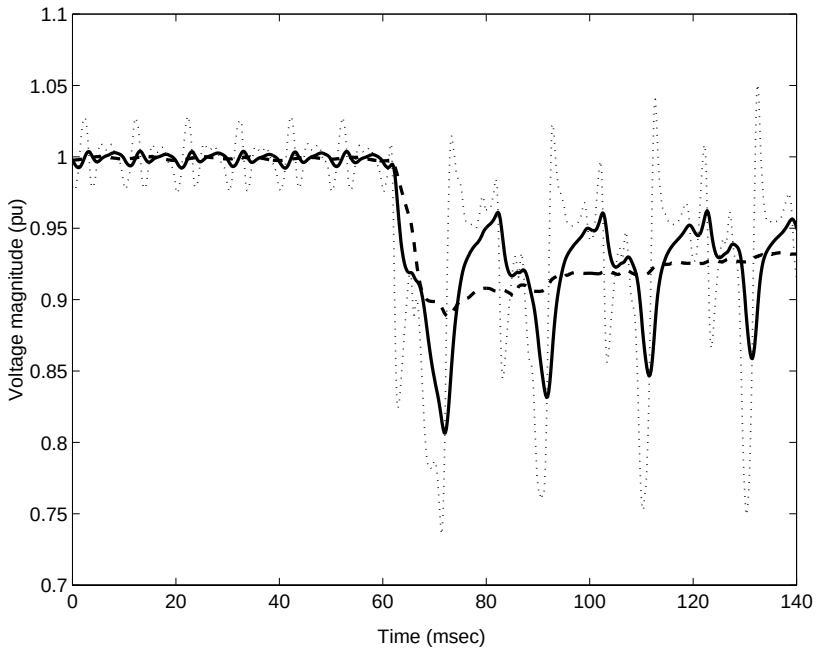

Figure 3.28: Estimated magnitude during transformer saturation using Kalman filter of order 1 (dotted line), Kalman filter of order 20 (dashed line) and Kalman filter of order 1 with a low-pass filter (solid line)

3.5.2 Transformer saturation

As shown in Section 3.3.1, the variation of voltage during transformer saturation is captured by the order-1 Kalman filter but not by that of order 20. The low-pass filter as described above moderately attenuates the oscillations. Figure 3.28 shows the corresponding estimated magnitudes for a measurement of transformer saturation.

Figure 3.29 shows the estimated magnitude using an order-1 Kalman filter with Butterworth low-pass filters of different orders. The increase in filter order does not influence the voltage dip magnitude significantly. Note also the delay in the initial response.

3.5.3 Distinguishing fault-induced dips and transformer saturation dips

If a voltage dip detection scheme does not need to produce a tripping signal for transformer saturation dips, it must wait for one cycle after the event initiation and verify that there is no voltage recovery in this time period because transformer saturation produces repeating voltage dips of duration approximately one cycle. In such a case either half-cycle rms or the order-1 Kalman filter can be used but not the higher order Kalman filter or the one-cycle rms because they need longer time to

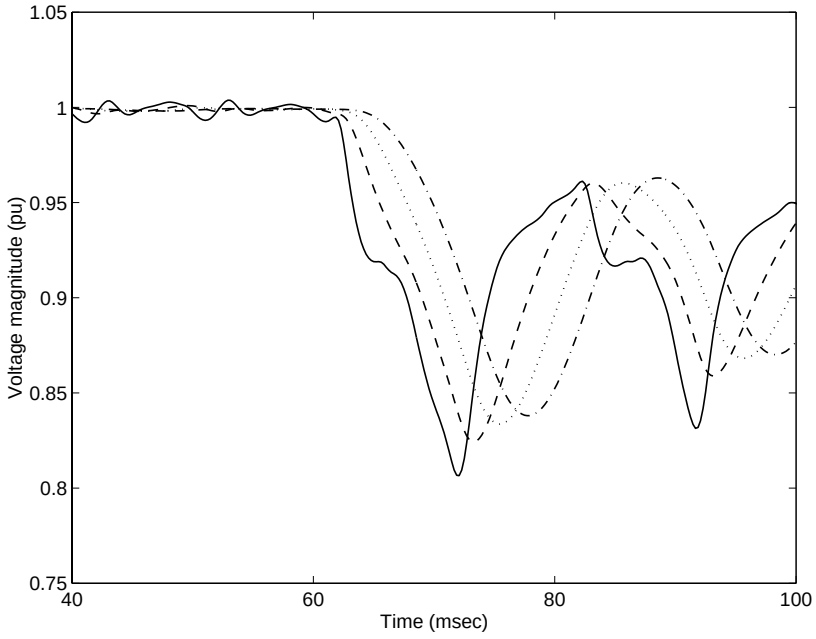

Figure 3.29: Estimated magnitude during transformer saturation using Kalman filter of order 1 with a low-pass filter of order 1 (solid line), 2 (dashed line), 3 (dotted line) and 4 (dash-dotted line)

capture the increase in voltage. The order-1 Kalman filter cascaded with a low-pass filter is used next.

The following measure is used to determine how much the voltage recovers within a one cycle window after it reaches its minimum point:

$$D = \frac{V_P - V_M}{1 - V_M} 100\% \tag{3.31}$$

where V_P and V_M are the values of estimated voltage at time instants that correspond to (referring to Figure 3.30):

- S the time instant the voltage magnitude crosses the 0.90 pu threshold
- M the time instant the voltage magnitude obtains its minimum value V_M within a window of one cycle starting from point S (analysis window)
- P the time instant the voltage magnitude obtains its maxim value V_P within a window w starting from point M until the end of the analysis window

The statistics on D shown in Figure 3.31, are obtained using one month measurements of fault-induced and transformer dips from a distribution network (33 and 11 kV). For each event, D is calculated for the phase that presents the most severe dip. Events that present voltage dips below 0.65 pu are not considered in these statistics. These events are classified as fault-induced dips because according to the statistics presented in Chapter 2, transformer dips do not exceed this value. It is obvious from

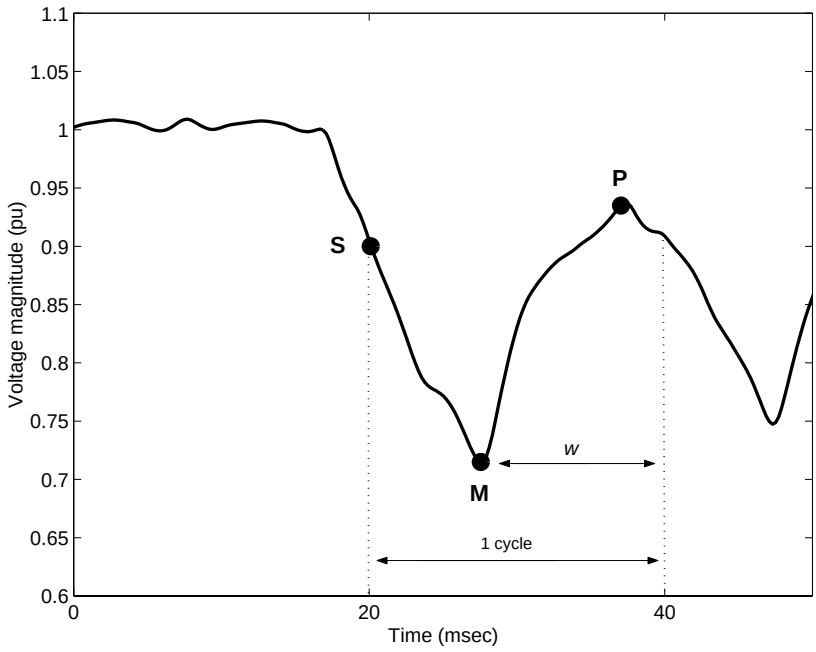

Figure 3.30: Voltage magnitude during transformer saturation (marked points refer to (3.31))

this figure that transformer saturation events are associated with a high value of D, unlike fault-induced dips.

Table 3.4 shows the classification results if a threshold of 50 % is used to D for distinguishing the two types of events. It means that if D is greater than this threshold, then the measurement is classified as transformer saturation and if smaller, it is classified as fault-induced event. In the first cycle, after the voltage magnitude exceeds the 0.90 pu threshold, all the transformer saturation events are classified correctly and only a small number of fault events are not classified correctly. These fault events are classified correctly in the second cycle using the same threshold for D. During the second cycle, all the transformer saturation events having magnitude below 0.90 pu even in the second cycle are also classified correctly.

However, an on-line scheme for distinguishing transformer events from fault events must consider the cost of misclassification for the two cases (transformer events classified as faults and faults classified as transformer events) as well as the time requirements for correct classification. Depending on the application, it might be more important that all the faults are detected even at the expense of some unnecessary operations due to transformer saturation. For other applications it might be more important to avoid unnecessary operations at the expense of some delay in detection.

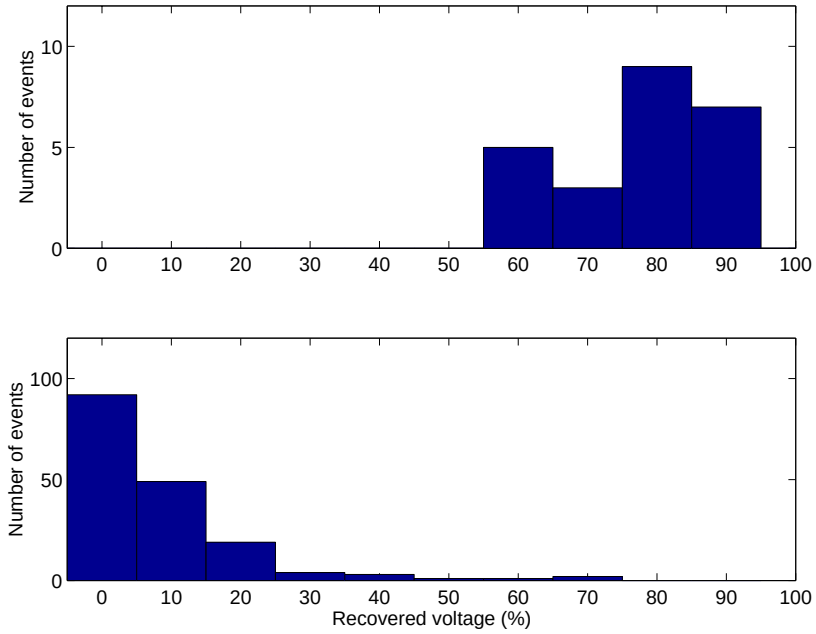

Figure 3.31: Statistics on D for (a) transformer saturation dips and (b) fault-induced dips

Table 3.4: Separating transformer and fault-induced dips using D

Type	1^{st} **cycle**	2^{nd} **cycle**
Fault-induced voltage dips	168/171	3/3
Transformer saturation	24/24	17/17

3.5.4 The dq-transform for the detection of voltage dips and transformer saturation

A common method for voltage dip detection is the one based on Park transform [72, 73]. The instantaneous three phase voltages $v_{\mathrm{a}}(t), v_b(t), v_c(t)$ are transformed into a fixed two-axis coordinate system called $\alpha\beta$-coordinate system by:

$$\begin{pmatrix} v_\alpha(t_k) \\ v_\beta(t_k) \\ v_0(t_k) \end{pmatrix} = \sqrt{\frac{2}{3}} \begin{pmatrix} 1 & -1/2 & -1/2 \\ 1 & \sqrt{3}/2 & -\sqrt{3}/2 \\ 1/\sqrt{2} & 1/\sqrt{2} & 1/\sqrt{2} \end{pmatrix} \begin{pmatrix} v_{\mathrm{a}}(t_k) \\ v_b(t_k) \\ v_c(t_k) \end{pmatrix} \tag{3.32}$$

where $v_0(t_k)$ is the zero sequence voltage component. The voltage vector obtained can be further transformed into a rotating dq-coordinate system using the following transformation (dq-transform):

$$\begin{pmatrix} v_d(t_k) \\ v_q(t_k) \end{pmatrix} = \mathrm{e}^{-j\theta(t_k)} \begin{pmatrix} v_\alpha(t_k) \\ v_\beta(t_k) \end{pmatrix} \tag{3.33}$$

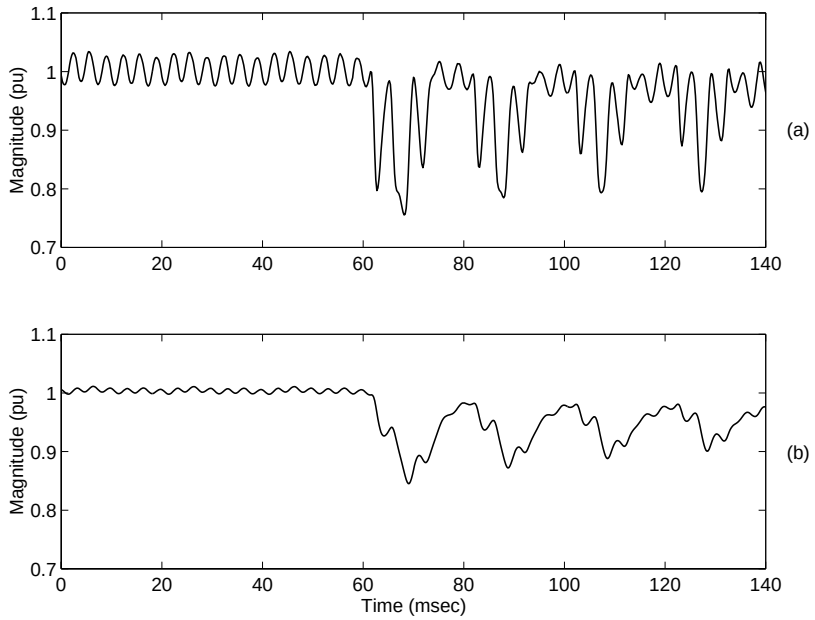

Figure 3.32: (a) V_{dq} calculated by (3.35) (b) Filtered V_{dq}

where $\theta(t_k)$ is the transformation angle obtained using $\omega = 2\pi 50$ rad/sec through the following formula:

$$\theta(t_k) = \theta(0) + \int_0^{t_k} \omega d\xi \tag{3.34}$$

The following value:

$$V_{dq}(t_k) = \sqrt{|v_d(t_k)|^2 + |v_q(t_k)|^2} \tag{3.35}$$

can be used for detection by comparing it with a user-set threshold. A low-pass filter must be used in order to remove frequency components higher than the fundamental.

Figure 3.32a shows V_{dq} calculated using the above formulas for the transformer saturation case used in the previous section. Figure 3.32b shows V_{dq} filtered with the low-pass filter used in the previous section.

The model used for the *dq*-transform considers only the fundamental frequency component. Therefore, V_{dq} has similar characteristics as compared to the magnitude estimated by an order-1 Kalman filter: it presents high variance due to harmonic distortion, and in the case of transformer saturation it captures the fast variations of voltage. Such a voltage dip detection scheme will be triggered by transformer saturation events. Furthermore, the estimated dip using this method will be deeper than the one calculated with order-20 Kalman filter or one-cycle rms. For the example of Figure 3.32, V_{dq} shows a drop of approximately 0.15 pu. The maximum drop of the three phases when the voltage magnitude is calculated with one-cycle rms or the order-20 Kalman filter is 0.10 pu.

3.5.5 Voltage dip detection and capacitor energising transients

Another type of transient that may trigger a voltage dip detection algorithm is the oscillatory transient caused by the energising of a capacitor bank. Although the energising of a capacitor bank increases the voltage of the system, the initial transient can be mistaken as a dip by fast detection algorithms, as shown in Table 3.3.

Capacitor energising causes a sudden drop in voltage towards zero followed by high frequency oscillatory transients superimposed to the voltage waveform (this type of event will be explained further in Chapter 6). The resulting overvoltage is usually between 1.1 and 1.7 pu, and the frequency of oscillation between 200 Hz and several thousand Hz.

If the voltage magnitude is estimated by the order-1 Kalman filter then it follows the high frequency oscillations because these oscillations cannot be accommodated by the filter. The low-pass filter that is used to filter this magnitude attenuates these oscillations. However, the performance of this filter is limited by the speed requirements as mentioned before. Therefore, attenuation of the oscillation becomes more difficult if the oscillation frequency is close to the cut-off frequency of the filter. Additionally, the filter must remove the initial instantaneous voltage dip (voltage drops to zero and increases towards its maximum value). The faster the increase in voltage after the initial drop to zero, the more is attenuated.

Figure 3.33 and Figure 3.34 show two cases of capacitor energising transients simulated in EMTP. The same system has been used for both cases for two different capacitor banks in order to obtain transients with different frequency (see Chapter 6). The oscillation frequency of the transient in Figure 3.33 is 300 Hz and in Figure 3.34, 600 Hz. Both transients start with an instantaneous voltage dip (voltage goes close to zero). The magnitude of voltage estimated by the order-1 Kalman filter oscillates from values close to zero to the maximum of the voltage waveform. In the first case, (Figure 3.33) the low-pass filter attenuates significantly the oscillation, and the minimum value of magnitude is 0.88 pu. In the case where the oscillation frequency is 600 Hz, the attenuation is more effective, as shown in Figure 3.34 and the minimum value of voltage is higher (0.95 pu). In both cases, the minimum estimated voltage magnitude corresponds to the initial instantaneous voltage dip.

It can be concluded that, whether a voltage dip detection scheme is triggered by a capacitor energising transient depends significantly on the oscillation frequency. Furthermore, the magnitude of the instantaneous voltage dip is important. If there are more capacitors in the bus where the capacitor bank is energised then the voltage will not initially go to zero. Therefore the estimated magnitude will be less effected by the initial voltage dip. High frequency transients are produced in this case. However, these transients are expected to be attenuated adequately by the low-pass filter. More important for the initial drop is the distance of the switching point from the measuring point. The initial drop in the measured voltage decreases with increasing distance from the switching point.

Another important parameter is the point on the wave where the capacitor switching transient takes place. Figure 3.35 shows a capacitor energising transient taken place at 90° and the corresponding magnitude estimates. The same system has been used for the simulation as in Figure 3.33, therefore the oscillation frequency is 300 Hz. It can be seen that the minimum dip as obtained by the Kalman filter is higher than the one in Figure 3.33. As shown in Section 3.5.1, the tracking speed of the Kalman filter depends on the point on the wave where a change takes place. Therefore, whether a voltage dip detection scheme is triggered by a capacitor energising transient depends significantly on the point on the wave where the transient starts.

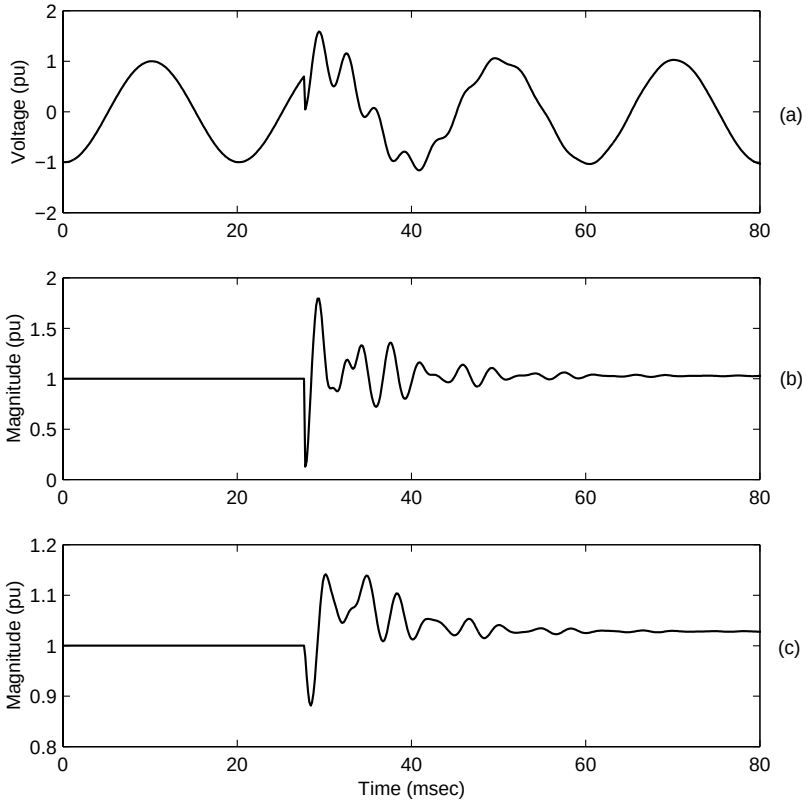

Figure 3.33: (a) Voltage waveform during capacitor energising (oscillation frequency 300 Hz) (b) Magnitude estimated by Kalman filter order 1 (c) Magnitude filtered by low-pass filter

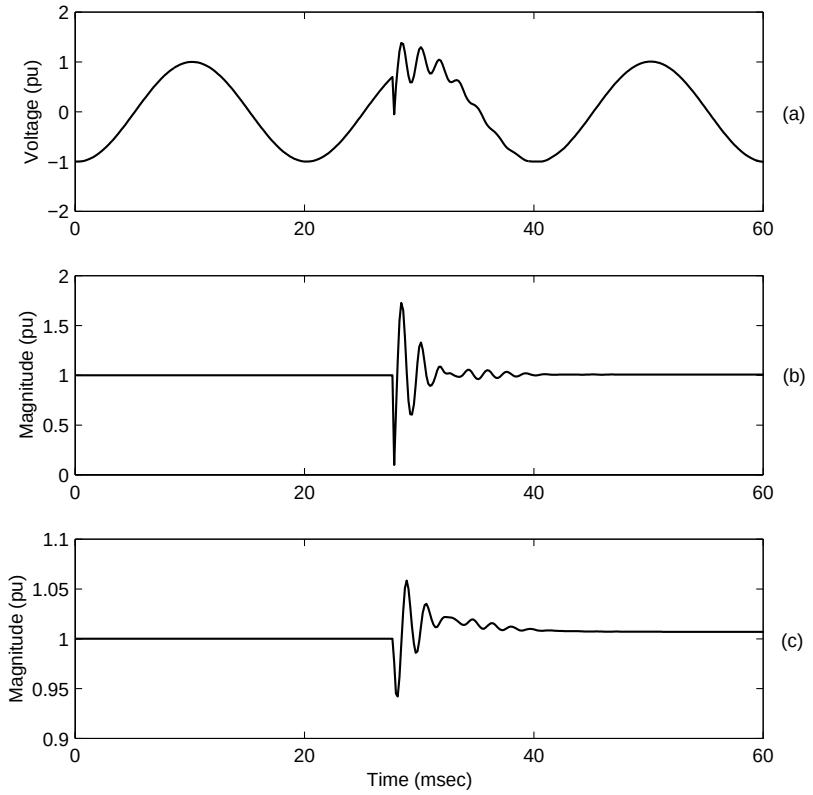

Figure 3.34: (a) Voltage waveform during capacitor energising (oscillation frequency 600 Hz) (b) Magnitude estimated by Kalman filter order 1 (c) Magnitude filtered by low-pass filter

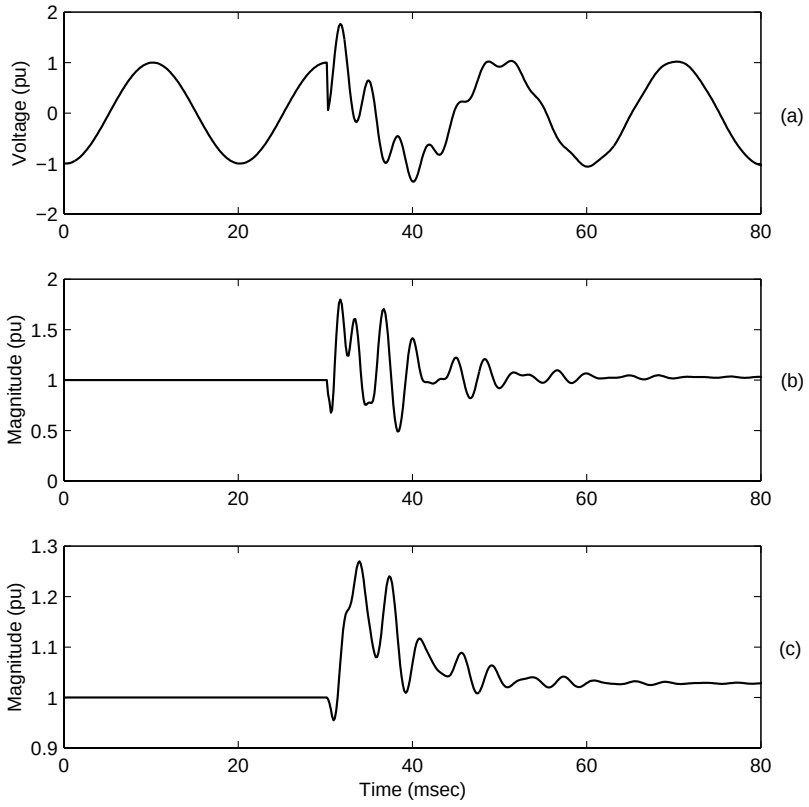

Figure 3.35: (a) Voltage waveform during capacitor energising (oscillation frequency 600 Hz) (b) Magnitude estimated by Kalman filter order 1 (c) Magnitude filtered by low-pass filter

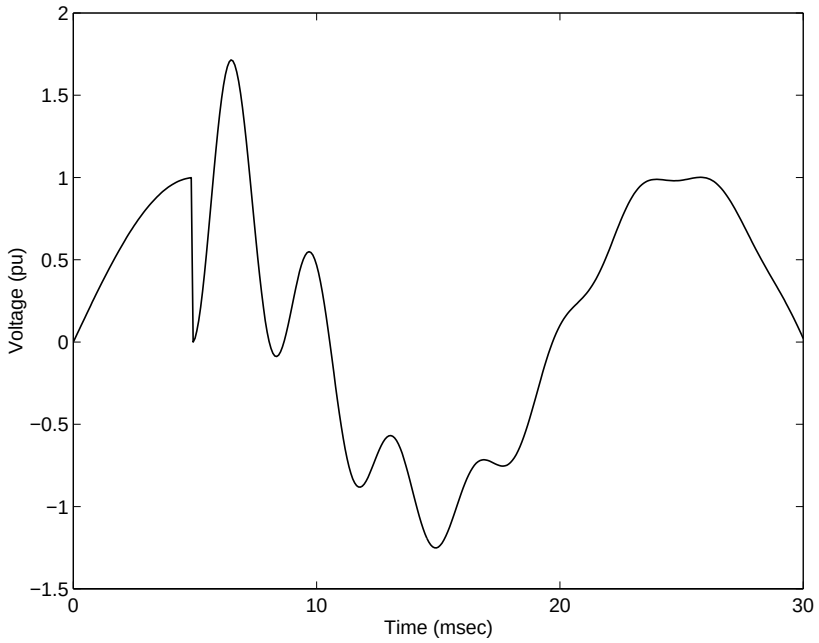

Figure 3.36: Synthetic signal for capacitor switching transient analysis

For a more systematic investigation of capacitor switching transients with respect to the voltage dip detection problem, synthetic signals were generated consisting of exponentially damped sinusoids of different frequencies superimposed to the fundamental frequency sinusoid causing a voltage drop at time instant t_0, to zero:

$$z(t_k) = \cos(\omega t_k + \theta) \qquad t_k < t_0 \quad (3.36)$$

$$z(t_k) = (1+\Delta)\cos(\omega t_k + \theta) - Ae^{-\alpha(t_k - t_0)}\cos(2\pi f_n(t_k - t_0) + \theta_s) \qquad t_k \geq t_0 \quad (3.37)$$

where A is the amplitude of the superimposed signal, α the damping factor and f_n is the oscillation frequency. The phase θ_s, is set according to:

$$\theta_s = \arccos\left(\frac{1+\Delta}{A}\cos(\omega t_0 + \theta)\right) \quad (3.38)$$

in order the oscillation to start from voltage equal to zero. Δ is used to represent the increase in voltage magnitude by connecting a capacitor bank to the network. This signal model is used to demonstrate the influence of the point on the wave and the oscillation frequency of the capacitor energising transient on voltage dip detection.

Figure 3.37 shows the estimated minimum voltage for synthetic signals generated using (3.37)-(3.38), and applying an order-1 Kalman filter cascaded with a low-pass filter. The signals were created with Δ =0.03, A =1.03, α =0.012, f_n =200-500 Hz, and different points on the wave (by varying θ). An example of such a waveform is given in Figure 3.36 where f_n was set to 300 Hz and the point on the wave is 90°.

The results of Figure 3.37 verify that the minimum voltage in these cases depends on the point wave and the frequency of the oscillation. For higher frequencies the minimum voltage is well above the 0.90 pu threshold.

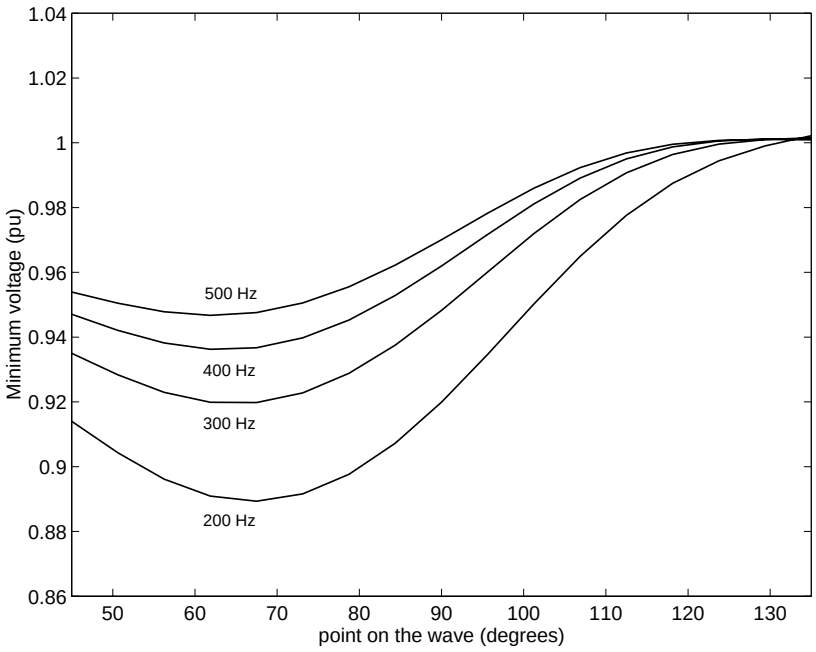

Figure 3.37: Minimum estimated voltage for capacitor energising transients with different oscillation frequencies f_n (synthetic signals)

Only points on the wave between 45° and 135° are considered. Other points on the wave do not cause significant changes in the estimated voltage at the instant of switching (less than 0.03 pu). For these points on the wave the initial voltage drop to zero is not captured by the magnitude estimator. Additionally, such high value for A is not realistic for other points on the wave (the capacitor switching overvoltage is maximum at 90° [74]).

One more point that must be mentioned here is that if the dip detection is based on using one-cycle data after the voltage magnitude goes below the 0.90 pu threshold, then capacitor switching transients can be easily ruled out as fault-induced dips. Within this time interval the voltage magnitude typically shows an increase (see the previous examples of capacitor switching simulations Figure 3.33 - Figure 3.35). This increase is the same for all three phases, unlike the case of voltage swell during a fault that appears in two of the three phases (the third one shows a voltage dip).

3.6 Conclusions

Estimation of voltage magnitude is important in terms of extracting information from measurements and characterising power system events. Following Chapter 2, where the different classes of power system events were presented, Chapter 3 shows the different types of voltage magnitude changes with respect to Kalman filtering.

Kalman filtering aspects are described. Emphasis is given to the time resolution properties. It is shown that there are three types of changes: fast, slow and fast

repeating changes corresponding to different power system phenomena. It is also shown that the model order used by the Kalman filter effects significantly the voltage magnitude estimates for the different types of changes. Especially for fast repeating changes (which are due to transformer saturation), a Kalman filter modelling only the fundamental frequency sinusoid is able to follow the variations but a filter that also models harmonics cannot follow the variations.

Basically, the voltage magnitude estimation is subjected to two facts:

- there are long duration power system events for which, the estimation of voltage magnitude does not impose problems in characterisation and extraction of their characteristics.

- there are power system events of a duration that coincides with the speed of the methods for voltage magnitude estimation.

Towards the automatic processing of power quality measurements, two approaches are proposed for the segmentation of voltage disturbance recordings. The first segmentation algorithm utilises a high order Kalman filter. Detection of sudden changes is based on how well a high order model (fundamental and harmonics) fits to the measurement data. Event segments (low detection index) and transition segments (high detection index) are obtained. Transient segments are typically parts of the voltage disturbance signals corresponding to fault initiation, fault clearing or switching actions. Event segments are the parts corresponding to the voltage during a fault or the recovery voltage during transformer saturation. It is demonstrated that the scheme is able to detect fast changes and is immune to slow changes in voltage magnitude.

Segmentation can also be performed using all three waveforms in a way that enables comparison between the phases. This is useful for classification purposes as explained in Chapter 4. The properties of the segmentation scheme are also extracted for rectangular dips using simulations. The detection index is sensitive to the point where the fast change takes place, the phase angle jump that might be present and the frequency contents of the voltage signals.

The time resolution of the above method is not adequate for events that contain transitions close in time. Therefore, a second method with better time resolution is proposed for identifying and locating stages of voltage between transition points. It utilizes a Kalman filter of order 1 and a simple detection scheme. This algorithm can be used for short duration events.

Segmentation offers the means for further analysis of the recordings. An expert system is presented in Chapter 4 for classification (in terms of underlying event) and analysis of power system events based on the above segmentation algorithms.

In this chapter the problem of voltage dip detection is also investigated. Simulations are used to show that a Kalman filter that considers only the fundamental frequency sinusoid combined with a low-pass filter has an overall better performance than purely using Kalman filters of either higher or lower order, and is not sensitive to high frequency transients. The influence of the characteristics of fault-induced

dips on the speed of a detection scheme is shown experimentally. The speed of detection depends on the voltage dip magnitude, the point on the wave where the dip starts, and the phase angle jump that is caused.

Special attention is also given to transformer-related events. Transformer saturation causes voltage dips that might trigger a voltage dip detection scheme. It is shown that the same problem exists even if the detection is based on the *dq*-transform. Considering the fast magnitude variation due to saturation, transformer dips can be distinguished from fault-induced dips within one or two cycles after the event initiation.

Capacitor switching transients have also been considered. They are characterised by the peak magnitude (overvoltage) and the frequency of the oscillation. They do not cause triggering of a voltage detection scheme that uses a Kalman filter of order 1 cascaded with a low-pass filter, as long as the oscillation is adequately attenuated by the low-pass filter. Overall, it is shown that voltage dip detection is subject to a trade-off between selectivity and speed.

Chapter 4

Expert System for Classification and Analysis of Power System Events

4.1 Introduction

In this chapter an expert system is presented which is able to classify different types of power system events, (presented in Chapter 2), according to the underlying causes and offer useful information in terms of power quality. The expert system uses the voltage waveforms as inputs and distinguishes the different types of voltage dips as well as interruptions. A method for event-based classification is proposed, where the segmentation algorithms presented in Chapter 3 are first applied to divide waveforms into several possible events. The classification scheme is based on identifying and characterising the different stages of voltage during an event.

Several approaches for automatic classification of power system disturbances have been presented in a number of papers [17, 18, 19, 20, 21, 22]. These systems classify recordings from power quality monitoring in terms of disturbances [17, 18, 20, 21] or in terms of underlying events [19, 22].

4.2 Automatic classification of power system events

The voltage events considered by the expert system can be divided into the following classes: fault-induced events, transformer events, induction motor events, interruptions and step-change events.

As explained in Chapter 2, the common feature of the first three classes is that they cause a temporary decrease in voltage magnitude (dip). Classification is possible using the following characteristics of voltage magnitude:

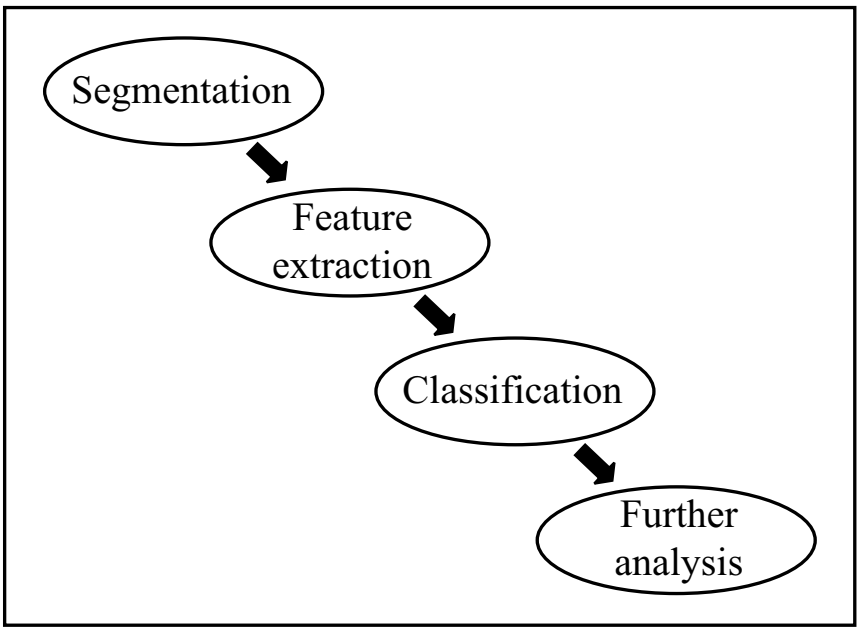

Figure 4.1: The elements of the expert system

- The way the fundamental component recovers back to normal: fault-induced events are rectangular dips due to protection operation. Transformer and motor dips are non-rectangular; voltage recovers gradually.
- The symmetry between the phases: transformer saturation events are asymmetrical dips (different degree of saturation for each phase) and motor events are symmetrical dips (balanced load).
- The distinctive signature that voltage magnitude presents during saturation, if a fast magnitude estimator is used.

Therefore, the strategy for classification must be based on:

- Segmenting the voltage waveforms by detecting fast changes in the fundamental frequency magnitude.
- Considering the number of segments and their types (transition or event segments).
- Characterising the segments.
- Comparing the segments in the same phase.
- Comparing the phases at the corresponding segments.

The classification results can be used for further analysis. Information like the type of voltage dip for fault-induced events, or the overvoltages present can be

extracted and explained in terms of the segmentation and classification results. The above-mentioned procedures are summarised in Figure 4.1.

The system also considers interruptions and distinguishes between fault and non-fault interruptions using the segmentation results. Finally, the expert system has an output for recordings presenting only a step change in voltage magnitude (load switching or voltage control related operations) and an output for energising from zero. To summarise, the system can classify the following nine events:

(a) Energising

(b) Non-fault interruption

(c) Fault interruption

(d) Transformer saturation

(e) Induction motor starting

(f) Step change

(g) Transformer saturation followed by protection operation

(h) Single stage dip due to fault

(i) Multistage dip due to fault

The case of transformer saturation followed by protection operation could be due to maloperation of protection during energising.

4.3 Segmentation of voltage waveforms

4.3.1 General

All the above mentioned events are associated with at least one sudden change in the voltage magnitude. These changes define the stages in the recording. Segmentation of the measurements is done in the following steps:

1. The segmentation scheme described in Sections 3.4.4-3.4.5 is applied considering all three phases. This way the measurement is split into transition and event segments.

2. For transition segments that contain a voltage dip of magnitude larger than 0.10 pu, the segmentation scheme for short duration events (presented in Section 3.4.6) is applied for the phase presenting the dip. This scheme identifies stages of constant magnitude. If stages of magnitude are found, the parts in the three voltage signals corresponding in time are considered as event segments.

3. The event segments are checked in order to find whether the measurement contains more than one event. This procedure is called multi-event segmentation and is described in the next section.

The segmentation procedure divides the voltage waveforms into parts with well-defined characteristics. Even in the case of events that present high harmonic distortion like transformer saturation, the different stages are revealed.

4.3.2 Multi-event segmentation

Analysis of several measurements showed that there might be more than one of the above-mentioned events in one single recording. Therefore, the parts of the signal associated with different events must be found and analysed separately. For this purpose, the expert system separates the recording into groups of segments that start and end with event segments for which all the phases have or tend to normal voltage, or zero voltage (interruption). Normal is considered a voltage with magnitude above 0.95 pu. In the case of energising, normal is consider a voltage with magnitude above 0.80 pu (to take into account the drop in voltage due to transformer saturation).

Figure 4.2 shows the voltage magnitude and the segmentation results of a measurement from an 11 kV network. This recording contains two events. First, transformer saturation takes place and then a fault-induced event follows. The multi-event segmentation splits the recording into two groups (G1 and G2) that start and end with segments that either have normal voltage (first and last segment of the recording) or tend to normal voltage (transformer saturation segment) for all three phases.

Figure 4.2 shows the voltage magnitude and the segmentation results of a measurement from an 11 kV network, where energising is followed by a non-fault interruption. The event is probably due to malfunctioning in the energising process. The multi-event segmentation splits the recording into two groups (G1 and G2) that start and end with segments that either have normal voltage or have or tend to zero voltage for all three phases.

Finally, if the second group in a recording is after a rectangular voltage dip then it is not considered separately but the whole recording is considered as a multistage dip. This is for multistage dips where the last stage before the final recovery is above 0.95 pu.

4.4 Classification strategy

4.4.1 Structure of the expert system

Before any processing is done, all the voltage waveforms are normalised with respect to the pre-event voltage. The magnitude of each phase then is estimated using order-20 Kalman filters (described in Chapter 3). The corresponding detection index is also obtained.

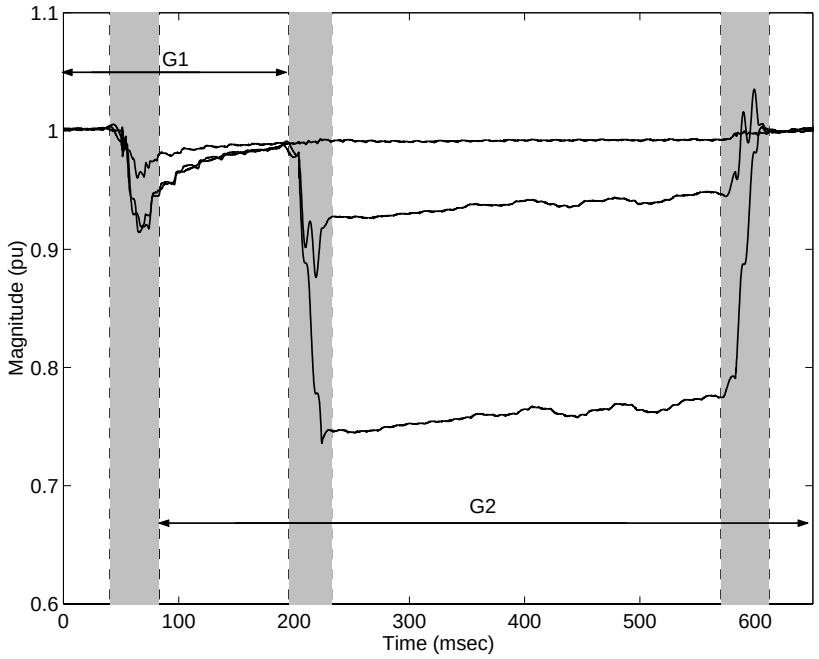

Figure 4.2: Voltage magnitude of a multi-event recording and segmentation results (shadowed parts: transition segments)

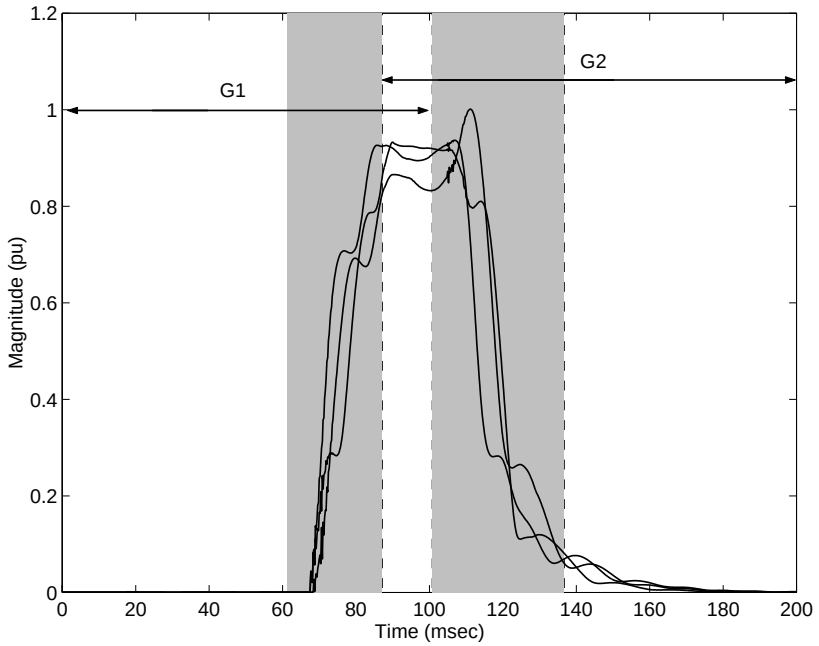

Figure 4.3: Voltage magnitude of a multi-event recording and segmentation results (shadowed parts: transition segments)

The system analyses recordings that present one of the following characteristics:

- a change in the estimated voltage magnitude higher than 0.05 pu.
- an overvoltage higher than 1.05 pu.

The structure of the expert system is shown in Figure 4.4. First, the segmentation algorithms are applied as described in the previous section. If more than one event exist in the recording, the classification procedure is repeated as many times as the number of these events (ne), each time using the corresponding parts of the measurement. For example, for the recordings shown in Figure 4.2 and Figure 4.3, ne is equal to 2.

Measurements that can be classified using the system information (protection time settings, scheduled switching operations) are transferred directly to the Further Analysis modules. The Classification Module classifies the rest of the measurements. The classification procedure terminates when all the events within the recording are classified.

If segments cannot be initially found and the measurement does not contain a dip, then the segmentation algorithm which uses the Kalman filter residues is applied again, with a lower threshold $\delta_{new} = \delta/2$, where δ is given in Chapter 2. Only the step change case is checked for these measurements.

4.4.2 Classification Module

The segmentation algorithms separate the events into subclasses according to the number of event segments. The possible options for an event are checked according to the number of event segments unless the recording contains zero values. The procedure ends when the event matches with the characteristics of one of the events in the knowledge base of the expert system. The modules corresponding to the events are called in the following order:

(a) If the recording contains zero voltage values:

1. energising
2. fault interruption
3. non-fault interruption

(b) If the number of event segments is two:

1. transformer saturation
2. induction motor starting
3. step change

(c) If the number of event segments is three:

1. transformer saturation followed by protection operation

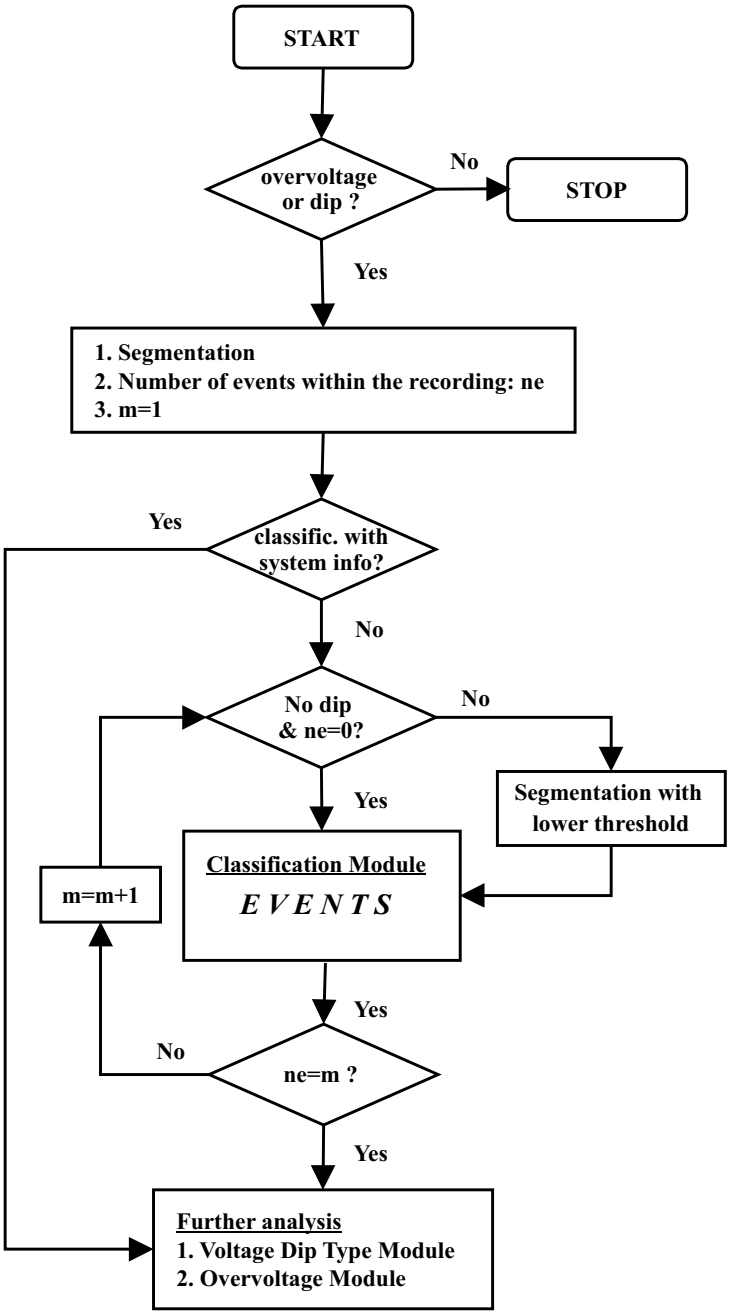

Figure 4.4: Structure of the expert system (flow chart)

2. single stage voltage dip due to fault

(d) If the number of event segments is higher than three:

1. multistage voltage dip due to fault.

After classification, the measurements, the estimated voltage magnitude for each phase as well as the segmentation and classification results are transferred to the Further Analysis modules.

4.5 Knowledge base: rules for classification

Next, the rules of the Classification Module are given for each event. Two points must be highlighted here. First, for the class of events that contain only one transition segment (and do not contain zero voltage parts), the segmentation as described in Chapter 3, provides transition segments that have clearly observed trend (increase or decrease). For the classification procedure of these events, it is checked whether the transition segment is a dip: the minimum value of magnitude is at least 0.10 pu below the magnitude of the event segment before the transition and at least 0.10 pu below the magnitude of the event segment after the transition segment. This way short duration voltage dips are detected and given as a separate output of the expert system. Second, for the extraction of features, the phase with the largest voltage dip is used. This phase is called *significant phase*.

Energising

The recording consists of two event segments. The first event segment corresponds to zero voltage for all phases, and the second one to normal voltage for all phases. An example is given in Figure 4.5.

Fault interruption

The recording consists of three or more event segments. An example is given in Figure 4.6. The last event segment corresponds to zero voltage for all the phases. The magnitude of the middle event segments of at least one of the three phases is below the 0.95 pu threshold and above 0.10 pu. The first transition segment corresponds to fault initiation, and the last transition segment to fault clearing.

Event segments of magnitude below 0.10 pu are not considered because interruptions might cause transformer saturation or current chopping. In these cases voltage waveforms are very distorted, and the results of the segmentation scheme are not reliable. Examples of these phenomena are given in Chapter 2.

Non-fault interruption

The recording consists of two or more event segments from which the last one corresponds to zero voltage magnitude for all the phases. An example is given in Figure

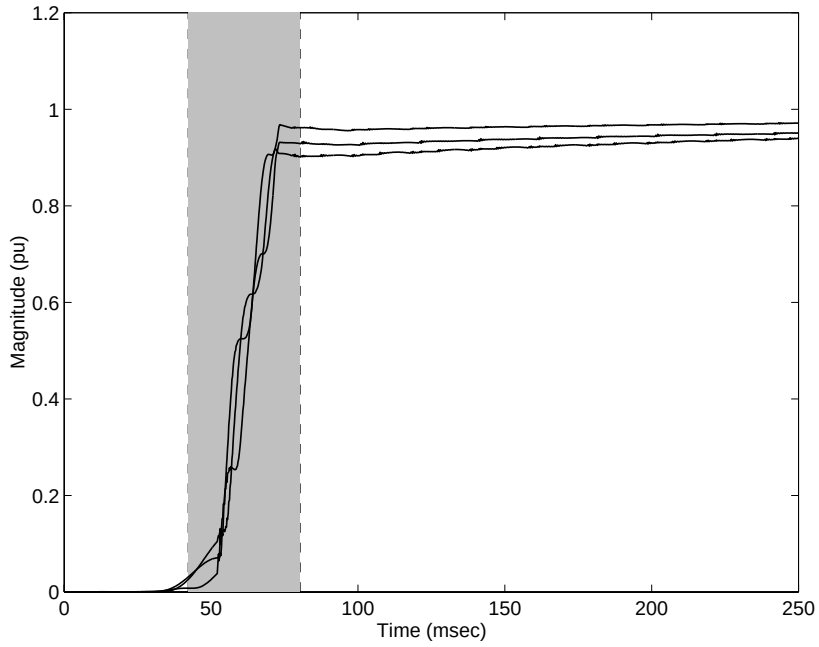

Figure 4.5: Energising: voltage magnitude and segmentation results (shadowed part: transition segment)

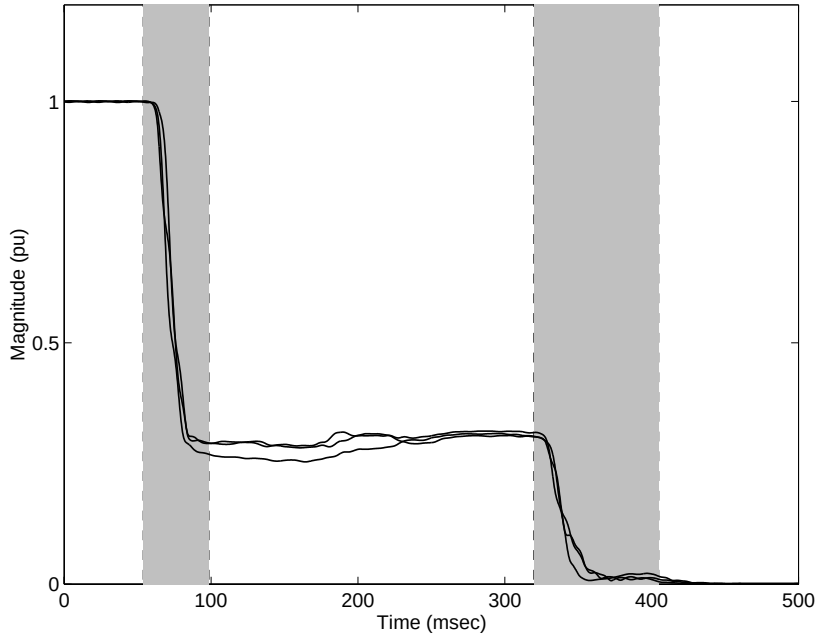

Figure 4.6: Fault interruption: voltage magnitude and segmentation results(shadowed parts: transition segments)

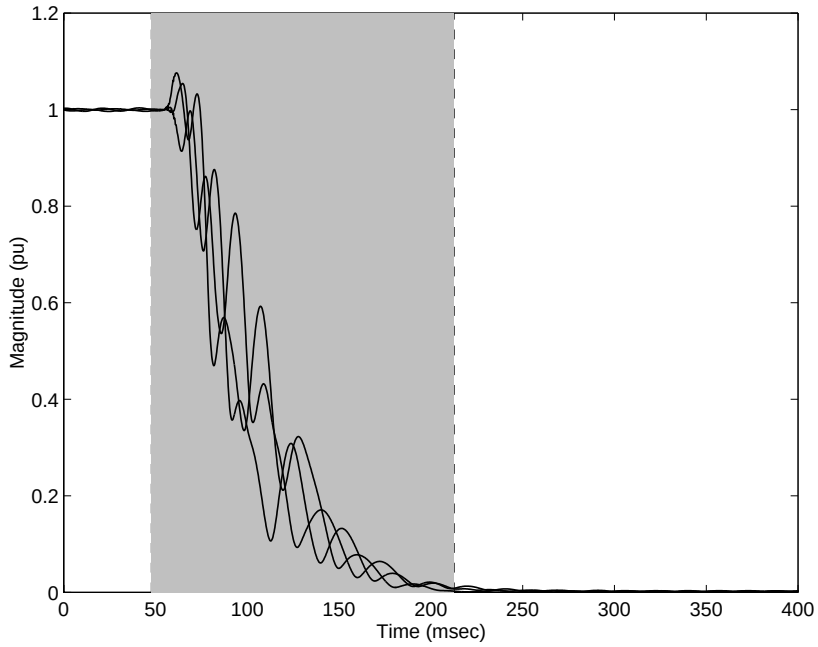

Figure 4.7: Non-fault interruption: voltage magnitude and segmentation results (shadowed part: transition segments)

4.7. None of the middle event segments has magnitude between 0.95 pu and 0.10 pu (for the same reason as in the case of fault interruption).

Transformer saturation

The recording consists of two event segments. The second event segment corresponds to a voltage drop that finally recovers for at least one phase. An example is given in Figure 4.8. Considering the significant phase , the following conditions must be fulfilled:

1. The minimum voltage of the recording is above 0.80 pu (the voltage magnitude estimated with an order-20 Kalman filter). This threshold, δ_{MD}, is set considering the statistics on transformer saturation dips (see Chapter 2).

2. The second event segment has increasing magnitude (voltage recovery): the end of the event segment has higher voltage magnitude than the beginning.

3. The increase in the voltage magnitude is gradual. Points are taken from the estimated magnitude every one cycle and the cycle-by-cycle increase should not exceed a threshold δ_{CBC}.

4. The estimated magnitude of the second event segment using a Kalman filter of order 1 varies significantly. The difference between the maximum and minimum values of this magnitude within one cycle exceeds a threshold which is set

as a percentage of the corresponding magnitude obtained using the order-20 Kalman filter.

Considering Figure 4.9, the deviation factor, DF is defined as:

$$DF = \frac{V_{P1} - V_{P2}}{1 - V_{P0}} \cdot 100\% \tag{4.1}$$

V_{P1} is the minimum value of voltage magnitude estimated using an order-1 Kalman filter cascaded with a low-pass filter (described in Chapter 2). V_{P2} is the maximum value of voltage magnitude in a window of one cycle that starts from the minimum voltage point P_1. V_{P0} is the minimum voltage magnitude in the same interval using an order-20 Kalman filter. The deviation factor DF is also calculated for the next two cycles. The same threshold is used for the three cycles, thus:

$$DF(i) \geq \delta_{DF} \qquad i = 1, 2, 3 \tag{4.2}$$

5. The initial drop of voltage is not the same for all the phases. The initial drop unbalance ID is calculated as:

$$ID = \frac{\max(|V_A - V_B|, |V_B - V_C|, |V_C - V_A|}{1 - \min(V_A, V_B, V_C)} \cdot 100\% \tag{4.3}$$

where V_A, V_B and V_C are the minimum voltage within the transition segment for the three phases estimated using the order-20 Kalman filter. The calculated initial drop unbalance must be higher than a threshold δ_{ID}:

$$ID \geq \delta_{ID} \tag{4.4}$$

Induction motor starting

The recording consists of two event segments. An example is given in Figure 4.10. The following conditions must be fulfilled:

1. The second event segment corresponds to a voltage drop that gradually recovers for all the phases, as in the case of transformer saturation.

2. The initial drop of voltage is the same for all the phases:

$$ID < \delta_{ID} \tag{4.5}$$

Points are taken from the estimated magnitude every one cycle, and the symmetry between the phases is also checked using these points.

3. The estimated magnitude using an order-1 Kalman filter and an order-20 Kalman filter do not differ significantly. Using the deviation factor DF:

$$DF(i) < \delta_{DF} \qquad i = 1, 2, 3 \tag{4.6}$$

An example is given in Figure 4.11, where it can be seen that the differences between the two estimators are minor.

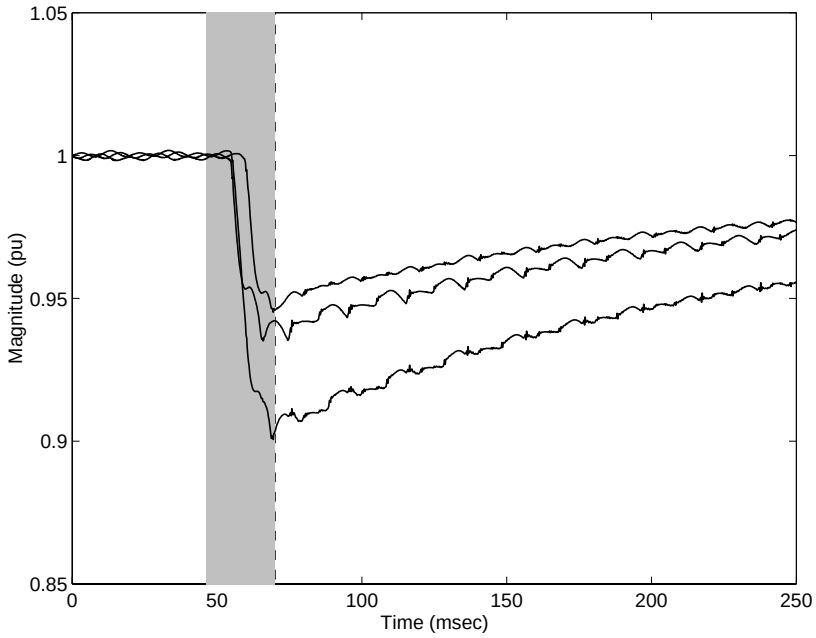

Figure 4.8: Transformer saturation: voltage magnitude and segmentation results (shadowed part: transition segment)

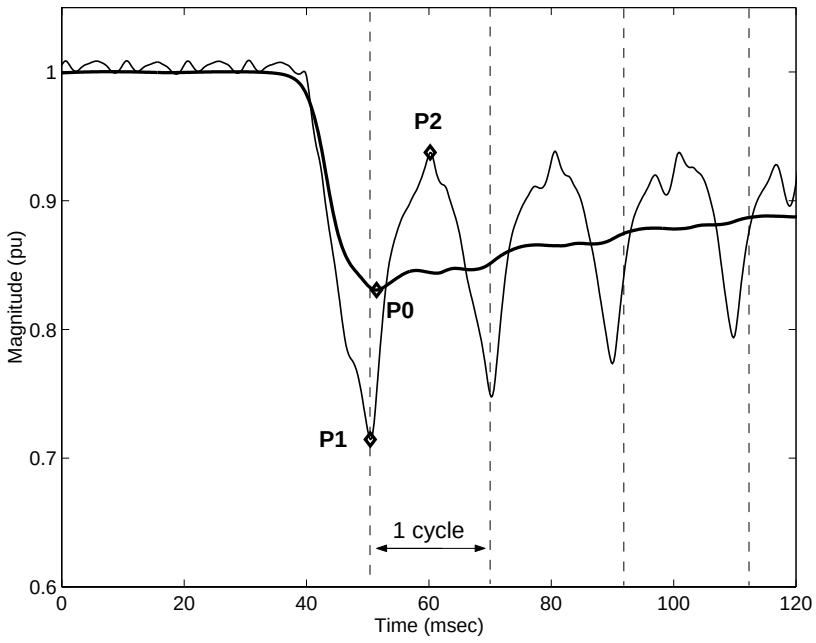

Figure 4.9: Deviation factor DF: estimated magnitude using order-1 Kalman filter (thin line) and estimated magnitude using order-20 Kalman filter (thick line)

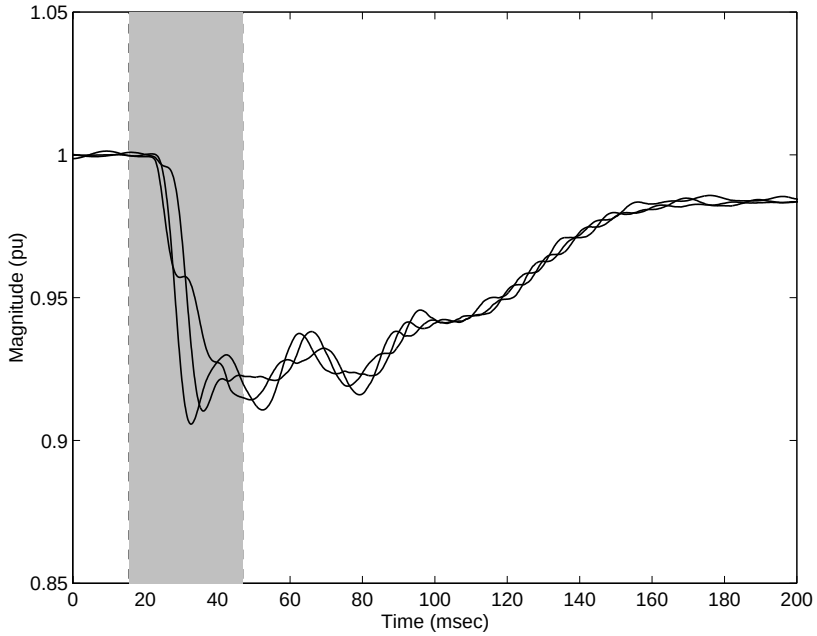

Figure 4.10: Induction motor starting: voltage magnitude and segmentation results (shadowed part : transition segment)

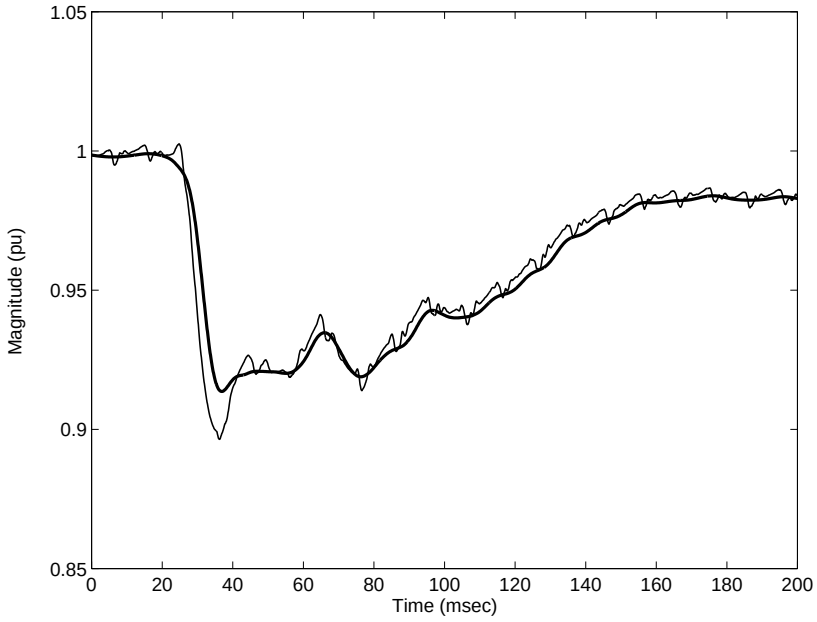

Figure 4.11: Deviation factor DF: estimated magnitude using order-1 Kalman filter (thin line) and estimated magnitude using order-20 Kalman filter (thick line)

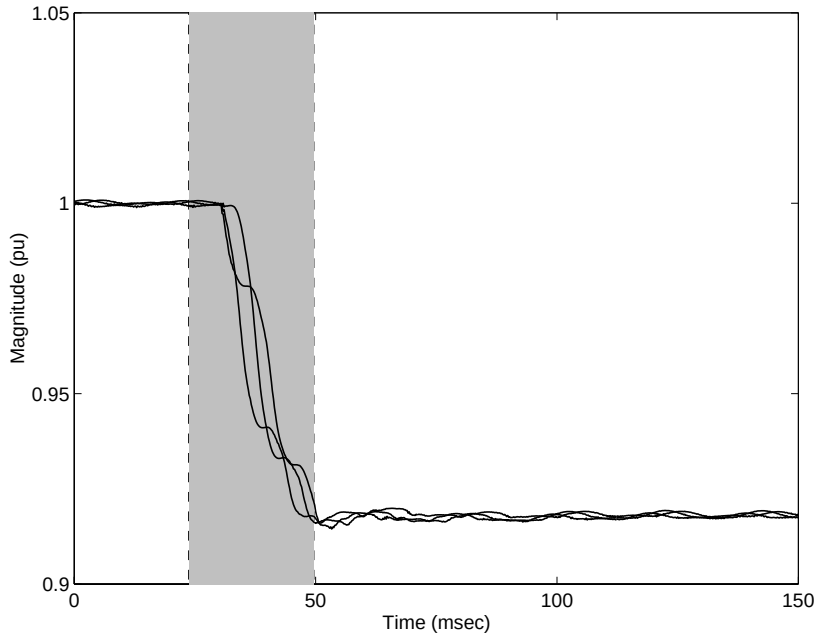

Figure 4.12: Step change: voltage magnitude and segmentation results (shadowed part: transition segment)

Step change

The recording consists of two event segments. An example is given in Figure 4.12. The transition segment is not a dip for any of the phases. The second event segment has either reduced or increased magnitude compared to the first event segment. The change is the same for all the phases (in sign and magnitude) and larger than 0.01 pu.

Transformer saturation and protection operation

The recording consists of three event segments where the middle event segment presents a voltage dip for at least one phase. An example is given in Figure 4.13. The first two event segments have the characteristics of transformer saturation (as described above). The second transition segment corresponds to protection operation and has increasing magnitude.

Single stage voltage dip due to fault

The recording consists of three event segments. An example is given in Figure 4.14. The magnitude of the middle event segment in the significant phase is below the 0.95 pu threshold. The first transition segment (fault initiation) of this phase has decaying magnitude, and the second transition segment (fault clearing) has increasing magnitude.

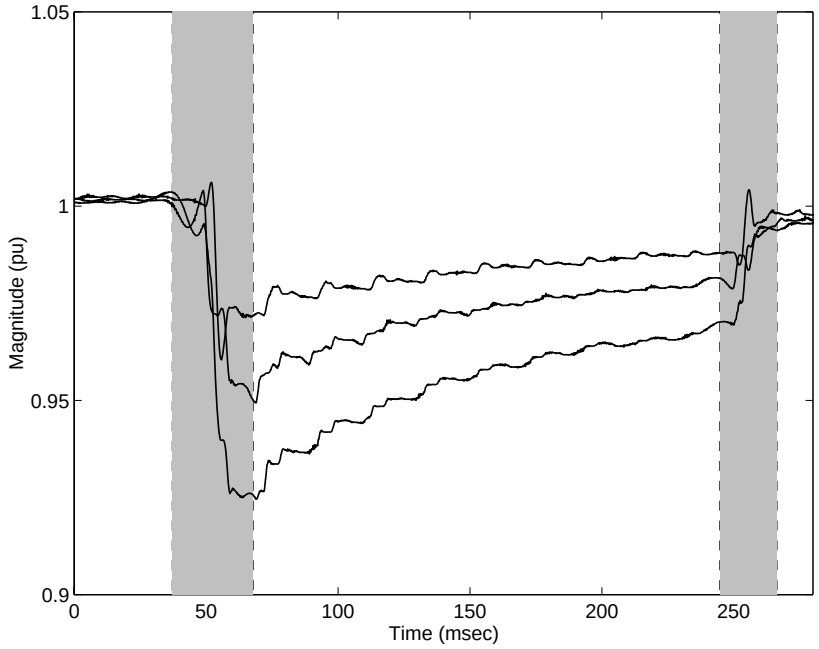

Figure 4.13: Transformer saturation followed by protection protection: voltage magnitude and segmentation results (shadowed parts: transition segments)

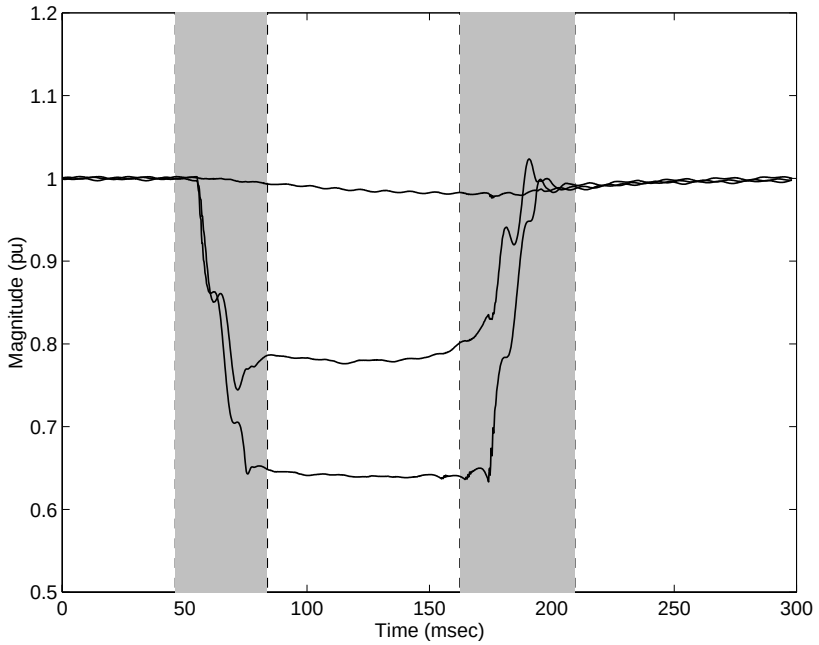

Figure 4.14: Single stage voltage dip: voltage magnitude and segmentation results (shadowed parts: transition segments)

Multistage voltage dip due to fault

The recording consists of more than three event segments. An example is given in Figure 4.15. The magnitude of the middle event segments of at least one of the three phases is below the 0.95 pu threshold. The first transition segment (fault initiation) of this phase has decaying magnitude, and the last transition segment (fault clearing) has increasing magnitude.

For multistage events, it must be determined whether the change in the magnitude of the dip is due to a system change or a fault type change. Based on the voltage dip characterisation method (Chapter 2), voltage dips can be classified into a number of different types, according to the fault that caused them. If during the dip the voltage dip type and the dip magnitude change, this is due to a change in the fault type. If the magnitude changes but the voltage dip type remains the same then the change is due to a change in the system as protection tries to clear the fault.

The number of stages is counted and the voltage dip type is found. If two consecutive stages have the same voltage dip type then the stage change is due to a change in the system while clearing the fault. If not, the change is due to a change in the fault type.

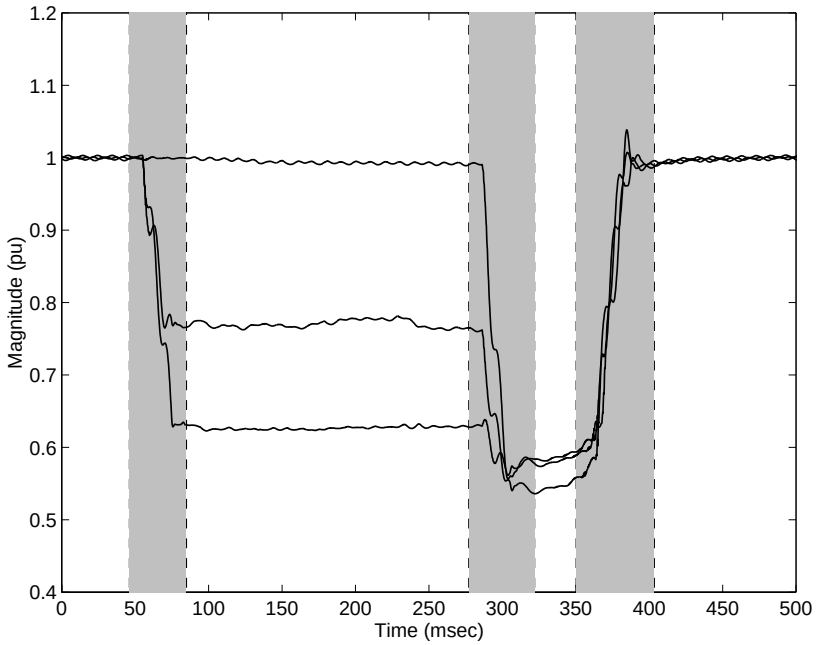

Figure 4.15: Multistage voltage dip: voltage magnitude and segmentation results (shadowed parts: transition segments)

4.6 Further Analysis: overvoltages

The Further Analysis module extracts information from the recordings like the voltage dip type (in case of single stage or multistage dips due to fault), the dip duration and the overvoltages that might be present.

The analysis of the measurements in terms of overvoltages is based on the segmentation and classification results. Overvoltages are found in the different segments of the measurement and the following cases are recognised (as explained in Chapter 2):

- Energising
  - Switching transients: overvoltage in the transition segment.
  - Harmonic overvoltages: overvoltage in the second event due to transformer saturation. segment
- Non-fault interruption: overvoltage in the transition segment (due to transformer saturation or current chopping).
- Transformer saturation: overvoltage in the second event segment (harmonic overvoltages).
- Step changes: overvoltage in the transition segment.
- Fault-related
  - Fault initiation: overvoltage in the corresponding transition segment.
  - Fault clearing: overvoltage in the corresponding transition segment.
  - Swell: overvoltage in the middle event segments.

Examples of these types of overvoltages can be found in Chapter 2. Figure 4.16 shows the segmentation results of three measurements that present overvoltages: two fault events and one step change.

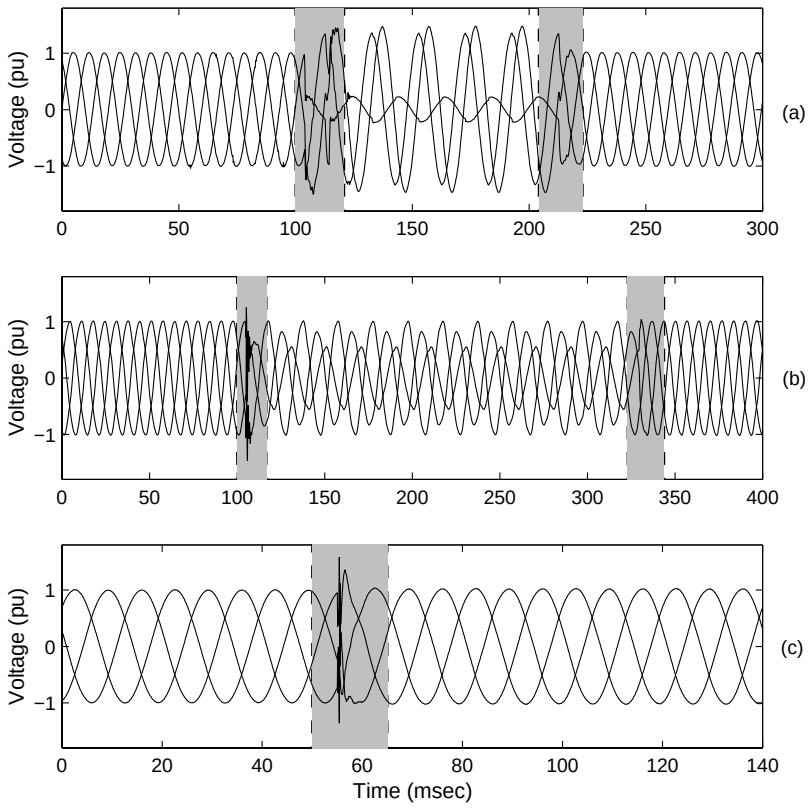

Figure 4.16: Voltage waveforms and segmentation results for (a) Fault-induced voltage dip with overvoltage during the fault (swell) (b) Fault-induced voltage dip with overvoltage during fault initiation (c) Step change with overvoltage (shadowed parts: transition segments)

4.7 Performance evaluation

4.7.1 Thresholds

The classification method presented above is based on segmenting the voltage signals. The output of the segmentation procedure not only provides the segments from which information is extracted but also creates subclasses of events considering the number of segments in the recording. Not considering events that contain zero voltage parts, there are events with only one transition segment (transformer saturation, induction motor starting, step change) and with two transition segments (transformer saturation followed protection operation, single stage dip due to fault). More than two transition segments are only present in multistage voltage dips due to faults. The extraction of features becomes important for correct classification within these subclasses.

For the class of events with one transition segment, the main challenge for the expert system is to distinguish transformer saturation events from motor starting events. A step change (the third item in this subclass) does not present a voltage dip hence it is easier to recognise.

For the subclass of events with one transition segment, some features are relatively easy to extract. For example the trend; increasing or decreasing. However other features are more difficult to extract. Transformer saturation is identified through the difference between the two Kalman filters, and the three phases present dips of different magnitude. Therefore, two thresholds must be set for these two features (δ_{DF} and δ_{ID}). These thresholds must be set considering transformer saturation and motor starting measurements.

Motor starting dips were not available however statistics are obtained for transformer saturation cases. Figure 4.17 shows statistics on the deviation factor DF obtained using transformer saturation measurements of one month of monitoring in a medium voltage network. The significant phase is used for the calculation of DF. DF is used for the first three cycles after transformer saturation starts. Statistics are shown for each cycle separately. It can be seen that DF obtains high values for the first three cycles, well above 50 %.

Figure 4.18 shows statistics on the initial drop ID obtained using the same transformer saturation measurements. ID, being a measure of the asymmetry between the phases during transformer saturation, is always above 20 %. An issue that rises at this point is to what extend the unbalance between the phases of the system could influence the initial drop and consequently the ability of the system to identify whether an event is symmetrical or not. The data presented here do not present significant unbalance. However, in the presence of high unbalance in the system the symmetry between the phases might not be a reliable feature for classification. In such a case (of high unbalance) the symmetry criterion can be omitted, and distinguishing between the two events (transformer saturation and motor starting) can be based entirely on the deviation between the fast and the slow magnitude estimators.

Another feature that could be used to distinguish transformer and motor start-

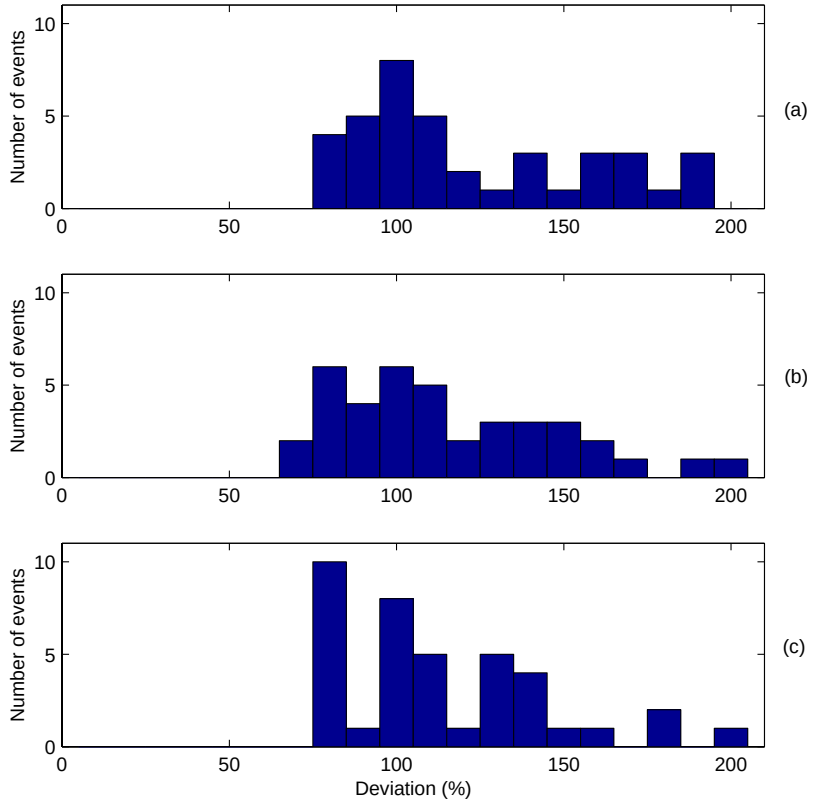

Figure 4.17: Statistics on the deviation factor DF for transformer saturation cases (a) first cycle (b) second cycle (c) third cycle)

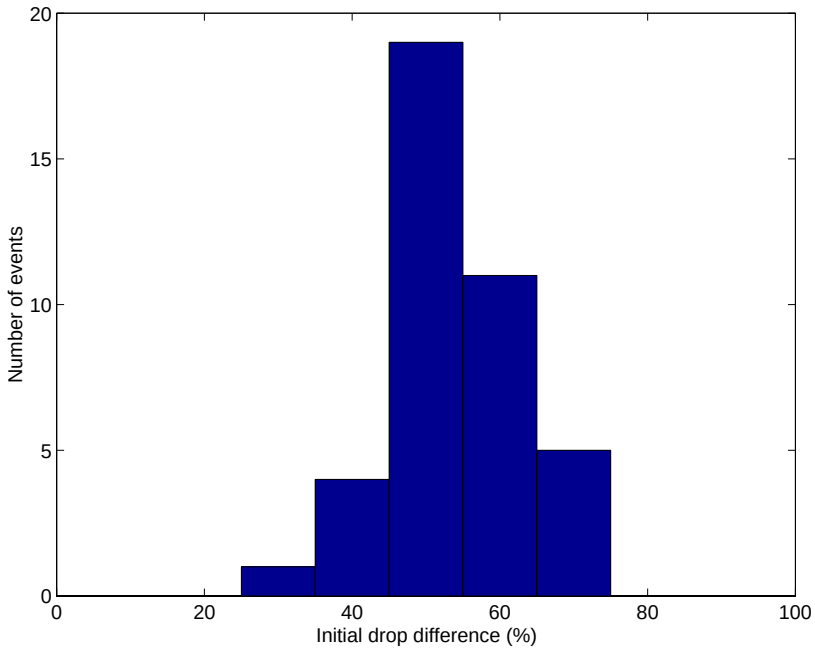

Figure 4.18: Statistics on the initial drop difference factor ID for transformer saturation cases

ing dips is the shape of voltage magnitude during voltage recovery. The available transformer saturation measurements show the magnitude of voltage in the second event segment is upwards convex. The magnitude of the recovering voltage in the available motor starting measurements is downwards convex.

Although there are no available motor starting statistics to compare with transformer saturation statistics, comparison can be made with single stage voltage dips for the deviation factor DF. This is important for the subclass of events with two transition segments (transformer saturation followed by protection operation and single stage voltage dips due to faults).

The statistics obtained from measurements of single stage voltage dips are shown in Figure 4.19. The measurements were obtained within the same time period and system as above. Single stage dips having magnitude above 0.80 pu are considered. In the opposite case the event cannot be transformer saturation hence distinguishing between the two classes becomes trivial. Comparing Figure 4.17 and Figure 4.19, the two cases can be clearly separated. Furthermore, these statistics show that there is no misclassification in the case of saturation during a fault (as explained in Chapter 2). A number of single stage voltage dips due to faults present this phenomenon, however DF is low for these cases. Note that the significant phase is used for the calculation of DF.

One more characteristic of the transformer saturation is the gradual voltage recovery unlike fault-induced voltage dips where voltage recovery is sudden upon fault clearing. Statistics on the cycle-by-cycle increase on the same group of transformer

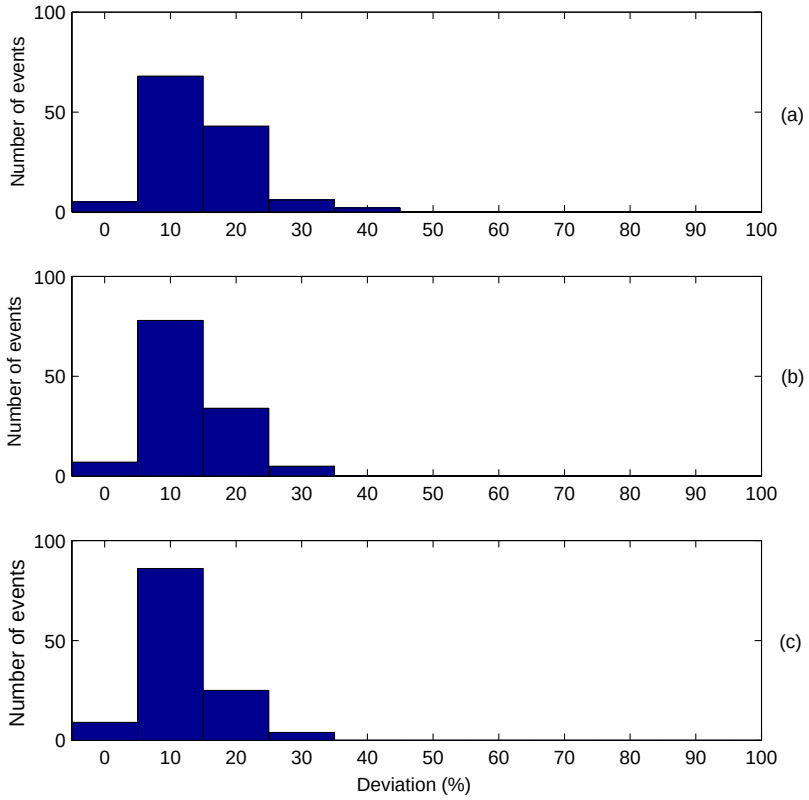

Figure 4.19: Statistics on the deviation factor DF for single stage voltage dips due to faults (a) first cycle (b) second cycle (c) third cycle

saturation measurements are shown in Figure 4.20. The significant phase is considered and the maximum cycle-by cycle increase in the second event segment is obtained for each measurement. Most of the events have a cycle-by-cycle increase less than 0.01 pu.

The thresholds set according to the above presented statistics are given in Table 4.1.

Table 4.1: Thresholds

Deviation factor (DF)	$\delta_{DF} = 60\%$
Cycle-by-cycle increase	$\delta_{cbc} = 0.05pu$
Initial drop (ID)	$\delta_{ID} = 20\%$

4.7.2 Testing of the expert system

The system has been applied to analyse measurements from a medium voltage network (33 and 11 kV). The measurements were obtained in a two-month period. The first month of measurements is used for setting the thresholds of the expert system

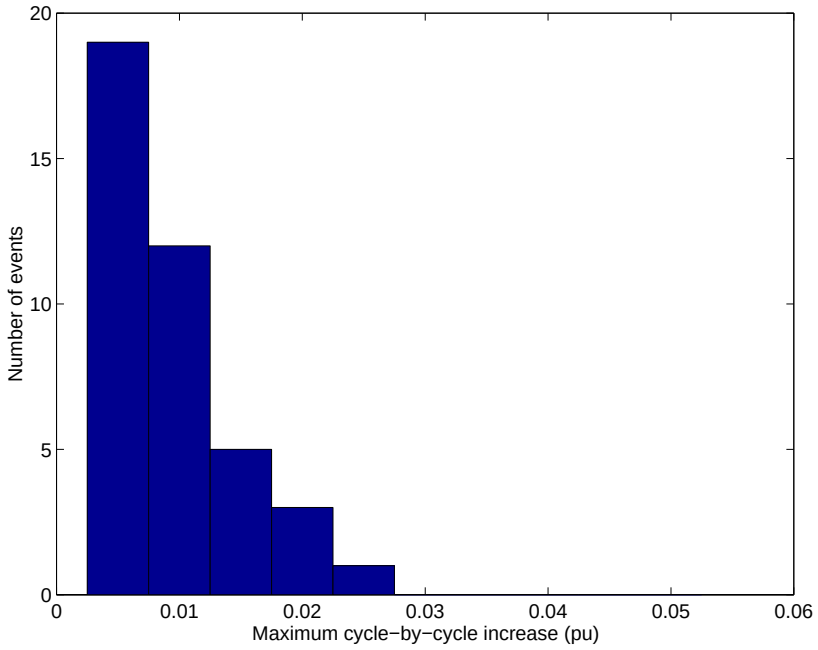

Figure 4.20: Statistics on the maximum cycle-by-cycle increase for transformer saturation cases

shown in the previous section. The data were captured using 90 fault recorders and the triggering was both on current and voltage disturbances. Severe voltage dips due to faults were captured by more than one fault recorder.

The classification results are given in Table 4.2. Further analysis results are also given: Table 4.3 gives the results of the analysis in terms of overvoltages; Table 4.4 the results of analysis of the single stage voltage dips due to fault in terms of the characterisation method presented in Chapter 2.

The class transformer saturation-reclosure is obtained by using system information: these events are non-rectangular voltage dips that take place within a certain time (10 sec) after a fault clearing operation.

Considering the records of the company that offered the data, verification was possible for 159 cases of faults (fault interruptions, single stage and multistage dips) and 37 reclosing operations after a fault leading to transformer saturation. No information was available regarding multistage dips and the cause of the changes in the magnitude.

Only 3 % of the recordings could not be classified by the system. These recordings (grouped as non-classified) are either voltage dips where no stage is found or overvoltages that do not cause a step change in the fundamental voltage.

Table 4.2: Classification results

Events	**Total number of events = 962**		
Energising	104		
	Fault		**Non-fault**
Interruption	13		88
	Reclosure	**Other type**	**Protection operation**
Transformer saturation	37	82	6
	Increase		**Decrease**
Step change	15		21
Single stage dip due to fault	455		
	Fault change		**System change**
Multistage dip due to fault	56		56
	Short duration dip		**Overvoltage**
Other,non-classified	16		13

Table 4.3: Further analysis results: voltage dip type (single stage dips only)

Single stage dip due to fault						
A	**Ca**	**Dc**	**Cb**	**Da**	**Cc**	**Db**
55	55	63	55	59	64	104

Table 4.4: Further analysis results: overvoltages

Analysis of overvoltages			
Energising (switching transient)	17		
Non-fault interruption	49		
	Harmonic overvoltage		
Transformer saturation	7		
	Increase		**Decrease**
Step change	13		6
	Start	**Swell**	**Clearing**
Fault related	10	86	8

4.7.3 Performance aspects

Segmentation

Apart from the group of thresholds discussed before regarding feature extraction, another group of thresholds is used by the segmentation schemes. The settings of the segmentation algorithms are given in Chapter 3. The selection of these thresholds is a trade-off between sensitivity and false alarms.

The thresholds of the segmentation algorithm based on the Kalman filter residues were set with respect to rectangular voltage dips (sudden changes larger than 0.05 pu). However, the tests showed that correct segmentation is also achieved in the case of transformer saturation. Also, for step changes, the segmentation algorithm is able to reveal the point of change even if the change is of low magnitude. Measurements classified as step change contain changes in magnitude between 0.01 pu and 0.09 pu. Finally, segmentation is trivial for cases such as energising and non-fault interruption.

The performance of the segmentation algorithm is limited only in a few cases where step changes (lower than 0.05 pu) in the voltage magnitude were not captured by the segmentation algorithm. These small steps are usually due to protection operation. Therefore, multistage events might be classified as single stage and protection operation after transformer saturation might not be detected. The number of events which contain small changes in magnitude (and are not detected by the segmentation algorithm) is less than 2 % of the total number of recordings. For most of these cases it is not clear whether a change takes place or not.

Short duration voltage dips

Changes in the voltage magnitude which are close in time might not be detected as described in Chapter 2. This might be the case for faults that are cleared by fuse blowing or self-extinguishing faults. For short duration events a segmentation algorithm is applied that searches for stages of almost constant voltage magnitude. If a stage is found, then the event is classified as a single stage voltage dip due to a fault. Events for which segmentation is not possible are grouped in Table 4.2 as non-classified short duration dips.

For the measurements used for testing, this segmentation algorithm was applied to 38 cases (10 % of the single stage dips due to fault). These are measurements of voltage dips with duration less than 3 cycles. In 22 cases a stage was found and in 16 cases no stage was found (short duration dips).

However, even in the case where the segmentation algorithm for short events reveals a stage of voltage magnitude, this should be used with caution. Two examples are given next. In Figure 4.21, the voltage magnitude of the significant phase is shown for the case of a short duration dip found in the available measurements. Kalman filters of order 1 and 20 are used. The order-1 Kalman filter reveals a stage of almost constant voltage magnitude that indicates protection operation that forced voltage recovery.

Figure 4.22 shows the voltage magnitude of a measurement of a self-extinguishing fault. A stage of voltage is also revealed in the shape obtained by the order-1 Kalman filter. However, this stage in voltage followed by fast recovery is not due to protection because the fault is self-cleared. Additionally, inspection of the voltage waveforms for this event (Chapter 2) shows that the fault extinguishes 1-2 msec after fault initiation. The almost constant magnitude stage of the voltage dip shown in Figure 4.22 is significantly longer therefore it does not correspond to the voltage during the fault.

It is interesting to notice that in the case of the self-extinguishing fault the voltage magnitude during recovery is almost the same for both estimators, unlike the case of Figure 4.21 where the differences are significant. In the case of self-extinguishing faults the recovery is slow, thus the difference in the speed of the two estimators is insignificant.

These two examples show that for short duration events more information is needed for correct classification. The limitations of the magnitude estimators impose a limitation on the extraction of features and consequently on the performance of the expert system.

Close-up three-phase faults

A three-phase fault forces the voltage of the fault point to zero for all three phases. Consider a monitor which is placed at the faulty feeder close to the fault point and at the line side of the circuit breaker that opens to clear the fault. In this case the captured voltage signature will be the same with the one during non-fault interruption. Therefore the event will be classified as a non-fault interruption followed by energising. Such case was not found in the measurements used for testing.

Additionally, for events that contain zero voltage parts, event segments of voltage magnitude below 0.10 pu are discarded. Interruptions might cause transformer saturation or current chopping which produce very distorted waveforms and the segmentation algorithm does not provide correct results (Section 4.5). Therefore, for three-phase faults that cause a drop in voltage below 0.10 pu, the expert system cannot distinguish between fault and non-fault interruptions. A possible solution to this problem is to use information from nearby monitors: at the same time with the event in question, nearby monitors will capture a three-phase voltage dip.

Finally, it is important to realise that for the classification procedure all the different stages of the event must be captured by the monitor. If, for example, the monitor does not capture the voltage recovery after fault clearing, then classification is not possible.

4.8 Applications of the system

The proposed expert system can be used for:

- Event statistics

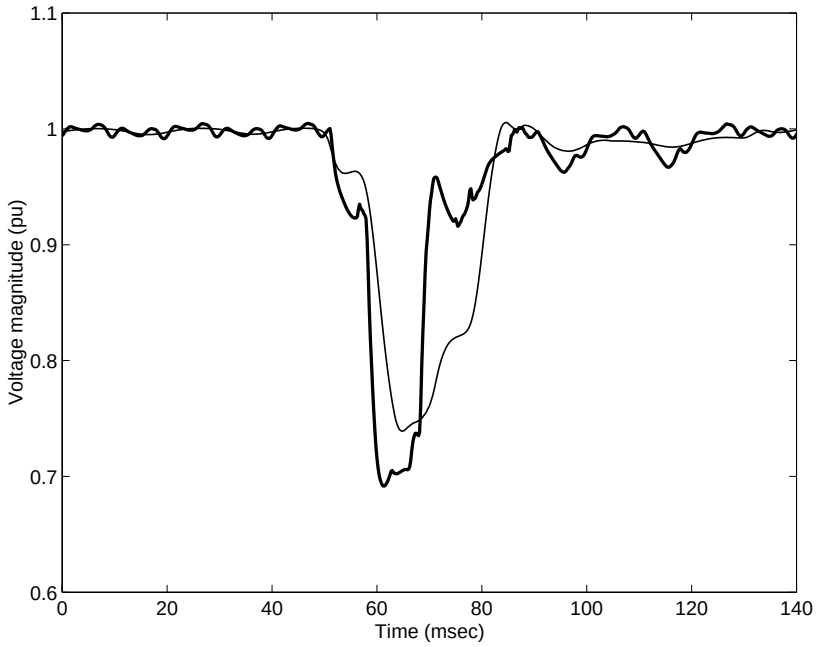

Figure 4.21: Short duration event: voltage magnitude estimated with order-20 Kalman filter and order-1 Kalman filter (thick line)

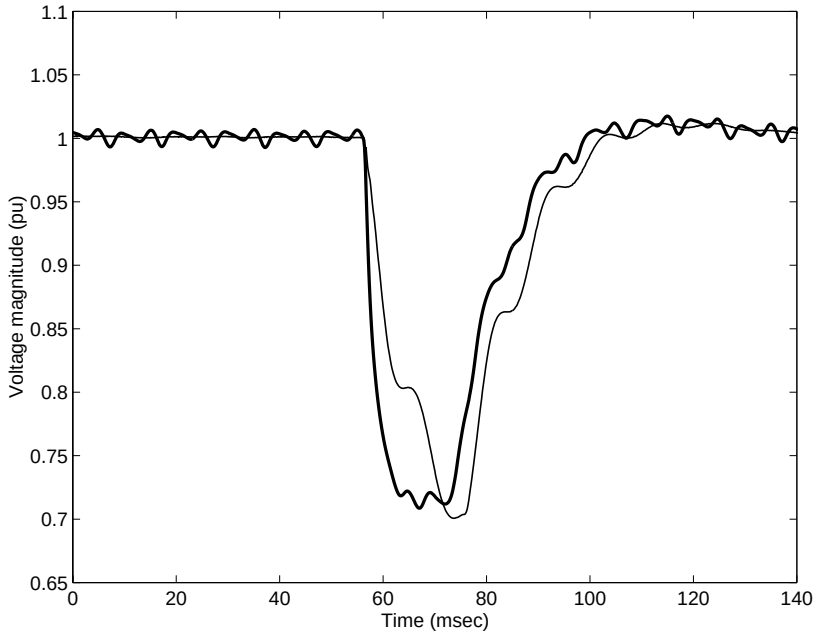

Figure 4.22: Self-extinguishing fault: voltage magnitude estimated with order-20 Kalman filter and order-1 Kalman filter (thick line)

- Automatic analysis of voltage dips and overvoltages
- Evaluation of the protection system

Event statistics, automatic analysis of voltage dips and overvoltages

The expert system can be used for in-depth analysis of power quality measurements not in terms of disturbance classification (dip, swell etc) but in terms of event classification. Event classification reveals the origin of a disturbance therefore better understanding of the system's performance can be obtained.

Additionally, the description of the events becomes more accurate. A voltage dip is presented in the statistics with its magnitude and duration using the assumption that the rms voltage has a rectangular shape. As magnitude is taken the minimum rms value of the recorded voltage and the duration is the time that the rms voltage is below a threshold. For events which are non-rectangular (transformer or motor events) or present different stages of voltage magnitude (multistage dips), the above assumption is not valid. The classification of the measurements into different types of events is the first step towards a better description of the collected data.

Multistage dips and transformer events are significant parts of the captured events. The results of Table 4.2 show that in two months of operation of a distribution network:

1. Fault-induced events (single stage dips,multistage dips, fault interruptions) are 60 % of the recordings that contain either a 0.05 pu change in the magnitude, or voltage above 1.05 pu.

2. Transformer saturation events are 13 % of these measurements.

3. Multistage dips are 18 % of the fault-induced events.

The system also offers information regarding the nature of multistage events (system or fault change) and faults in general (Table 4.2 and Table 4.3). Additionally, overvoltages are linked with the underlying events (Table 4.4) and potentially dangerous cases can be automatically identified.

After classification, statistics can be obtained for each event separately. Figure 4.23 shows statistics on the single stage voltage dips due to faults, as found in the data used for testing the expert system. For each event the minimum voltage dip is found and the time that the voltage magnitude is below 0.95 pu. Each phase is considered separately and only dips with magnitude below 0.90 pu are plotted. It can be seen that the majority of dips are of duration less than 10 cycles and of magnitude above 0.50 pu. These dips are typically due to faults on transmission level [6]. Voltage dips of longer duration (typically due to faults in distribution level) are less severe with a few exceptions.

Magnitude and duration, although generally accepted for describing rectangular dips, is not accurate for events like transformer dips. One possible way to describe transformer dips is the minimum dip and the half-life constant: the time it takes for

the voltage magnitude to increase by half the voltage difference between its minimum voltage and the final value of voltage. Figure 4.24 shows statistics on voltage dips due to transformers, as found in the data used for testing the expert system. The order-20 Kalman filter has been used for estimation of voltage magnitude. Each phase is considered separately. Dips with magnitude below 0.95 pu are considered. Transformer dips are in general shallow and there is no obvious relationship between the minimum dip and the duration. The same group of measurements is used for the statistics presented in Chapter 2.

Evaluation of the protection system

The expert system can be the basis for evaluating the performance of the protection system in terms of time and co-ordination. The data obtained by fault recorders can be used to:

- find transitions in the voltage signals that correspond to fault initiation and fault clearing, and then compare them with the information obtained by the circuit breakers in order to find whether the system operated as expected [75].
- discard events that are not fault-related, such as transformer saturation or induction motor starting.
- identify cases of protection malfunctioning. This could be the case of transformer saturation followed by protection operation.

4.9 Conclusions

The increased requirements on supervision, control and performance in modern power systems make power quality monitoring a common practice for utilities. With the growth of the number of monitors installed in the system, the amount of data collected is growing, making individual inspection of all the waveshapes no longer an option. This chapter presents an expert system for automatic classification of power quality recordings. This expert system extracts all relevant information from the recordings, in an automatic way.

The main objective of the system is to distinguish between the different types of power system events according to their causes. The expert system considers events that present a considerable change in voltage. These events are mainly voltage dips (fault-induced, transformer saturation and induction motor starting dips) and interruptions (fault and non-fault) as explained in Chapter 2.

The suggested classification method is based on segmenting the voltage waveforms in points of sudden changes in the fundamental magnitude. The segmentation methods presented in Chapter 3 are used for this purpose. Based on the segmentation results a set of classification modules is utilised to classify the event. Classification is based on features extracted from the voltage waveforms. The magnitude of voltage and its characteristics are the most important features.

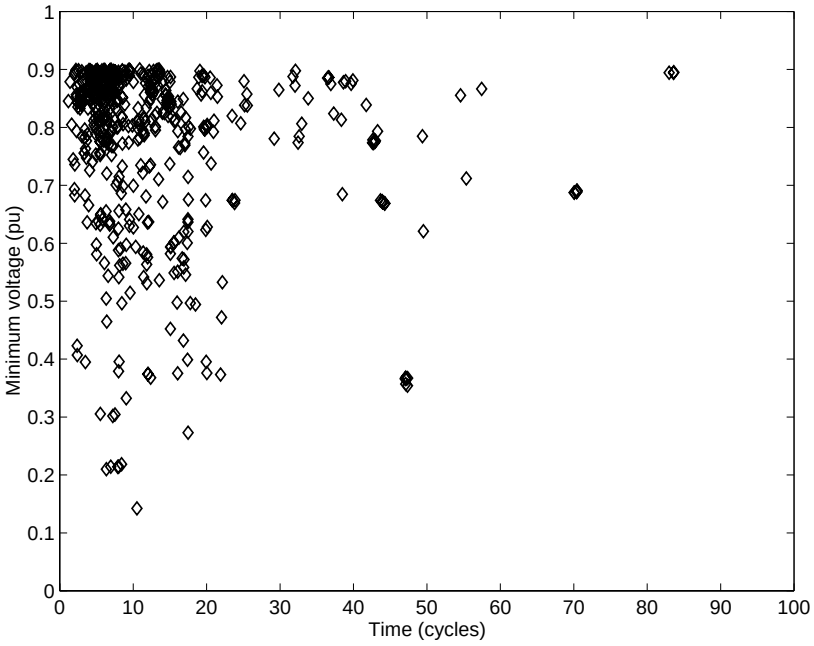

Figure 4.23: Statistics on the single stage voltage dips due to faults

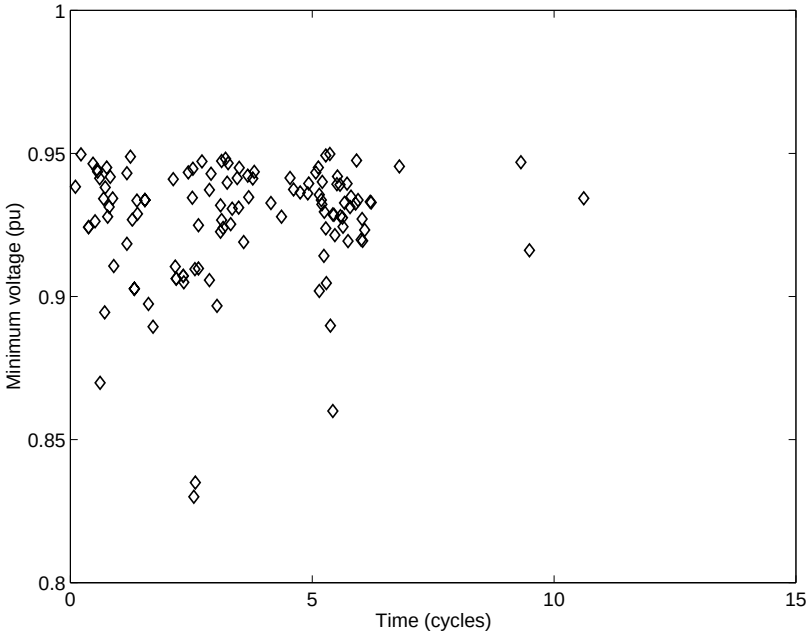

Figure 4.24: Statistics on voltage dips due to transformers

The system is used to analyse measurements from a medium voltage network. The results showed that the system successfully classifies the largest part of the recordings into a number of classes. The results also verify that the segmentation-based approach is suitable for the classification of power system events that present significant changes in the fundamental frequency magnitude. This approach also provides the means for introducing new events to the expert system as long as these new events present identifiable changes in the voltage magnitude.

Analysis of the features and the corresponding thresholds is presented for the case of transformer saturation. It is shown that the features extracted for identifying transformer saturation are reliable. For the case of induction motor starting, analysis was not possible due to insufficient number of measurements.

Several aspects regarding the performance of the system are also presented and discussed. The major problem arises in the cases of short duration events where the time resolution provided by the magnitude estimators is not adequate for extracting the required features.

The expert system enables fast and accurate analysis of large databases and classification of the recordings according to their origin. Event classification (instead of disturbance classification) offers the means for better understanding and description of the operation of the system in terms of voltage dips and overvoltage analysis. Other possible applications can be the evaluation of the protection system performance.

The results of the testing of the expert system show that multistage and transformer dips are a significant part of the captured events.

Chapter 5

Automatic Classification of Power System Events using rms Voltage Measurements

5.1 Introduction

Power quality monitors in the occasion of a disturbance can either save the actual voltage waveform that contains the event or the corresponding rms values. The later option combined with updating the rms with a time interval, reduces significantly the memory needed for saving the event. Several issues arise regarding this type of monitoring: to what extend can the discrete rms voltage be useful, what kind of information can be obtained by it and which information is lost when a monitor saves the discrete rms voltage instead of the actual voltage waveforms.

This chapter shows that even with rms monitoring the measurements can be analysed in depth. A method is proposed for automatic classification of power system events using rms voltage measurements. The method is similar to the classification method presented in Chapter 4. The classification system is tested with measurements from a distribution network and the results show that classification is possible for the considered types of events. Finally, the limitations of this type of monitoring are discussed.

5.2 Calculation of rms: discrete and continuous

Rms (voltage or current) is a quantity commonly used in power systems as an easy way of accessing and describing power system phenomena [6, 36]. The rms values can be computed each time a new sample is obtained, but generally these values are updated each cycle or half cycle, thus the required memory is significantly reduced. If

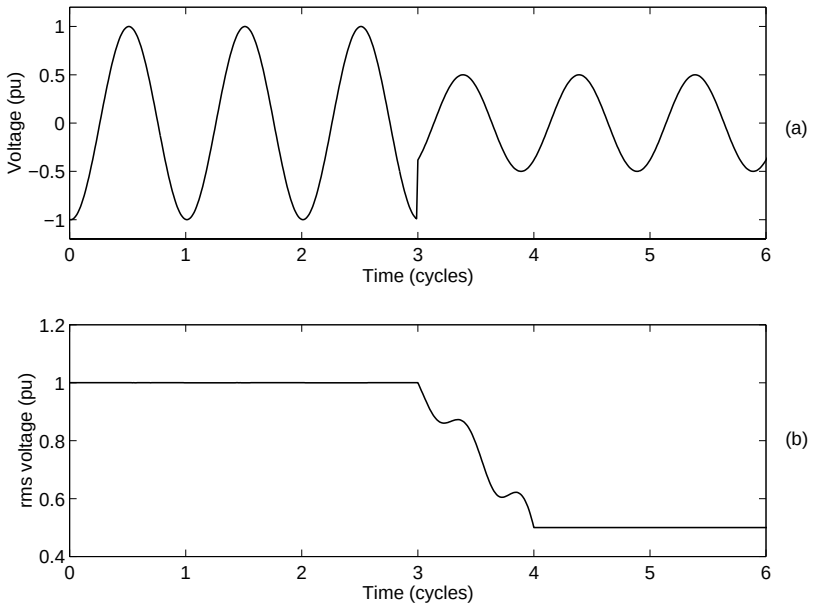

Figure 5.1: (a) Step change in voltage (b) the corresponding continuous rms voltage

the rms values are updated every time a new sample is obtained, then the calculated rms series is called *continuous*. If the updating of rms is done with a certain time interval, then the obtained rms is called *discrete*.

Rms is defined for periodic signals although it is generally used to extract information from power system disturbance measurements which are non-periodic. In case of a transition, the computed rms does not give the correct value for the new state until the window over which the rms is calculated contains only samples of the new state. This can be seen in Figure 5.1. Figure 5.1b shows the calculated continuous rms voltage of a sudden step change in the amplitude of the voltage shown in Figure 5.1a. Although the change is sudden, it takes one cycle for the rms to reach the correct new value. This is important if the measurement under analysis contains changes in voltage that are close in time (closer than one cycle).

The discrete rms voltage has the same properties: the rms value calculated within a window that contains both pre-event and post-event samples will give an rms value which is normally between the previous and the new rms voltage.

5.3 Automatic classification of rms voltage measurements

The automatic classification system proposed for event classification considers discrete rms voltage measurements where the time interval between two rms values is one cycle. The classification approach is similar to the one described in Chapter

4 and tailored to use only rms voltage measurements. Seven types of events are considered here:

(a) Energising

(b) Non-fault interruption

(c) Fault interruption

(d) Transformer saturation

(e) Induction motor starting

(f) Step change

(h) Fault (single stage dip or multistage dip)

The rms signatures of the above mentioned events are used as the features for classification. These events present a distinctive rms signature as described in Chapter 2. Classification of these events is done by considering the changes in the voltage magnitude, the way that voltage recovers after a dip, and the relationship between the phases.

5.3.1 Segmentation of recordings of rms voltage

The classification strategy is based on separating the computed rms values into event and transition segments as in the case of using the actual voltage waveforms.

Transition segments correspond to abrupt changes in voltage magnitude. Regarding the above mentioned events, these abrupt changes are caused by fault initiation, fault clearing by protection operation and other switching actions like induction motor starting, transformer energising, reclosing actions following fault clearing, load switching, capacitor switching etc. as described in Chapters 2 and 3.

Detection of changes is based entirely on the changes in rms magnitude. The segmentation is done using a detection index, di_{rms}, which is obtained by calculating the differences between two consecutive values of the rms voltage, u_{rms}:

$$di_{rms}^{phase}(n) = \mid u_{rms}^{phase}(n+1) - u_{rms}^{phase}(n) \mid \quad n = 1, \ldots, L-1 \tag{5.1}$$

where L is the number of available values of rms voltage for each phase. One detection index is calculated for each phase. The detection index used for segmentation is obtained by selecting the maximum value among the three detection indices for each cycle:

$$di_{rms}(n) = max(di_{rms}^{\mathrm{a}}(n), di_{rms}^{b}(n), di_{rms}^{c}(n)) \quad n = 1, \ldots, L-1 \tag{5.2}$$

Segmentation is done under the following conditions:

- If $di_{rms}(n) \geq \delta$ then point n belongs to a transition segment.

- If $di_{rms}(n) < \delta$ then point n belongs to an event segment.

Transition segments end with the first point for which $di_{rms}(n) < \delta$ after transition is detected.

The value of di_{rms} depends not only on the magnitude of the change in the voltage but also on the position of the window used for the calculation of the rms voltage as explained before. For our tests δ was set to 0.02 pu. This threshold normally is adequate for detecting fast changes in the voltage magnitude which are larger than 0.04 pu. Notice that for a fast change in the voltage magnitude of 0.04 pu, the discrete rms will capture a change at least 0.02 pu (half of the actual change). That is the case for a window that contains equal amount of pre-event and post event voltage samples, i.e. the center of this window is exactly at the point of change). For any other position of this window, the captured rms change will be larger than 0.02 pu.

Figure 5.2a shows the results of the segmentation method to rms voltages calculated using a measurement in a distribution system. The voltage presents three different stages of magnitude. The corresponding detection index is shown in Figure 5.2b. The transition segments 1 and 4 correspond to fault initiation and fault clearing. Transition segments 3 and 4 correspond to two changes in the voltage dip magnitude. The dip is due to an evolving fault (single-phase fault becomes two-phase-to-ground fault and finally three-phase-to-ground fault). The segmentation scheme detects the sudden changes successfully. The number of transition segments is 4, and the number of event segments is 5. The transition segments duration are longer than one cycle due to the effect of the window, and due to the fact that changes in the different phases might not be simultaneous (an example is the fault clearing operation). The same measurement (the actual voltage waveforms) is used in Chapter 3 for testing the segmentation algorithm that is based on Kalman filtering. For this measurement, the results of both methods are similar.

As explained in Chapter 4, there might be more than one event in a recording, therefore the system separates the recording into groups of segments that start and end with segments for which all the phases have rms voltage above 0.95 pu, or zero (interruption).

5.4 Structure of the expert system

5.4.1 Classification strategy

The structure of the expert system is shown in Figure 5.3. The classification strategy of this system is similar to the expert system of Chapter 4. The system analyses recordings that present a change in the rms voltage larger than 0.05 pu. If more than one event exist in the recording, the classification procedure is repeated as many times as the number of events (ne) found using the multi-event segmentation, each time using the corresponding parts of the measurement.

As explained in Chapter 4, there are measurements that can be classified using the

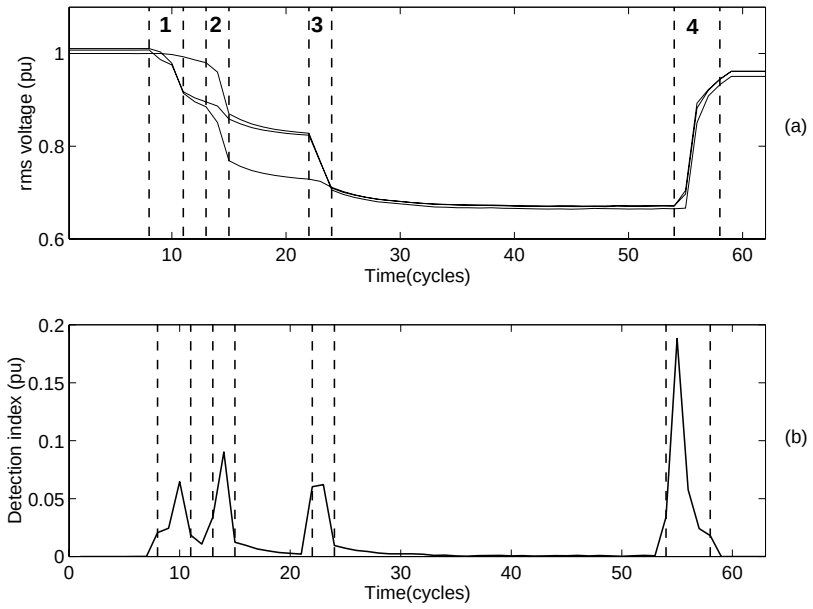

Figure 5.2: rms voltage segmentation (a) rms voltage and (b) detection index (vertical lines: segmentation results)

system data (protection time settings, scheduled switching operations). The classification procedure described in Figure 5.3 is used for the rest of the measurements. The classification procedure terminates when all the events within the recording are classified. The possible options for an event are checked according to whether the recording contains zero values or according to the number of segments. The procedure ends when the event matches with the characteristics of one of the events in the knowledge base of the expert system.

5.4.2 Rules

The rules of the system are described below.

Energising

The recording consists of two event segments. The first corresponds to zero voltage for all phases and the second one to normal voltage. Figure 5.4a shows the rms voltage signature of a measurement of this event in an 11 kV system and the segmentation results.

Non-fault interruption

The recording consists of two event segments from which the last one has or tends to zero voltage magnitude for all the phases. Segmentation results for parts of the signal

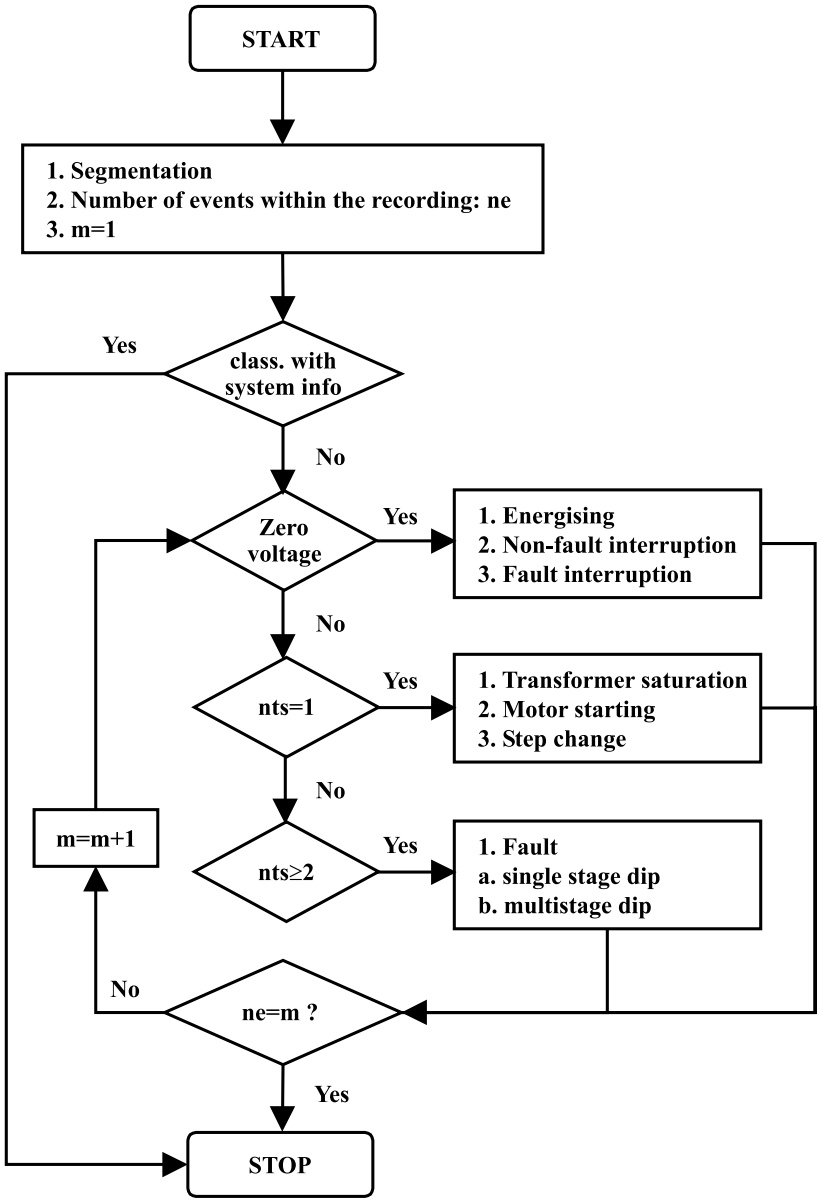

Figure 5.3: The structure of the classification system

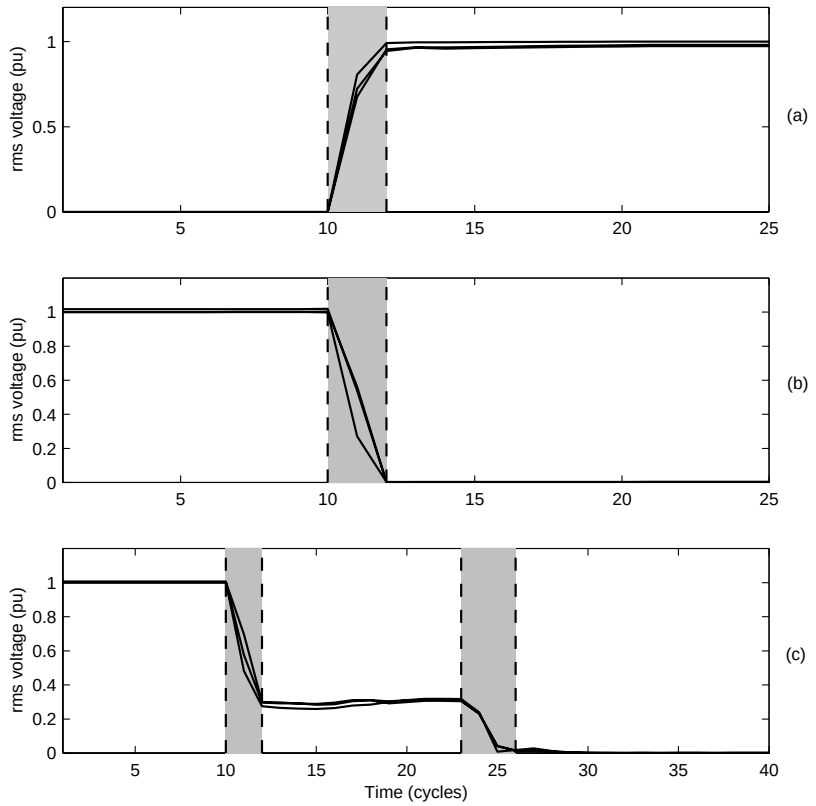

Figure 5.4: rms voltages and segmentation results (shadowed parts: transition segments) for (a) Energising (b) Non-fault interruption (c) Fault interruption

where voltage goes below 0.10 pu are ignored due to transients which might appear during interruption. Figure 5.4b shows the rms voltage signature of a measurement of this event in an 11 kV system and the segmentation results.

Fault interruption

The recording consists of two or more event segments from which the last one corresponds to zero voltage magnitude for all the phases. At least one of the middle event segments has magnitude between 0.95 pu and 0.10 pu. The first transition segment corresponds to fault initiation and the last transition segment to fault clearing. Figure 5.4c shows the rms voltage signature of a measurement of this event in an 11 kV system and the segmentation results. In this case, voltage for all three phases presents one stage of magnitude before fault clearing which leads to an interruption.

Transformer saturation

The recording consists of two event segments. The second event segment corresponds to a voltage drop that finally recovers for at least one phase. Figure 5.5a shows the rms voltage signature of a measurement of transformer saturation in an 11 kV system

and the segmentation results. The following conditions must be fulfilled for such an event:

(a) The second event segment (voltage recovery) should have gradually increasing magnitude. The increase between two consecutive values (first derivative) should not exceed a threshold (gradual increase). The phase that presents the most severe dip is used for these calculations.

(b) The initial drop of voltage is not the same for all the phases. The initial drop ID is calculated as in Chapter 3 for rms values, in order to decide whether the dip is symmetrical or not.

As shown in Chapter 2, high harmonic distortion during transformer saturation might be captured as an increase in the rms voltage contrary to the estimated voltage magnitude using the STFT or Kalman filtering which shows a decrease. For the available measurements of transformer saturation, in the case of high distortion, at least one phase shows a dip in the rms magnitude.

Induction motor starting

The recording consists of two event segments. The second event segment corresponds to a voltage drop that gradually recovers for all the phases. The initial drop of voltage is the same for all the phases. The initial drop ID is used as in the case of transformer saturation. The symmetry between the phases is also checked for all the values following the minimum voltage value. Figure 5.5b shows the rms voltage signature of a measurement of motor starting in a 400 V system and the segmentation results.

Step change

The recording consists of two event segments. The transition segment is not a voltage dip for any of the phases. The second event segment has either reduced or increased magnitude compared to the first segment. The sign of the change is the same for all the phases. Figure 5.5c shows the rms voltage signature of a measurement of a step change event in an 11 V system and the segmentation results.

Dip due to fault

There are two types of rms signatures related with fault-induced events. The first type is the single stage voltage dip. Figure 5.6a shows the rms voltage signature of a measurement of a single stage voltage dip in an 11 V system and the segmentation results. Such an event consists of three event segments. The magnitude of the middle event segment of at least one of the three phases is below the 0.95 pu threshold. The first transition segment (fault initiation) of this phase has decaying magnitude and the second transition segment (fault clearing) has increasing magnitude.

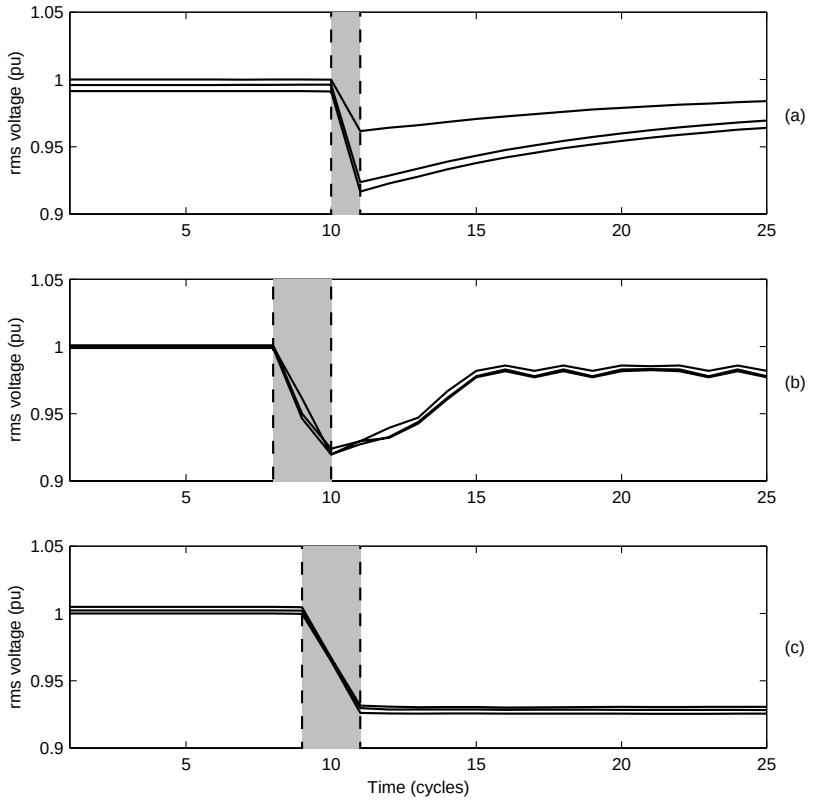

Figure 5.5: rms voltages and segmentation results (shadowed parts: transition segments) for (a) Transformer saturation (b) Induction motor starting (c) Step change

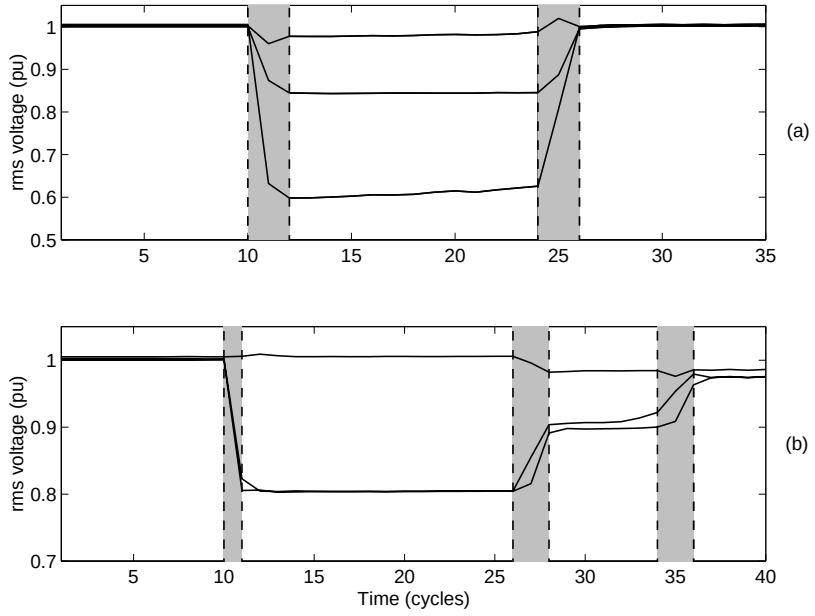

Figure 5.6: rms voltages and segmentation results (shadowed parts: transition segments) for (a) Single stage dip due to fault (b) Multistage dip due to fault

The second type of fault-induced events is the multistage voltage dip. Figure 5.6b shows the rms voltage signature of a multistage voltage dip in an 11 kV system and the segmentation results. Such an event consists of more than three event segments. The magnitude of the middle event segments of at least one of the three phases is below the 0.95 pu threshold. The first transition segment (fault initiation) of this phase has decaying magnitude and the last transition segment (fault clearing) has increasing magnitude.

5.4.3 Application of the classification system

The measurements used for testing the expert system of Chapter 4 are used also for testing of the rms classification system. The discrete rms is calculated first. As mentioned already only measurements which present a voltage change higher than 5 % are considered by the classification system. The same thresholds are used as given in Chapter 4 for the features that can be applied for rms measurements (initial drop, gradual increase, etc)

The results are given in Table 5.1. These results are compared with the results obtained with the expert system that utilises the actual voltage waveforms. The system is able to classify correctly 92 % of the data. Analysis of the results is given in the next section.

Table 5.1: Classification results using rms

Type of event	*Number of events*	*Classified correctly*
Energising	104	100%
Non-fault interruption	88	97%
Fault interruption	13	84%
Transformer saturation	125	88%
Step change	18	100%
Fault	567	91%

5.5 Performance aspects when using rms measurements

5.5.1 Short duration events

Time resolution problems might arise for short duration voltage dips due to the calculation of rms using a one-cycle window. As mentioned already, time equivalent to the length of the window is required for the rms to obtain the correct value after a change. If a second change takes place before that time interval, then the correct rms value will not be obtained. Additionally, the segmentation algorithm which is described above cannot detect the stage between two changes close in time. In the case of discrete rms, the problem is aggravated by the fact that the position of the calculation window is random, thus the error might be higher.

Discrete rms can be seen as sampling the continuous rms every cycle. Figure 5.7 shows the voltage waveform of a short duration dip (1.5 cycles), the continuous and discrete rms calculated using a window of one cycle. The duration of the dip is such that the continuous rms shows, as expected, a stage of constant magnitude (0.40 pu) and duration around one and a half cycles. For the discrete rms, not only the stage of voltage cannot be seen (thus segmentation of this event is not possible) but also the minimum voltage is 0.50 pu; different than the correct one as calculated by the continuous rms.

Figure 5.8 shows the maximum possible error that can appear when calculating the minimum voltage magnitude of short duration dips using the discrete rms. The error can be very large for short duration and severe dips. The maximum possible error is found using synthetic voltage dips by changing the position of the window for the calculation of the rms voltage.

Fault events which are not classified correctly by the rms classification system are short duration events where the segmentation method failed to capture the beginning and the end of the dip. These events are approximately 9 % of the total fault-induced events found using the expert system of Chapter 4.

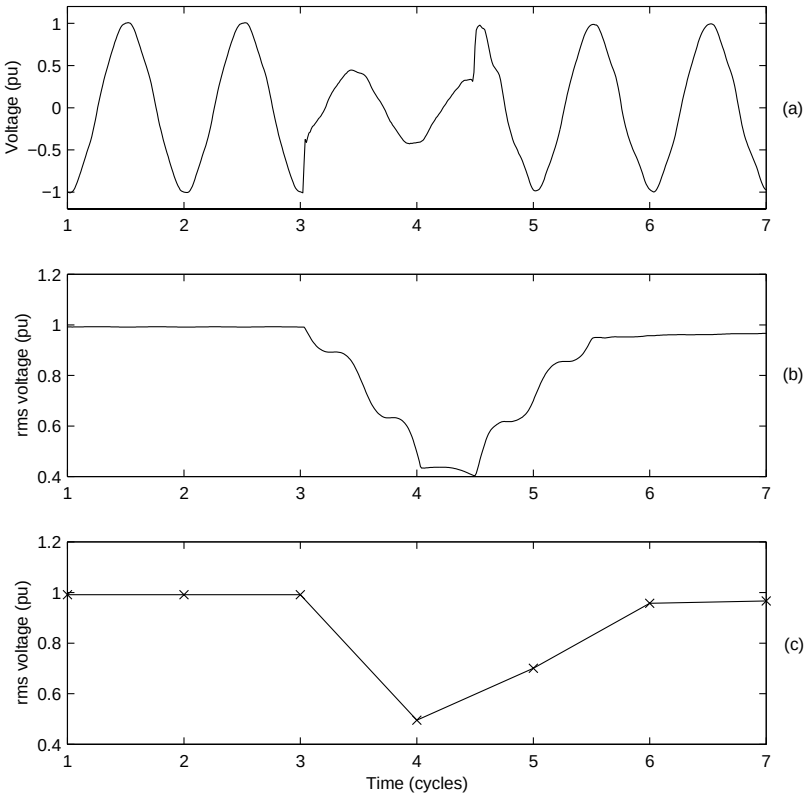

Figure 5.7: Measurement (a) Voltage waveform (b) Continuous rms (c) Discrete rms

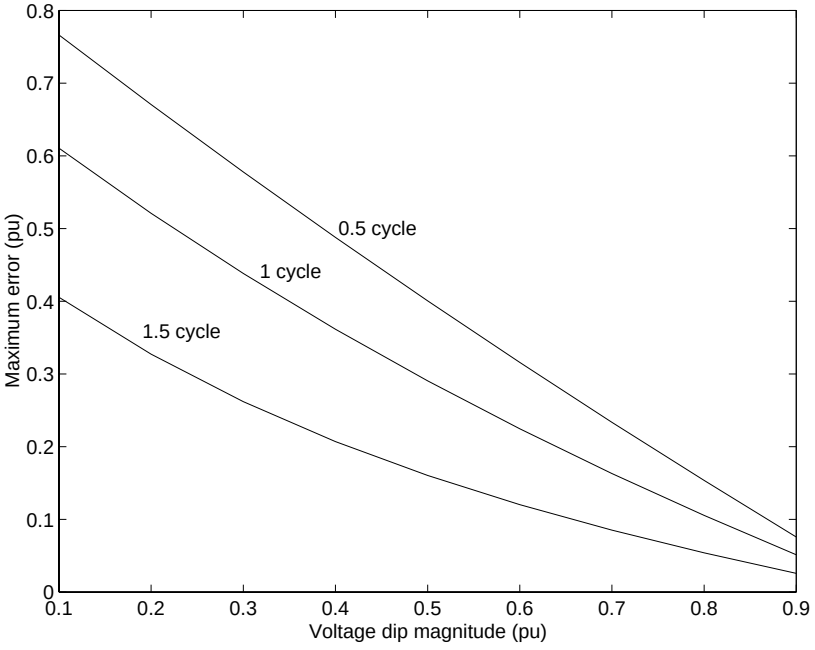

Figure 5.8: Error in calculating discrete rms voltage of short duration dips

5.5.2 Transformer saturation

If the actual voltage waveforms are available, additional information and features can be extracted for classification, for example the signature of transformer saturation during the event or the voltage dip type. Additionally, multistage dips can be further classified as fault change or system change dips if the voltage dip type is found. Short events are also more difficult to be analysed as shown in the previous section.

The use of rms voltage limits the amount of available information, however the results show that classification is possible. It must highlighted that, as in the case of the expert system of Chapter 4, motor starting dips were not available. Therefore, the system has not been tested for this type of event. It is not clear whether motor dips and transformer dips (which share similar characteristics) can be distinguished by considering only the rms signatures. Using rms voltage, the main difference of these two events is that transformer events cause asymmetrical dips and motor starting events cause symmetrical dips. Classification can be difficult based on this feature only, especially in the case of large voltage unbalance in the system.

Compared to the events considered by the expert system of Chapter 4, the above list of events does not contain the case of transformer saturation followed by protection operation and two classes for faults (single stage and multistage dips are in one class). The reason for not considering this class of events is the fact that the discrete rms voltage using one cycle for the calculation and as an interval does not provide the distinctive characteristic that can be obtained using a Kalman filter of order 1. Therefore, this event cannot be classified using rms measurements. Such an event gives an asymmetrical voltage dip that recovers like a fault-induced dip. Therefore, when rms measurements are used, this event is classified as a single stage voltage dip due to fault.

An example of this event is given in Figure 5.9. Figure5.9a shows the discrete rms voltage of a measurement in a distribution system, and Figure 5.9b the corresponding continuous rms calculated over a half cycle window. As explained in Chapter 2, this signature is characteristic of transformer saturation. However, unlike the typical transformer saturation dip that recovers gradually, this case shows a step change that brings the voltage back to normal. The discrete rms signature is not enough for identifying the event because it is similar to a single stage dip due to fault.

The distinctive signature of transformer saturation can be obtained even for discrete rms as long as the rms is calculated over a half-cycle window. Figure 5.10 shows an rms measurement of voltage in a 10 kV system using a half-cycle window for the calculation of the rms, and a half-cycle window for updating.

5.5.3 Segmentation

Segmentation using rms limits the possibilities for analysis of short duration events as shown in Section 5.5.1. For the analysed measurements this is only a small fraction of the data (10 % of the single stage dips due to fault).

The segmentation method used in this chapter is based on detecting sudden changes in the rms voltage. Compared to the segmentation algorithm based on

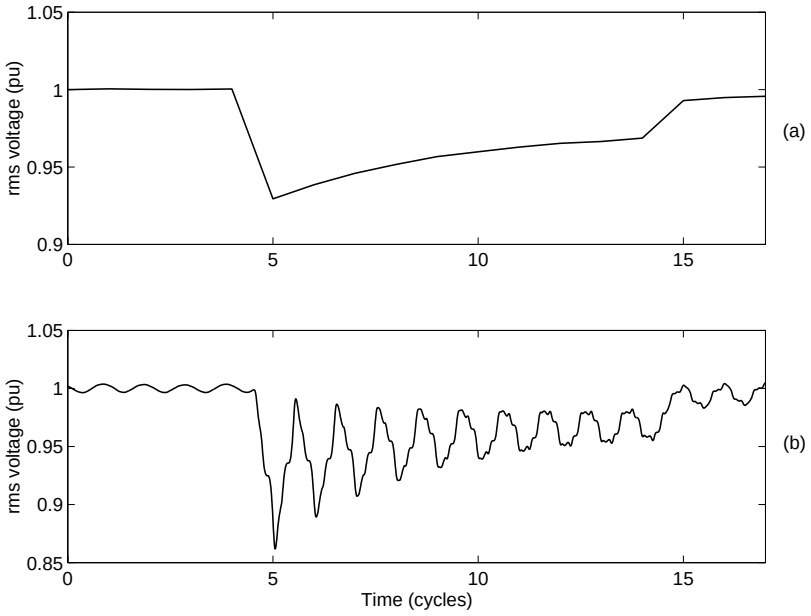

Figure 5.9: (a) Discrete rms voltage of a transformer saturation event followed by protection operation (b) Continuous rms of the same voltage measurement calculated over a half cycle window

Kalman filtering for cases other than short duration events, the rms segmentation offers reliable results similar to the results obtained using Kalman filtering. Differences were observed in a number of cases of voltage dips due to faults and transformer saturation.

However, the segmentation scheme using Kalman filtering is able to detect even small changes in the voltage magnitude if these changes are accompanied by high frequency transients. This is the case for some switching events like capacitor energising. Using the rms voltage, detection of small changes becomes difficult and a lower threshold δ must be used. However, a lower threshold δ increases the probability of false alarms. Therefore, step changes of magnitude less than 0.05 pu are not considered by the rms classification scheme.

For 10 % of the total number of fault-induced dips, the two segmentation algorithms provide different results however the event is not incorrectly classified in terms of whether is a fault or not, but in terms of whether the event is multistage or not. An example is given in Figure 5.11. The rms segmentation detects three changes in voltage because the rms magnitude during the fault varies. The segmentation algorithm based on Kalman filtering does not detect this middle stage. Therefore, this event is classified by the expert system of Chapter 4 as a single stage dip, but by the system of this chapter as multistage. In other cases multistage events are classified as single stage events when rms voltage is used because one stage is of short duration and is not revealed.

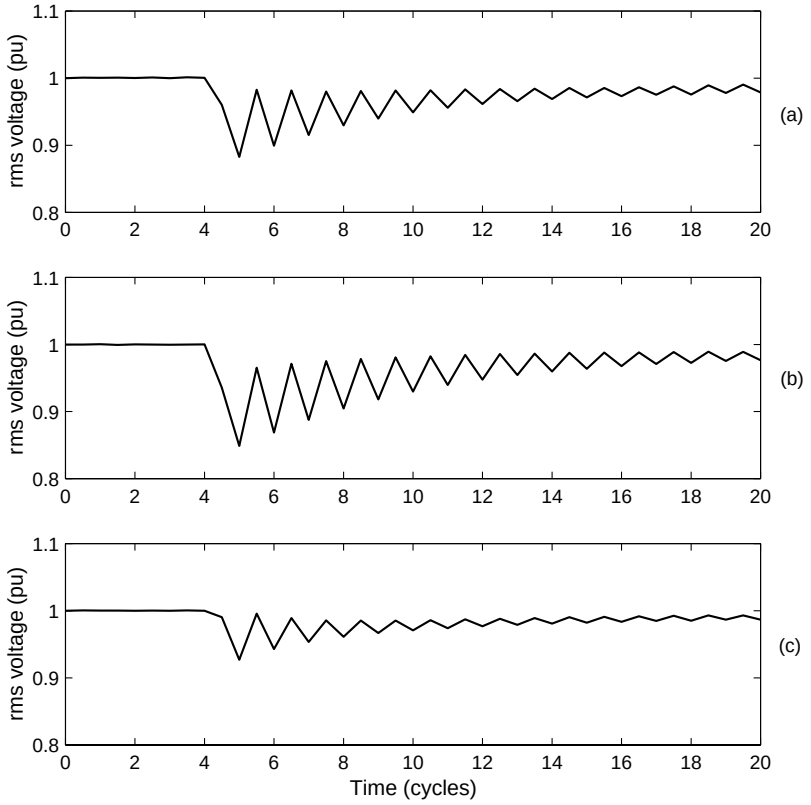

Figure 5.10: rms voltage in a 10 kV network - half-cycle update half-cycle window (a) phase a (b) phase b (c) phase c

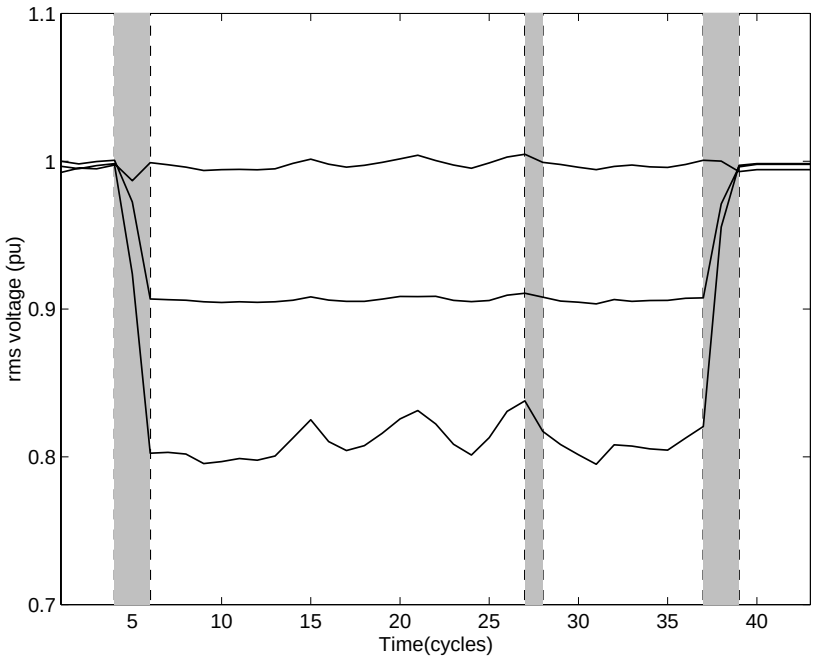

Figure 5.11: rms voltage and segmentation results for a voltage dip due to fault

For 10 % of the transformer saturation events, classification is incorrect due to incorrect segmentation. An example is shown in Figure 5.12. The rms magnitude has not the same shape as the one obtained using STFT or Kalman filtering. The segmentation gives more than one transition segment thus the event is classified as single stage dip due to fault.

Incorrect segmentation is also the reason for misclassification in the case of interruptions. The reason is the presence of strong transients either due to transformer saturation or current chopping. Therefore, non-fault interruptions are classified as fault interruptions.

Overall, the segmentation using rms voltage is a good alternative to the segmentation based on waveform Kalman filtering especially if the measurements do not contain short duration events. The successful application of the rms segmentation in this set of measurements also indicates that the rms magnitude during a dip does not present fast and large changes.

5.6 Conclusions

One of the objectives of a power quality monitor is to capture power system events without running out of memory. By saving only the computed discrete rms values the monitor is able to capture more events before it runs out of memory.

This chapter describes an automatic event classification system which uses discrete rms voltage measurements. Discrete rms voltage measurements is a memory saving option that power quality monitors offer instead of saving the actual voltage

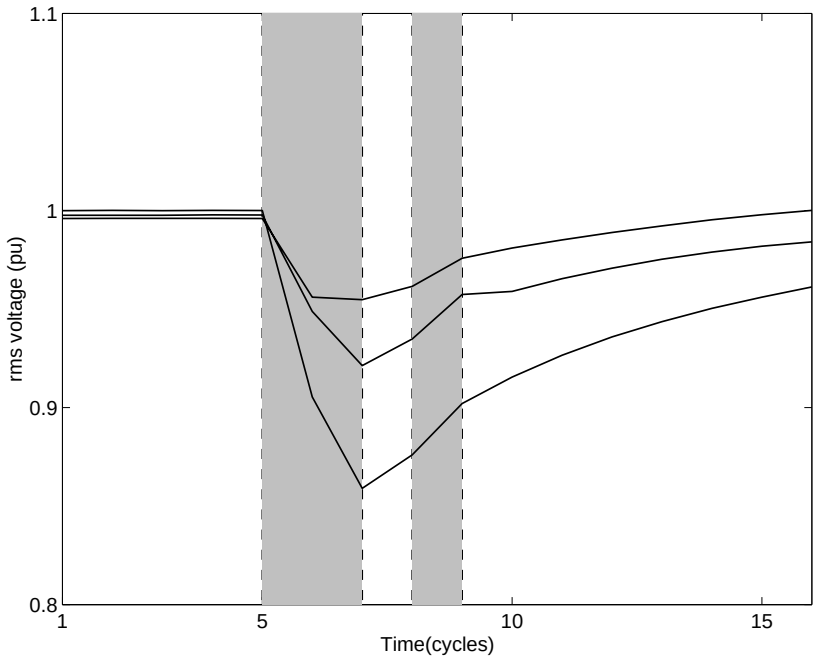

Figure 5.12: rms voltage and segmentation results for a voltage dip due to transformer saturation

waveforms. It is shown that automatic event classification is possible even if only the rms signatures are available as obtained by the monitors.

The classification method starts with segmenting the rms voltage series into event and transition segments. The segmentation is based on detecting sudden changes in the voltage magnitude. Classification is done by characterising the segments of each phase as well as comparing the corresponding segments between the phases.

Seven types of events are considered. The classification system is tested using measurements from a distribution network. The classification rate is 92 %.

Finally, the limitations with the rms voltage monitoring are discussed. Attention was given to short duration events. Significant errors might exist in the calculation of the dip magnitude when using the discrete rms calculation. It is shown also that in the case of transformer saturation events, classification can be difficult if only the one-cycle discrete rms is available. The classification can be improved if the rms is calculated over a half-cycle window and two values per cycle are stored.

Overall, the method offers a simple way for more sophisticated analysis of power quality measurements. The method can be implemented on a monitor and can provide automatically more information about the captured events.

Chapter 6

Characterisation and Analysis of Power System Transients

6.1 Introduction

In terms of classification, from the analysis presented in the previous chapters, power system phenomena can be divided into three classes:

- Events that can be classified by their fundamental frequency magnitude. These events contain parts where the voltage goes through significant changes for long periods. These changes are well apart in time so the magnitude estimators have no difficulties in resolving them. This class consists of the majority of fault induced events, transformer saturation, induction motor starting, etc.

- Events that present significant changes in the fundamental frequency magnitude but of short duration. The extraction of the voltage magnitude becomes problematic for these events. This class contains fuse-cleared faults and self-extinguishing faults.

- Events of very short duration (transients) for which the voltage magnitude does not offer important information. For this class, the higher frequency components of the signal must be considered for a thorough characterisation and classification.

Aim of this chapter is to present power system events of the last class, highlight their characteristics, and show how signal processing tools can be used to extract useful information from the captured voltage waveforms. Both measurements and simulations are used. The events presented either a step-like signature in the funda-

mental magnitude voltage or no change. The Electromagnetic Transients Program (EMTP) is used for simulations.

6.2 General classification of voltage transients

Voltage transients can be grouped according to their waveform characteristics in the following categories [4]:

1 Oscillatory transients

2 Impulsive transients

Further subclasses are suggested in [4] according to the frequency components and the time characteristics of these transients (Table 1.1 in Chapter 1). Next, some types of transients are presented in terms of the underlying cause.

6.3 Oscillatory transients

Oscillatory transients are the ones whose instantaneous value of voltage changes polarity rapidly. They are described by their spectral content, duration and magnitude. The most common causes of oscillatory transients are:

- Capacitor energising
- Restrike during capacitor de-energising
- Line or cable energising

In the following sections these events are presented in more detail.

6.3.1 Capacitor energising

Capacitor energizing is one of the most common transient events present in power systems. The overvoltage produced can reach values up to 2.0 pu and can cause problems to sensitive equipment like adjustable speed drives [76, 77].

When a capacitor is switched on, an oscillatory transient is produced because the voltage of the capacitor cannot change instantaneously. The voltage at the point of switching initially drops because the capacitor is uncharged and behaves as a short circuit. If the capacitor bank is uncharged the voltage initially will drop to zero. The initial drop is followed by an overshoot and an oscillation that decays until the voltage returns to steady state. The worst overvoltage occurs when energising takes place at a peak of the supply voltage. Without damping this overvoltage will be twice the maximum supply voltage [32, 78].

The transient's frequency f is determined by the combination of the capacitance of the capacitor bank C and the source inductance at the point of switching L:

$$f = \frac{1}{2\pi\sqrt{LC}} \tag{6.1}$$

The oscillation frequency can be also expressed as:

$$f = f_o\sqrt{\frac{\text{MVA}_{sc}}{\text{MVA}_c}} \tag{6.2}$$

where f_o is the fundamental frequency of the system, MVA_{sc} is the short circuit capacity of the source, and MVA_c is the capacitor bank rating.

The oscillation frequency in the voltage waveform is typically between 250 and 1000 Hz and lasts for less than half a cycle. The decay of the transient (damping) is exponential as shown in [32] and in [79], and depends strongly on the resistance of the network.

Capacitors are used for power factor correction or voltage support. The voltage rise due to the connection of a capacitor bank is given approximately by [80]:

$$\Delta V = \frac{\text{MVA}_c}{\text{MVA}_{sc}} 100\% \tag{6.3}$$

Capacitor energising and travelling waves

The sudden drop of voltage when the capacitor is energised initiates travelling waves that propagate in the system along the lines connected to the bus where the energising takes place. At points of discontinuity the waves are reflected back to the capacitor bank. The reflection and refraction coefficient of the point of discontinuity determines the portion of the wave that returns back to the capacitor bank and the portion that passes through. The capacitor due to its low surge impedance is seen by the waves as a short circuit. So the waves are inverted and reflected back to the lines. These travelling waves can travel between two locations many times before being damped due to the losses of the line [32]. If the travelling wave arrival at a remote location coincides with the peak of the oscillatory transient at that location, high magnitude overvoltages might appear [81, 82]. In [81] a case is shown where the travelling wave initiated by the switching of a capacitor bank in a 230 kV system produces a phase-to-phase overvoltage of 2.0 pu.

An example is given next using a simulation in EMTP of the network in Figure 6.1. The frequency dependent model (JMARTI's model) is used for the modelling of the 160 km transmission line in order to take into account the propagation of travelling waves. The characteristics of the line can be found in Appendix A. The short circuit level of the source is 5000 MVA and the 115 kV capacitor bank is 64 MVAr.

Figure 6.2 shows the oscillatory transient at the 115 kV busbar of the circuit in Figure 6.1, when the capacitor bank is energised. The transmission line is connected

to this busbar (CB_1 is closed). Figure 6.3 shows the voltage waveform at the 115 kV side of the transformer. The peak voltage (2.1 pu) is significantly higher than the peak voltage in Figure 6.2. The increased overvoltage is due to the reflection of the travelling wave (initiated by the capacitor energising) at the transformer terminals for the second time (the first reflection causes the sudden drop of voltage as it can be seen in Figure 6.3). The transformer terminal appears as virtually an open circuit refraction coefficient to the high rate-of-rise transient [81].

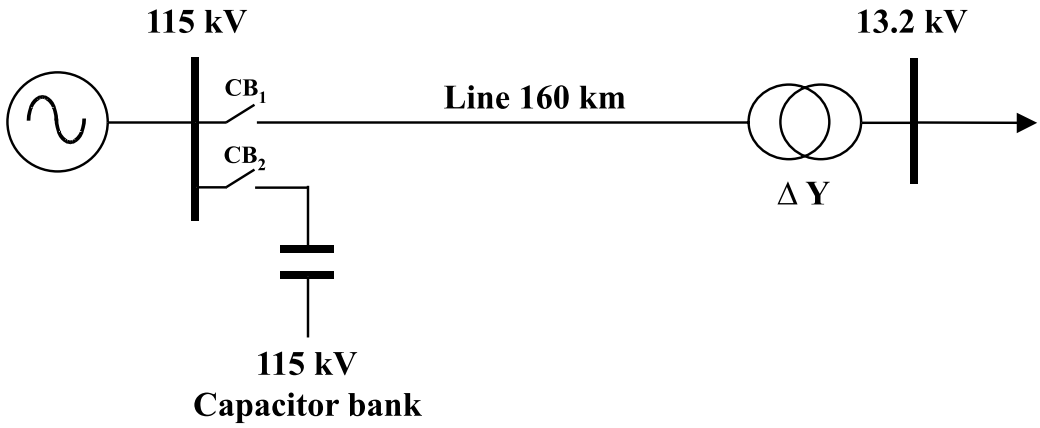

Figure 6.1: Sub-transmission system for the simulation of capacitor energising

Figure 6.4 shows the spectrum of these voltage transients as well as the spectrum of the transient when the transmission line in Figure 6.1 is not connected to the busbar (CB_1 is opened). The spectrum of the transient is estimated after the fundamental frequency is removed. First, a high-pass FIR filter with 128 taps and a cut-off frequency of 200 Hz is applied to the voltage signals, and then Fourier transform is calculated for a one-cycle window that starts from the point that corresponds to maximum voltage.

The spectrum of the transient at the 115 kV busbar shows a peak at around 400 Hz due to the oscillatory transient caused by the energising (the resonance frequency at the 115 kV busbar is 442 Hz, according to (6.2)). The spectrum of the energising transient at this busbar does not change significantly when the line is disconnected. The spectrum of the transient at the transformer presents a peak at the same frequency but has also peaks at higher frequencies due to the effect of travelling waves.

Influence of other capacitor banks - Voltage amplification

Not only travelling waves influence the characteristics of the capacitor energising transient. Other capacitors in the network can create resonances and introduce more than one frequency in the oscillatory transient. This phenomenon is important in the case of voltage amplification. Voltage amplification occurs when the oscillation

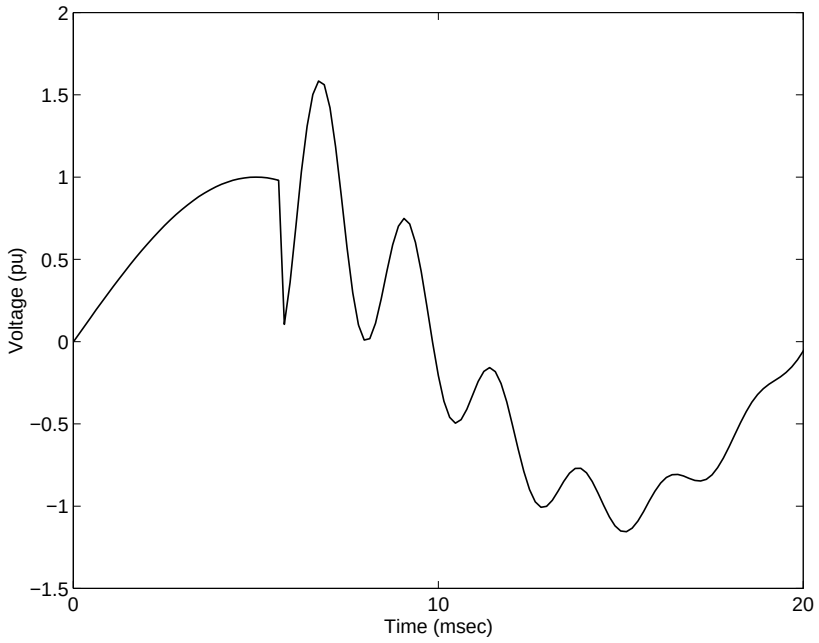

Figure 6.2: Voltage waveform during capacitor energising at the 115 kV busbar (EMTP simulation)

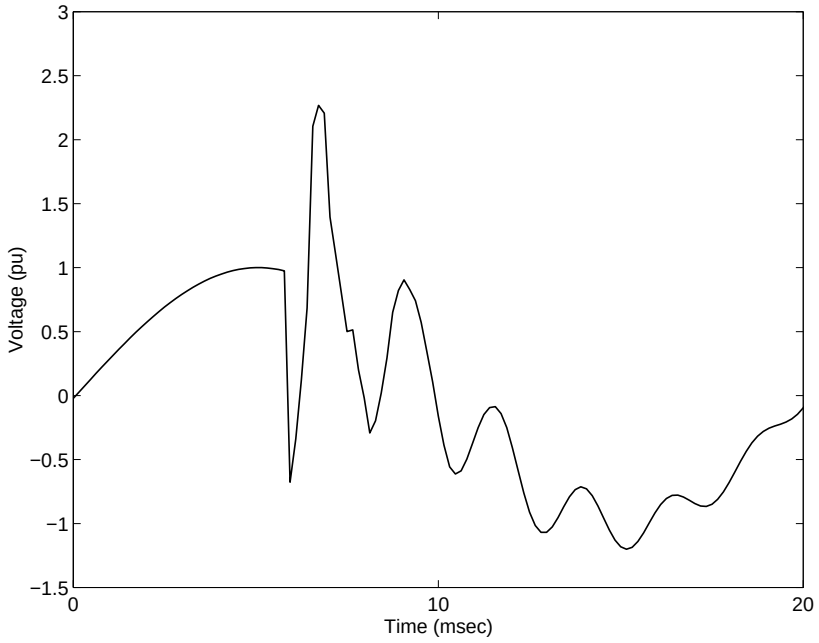

Figure 6.3: Voltage waveform during capacitor energising at the high voltage side of the 115/13.2 kV transformer (EMTP simulation)

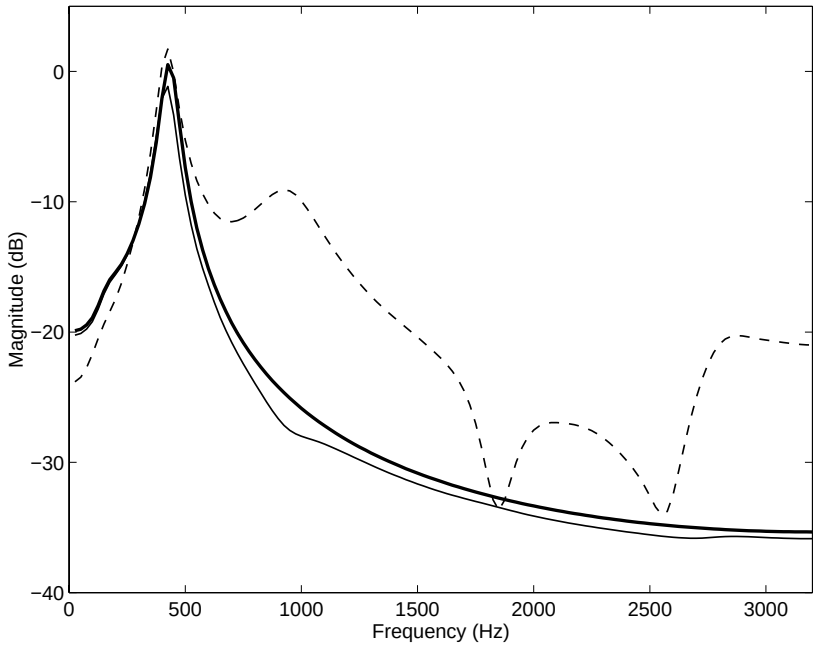

Figure 6.4: Spectrum of capacitor energising transients: voltage measured at the 115 kV busbar (solid line), voltage measured at the transformer (dashed line) and voltage measured at the 115 kV busbar when the line is disconnected (thicker line)

caused by the energising of a distribution capacitor bank excites the L-C circuit formed by the inductance between the switched capacitor bank and the utilisation-voltage busbar, and the capacitance of the capacitors connected to it. The result is a higher overvoltage at the utilisation-voltage busbar [82, 83, 84, 85, 86]. The overvoltage can be significant in low voltage networks with primarily motor load and low resistive load (less damping).

The system of Figure 6.5 is simulated in EMTP for energising the 12.5 kV capacitor bank when a capacitor bank is connected to the 480 V busbar (CB_{CL} is closed). The line between the two busbars is modelled using lumped elements, therefore the influence of travelling waves is neglected. This simplification is acceptable for lines that have short length compared to the wavelength of the transients [87]. The transformer is also modelled using lumped elements. The short circuit level of the source is 250 MVA. The capacitor being switched is 2.5 MVAr and the capacitor bank at 480 V is 170 kVAr delta connected. The resulting transients at the high and low voltage busbars are shown in Figure 6.6. The peak voltage at the low voltage busbar is 2.5 pu, significantly higher than the peak voltage at the high voltage busbar.

Figure 6.7 shows the spectrum of the transients. The spectrum of the transient at the 12.5 kV busbar shows a peak close to 450 Hz. The spectrum of the transient at the 480 V shows two peaks: one at the same frequency as the transient at the 12.5 kV busbar and another around 700 Hz. Their amplitudes are almost equal. As described in [86], the presence of a second capacitor in the vicinity of the ca-

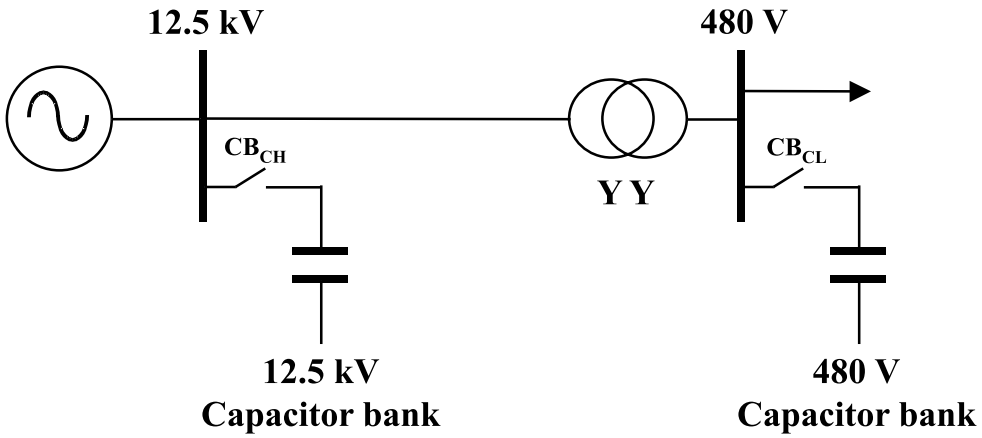

Figure 6.5: Distribution system for the simulation of voltage amplification due to capacitor energising

pacitor that is being switched produces a transient which is the combination of two frequency components. These two frequencies cannot be calculated using simple formulas like (6.1). Formulas for the calculation of these frequencies are given in [86]. Furthermore, more resonance frequencies appear if more capacitors are close.

For a different capacitor bank at the low voltage busbar the peak voltage is reduced significantly. If the 480 V capacitor bank is reduced to 40 kVAr then the switching of the 2.5 MVAr capacitor bank at the 12.5 kV busbar produces an overvoltage of 1.5 pu at the 480 V busbar (Figure 6.8). This is almost equal to the overvoltage of the high voltage side and significantly lower than the overvoltage of Figure 6.6.

The influence of other capacitor banks to the energising transient is also important in the case of back to back capacitor energising. Back to back capacitor energising is the energising of a capacitor bank from a busbar on which other capacitor banks are already connected. This type of switching produces transients with two frequency components: first, a very rapid transient brings about an exchange of charge between the capacitors so they are brought to a common voltage and then a second transient follows during which the two capacitor banks reach the source potential [32]. The first transient is of high frequency (C in (6.1) is the series combination of the capacitances of the capacitor banks and L is the inductance between them) and the second transient has significantly lower frequency (C in (6.1) is the parallel combination of the capacitances of the capacitor banks and L is the source inductance) [32].

In the same manner, the spectrum of a capacitor energising transient will be effected by cables due to their high capacitance [32].

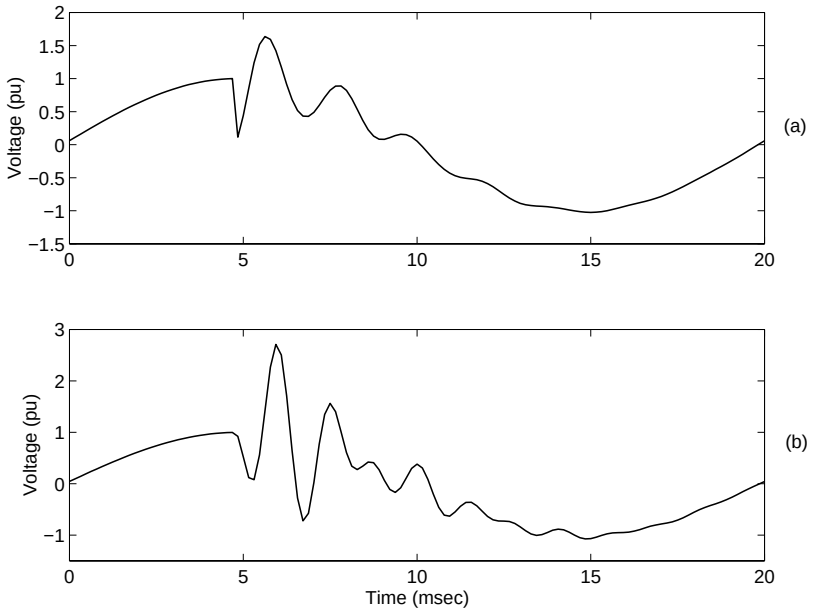

Figure 6.6: Voltage waveforms during capacitor energising (a) at the 12.5 kV busbar (b) at the 480 V busbar (EMTP simulation)

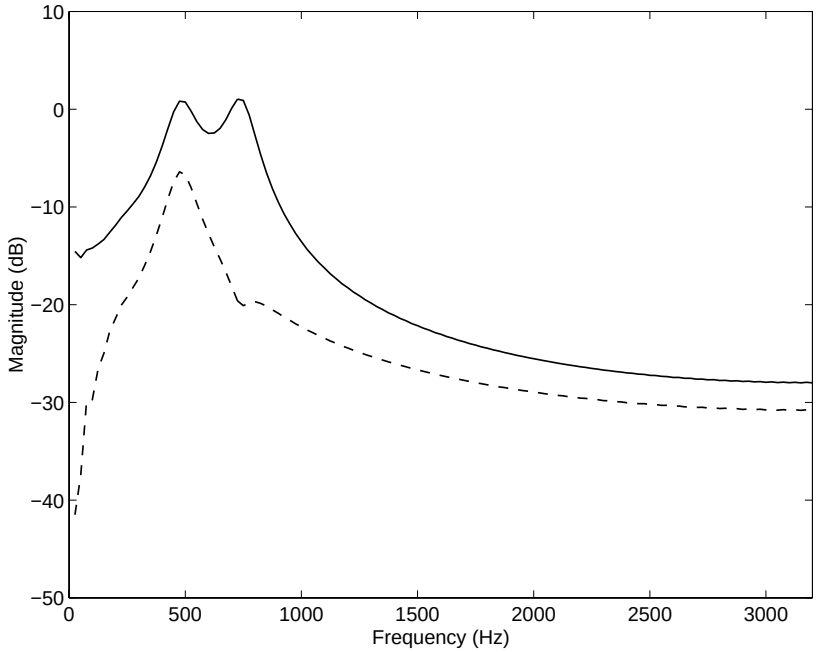

Figure 6.7: Spectrum of transients of capacitor switching: voltage measured at the 12.5 kV busbar (dashed line) and voltage measured at the 480 V busbar (solid line)

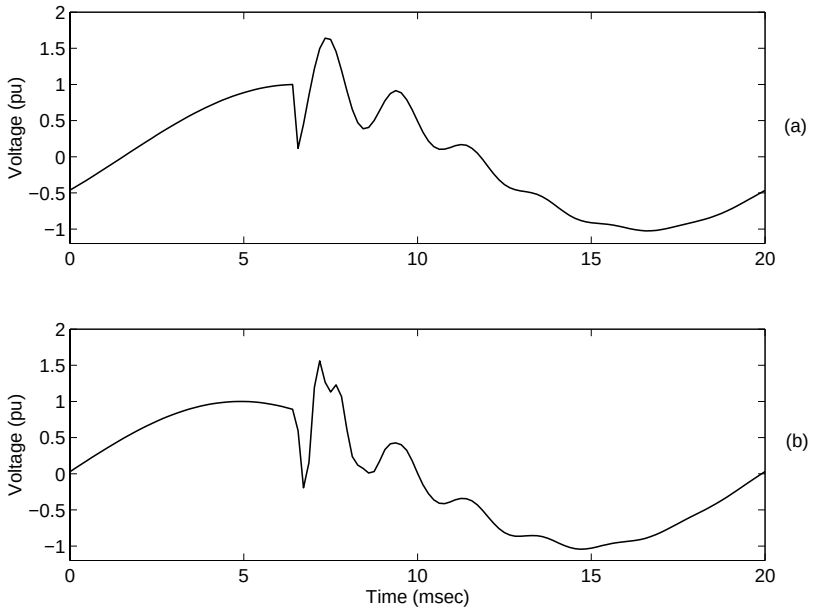

Figure 6.8: Voltage waveform during capacitor energising (EMTP simulation) (a) at the 12.5 kV busbar (b) at the 480 V busbar (EMTP simulation)

6.3.2 Restrike-reignition during capacitor de-energising

Switching off a capacitor bank (i.e., capacitor de-energising) does not usually result in any transient oscillation. The bus voltage will drop up to a few percent due to the loss of voltage support provided by the capacitor. During the de-energizing process, the contactor of a capacitor opens and discontinues the current flow. If the contactor does not open successfully, an arc will be established between the contacts and the capacitor will reignites or restrikes. The event is called reignition if current conduction is re-established within half a cycle of current interruption. If current conduction occurs later, the event is called a restrike [32]. The contactor might open and restrike later. The same event might be repeated several times (multiple restrikes).

Figure 6.9 shows a damped oscillation transient caused by restrike during capacitor de-energising. The voltages at both the line side and the capacitor side are shown as obtained by an EMPT simulation. The capacitor is disconnected at current zero when voltage is at its maximum (current leads voltage by approximately 90°. Therefore, the capacitor is charged to maximum voltage. Half a cycle later the voltage difference between the line side and the capacitor side is 2.0 pu and this could lead to reignition as shown in Figure 6.9. The case of multiple restrikes is shown in Figure 6.10.

For the cases shown in Figure 6.9 and Figure 6.10, the voltage initially changes sign due to the fact that the capacitor is charged with a voltage of opposite sign than the line voltage at the moment of reignition. The amplitude of the overvoltage due

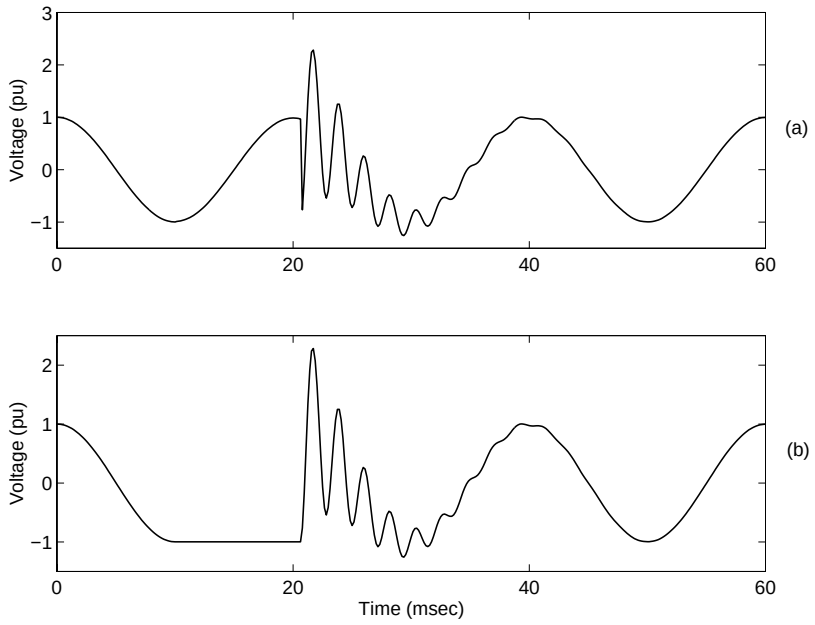

Figure 6.9: Voltage waveform of a restrike during capacitor de-energising (a) line side (b) capacitor side

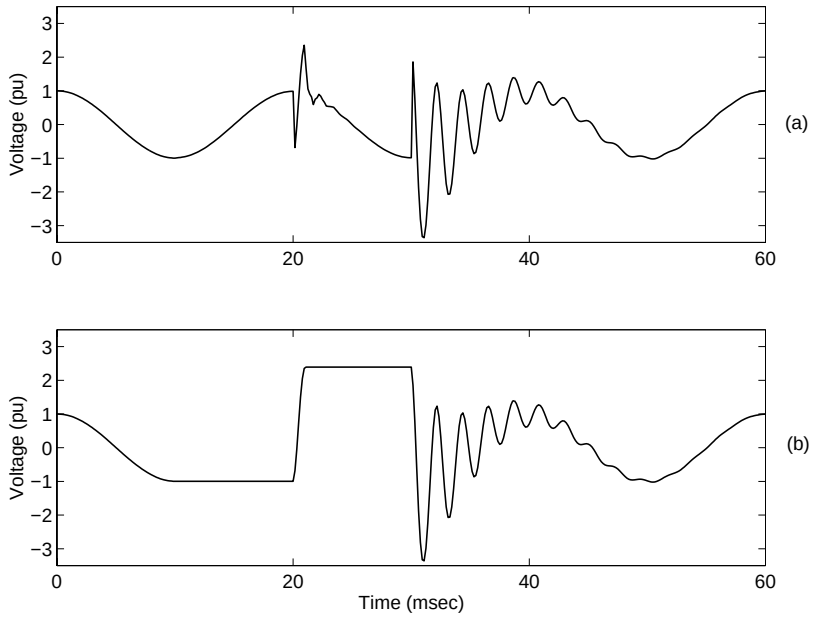

Figure 6.10: Voltage waveform for multiple restrikes during capacitor de-energising (a) line side (b) capacitor side

to this phenomenon depends on the trapped charge in the capacitor. The voltage at the instant of restrike will oscillate at the natural frequency characterised by the capacitance of the capacitor and the system inductance like in the case of capacitor energising.

6.3.3 Energising of open-ended line

Energizing of transmission lines can lead to high overvoltages especially if the end of the line is open [32]. When the circuit breaker at the sending terminal of the line is switched on, an electromagnetic wave propagates along the line with the polarity of the voltage at the instant of switching. The wave reaches the open end of the line and reflects without changing polarity. Part of the reflected wave is refracted to the source side and the remaining part reflects back to the receiving terminal. If the line is energised at a peak of the supply voltage (1 pu) then 2 pu voltage will be produced at the open end of the line. The shape of the travelling wave depends on the characteristics of the source and the propagation time of the line (the time it takes for the travelling wave to propagate from one end of the line to the other) [78]. Reflections to other points of the system will also effect the shape of the resulting transient. The amplitude of the travelling waves is exponentially decreased with a time constant that depends on the characteristics of the line.

In the following example the voltage transient at the open end of a line and at the source side of a line are considered. Figure 6.11 shows the voltage transient caused by the energising of the 160 km open-ended line at the source side and at the end of the line. The 132 kV circuit of Figure 6.1 is used for the EMTP simulation with the transformer and the capacitor banks disconnected and with the fault level of the source equal to 2500 MVA. The voltage at the end of the line approaches 2.0 pu and this is the main concern from an insulation point of view. The overvoltage at the source side is approximately 1.4 pu. The initial overshoot is followed by an oscillatory transient. Figure 6.12 shows the beginning of the voltage transient that is caused by open-ended line energising at the source side. The arrival of the travelling wave at this busbar after its reflection at the open end of the line causes a 0.40 pu fast increase in the voltage waveform. The propagation time, τ, of the line is:

$$\tau = \frac{L}{v} \tag{6.4}$$

where L is the length of the line and v the propagation speed. The propagation speed depends on the line characteristics. For an overhead line, the propagation speed is close to the speed of light [87].

Figure 6.13 shows the spectrum of the voltage transients of Figure 6.12 and the transient of the energising of a line with the same characteristics but half the length (80 km). The spectrum of the transient of the 160 km line has a peak at around 400 Hz (the oscillation frequency) and a number of lower peaks. The spectrum of the transient has a peak at around 800 Hz. As expected a shorter line produces an oscillatory transient of higher frequency due to a shorter propagation time. The

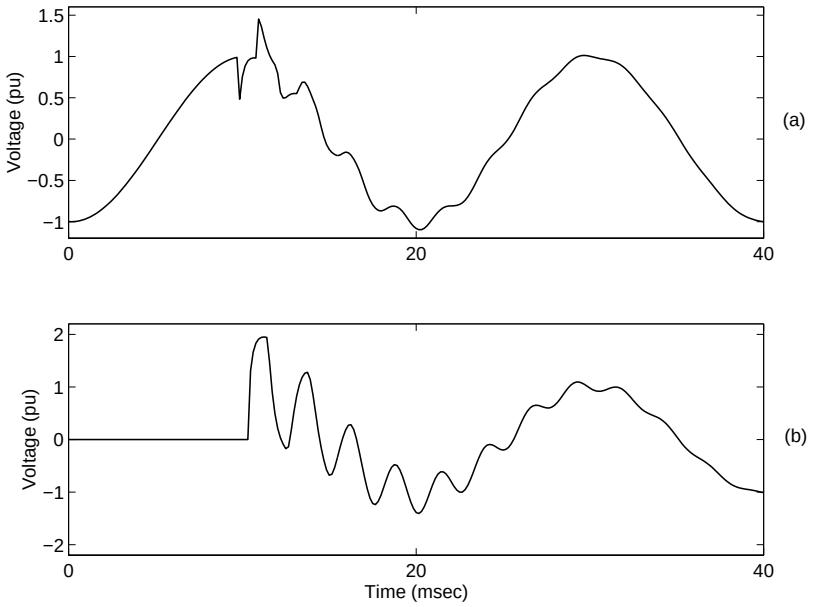

Figure 6.11: Voltage waveform of line energising (a) source side (b) end of the line

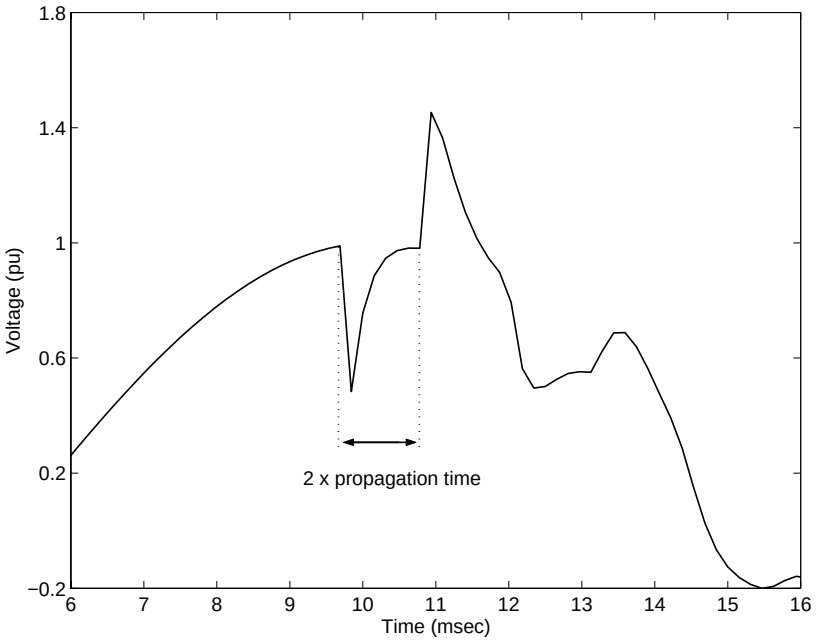

Figure 6.12: Voltage waveform of line energising at the source side

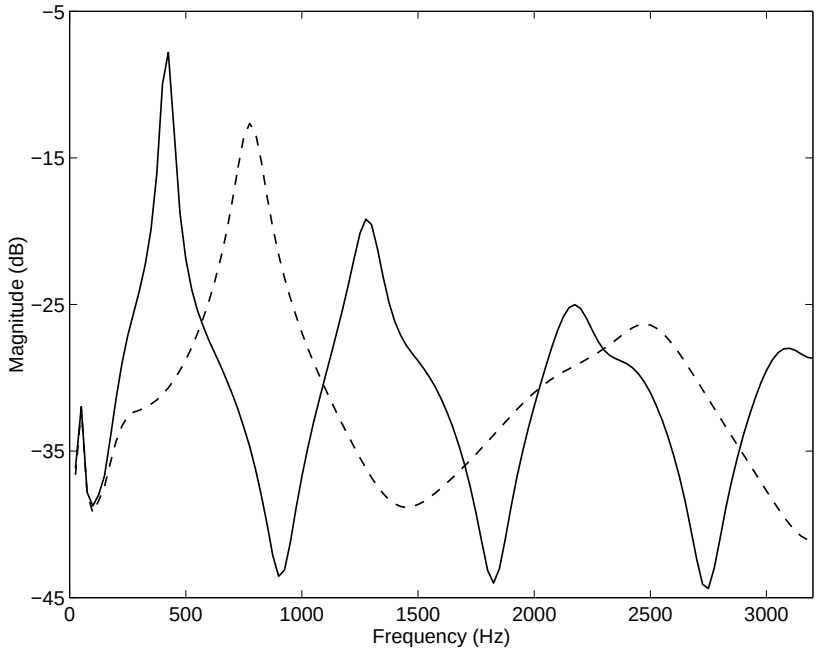

Figure 6.13: Spectrum of line energising transients: voltage transient for a 160 km line (solid line) and for an 80 km line (dashed line)

spectrum of line energising transient is similar to the frequency response of the line to a step voltage applied to one of its ends [32]. A number of natural frequencies appear at regular intervals along the frequency axis. The lowest natural frequency is $v/4L$, and the higher natural frequencies are multiples of 3,5,7,... of this.

6.4 Impulsive transients

An impulsive transient is a sudden change in the steady state condition of voltage, current or both, that is unidirectional in polarity (primarily either positive or negative) [4]. Impulsive transients are normally characterized by their rise and decay times. They are damped quickly by the resistive circuit elements and do not propagate far from their source. Figure 6.14 shows an impulsive transient measured in a 132 kV network.

The most common cause of impulsive transients is lightning. When a lightning stroke hits a transmission line (direct stroke) an impulsive overvoltage is induced [88, 89]. The maximum value of the lightning current I_{max} can be between 1 kA and 200 kA and the duration can be 1 μsec or less. The maximum voltage V_{max} due to the maximum current is found from [87]:

$$V_{max} = \frac{1}{2} \cdot I_{max} \cdot Z_0 \tag{6.5}$$

where Z_0 is the wave impedance of the line (typical values of wave impedance are

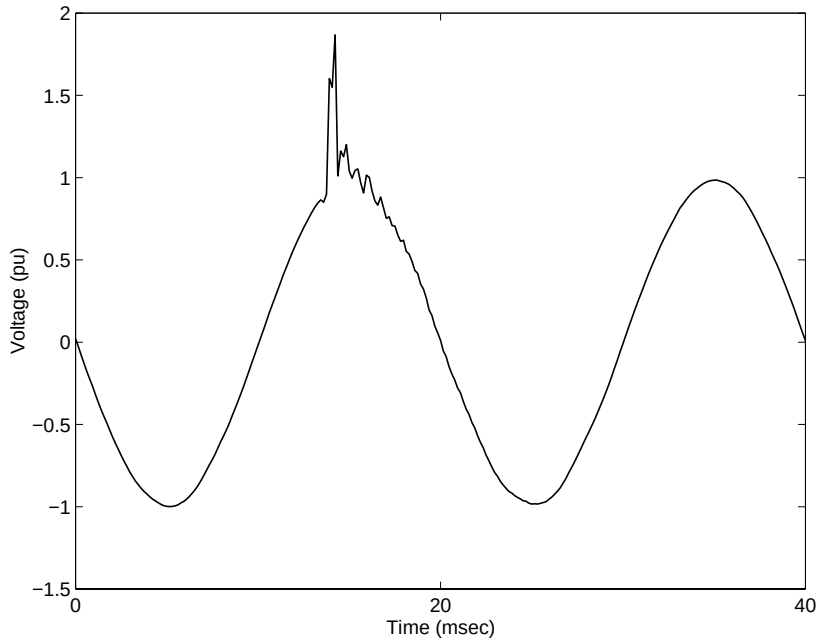

Figure 6.14: Voltage waveform of impulsive transient (measurement in a 132 kV network)

between 150 ohms and 400 ohms). Lightning overvoltages can also be induced by nearby strokes to the ground or between clouds. These overvoltages are of lower magnitude than those produced by direct strokes.

Impulsive transients might excite power system resonance circuits and produce oscillatory transients [4].

6.5 Further characterisation of power system transients

6.5.1 Pre-event/post-event characterisation

Some of the above mentioned events produce changes in the voltage profile. These changes might be in the fundamental voltage magnitude or in the harmonics or in both.

Voltage magnitude

Changes in the fundamental voltage magnitude due to the switching actions described so far are fast and step-like. By comparing the pre-event and post-event characteristics of voltage in terms of magnitude, the following classes can be defined:

- Increase in voltage magnitude: this can be caused by capacitor energising and open-ended line energising.
- Decrease in voltage magnitude: this can be caused by capacitor de-energising.

A change in voltage magnitude is also caused by shunt reactor switching. The energising of a reactor causes a drop in voltage and the de-energising an increase.

The increase in voltage magnitude in the case of energising capacitor banks and lines is due to the capacitance. The capacitance acts as a source of reactive power and increases the voltage. The increase in voltage for the case of line energising is expected to be lower than that in the case of energising a capacitor bank, because in the later case the capacitance is significantly larger.

The opposite effect (voltage drop) is observed upon capacitor de-energising. If a restrike takes place during capacitor de-energising then the voltage magnitude before the de-energising process is higher than the voltage magnitude after de-energising is successfully completed for all phases. Table 6.1 summarises the above-mentioned changes of magnitude for the different types of transients.

Table 6.1: Transients and their effects on voltage magnitude

Type	**Voltage magnitude**
Capacitor energising	Increase
Restrike during capacitor de-energising	Decrease
Open-ended line energising	Small increase

Two examples are given next. Figure 6.15 shows the voltage waveforms and their magnitude before and after a capacitor energising transient. This is a measurement in a 22 kV network. It can be seen that the switching causes an increase in the magnitude of all phases. The change is the same for all three phases, approximately 0.03 pu. Figure 6.16 shows the voltage waveforms and their magnitude before and after an open-ended line energising. The voltage waveforms are obtained from the EMTP simulation shown in Figure 6.11. Upon switching the voltage magnitude increases by approximately 0.003 pu for all phases.

Harmonic distortion

By comparing the pre-event and post-event characteristics of voltage in terms of harmonic distortion, the following classes can be defined:

- Increase in harmonic distortion: this can be caused by capacitor energising.
- Decrease in harmonic distortion: this can be caused by capacitor de-energising or the energising of a special case of a capacitor, the harmonic filter.

Capacitor energising might increase the harmonic distortion depending on the resonances of the system and the harmonics produced by the loads. The phenomenon is commonly known as harmonic amplification [90].

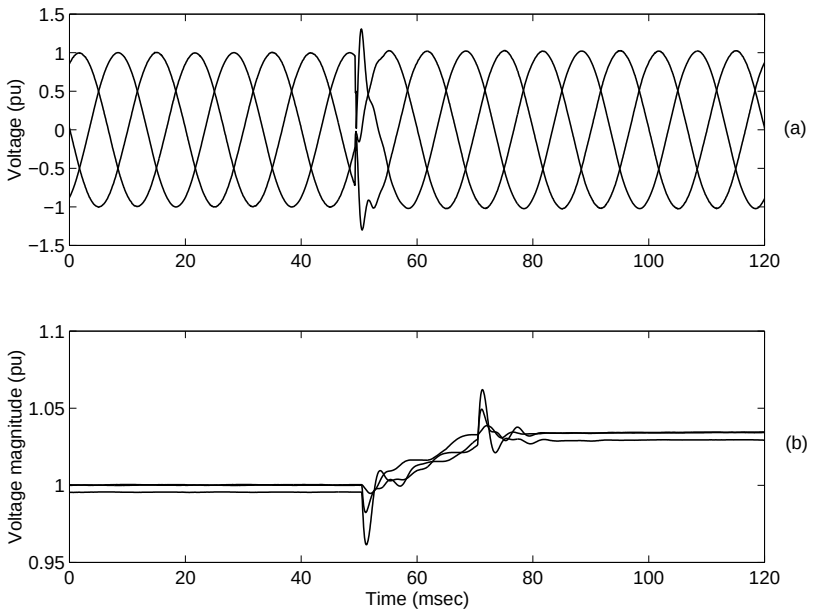

Figure 6.15: (a) Voltage waveforms during capacitor energising (b) corresponding voltage magnitude (measurement in a 22 kV network)

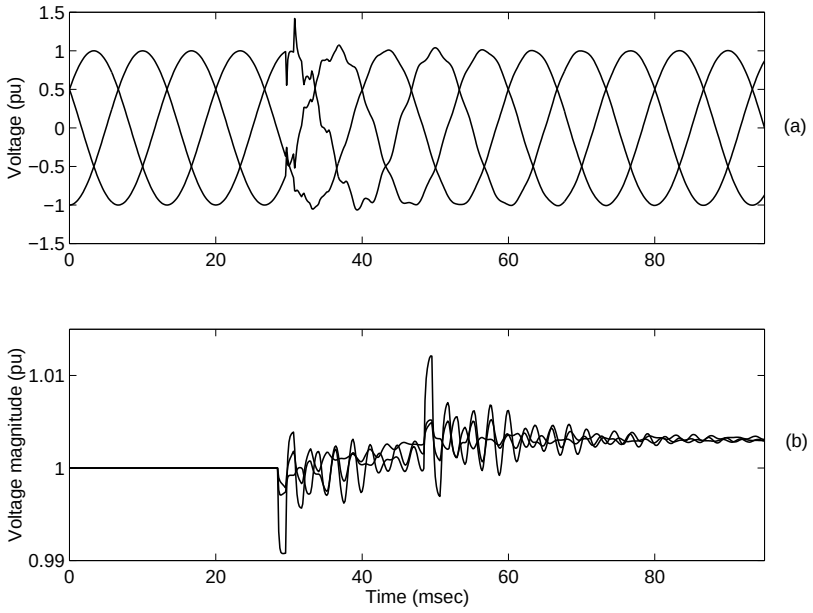

Figure 6.16: (a) Voltage waveforms during line energising (b) corresponding voltage magnitude (EMTP simulation)

Consider the simplified circuit of Figure 6.17. The loads are modelled as current sources. The h^{th} harmonic current $I_{sys,h}$ that flows to the system is given by the following formula:

$$I_{sys,h} = \frac{Z_{cap}(\omega_h)}{Z_{cap}(\omega_h) + Z_{sys}(\omega_h)} I_h \tag{6.6}$$

where $Z_{cap}(\omega_h)$ and $Z_{sys}(\omega_h)$ are the impedance of the capacitor and the system respectively at the h^{th} harmonic. The current $I_{sys,h}$ flowing into the system has its maximum value when the denominator of (6.6) is minimum. This is the case when the impedance of the capacitor $(-j/h\omega C)$ is equal to $(jh\omega L)$ where L is the inductance of the source. The value of h which satisfies this requirement is called the resonant harmonic frequency.

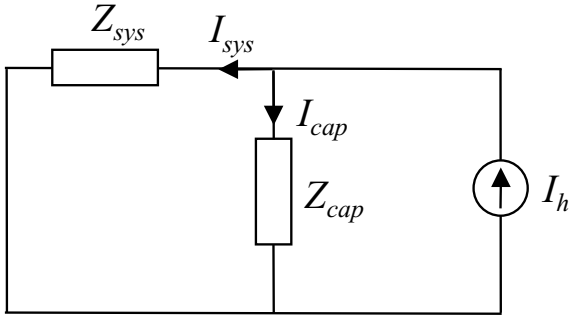

Figure 6.17: Equivalent network model for harmonic amplification

Figure 6.18 shows the harmonics of the phase a voltage of Figure 6.15 which is a measurement of a capacitor energising transient. There is an increase in the 5^{th} harmonic after the switching, and a smaller increase in the 3^{rd} harmonic. Small changes can be observed in the other harmonics. The total harmonic distortion also increases. The switching of the capacitor by changing the resonances of the system led to increased harmonic distortion.

At this point it is important to add the case of harmonic filter energising. Filters are combinations of resistance, inductance and capacitance tuned to present a low impedance to a particular frequency in order to reduce the harmonic distortion. Due to the presence of capacitance, filter energising presents similar characteristics as capacitor energising: overvoltage, oscillatory transient and step increase in voltage magnitude [91, 92]. However, unlike the case of harmonic amplification due to capacitor energising, filter energising has exactly the opposite effect on the harmonics: the harmonic for which the filter is tuned, is significantly reduced after the switching.

Figure 6.19 shows the voltage waveforms and their magnitude before and after the filter energising. This is an EMTP simulation using the 12.5 kV / 480 V distribution network of Figure 6.5. The load at 480 V is modelled as current sources that produce

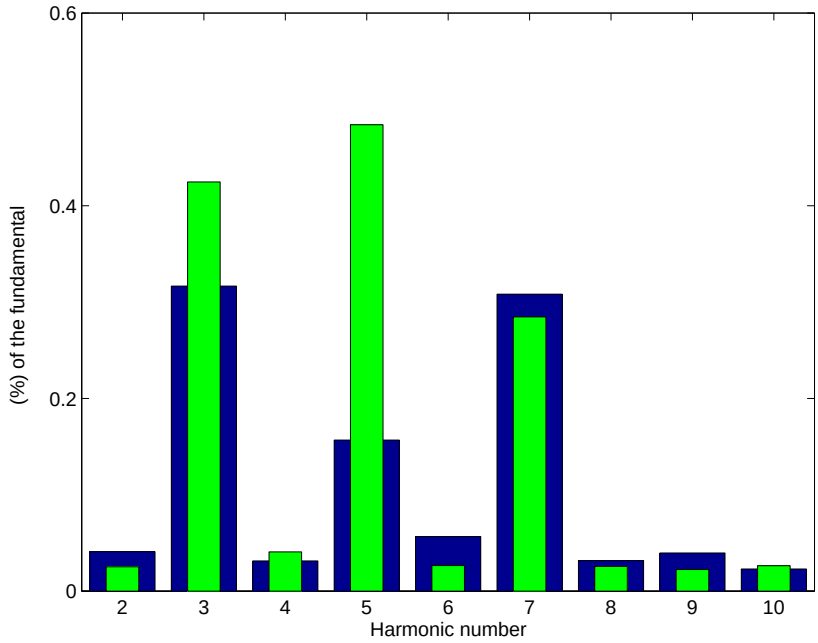

Figure 6.18: Voltage harmonics before (wide bars) and after (narrow bars) capacitor energising (measurement in a 22 kV network)

5^{th} and 7^{th} harmonic currents . The filter (a series combination of inductance and capacitance) is tuned to the 5^{th} harmonic, and is switched on the 12.5 kV busbar. It can be seen that the filter connection causes an oscillatory transient and an increase in the magnitude of all phases due to the filter's capacitor. Figure 6.20 shows the harmonics of the phase a voltage before and after the switching at the 12.5 kV busbar. The 5^{th} harmonic is completely eliminated.

6.5.2 Characterisation by comparing the phases

Considering the number of phases where an event takes place as well as the way the other phases are effected, transients can be divided into the following classes:

Three-phase events

These events are due to switching actions that take place in all phases. Typical examples are capacitor bank energising and line energising. In these cases the switching leads to an increase in voltage magnitude for all three phases. The characterisation of these events as three-phase can also be done by only considering the voltage magnitude.

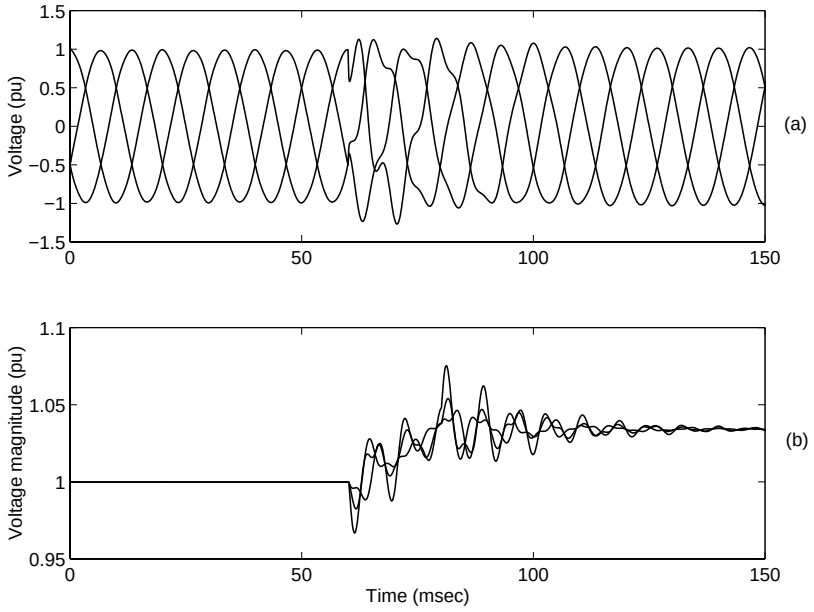

Figure 6.19: (a) Voltage waveforms during filter energising (b) corresponding voltage magnitude (EMTP simulation)

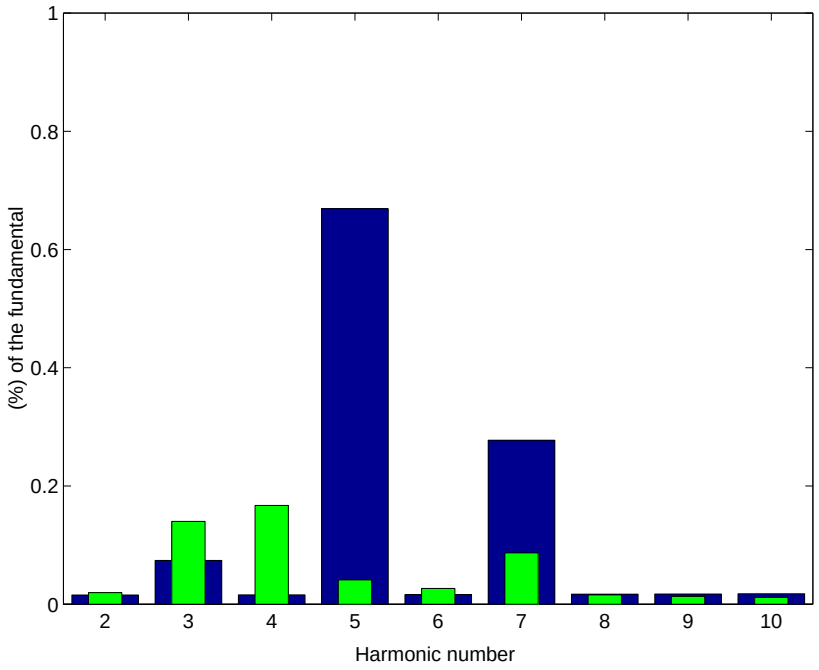

Figure 6.20: Voltage harmonics in a medium voltage network before (wide bars) and after (narrow bars) filter switching (EMTP simulation)

Single-phase events

These events are caused by switching or other phenomenon in only one phase. An example is a restrike during capacitor de-energising. For this case the change in the voltage magnitude must lead to characterisation of the event as a three-phase event because all phases will eventually present a decrease in voltage magnitude as soon as all three capacitor banks are successfully disconnected. Differences between the phases are difficult to be observed because these changes in magnitude are too close in time for a magnitude estimator to capture.

It is important to note that although an event takes place in one phase, transients are induced to another due to the capacitive coupling between phases (Figure 6.21). Additionally, if a single-phase transient propagates through a delta star transformer (Figure 6.22), then at the other side of the transformer, the transient appears in two phases.

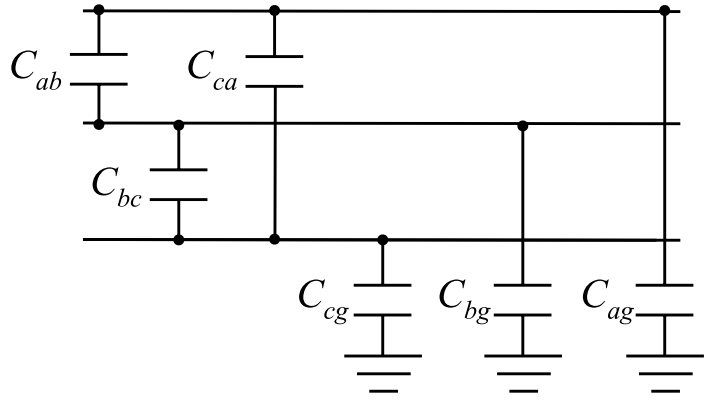

Figure 6.21: Line capacitances

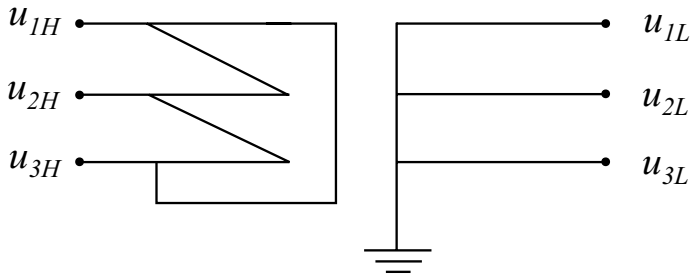

Figure 6.22: Delta-star transformer

Restrike is typically a single-phase event: only one phase restrikes. Figure 6.23 shows the voltage waveforms of restrike during capacitor switching. The waveforms are obtained by simulating a restrike in the 132 kV network of Figure 6.1. The restrike takes place in one phase (Figure 6.23a). However, transients are also induced

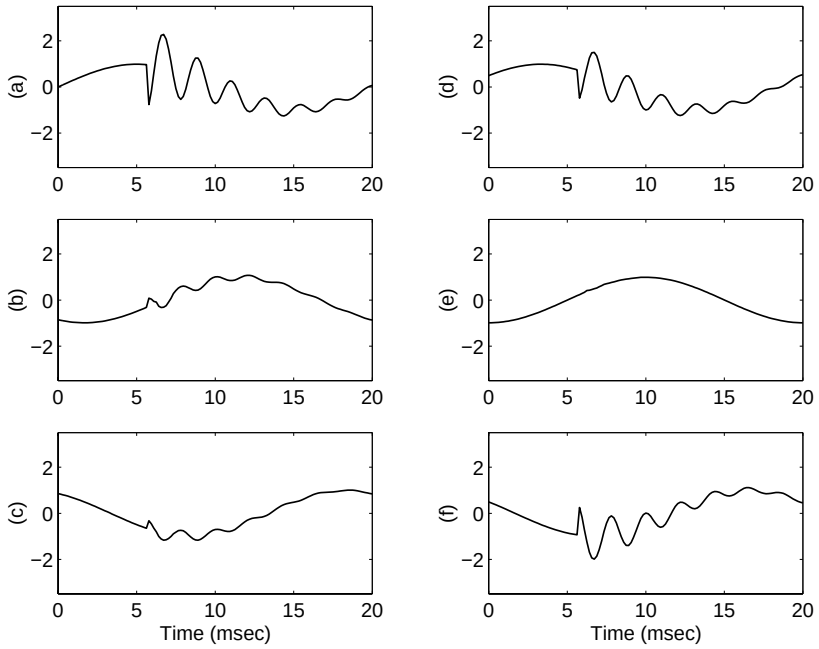

Figure 6.23: (a)-(c) Phase-to-ground voltage waveforms and (d)-(f) Phase-to-phase voltage waveforms during a restrike (EMTP simulation)

to the other two phases (Figure 6.23b and Figure 6.23c).

Figures 6.23d-6.23f show the phase-to-phase voltage waveforms of the previous event. The restrike transient appears in two-phase-to-phase voltages and the transient in one of the phase-to-phase voltages is very low. This means that the transients induced in the phase-to-ground voltages of the other two phases (due to the restrike in the third) are similar so they cancel in the phase-to-phase voltages. Similar waveforms are shown for this event in [22].

Phase-to-phase events

These are cases where two phases present transients of equal magnitude but opposite polarity. This case could be due to a switching action or a fault between two phases. It could also be due to a single-phase event that propagates through a delta-star transformer, as shown in Figure 6.23. Figure 6.24a shows the voltage waveforms of a measurement in a medium voltage network. The cause of the transient is unknown. It can be seen that almost the same transients appear in two of the phases. The third phase does not present any noticeable disturbance. Figure 6.24b shows the sum of these two phases: there is no obvious disturbance which proofs that the transients in these phases are equal but of opposite polarity. No change in the voltage magnitude is observed for this measurement.

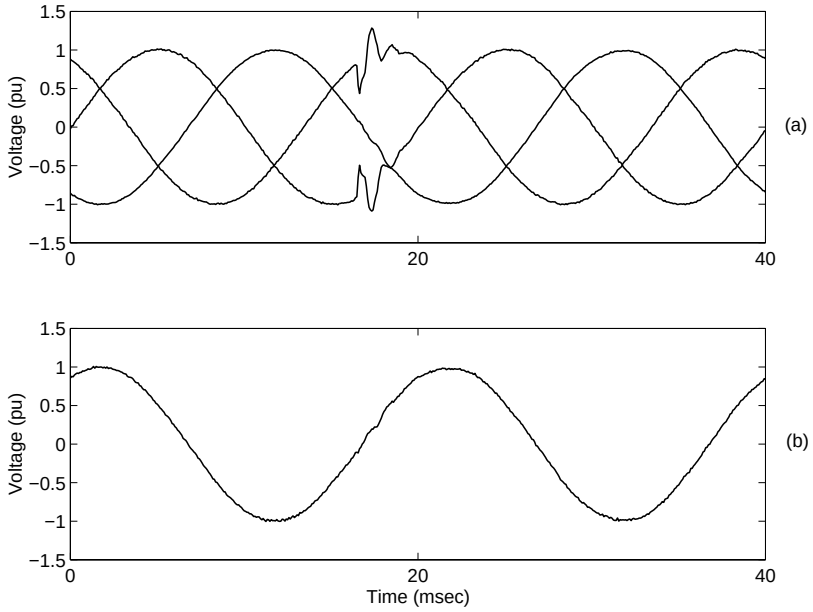

Figure 6.24: Phase-to-phase event (a) Phase-to-ground voltage waveforms (b) Sum of phases a and b (measurement in a 21.7 kV network)

Common mode events

These events present the same transient in all three phases. An example is given in Figure 6.25. The measured transient in the three phases (Figures 6.25a-6.25c) almost disappears in the corresponding phase-to-phase voltages (Figures 6.25d-6.25f). This proves that the transient is the same in all three phases. The cause of this measurement is unknown.

6.5.3 Characterisation of the initial change of voltage

From the examples given above, the initial change of voltage can be a characteristic of transients. The different cases are shown in Figure 6.26. Here, *increase* is defined as *away from zero* and *decrease* as *towards zero*.

Initial decrease in voltage

This takes place in capacitor energising (an uncharged capacitor behaves initially as a short circuit) and line energising (for the same reason due to the capacitive coupling of the line to earth). A lightning impulse can cause a decrease in voltage depending on its polarity.

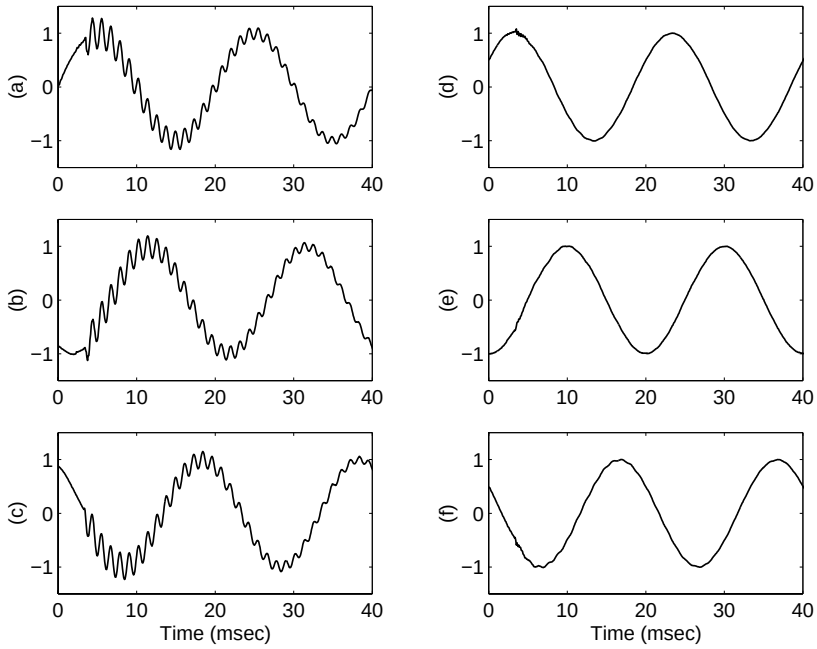

Figure 6.25: (a)(b)(c) Phase-to-ground voltage waveforms (d)(e)(f) Phase-to-phase voltage waveforms (measurement in a 76.2 kV network)

Initial increase in voltage

Depending on its polarity, a lightning impulse could cause an initial increase in voltage.

Initial change in the three phases

Capacitor energising and line energising cause an initial decrease in voltage for all three phases. Figures 6.27a-6.27c show the case of capacitor energising. However, measurements showed that there are cases where the initial change might not be the same for all three phases. Figures 6.27d-6.27f show a measurement in a sub-transmission network where an impulsive transient presents different initial change for the three phases: for the phase shown in Figure 6.27d the voltage shows an increase and for the phases of Figure 6.27e and Figure 6.27f shows a decrease.

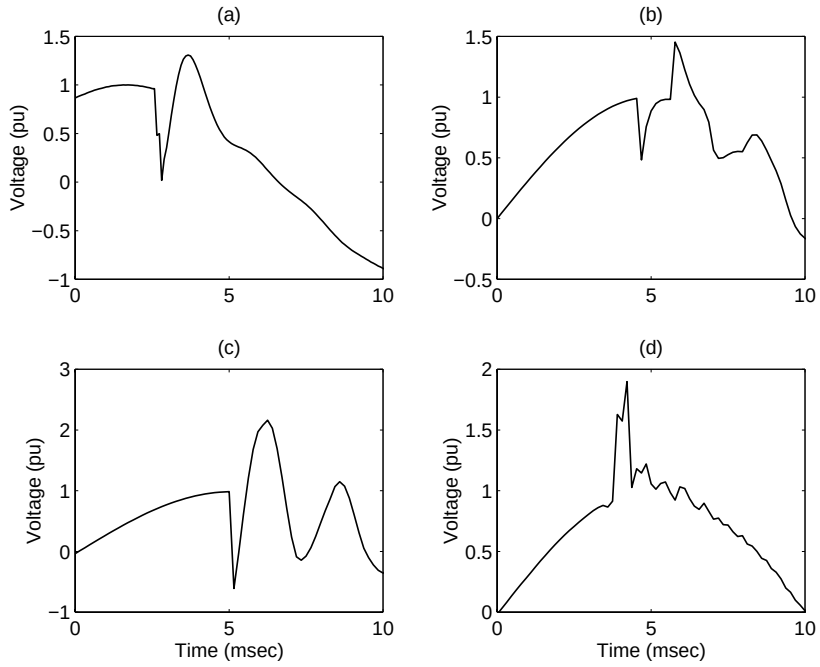

Figure 6.26: (a) Capacitor energising (measurement) (b) Line energising (EMTP simulation) (c) Restrike during capacitor switching (EMTP simulation) and (d) Impulsive transient (measurement in a 132 kV network)

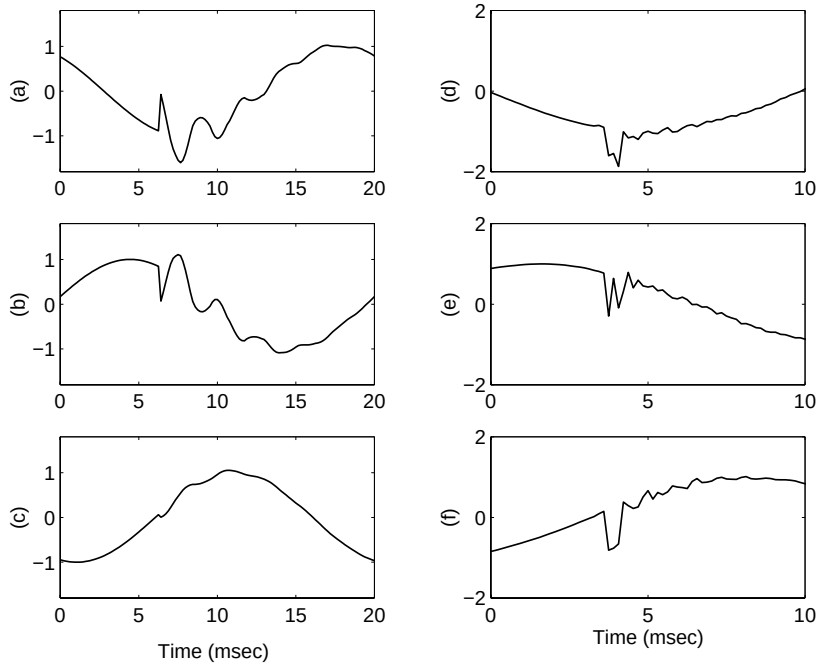

Figure 6.27: (a)-(c) Voltage waveforms during capacitor energising (EMTP simulation) and (d)-(f) Voltage waveforms - measurement of an impulsive transient in a 132 kV network

6.6 Frequency components and propagation of power system transients

6.6.1 Frequency components of power system transients

The spectrum of the voltage transients presented so far consists of:

- damped oscillations due to the resonances of the system, and the exchange of energy between inductances and capacitances.
- travelling waves initiated by the switching operations.
- phenomena related to the switching process and the switching equipment (like restrike and reignition)

The resonances of the system are responsible for strong frequency components. The oscillations produced by the resonances decay exponentially and they vanish in short time. The effect of travelling waves is of even shorter duration: as travelling waves propagate, their energy is spread over a large part of the system. Therefore, the effect of travelling waves at one location is of very short duration.

In addition to the restrike-reignition phenomenon, switching might introduce one more type of disturbance. During the closing of a switch a position is reached where the dielectric strength between closing contacts falls below the voltage across the contacts. At this point, a flashover, termed a prestrike will occur. Then the voltage across the terminals of the switch falls to a very low value. This rapid change of voltage results in the injection of a steep-fronted transient voltage wave into the load side as well as the source side [93]. In the case of capacitive load, the phenomenon might be aggravated if the capacitive load contains a trapped charge. Prestrike might occur in this case when the source side voltage reaches its maximum, and the trapped charge has polarity opposite to the polarity of the source voltage [87]. As shown in [93], a prestrike results in high frequency voltage oscillations. Figure 6.28 shows a measurement of a damped oscillation starting with a short duration high frequency transient. The voltage magnitude increase after the transient approximately 0.03 pu. Therefore, the event could be due to capacitor energising.

One more source of frequency components in the transients is the non-simultaneous switching of the phases. As shown in the case of single-phase events, a transient in one phase is coupled to the other. Therefore, for switching events, if the time instant is different for each phase, transients are induced to the other phases due to coupling. The random fluctuations in the angle of switching are recognised as being due to imperfections in the mechanical system of closure and/or possible prestriking of the breaker poles. According to published practical experience the distribution of the angle of switching around its aiming value can be considered to be Gaussian with a standard deviation of 20° (1.11 msec in a 50 Hz system) [94]. An example is given in the next section.

The transients might be also effected by the operation of equipment like surge arrestors which protect the power system from overvoltages [95].

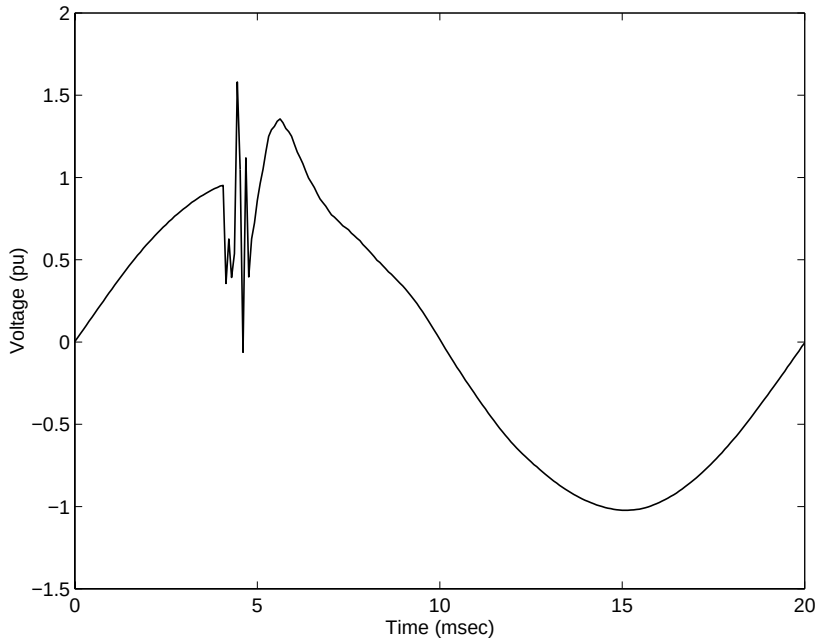

Figure 6.28: Voltage waveform of an short duration transient (measurement in a 22 kV network)

6.6.2 Propagation of power system transients

In general, power system events propagate through the system and are captured by monitors at different locations. Considering the events presented in Chapters 2-6, voltage dips due to faults effect a large part of the network. The voltage dip will be different at different locations depending on the system configuration, the distance from the fault point, the dip type and the types of transformers from which the voltage dip propagates as explained in Chapter 2. Contrary to fault-induced dips, dips due to induction motor or transformer saturation are shallow and do not propagate far; they are local events.

The events presented in this chapter are also local: the produced transients cannot propagate far because they are damped fast by the resistive part of the system. Therefore, they effect only a small part of the network.

As shown in Section 6.3, the characteristics of the transients produced by a certain event are different at different locations in the system. Depending on the characteristics of the location where voltage is measured (monitoring location), the maximum voltage, the underlying frequencies and the relationship between the phases change. The distance between the monitoring location and the origin of the transient, capacitors or cables connected near it and its response to travelling waves effect significantly the voltage transient. Capacitor switching is a very good example of how an event produces significantly different transients at different points of the system.

One more that must be taken into account regarding propagation of transients is that the response of the elements of the system (lines, transformers, etc) is fre-

quency dependent: these elements behave as filters suppressing some frequencies and passing others. Therefore, transients measured at both sides of a transformer present differences depending of the frequency response of the transformer. In the case of voltage dips the frequency dependence of the transformer is insignificant (the frequency response of the transformer at the fundamental frequency is unity).

6.7 Analysis of power system transients using ESPRIT

6.7.1 Further analysis of power system transients

Spectrum analysis of transients produced by the above mentioned events reveals several frequency components. For further investigation of the characteristics of the frequency components time-frequency analysis can be applied. Time-frequency analysis reveals the time evolution of the underlying frequency components of a non-stationary signal. STFT presented in chapter 2 is one way of performing this kind of analysis. STFT belongs to a class of time-frequency methods that are based on constructing filter banks that split the signal into different frequency bands by locating the filters at appropriate frequencies. Wavelet filter banks belong also to this class [96]. These methods have been utilised for the analysis of power system transients [19, 26, 28, 68].

Analysis using filter banks suffers from the time-frequency resolution problem (constrained by the uncertainty principle): one can only trade time resolution for frequency resolution [96]. This is already explained in the case of STFT in Chapter 2: a short time window provides better time resolution but gives a bandpass filter of larger bandwidth thus worse frequency resolution. The trade off between time and frequency resolution imposes problems in the analysis of signals that contain components with closely spaced frequencies.

Alternatively to the filter bank approach, where no model is considered for the signal under analysis, a model-based approach can be used in order to extract the different frequency components and their characteristics. For most of the transients presented so far, the main frequency components are due to the resonances of the system. Frequency components of these types can be described as a sum of exponentially decaying sinusoids. Providing that the characteristics of the signal do not change with time, Prony's method and ESPRIT are two ways of estimating the parameters of such a model (the frequencies, the damping coefficients, the initial phases and the amplitudes). Both methods have been suggested for the analysis of short duration transients in power systems: Prony's method has been used for the analysis of earth fault currents [97] and ESPRIT for the analysis of capacitor energising transients [98]. Assuming that the underlying frequency components are exponentially damped sinusoids, ESPRIT is found to be able to resolve closely spaced frequencies [99]. Next, ESPRIT is utilised for the analysis of the transients presented in this chapter.

6.7.2 ESPRIT

ESPRIT (Estimation of Signal Parameters via Rotational Invariance Techniques) decomposes the signal into a sum of sinusoids using an eigen-decomposition approach [99]. Consider a signal $z(t_k)$, being the sum of p exponentially damped sinusoids in additive noise $e(t)$:

$$z(t_k) = \sum_{i=1}^{p} A_i e^{-\alpha_i t_k} cos(2\pi f_i t_k + \phi_i) \; + \; e(t_k) \tag{6.7}$$

The number of sinusoids p is assumed known.

The ESPRIT method for estimating the parameters of the model can be implemented as follows [100]:

1. For $y(t_k) = [z(t_k) \dots z(t_{k+M-1})]^T$ with $(M > p)$, the sample estimate of the corresponding covariance matrix R is computed by:

$$R = \frac{1}{M} \sum_{t_k=1}^{M} y(t_k) y^T(t_k) \tag{6.8}$$

2. The eigenvalues (λ) and the corresponding eigenvectors (s) of R are found. The eigenvalues are arranged in a decreasing order.

3. Considering the first p eigenvectors, the matrix S is formed as:

$$S = (s_1 \dots s_p) \tag{6.9}$$

and the matrices S_1 and S_2 as:

$$S_1 = (\mathrm{I}_{M-1} \quad 0)S \tag{6.10}$$

$$S_2 = (0 \quad \mathrm{I}_{M-1})S \tag{6.11}$$

where I_{M-1} is the identity matrix of dimension $M-1$ by $M-1$.

4. The eigenvalues of the matrix $\psi = (S_1^T S_1)^{-1} S_1^T S_2$ are found. These eigenvalues $(c_1, \dots, c_p)$ determine the frequencies f_i and the damping factors α_i:

$$f_i = \frac{angle(c_i)}{\Delta t \; 2\pi} \tag{6.12}$$

$$\alpha_i = -\frac{\ln(|c_i|)}{\Delta t} \tag{6.13}$$

where Δt is the sampling period.

For the calculation of the other parameters in the signal model, the following system is solved using N signal samples $(N > M)$ [98]:

$$X = VH \tag{6.14}$$

where

$$V = \begin{pmatrix} 1 & 1 & 1 & 1 \\ c_1 & c_2 & \cdots & c_p \\ \vdots & \vdots & \vdots & \vdots \\ c_1^{N-1} & c_2^{N-1} & \cdots & c_p^{N-1} \end{pmatrix} \tag{6.15}$$

$$X = [z(t_0) \quad z(t_1) \quad \ldots \quad z(t_{N-1})]^T \tag{6.16}$$

and

$$H = [h_1 \quad h_2 \quad \ldots \quad h_p]^T \tag{6.17}$$

The least squares solution to (6.14) is

$$H = (V^H V)^{-1} V^H X \tag{6.18}$$

Having computed H, the amplitude is calculated as:

$$A_i = 2|h_i| \tag{6.19}$$

and the initial phase is the angle of h_i, i.e.:

$$\phi_i = angle(h_i) \tag{6.20}$$

For real-valued signals (as the ones used next), the frequencies obtained by ESPRIT appear in pairs of frequencies of opposite sign. The order of the model p is therefore set equal to twice the number of frequencies expected in the signal.

6.7.3 Application of ESPRIT

Pre-filtering is applied to the voltage waveforms before ESPRIT is applied. First, a high-pass linear phase FIR filter with 128 taps with a cut-off frequency of 200 Hz is used to the voltage signals to remove the fundamental frequency component. The high-pass FIR filter is constructed with the window method of FIR filter design using a Hamming window [101]. The frequencies under consideration are much higher than the fundamental frequency and no harmonic distortion due to loads is present, so artifacts of the pre-filtering are not expected to be important. In the presence of harmonic distortion due to loads, problems are not expected as long as the transient is much higher than the harmonics. Then, the method described in the previous section is applied to the data interval that starts from the point of maximum voltage and ends where the transient is completely damped. The first half of this data interval is used for the estimation of the frequencies f_i and the damping factors α_i (with ESPRIT) and the whole data interval for the estimation of the amplitudes A_i and the initial phases ϕ_i.

After parameter estimation, the transient is reconstructed using the obtained results and (6.7). The reconstructed signal can be used as a measure of how well the original transient is modelled by the underlying model and its estimated parameters.

The order of the model (the number of damped sinusoids that exist in the signal) is user-selected. For the results shown next, the order of the model p in (6.7) is set as high as needed to reduce the maximum difference between the original transient and the reconstructed transient below 5 % of the maximum value of the transient. For the examples shown next the simulations presented in the previous sections are used.

Voltage amplification due to capacitor energising

Figure 6.29 shows the results of ESPRIT for the transient that corresponds to the voltage amplification case of Figure 6.6b. ESPRIT successfully resolves the two frequencies as shown in the spectrum of the transient (Figure 6.7). The two sinusoids have frequencies 477 and 742 Hz. At the beginning of the transient, the two sinusoids are in phase, and as they sum, contribute equally to the resulting overvoltage. This feature provided by ESPRIT can be used for identifying the voltage amplification phenomenon: in the low voltage transient there are two strong frequencies which contribute significantly to the overvoltage.

Figure 6.30 shows the results of ESPRIT for the transient that corresponds to the voltage of Figure 6.8b. Two sinusoids are found adequate in modelling the signal (frequencies 484 and 1507 Hz). However, the higher frequency sinusoid has low magnitude, decays fast, and its phase is almost opposite to the phase of the other sinusoid. The resulting overvoltage is significantly lower than the one in Figure 6.29. In this case, the low voltage capacitor bank does not cause voltage amplification.

Line energising

Figure 6.31 shows the results of ESPRIT for the transient due to line energising (Figure 6.12). The decomposition shows that there is one strong frequency component (418 Hz) and two other fast decaying sinusoids of higher frequency (1283 and 1865 Hz). These sinusoids model the effect of the travelling waves on the voltage waveform. It is important to notice that these two sinusoids initially contribute almost equally to the voltage maximum as the low frequency sinusoid. This is indicates that the maximum voltage in the case of line energising is not due to the long duration low frequency oscillation but due to the arrival of the travelling wave from the open end of the line. The sinusoids that model the effect of the travelling wave decay fast.

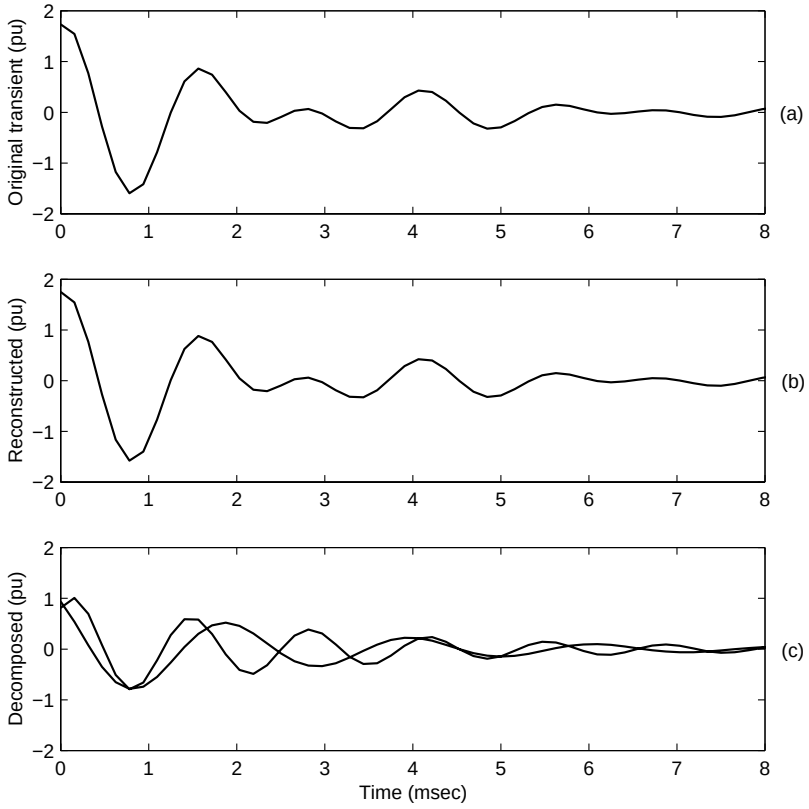

Figure 6.29: (a) Original transient (b) Reconstructed transient using ESPRIT results (c) Decomposition using ESPRIT results

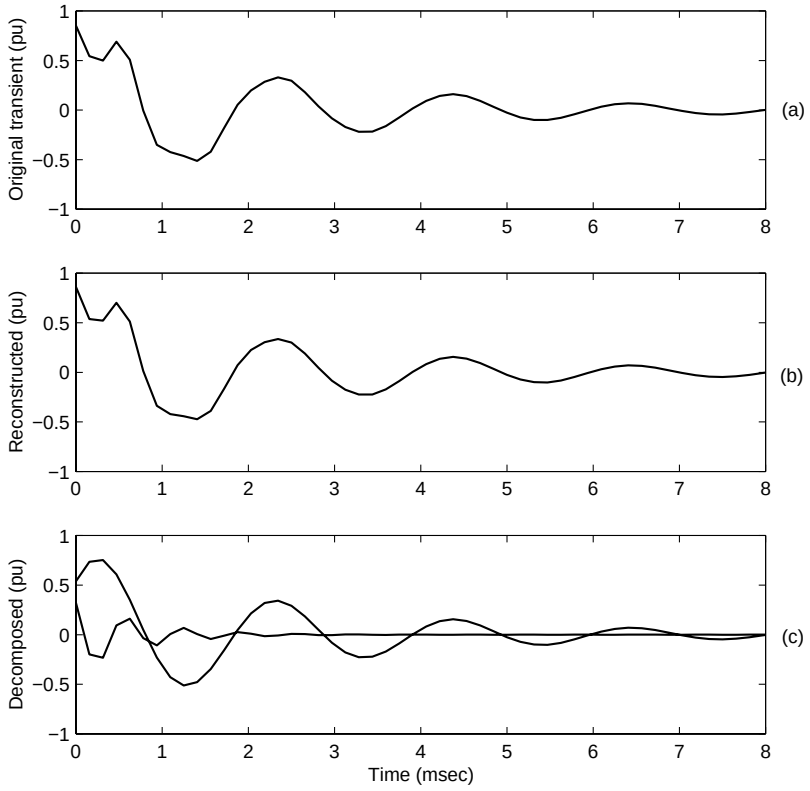

Figure 6.30: (a) Original transient (b) Reconstructed transient using ESPRIT results (c) Decomposition using ESPRIT results

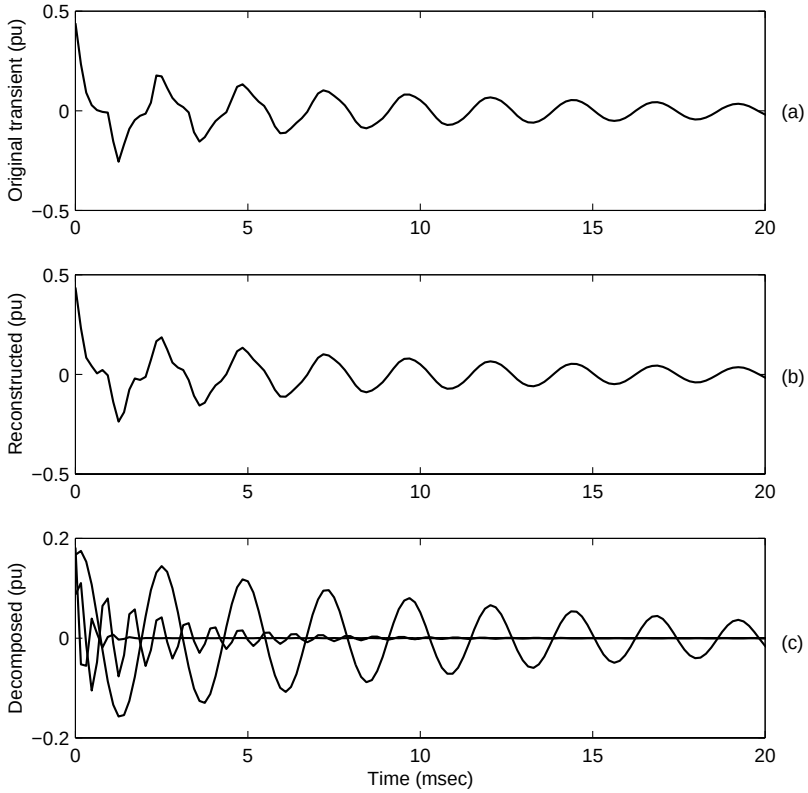

Figure 6.31: (a) Original transient (b) Reconstructed transient using ESPRIT results (c) Decomposition using ESPRIT results

Capacitor energising and travelling waves

The effect of the travelling waves is also shown in Figure 6.32, which shows the results of ESPRIT for the transient of Figure 6.3. This is the case of capacitor switching in a sub-transmission system where the presence of travelling waves leads to high overvoltages. Four sinusoids resulted from the decomposition. The low frequency (421 Hz) sinusoid corresponds to the oscillatory transient due to the resonance, and the other three sinusoids model the influence of the travelling wave on the signal. The high frequency sinusoids contribute up to 50 % of the maximum voltage.

The capacitor energising transient at the busbar where the switching takes place (Figure 6.2) is also analysed using ESPRIT. The results (Figure 6.33) show that the transient can be modelled with two sinusoids: one sinusoid of high energy with frequency 421 Hz, and one of very low energy and rapidly decaying sinusoid of frequency 239 Hz. The high energy sinusoid has frequency equal to that of the high energy sinusoid of the decomposition in Figure 6.32. This frequency is due to the excitation of the resonance created by the capacitor being switched and the source inductance. The low energy sinusoid models the effect of the travelling waves. For this point of the system the effect of travelling waves is minor because the capacitor bank connected to it does not allow sudden changes in voltage.

Influence of non-simultaneous switching

Finally, the influence of different switching angles between phases is shown. For all the simulations shown previously the three phases are switched at exactly the same time instant. The simulation that produced Figure 6.2 is repeated, but this time the switching angles of the three phases are not the same: phase a is switched first and phases b and c are switched 0.5 msec later.

Figure 6.34 shows the three phase voltages for the simultaneous switching case and the non-simultaneous switching case. It can be seen that the resulting waveforms differ considerably, and that the switching of one phase induces transients to the other two.

The results of ESPRIT for phase a (Figure 6.35) show that the transient can be decomposed into three sinusoids. The highest energy sinusoid has a frequency of 420 Hz almost equal to the frequency of the highest energy sinusoid of the decomposition of the simultaneous switching case (Figure 6.33). From the other two sinusoids, one has significant energy (frequency of 605 Hz). This frequency component is induced by the switching of phases b and c. The other very low energy sinusoid (frequency of 181 Hz) models the influence of the travelling waves.

It must be highlighted here that the analysis using ESPRIT is applied to a part of the transient that starts after all switching actions are completed. ESPRIT considers that all the components start at the same time instant, therefore if the transient under analysis contains frequency elements that start later, then the results of ESPRIT will not be reliable.

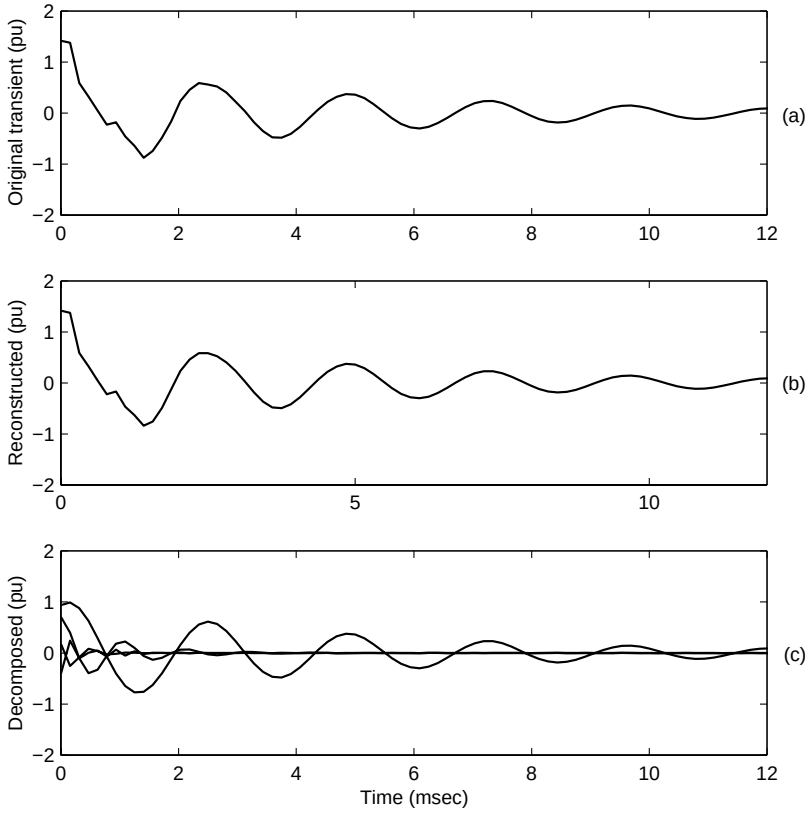

Figure 6.32: (a) Original transient (b) Reconstructed transient using ESPRIT results (c) Decomposition using ESPRIT results

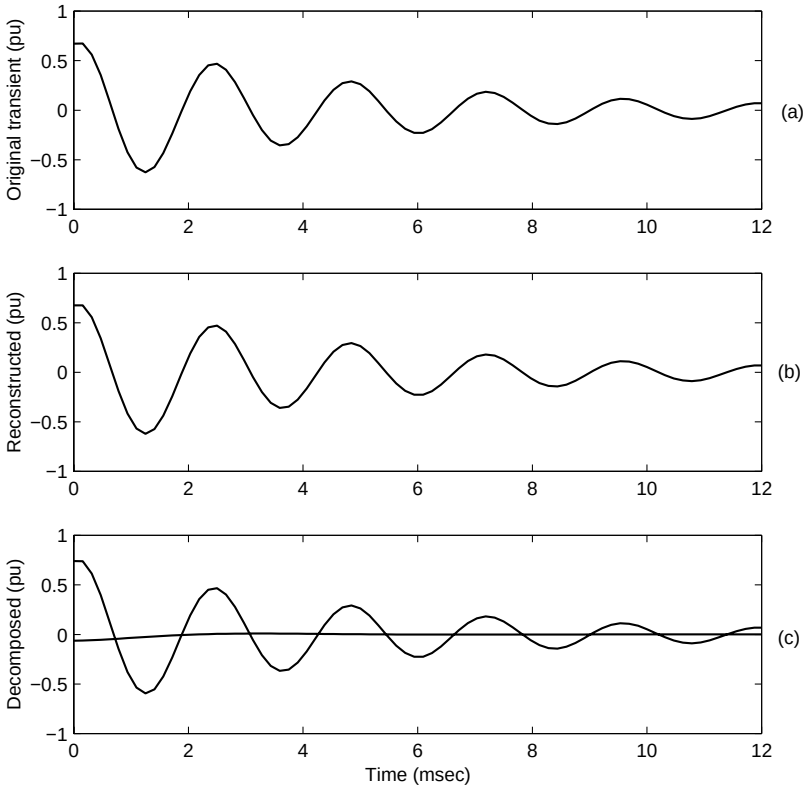

Figure 6.33: (a) Original transient (b) Reconstructed transient using ESPRIT results (c) Decomposition using ESPRIT results

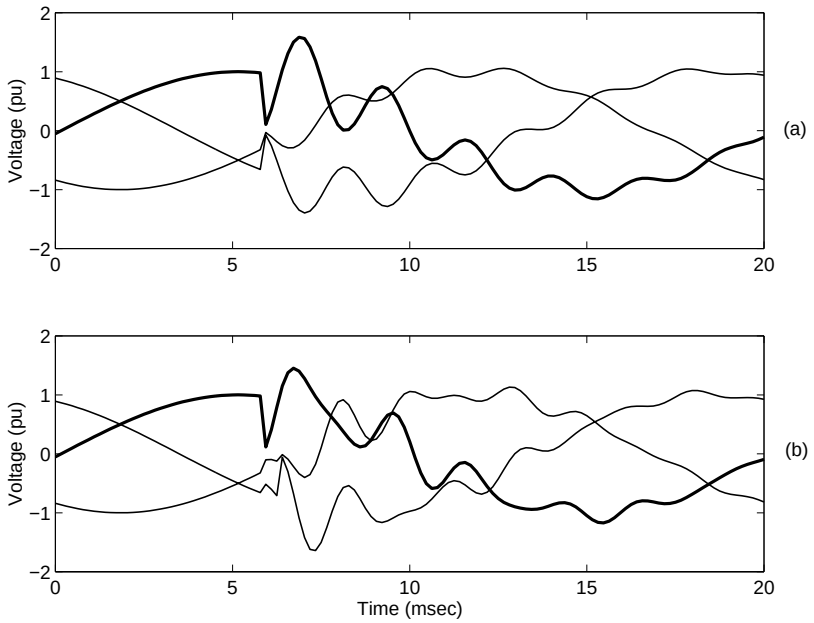

Figure 6.34: (a) Voltage waveforms for (a) simultaneous capacitor energising (b) non-simultaneous capacitor energising (thicker line: phase a) (EMTP simulation)

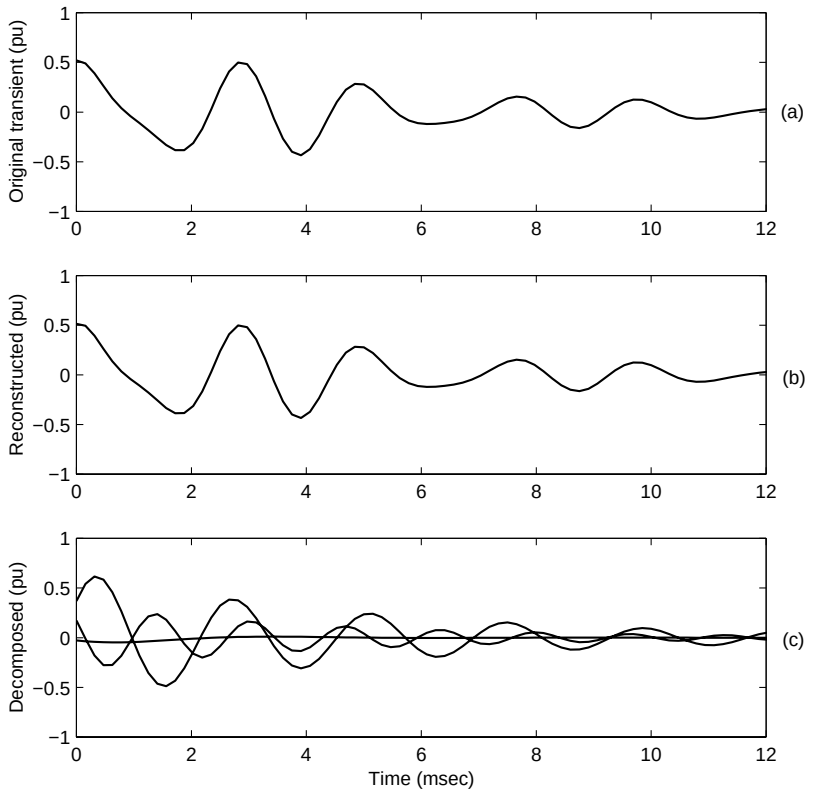

Figure 6.35: (a) Original transient (b) Reconstructed transient using ESPRIT results (c) Decomposition using ESPRIT results

6.8 Conclusions

In this chapter a number of power system phenomena is presented which are associated with high frequency characteristics and overvoltages. The magnitude of these overvoltages is dangerous for certain types of loads and the insulation of the elements of the system.

The events considered here are:

- Capacitor energising
- Restrike during capacitor de-energising
- Line energising

Simulations are used for presenting the characteristics of these events in voltage. Compared with the events presented in previous chapters, these high frequency transients cannot be described adequately by considering only the fundamental frequency magnitude. In terms of the fundamental frequency magnitude, these events present a step increase (capacitor and line energising) or a decrease (capacitor de-energising).

The events under consideration produce oscillatory transients. One more type of transient also appears in power systems: impulsive transients. Lightning is a typical cause of this type of transients.

For extracting information from transients two options are considered:

- The time domain
- The frequency domain

In the time domain the phases can be compared. It is shown that there are three-phase events where switching takes place in all the phases (capacitor energising and line energising) and single-phase events where only one phase is subject to the phenomenon. Measurements of power system transients show that there are also phase-to-phase events (equal in magnitude but opposite in polarity) and common mode events where the same transient appears in all three phases. The interaction between the phases is briefly discussed as well as how transients change as they propagate in the system (for example a single-phase event becomes a phase-to-phase event due to delta-star transformer). Furthermore, it is shown that the initial change of voltage is also a feature that can be used for characterisation of transients.

In the frequency domain, events like capacitor switching might be responsible for changes in the harmonic distortion due to a phenomenon known as harmonic amplification. The opposite effect is produced by the connection of a harmonic filter. Changes in the voltage profile can be easily observed by comparing the pre-event and post-event parts of the signal, or in terms of the segmentation algorithm presented in Chapter 3, by comparing the event segments of the voltage measurement.

It is also shown that the frequency contents (spectrum) of the transient voltage signals are influenced not only by the resonances of the network which are excited by the switching actions (this is clear in the case of capacitor switching) but also

by the propagation of travelling waves initiated by the switching. Furthermore, it is shown that the spectrum of transients caused by switching actions is different at different points in the system. In the case of capacitor energising, this is either due to travelling waves or due to other capacitors of the system connected close to the one being switched.

Motivated by the fact that resonance-related transients have fast decaying oscillatory nature, ESPRIT is used for the analysis of the events under consideration. ESPRIT models the signal as a sum of exponentially damped sinusoids. Decomposition of transients using ESPRIT shows that voltage amplification due to capacitor energising is the combined effect of two sinusoids at different frequencies and appropriate phases. This feature can be used for the identification of the phenomenon.

It is also shown that the influence of travelling waves on the transients is modelled by ESPRIT with very fast decaying sinusoids. In cases where the overvoltage is a result of travelling waves (line energising or capacitor energising) these sinusoids contribute significantly to the maximum voltage. Apart from resonances and travelling waves, other frequency components might be present in the transients due to differences in the switching angles of the phases. An example is shown where analysis using ESPRIT reveals these components.

Classification (automatic or not) of the above mentioned events is a task subject to a number of problems. Different events present similar characteristics; for example capacitor switching and line energising. Both events cause oscillatory transients that lead to a step increase in voltage. Additionally, although the time-frequency analysis of the signals decomposes the signals into a number of frequency components, the origin of these components cannot be found (resonances, travelling waves, prestrike or others). However, as shown with simulations, resonance frequency components are expected to last longer than frequency components due to travelling waves.

Automatic classification of transients must be supported by information on the system characteristics such as the types of switchings taking place in the system, the system resonances, and the influence of the switchings on the voltage profile.

Chapter 7

Conclusions and Future work

Next, the main results from the different chapters together with some general conclusions are presented. Finally, some potential extensions of this work are proposed.

7.1 Conclusions

Aim of the work presented in this thesis is the development of tools for automatic analysis of monitoring data and in particular measurements of voltage events. The objectives of the analysis include the identification of the event origin, the accurate description of the voltage characteristics in a compact way and the interpretation of all phenomena related to the event.

The first step towards automatic analysis of monitoring data is the so-called event classification (contrary to the commonly used disturbance classification): grouping of the measurements not according to the dominating change in voltage but according to the event that caused the change. A large number of measurements from different networks was used combined with the knowledge available in the literature to develop an event classification method. The proposed method is the basis for the automatic classification tools presented in this thesis and can also be used for visual inspection of the individual events.

Chapter 2 shows that event classification can be achieved by considering the voltage magnitude of the three phases. Disturbances are divided into three groups (voltage dips, interruptions and step changes). Event classification for the case of voltage dips can be achieved by considering the way of voltage recovery, the relationship between the phases and other distinctive features that voltage presents for some of these events. Interruptions can be classified as fault and non-fault. In the group of voltage dips, three types of events were found: faults, induction motor starting and transformer saturation.

In the class fault-induced events, a new subclass was added and analysed: the multistage dips. It is shown that the different stages in the dip magnitude are either

due to changes in the system as it tries to isolate the fault or due to changes in the nature of the fault.

Special attention is given to the class of transformer saturation events. Previous analysis of this phenomenon was focused on the characteristics of current and its impact on transformer protection. Chapter 2 describes the effect of transformer saturation on voltage. Transformer saturation produces voltage dips that are non-rectangular (gradual recovery), asymmetrical (each phase presents different dip magnitude) and can reach considerable magnitude. It is also shown that due to the nature of the phenomenon the rms voltage using a window of one cycle differs significantly from the rms voltage calculated using a window of half cycle. The half-cycle rms voltage presents a distinctive signature of repeating short duration voltage dips. The magnitude of these dips is significantly larger that that calculated with a window of one cycle.

For automatic analysis of power system events a method is suggested which splits the classification task into three subtasks:

1. Segmentation of the voltage signals
2. Feature extraction from the segments
3. Rule-based classification using the segmentation results and the extracted features

Segmentation is based on the detection of abrupt changes in the voltage signals (Chapter 3). A segmentation method based on Kalman filtering is suggested. With this method the voltage signals are split into event and transition segments according to how well the model of the Kalman filter fits the measurement data. The method performs well for the majority of available measurements (Chapters 3 and 4). The performance of the segmentation scheme depends, among other factors, on the time properties of the magnitude estimator. The voltage magnitude of short duration events cannot be extracted accurately and segmentation becomes difficult. A scheme based on Kalman filtering is suggested for the segmentation of short duration events. Evaluation of the performance of this scheme is limited by the lack of information for the available measurements.

Based on the segmentation results a set of rules is utilised to classify the events (Chapter 4). The segmentation algorithms separate the events into subclasses and classification is made using features extracted from the different segments of the voltage waveforms. Analysis of the features and the corresponding thresholds is presented for the case of transformer saturation.

The system is used to analyse real measurements from a medium voltage network and the results are presented. The system successfully classifies the largest part of the recordings into a number of classes. It also provides information in terms of overvoltages and their origin. The results verify that the segmentation-based approach is suitable for the classification of power system events that present changes in the fundamental frequency magnitude. It is also found that multistage and transformer dips are a significant part of the captured events.

One more method for automatic event classification is presented in Chapter 5. The method uses discrete rms voltage measurements. Discrete rms voltage measurements form a memory saving option that power quality monitors offer instead of saving the actual voltage waveforms. It is shown that classification is possible even with rms measurements using the segmentation-based approach. A segmentation scheme is proposed based on detecting fast changes in the rms magnitude. The limitations in the segmentation and the extraction of features are also discussed. The segmentation using rms voltage is a good alternative to the segmentation based on Kalman filtering especially if the measurements do not contain short duration events.

Overall, this thesis shows that automatic processing of power quality monitoring can be achieved by following a number of well-defined steps. Automatic classification can be applied to large databases and simplify the processing and analysis of monitoring data. Compared to the existing methods of automatic processing the suggested method provides more accurate analysis and description of the measurements. Event statistics can be obtained instead of disturbance statistics and the characteristics of each class can be investigated separately. The proposed classification and segmentation methods can also be used to evaluate the performance of the protection system.

This type of automatic processing can also be implemented in the monitor. The results of the classification can be used to decide whether a captured event must be stored and thus more efficient use of the monitor's memory can be achieved. Furthermore, by on-line classification of the events, the monitor can be set to sent an alarm to the system operator in the occasion of an important event.

The problem of voltage dip detection is also investigated. The main conclusion of the analysis (Chapter 3) is that voltage dip detection is subject to a trade-off between selectivity and speed. Transformer saturation and capacitor switching transients can trigger a fast dip detection scheme that should typically operate only for fault-induced events that cause a drop in magnitude below a certain threshold. Considering the fast magnitude variation due to saturation, transformer dips can be distinguished from fault-induced dips within one or two cycles after the event initiation as verified by analysing a number of measurements. Using this idea the number of unnecessary operations of voltage dip protection equipment can be reduced.

Chapter 6 presents events that cannot be characterised adequately using the voltage magnitude and present high frequency components. The analysis is focused on events like capacitor energising, restrike during capacitor de-energising and line energising. Measurements and EMTP simulations are used. This class of events is important because the produced transients are usually of high magnitude and can be dangerous for the elements of the system.

Time domain and frequency domain information can be used for more accurate characterisation of these events. Different classes of transients are found depending on how the underlying event effects the phases and their voltage profile (magnitude and harmonics).

Regarding the spectrum of these transients, it is shown that their frequency contents are influenced non only by the resonances of the network which are excited

by the switching actions but also by the propagation of travelling waves (initiated by the switching) and the non-simultaneous switching of the phases. Phenomena related with the circuit breakers also introduce specific frequency components. Furthermore, it is shown that the spectrum of the transients caused by switching actions is different at different points in the system.

ESPRIT is used for the analysis of the events under consideration. ESPRIT models the signal as a sum of exponentially damped sinusoids. Decomposition of transients using ESPRIT shows that voltage amplification due to capacitor energising is the combined effect of two sinusoids at different frequencies and appropriate phases. This feature can be used for the identification of the phenomenon. A problem that arises with this analysis is that although the signals are decomposed into a number of frequency components, the origin of these components cannot be directly found (resonances, travelling waves, prestrike or others).

7.2 Future work

The main conclusions presented in this thesis are drawn after analysing real measurements. Simulations were used only to verify the signal models. Testing of the developed methods was also done using measurements. Although a large number of data was available, not much information was known regarding the type of captured events, their location or the response of the protection system. More knowledge about the measurements will allow better understanding of the phenomena and extraction of more information in a automatic way. It would be also interesting to investigate the effect of transformer saturation on loads and on control algorithms of power electronic equipment.

Knowledge of the operation characteristics of the system that is monitored (protection system, voltage control methods, load characteristics) can be incorporated into the knowledge base of the expert system for automatic classification and analysis of power system events. The classification system can be supported by considering information on the protection strategies used in the system (an example is given in Chapter 4) or on the types of loads connected (induction motor load, harmonic loads etc). Knowledge of the protection characteristics can be also used by the expert system to evaluate the time response of the protection system and identify cases of maloperation.

The analysis of transients presented in Chapter 6 was based mostly on simulations. Simulation of some events is particularly difficult especially if phenomena like prestriking or current chopping are to be included. Measurements are required for a more thorough investigation of the characteristics of transients. The potential in using pattern recognition methods for automatic classification of transients can be also investigated. Information about the characteristics of transients at a particular point of the network can be incorporated in the classification process. Such information can be the main frequencies of a switching action or the changes in the voltage profile. Combining features extracted from the signals with information of

the system, diagnostic tools can be developed that will identify problems or potential problems for the system or the customers. Such diagnostic tools will be able to automatically identify phenomena like voltage amplification or harmonic amplification. Measurements of the event at different locations in the system can also be combined to identify the nature of the different frequency components (resonances, travelling waves etc) in the voltage transient.

The available measurements were mainly from medium voltage networks. A small number of measurements was available from low voltage networks. A number of the events captured at these voltage levels originate at higher or lower voltage levels and propagate in the system (a typical example are the fault-induced dips). However, measurements from other voltage levels are needed for further testing of the automatic classification methods. Furthermore, the list of events considered in this thesis can be expanded by considering power generation and load switching events. For example, connection of induction generators causes voltage dips [102] thus further analysis is required for distinguishing this type of dip from the types considered in this thesis. Regarding load switching, the thesis considers only the case of induction motor starting. Only few measurements of this event were available. Additional work is needed in order to evaluate the performance of the segmentation and classification methods for the motor starting event.

The expert system for automatic classification determines the underlying cause of an event, analyses the related overvoltages and by segmentation offers the means for systematic analysis of a measurement. Other information that can be of interest is the event location. For event location, measurements of current are required. If current measurements are available the power flow can also be calculated. The changes that power flow undergoes during an event can be used for analysing the load response as shown in [103] for fault-induced dips. The power flow during an event can also be exploited as a feature for classification. Information on the event location can be extracted by combining measurements of an event from different locations. Furthermore, using measurements from different voltage levels, the propagation of events can be studied.

In terms of signal processing the methods used present certain limitations. For example, the magnitude estimation becomes problematic for short duration events and segmentation is not always possible. Investigations must be made to find appropriate signal processing methods for extracting the necessary features from short duration events.

Another problem that requires attention from a signal processing point of view is voltage dip detection. As shown in Chapter 3, the voltage dip detection problem has several parameters and one of them is the identification of events for which no action should be taken. These events are capacitor switching and transformer saturation. One or two cycles are required for ruling out these two cases. The possibility of faster classification can be investigated. Appropriate transforms must be applied to the voltage signals and reveal their distinctive characteristics within a very short time interval and classification methods must be applied that will allow reliable classification. In [104] a statistical method is proposed for discriminating faults and

capacitor switching transients in less than one half-cycle. The case of transformer saturation must be included in such methods.

Bibliography

[1] A. McEachern, "Designing electronic devices to survive power-quality events," *IEEE Industry Applications Magazine*, vol. 6, no. 6, pp. 66–69, Novemer-December 2000.

[2] M.F. McGranaghan, "Economic evaluation of power quality," *IEEE Power Engineering Review*, vol. 22, no. 2, pp. 8–12, February 2002.

[3] J. Arrillaga, M.H.J. Bollen, and N.R. Watson, "Power quality following deregulation," *Proceedings of the IEEE*, vol. 88, no. 2, pp. 246–261, February 2000.

[4] *IEEE Std 1159-1995, IEEE recommended practice for monitoring electric power quality*, 1995.

[5] Dranetz Technologies Incorporated, *The Dranetz field handbook for Power Quality Analysis*, Edison, New Jersey, 1991.

[6] M.H.J. Bollen, *Understanding power quality problems: voltage sags and interruptions*, IEEE Press, New York, 1999.

[7] I. Hunter, "Power quality issues-a distribution company perspective," *Power Engineering Journal*, vol. 15, no. 2, pp. 75–80, April 2001.

[8] S. Peeran, T. Barclay, K. Sanborn, R. Schnorr von Carolsfeld, and M. Shields, "Fault analysis through power quality metering," *IEEE Industry Applications Magazine*, vol. 5, no. 2, pp. 28–31, March-April 1999.

[9] Fan Wang, "Power quality and protection," Licentiate Thesis 372L, Chalmers University of Technology, 2001.

[10] A.K. Khan, "Monitoring power for the future," *Power Engineering Journal*, vol. 15, no. 2, pp. 81–85, April 2001.

[11] R. Tsukui, P. Beaumont, T. Tanaka, and K. Sekiguchi, "Power system protection and control utilising intranet technology," *Power Engineering Journal*, vol. 15, no. 5, pp. 249–255, October 2001.

[12] D.S. Dorr, "Point of utilization power quality study results," *IEEE Transactions on Industry Applications*, vol. 31, no. 4, pp. 658–666, July-August 1995.

[13] W.W. Dabbs, D.D. Sabin, T.E. Grebe, and H. Mehta, "Probing power quality data," *IEEE Computer Applications in Power*, vol. 7, no. 2, pp. 8–14, April 1994.

[14] S. Santoso, J.D Lamoree, and R.P. Bingham, "Answermodule: autonomous expert systems for turning raw PQ measurements into answers," *9th International IEEE Conference on Harmonics and Quality of Power, Orlando, Florida USA*, vol. 2, pp. 449–503, 2000.

[15] S. Santoso and J.D Lamoree, "Power quality data analysis: from raw data to knowledge using knowledge discovery approach," *Power Engineering Society Summer Meeting*, vol. 1, pp. 172–177, 2000.

[16] M.F. McGranaghan, "Trends in power quality monitoring," *IEEE Power Engineering Review*, vol. 21, no. 10, pp. 3–9, October 2001.

[17] A.M. Gaouda, M.M.A Salama, M.R. Sultan, and A.Y. Chikhani, "Power quality detection and classification using wavelet-multiresolution signal decomposition," *IEEE Transactions on Power Delivery*, vol. 14, no. 4, pp. 1469–1476, July 1999.

[18] P.K. Dash, M.M.A. Salama, S. Mishra, and A.C. Liew, "Classification of power system disturbances using a fuzzy expert system and a fourier linear combiner," *IEEE Transactions on Power Delivery*, vol. 15, no. 2, pp. 472–477, April 2000.

[19] S. Santoso, W.M. Grady, E.J. Powers, J. Lamoree, and S.C. Bhatt, "Characterization of distribution power quality events with fourier and wavelet transforms," *IEEE Transactions on Power Delivery*, vol. 15, no. 1, pp. 247–254, January 2000.

[20] S. Santoso, E.J. Powers, W.M. Grady, and A.C. Parsons, "Power quality disturbance waveform recognition using wavelet-based neural classifier. i. theoretical foundation," *IEEE Transactions on Power Delivery*, vol. 15, no. 1, pp. 222–228, January 2000.

[21] S. Santoso, E.J. Powers, W.M. Grady, and A.C. Parsons, "Power quality disturbance waveform recognition using wavelet-based neural classifier. ii. application," *IEEE Transactions on Power Delivery*, vol. 15, no. 1, pp. 229–235, January 2000.

[22] S. Santoso, J.D. Lamoree, W.M. Grady, E.J. Powers, and S.C. Bhatt, "A scalable PQ event identification system," *IEEE Transactions on Power Delivery*, vol. 15, no. 2, pp. 738–742, April 2000.

[23] C.H. Lee and S.W. Nam, "Efficient feature vector extraction for automatic classification of power quality disturbances," *Electronics Letters*, vol. 34, no. 11, pp. 1059–1061, May 1998.

[24] L. Angrisani, P. Daponte, and M. D'Apuzzo, "Wavelet network-based detection and classification of transients," *IEEE Transactions on Instrumentation and Measurement*, vol. 50, no. 5, pp. 1425–1435, October 2001.

[25] J. Chung, E.J. Powers, W.M. Grady, and S.C. Bhatt, "Power disturbance classifier using a rule-based method and wavelet packet-based hidden Markov model," *IEEE Transactions on Power Delivery*, vol. 17, no. 1, pp. 233–241, January 2002.

[26] I.Y.H. Gu and M.H.J. Bollen, "Time-frequency and time-scale domain analysis of voltage disturbances," *IEEE Transactions on Power Delivery*, vol. 15, no. 4, pp. 1279–1284, October 2000.

[27] *European Standard EN-50160, Voltage characteristics of electricity supplied by public distribution systems*, CENELEC, Brussels, Belgium, 1994.

[28] G.T. Heydt, P.S. Fjeld, C.C. Liu, D. Pierce, L. Tu, and G. Hensley, "Time-frequency and time-scale domain analysis of voltage disturbances," *IEEE Transactions on Power Delivery*, vol. 14, no. 4, pp. 1411–1416, October 1999.

[29] C. Grigg L. Conrad, K. Little, "Predicting and preventing problems accosiated with remote fault-clearing voltage dips," *IEEE Transactions on Industry Applications*, vol. 27, no. 1, pp. 167–172, January-February 1991.

[30] L.A. Kojovic, S.P. Hassler, K.L. Leix, C.W. Williams, and E.E.Baker, "Comparative analysis of expulsion and current-limiting fuse operation in distribution systems for improved power quality and protection," *IEEE Transactions on Power Delivery*, vol. 13, no. 3, pp. 863–869, July 1998.

[31] M.A. Chapman, A. Martinez, E. Sabir, K.Wang, and Y. Liu, "Switching and fault caused transients in electric power systems," *IEEE Power Engineering Society Winter Meeting 1999*, vol. 2, pp. 1015–1021, 1999.

[32] A. Greenwood, *Electrical Transients in Power Systems*, JohnWiley and Sons, New York, 1991.

[33] A. Nikander and E. Lakervi, "A philosophy and algorithms for extinguishing earth fault arcs in suppressed medium voltage networks," *14th International Conference and Exhibition on Electricity Distribution*, vol. 4, pp. 20/1–20/6, 1997.

[34] T. Henriksen, "Single phase fault clearance in solid grounded network," *Proceedings of the Nordic Distribution Automation Conference*, 2000.

[35] S. Hanninen, M. Lehtonen, T. Hakola, E. Antila, J. Strom, and S. Ingman, "Characteristics of earth faults in power systems with a compensated or an unearthed neutral," *14th International Conference and Exhibition on Electricity Distribution. Part 1: Contributions. CIRED*, vol. 1, pp. 2.16.1–2.16.5, 1997.

[36] D.L. Brooks, R.C. Dugan, M. Waclawiak, and A. Sundaram, "Indices for assessing utility distribution system rms variation performance," *IEEE Transactions on Power Delivery*, vol. 13, no. 1, pp. 254–259, January 1998.

[37] L. Zhang and M.H.J. Bollen, "Characteristic of voltage dips in power systems," *IEEE Transactions on Power Delivery*, vol. 15, no. 2, pp. 827–832, April 2000.

[38] M.H.J. Bollen and E. Styvaktakis, "Characterization of three-phase unbalanced dips (as easy as one-two-three?)," *9th International IEEE Conference on Harmonics and Quality of Power, Orlando, Florida USA*, vol. 1, pp. 81–86, October 1-4, 2000.

[39] B.R. Williams, W.R. Schmus, and D.C. Dawson, "Transmission voltage recovery delayed by stalled air conditioner compressors," *IEEE Transactions on Power Systems*, vol. 7, no. 3, pp. 1173–1179, August 1992.

[40] M. Kezunovic and Y. Liao, "A new method for classification and characterization of voltage sags," *Electric Power Systems Research*, vol. 1, no. 3, pp. 27–35, May 2001.

[41] M.H.J. Bollen, "The influence of motor re-acceleration on voltage sags," *IEEE Transactions on Industry Applications*, vol. 31, no. 4, pp. 667–674, July-August 1995.

[42] L. Ran K.S. Smith and B. Leyman, "Analysis of transformer inrush transients in offshore electrical systems," *IEE Proceedings-Generation, Transmission, Distribution*, vol. 146, no. 1, pp. 89–95, January 1999.

[43] M.A. Rahman and B. Jeyasurya, "A state-of-the-art review of transformer protection algorithms," *IEEE Transactions on Power Delivery*, vol. 3, no. 2, pp. 534–544, April 1988.

[44] H.S. Bronzeado, P.B. Brogan, and R. Yacamini, "Harmonic analysis of transient currents during sympathetic interaction," *IEEE Transactions on Power Systems*, vol. 11, no. 4, pp. 2051–2056, November 1996.

[45] A. Hamel, G. St-Jean, and M. Paquette, "Nuisance fuse operation on medium voltage transformers during storms," *IEEE Transactions on Power Delivery*, vol. 5, no. 4, pp. 1866–1874, November 1990.

[46] O. Bourgault and G. Morin, "Analysis of harmonic overvoltage due to transformer saturation following load shedding on Hydro-Quebec-Nypa 765 kV

interconnection," *IEEE Transactions on Power Delivery*, vol. 5, no. 1, pp. 397–405, January 1990.

[47] D.H. Boteler, R.M. Shier, T. Watanabe, and R.E. Horita, "Effects of geomagnetically induced currents in the BC Hydro 500 kV system," *IEEE Transactions on Power Delivery*, vol. 4, no. 1, pp. 818–823, January 1989.

[48] G. Sybille, M.M. Gavrilovic, J.Belanger, and V.Q. Do, "Transformer saturation effects on EHV system overvoltages," *IEEE Transactions on Power Apparatus and Systems*, vol. 104, no. 3, pp. 671–680, March 1985.

[49] E. Styvaktakis, M.H.J. Bollen, and I.Y.H. Gu, "Transformer saturation after a voltage dip," *IEEE Power Engineering Review*, vol. 20, no. 4, pp. 60–62, April 2000.

[50] B. Blez, J. Gauthier, and D.Koch, "Statistical processing of chopped currents and overvoltages in two types of sulphur hexafluoride breaker technology," *IEE Proceedings-Generation, Transmission and Distribution*, 1990.

[51] H. Kuisti and F. Oyj, "The commutation failure of a HVDC converter bridge when energising a power transformer," *Proceedings of Nordic and Baltic workshop on power system, Tampere, Finland*, 2002.

[52] J.E. Jipping and W.E. Carter, "Application and experience with a 15 kV static transfer switch," *IEEE Transactions on Power Delivery*, vol. 14, no. 4, pp. 1477–1481, October 1999.

[53] R.G. Brown and P.Y.C. Hwang, *Introduction to random signals and applied Kalman filtering with* MATLAB *exercises and solutions*, John Wiley and Sons, New York, 1997.

[54] V.M.M. Saiz and J.B. Guadalupe, "Application of Kalman filtering for continuous real-time tracking of power system harmonics," *IEE Proceedings-Generation, Transmission and Distribution*, vol. 144, no. 1, pp. 13–20, January 1997.

[55] I. Kamwa, R. Grondin, and D. McNabb, "On-line tracking of changing harmonics in stressed power systems: application to Hydro-Quebec network," *IEEE Transactions on Power Delivery*, vol. 11, no. 4, pp. 2020–2027, October 1996.

[56] J. Barros and J.M. Drake, "Realtime fault detection and classification in power systems using microprocessors," *IEE Proceedings-Generation, Transmission and Distribution*, vol. 141, no. 4, pp. 315–322, July 1994.

[57] A.A. Girgis, D.G. Hart, and W.B. Chang, "An adaptive scheme for digital protection of power transformers," *IEEE Transactions on Power Delivery*, vol. 7, no. 2, pp. 546–553, April 1992.

[58] A.A. Girgis and J. Qiu, "Measurement of the parameters of slowly time varying high frequency transients," *IEEE Transactions on Instrumentation and Measurement*, vol. 38, no. 6, pp. 1057–1063, December 1989.

[59] A.A. Girgis, W.B. Chang, and E.B. Makram, "A digital recursive measurement scheme for on-line tracking of power system harmonics," *IEEE Transactions on Power Delivery*, vol. 6, no. 3, pp. 1153–1160, July 1991.

[60] F. Gustafsson, "Monitoring tire-road friction using the wheel slip," *IEEE Control Systems Magazine*, vol. 18, no. 4, pp. 42–49, August 1998.

[61] L. Wang, "Frequency responses of phasor-based microprocessor relaying algorithms," *IEEE Transactions on Power Delivery*, vol. 14, no. 1, pp. 98–105, January 1999.

[62] R.P. Bitmead, A.C. Tsoi, and P.J. Parker, "A Kalman filtering approach to short-time Fourier analysis," *IEEE Transactions on Acoustics, Speech and Signal Processing*, vol. 34, no. 6, pp. 1493–1501, December 1986.

[63] M.B. Djuric and C.V. Terzija, "A new approach to the arcing faults detection for fast autoreclosure in transmission systems," *IEEE Transactions on Power Delivery*, vol. 10, no. 4, pp. 1793–1798, October 1995.

[64] B.D. Russell and C.L. Benner, "Arcing fault detection for distribution feeders: security assessment in long term field trials," *IEEE Transactions on Power Delivery*, vol. 10, no. 2, pp. 676–683, April 1995.

[65] Li Ta-Hsin and J.D. Gibson, "Speech analysis and segmentation by parametric filtering," *IEEE Transactions on Speech and Audio Processing*, vol. 4, no. 3, pp. 203–213, May 1996.

[66] M. Khalil and J. Duchene, "Uterine EMG analysis: a dynamic approach for change detection and classification," *IEEE Transactions on Biomedical Engineering*, vol. 47, no. 6, pp. 748–756, June 2000.

[67] F. Gustafsson, *Adaptive filtering and change detection*, John Wiley and Sons, New York, 2000.

[68] O. Poisson, P. Rioual, and M. Meunier, "Detection and measurement of power quality disturbances using wavelet transform," *IEEE Transactions on Power Systems*, vol. 15, no. 3, pp. 1039–1044, July 2000.

[69] H. Shyh-Jier, H. Cheng-Tao, and H. Ching-Lien, "Application of morlet wavelets to supervise power system disturbances," *IEEE Transactions on Power Delivery*, vol. 14, no. 1, pp. 235–243, January 1999.

[70] K. Matsushita, Y. Kataoka, and M. Ono, "High speed switchgear protecting power generating facilities against voltage dip and interruption," *Proceedings of 1995 International Conference on Power Electronics and Drive Systems*, vol. 2, pp. 726–731, 1995.

[71] J. Chung, E.J. Powers, W.M. Grady, and S.C. Bhatt, "New robust voltage sag disturbance detector using an adaptive prediction error filter," *IEEE Power Engineering Society Summer Meeting*, vol. 1, pp. 512–517, 1999.

[72] H. Mokhtari, S.B. Dewan, and M.R. Travani, "Performance evaluation of thyristor based static transfer switch," *IEEE Transactions on Power Delivery*, vol. 15, no. 3, pp. 960–966, July 2000.

[73] A. Sannino, "Static transfer switch: analysis of switching conditions and actual transfer time," *Power Engineering Society Winter Meeting*, vol. 1, pp. 120–125, 2001.

[74] E.P. Dick, D. Fischer, R. Marttila, and C. Mulkins, "Point-on-wave capacitor switching and adjustable speed drives," *IEEE Transactions on Industry Applications*, vol. 11, no. 3, pp. 1367–1372, July 1996.

[75] M. Chantler, P. Pogliano, A. Aldea, G. Tornielli, T. Wyatt, and A. Jolley, "The use of fault-recorder data for diagnosing timing and other related faults in electricity transmission networks," *IEEE Transactions on Power Systems*, vol. 15, no. 4, pp. 1388–1393, November 2000.

[76] M.F. McGranaghan, T.E. Grebe, G. Hensley, and M. Samotyj T. Singh, "Impact of utility switched capacitors on customer systems. II. adjustable-speed drive concerns," *IEEE Transactions on Power Delivery*, vol. 6, no. 4, pp. 1623–1628, October 1991.

[77] M. F. McGranaghan, "Do capacitor switching transients still cause problems?," *Power quality assurance*, pp. 28–33, January-February 1998.

[78] J.P. Bickford and A.G. Heaton, "Transient overvoltages on power systems," *IEE Proceedings-Generation, Transmission, Distribution*, vol. 133, no. 4, pp. 201–225, May 1986.

[79] M.M. Forti and L.M. Millanta, "Power-line impedance and the origin of the low-frequency oscillatory transients," *IEEE Transactions on Electromagnetic Compatibility*, vol. 32, no. 2, pp. 87–97, May 1990.

[80] *IEEE Std 1036-1992 IEEE guide for application of shunt power capacitors*, 1992.

[81] R.S. Bayless, J.D Selman, and D.E. Truax W.E. Reid, "Capacitor switching and transformer transients," *IEEE Transactions on Power Delivery*, vol. 3, no. 1, pp. 349–357, January 1988.

[82] CIGRE Working group 13.04, "Shunt capacitor bank switching stresses and test methods. (part I)," *Electra*, vol. 182, pp. 165–189, February 1999.

[83] R.A. Adams, S.W. Middlekauff, and E.H. Camm J.A. McGee, "Solving customer power quality problems due to voltage magnification," *IEEE Transactions on Power Delivery*, vol. 13, no. 4, pp. 1515–1520, October 1998.

[84] T.A. Bellei, R.P. O'Leary, and E.H. Camm, "Evaluating capacitor-switching devices for preventing nuisance tripping of adjustable-speed drives due to voltage magnification," *IEEE Transactions on Power Delivery*, vol. 11, no. 3, pp. 1373–1378, July 1996.

[85] M.F. McGranaghan, R.M. Zavadil, G. Hensley, T. Singh, and M. Samotyj, "Impact of utility switched capacitors on customer systems-magnification at low voltage capacitors," *IEEE Transactions on Power Delivery*, vol. 7, no. 2, pp. 862–868, April 1992.

[86] D.M. Dunsmore, E.R. Taylor, B.F. Wirtz, and T.L. Yanchula, "Magnification of transient voltages in multi-voltage-level, shunt-capacitor-compensated, circuits," *IEEE Transactions on Power Delivery*, vol. 7, no. 2, pp. 644–673, April 1992.

[87] L. van der Sluis, *Transients in Power Systems*, JohnWiley and Sons, New York, 2001.

[88] C.A. Nucci, F. Rachidi, M.V. Ianoz, and C. Mazzetti, "Lightning-induced overvoltages on overhead lines," *IEEE Transactions on Electromagnetic Compatibility*, vol. 35, no. 1, pp. 75–86, February 1993.

[89] C. Mirra, A. Porrino, A. Ardito, and C.A. Nucci, "Lightning overvoltages in low voltage networks," *Proceedings of 14th Biennial International Conference and Exhibition on Electricity Distribution*, pp. 2.19.1–2.19.6, 1997.

[90] A.A. Girgis, C.M. Fallon, J.C.P. Rubino, and R.C. Catoe, "Harmonics and transient overvoltages due to capacitor switching," *IEEE Transactions on Industry Applications*, vol. 29, no. 6, pp. 1184–1188, November/December 1993.

[91] R.F. Dudley, C.L. Fellers, and J.A. Bonner, "Special design considerations for filter banks in arc furnace installations," *IEEE Transactions on Industry Applications*, vol. 33, no. 1, pp. 226–233, January-February 1997.

[92] N.K. Medora and A. Kusko, "Computer-aided design and analysis of power-harmonic filters," *IEEE Transactions on Industry Applications*, vol. 36, no. 2, pp. 604–613, March-April 2000.

[93] J.D. Gibbs, D. Koch, P. Malkin, and K.J. Cornick, "Investigations of prestriking and current chopping in medium voltage SF6 rotation arc and vaccum switchgear," *IEEE Transactions on Power Delivery*, vol. 4, no. 1, pp. 308–316, January 1989.

[94] M. Morcos and H. Anis, "Random energisation transients in EHV systems," *IEE Proceedings-Generation, Transmission and Distribution*, vol. 136, no. 6, pp. 325–330, November 1989.

[95] D. Paul and S.I. Venugopalan, "Power distribution system equipment overvoltage protection," *IEEE Transactions on Industry Applications*, vol. 30, no. 5, pp. 1290–1297, September-October 1994.

[96] O. Rioul and M. Vetterli, "Wavelets and signal processing," *IEEE Signal Processing Magazine*, vol. 8, no. 4, pp. 14–38, October 1991.

[97] O. Chaari, P. Bastard, and M. Meunier, "Prony's method: an efficient tool for the analysis of earth fault currents in petersen-coil-protected networks," *IEEE Transactions on Power Delivery*, vol. 10, no. 3, pp. 1234–1241, July 1995.

[98] C.J. Dafts, C.O. Nwankpa, and A. Petropoulu, "Analysis of power system transient disturbances using an ESPRIT-based method," *IEEE Power Engineering Society Summer Meeting*, vol. 1, pp. 437–442, 2000.

[99] R. Roy, A. Paulraj, and T. Kailath, "ESPRIT-a subspace rotation approach to estimation of parameters of cisoids in noise," *IEEE Transactions on Acoustics, Speech, and Signal Processing*, vol. 34, no. 5, pp. 1340–1342, October 1986.

[100] A. Eriksson, P. Stoica, and T. Soderstrom, "Second-order properties of MUSIC and ESPRIT estimates of sinusoidal frequencies in high SNR scenarios," *IEE Proceedings-Radar and Signal Processing*, vol. 140, no. 4, pp. 266–272, August 1993.

[101] J. Proakis and D. Manolakis, *Digital Signal Processing: principles, algorithms and applications*, Prentice Hall, New Jersey, 1996.

[102] T.J. Hammons and S.C. Lai, "Voltage dips due to direct connection of induction generators in low head hydro electric schemes," *IEEE Transactions on Energy Conversion*, vol. 9, no. 3, pp. 460–465, September 1994.

[103] M.H.J. Bollen, "On voltage dip propagation," *Power Engineering Society Summer Meeting*, vol. 1, pp. 665–670, 2001.

[104] M. Karimi, H. Mokhtari, , and M.R. Iravani, "Wavelet based on-line disturbance detection for power quality applications," *IEEE Transactions on Power Delivery*, vol. 15, no. 4, pp. 1212–1220, October 2000.

[105] Electrotek Concepts, *EMTP Modelling and Analysis Tutorial*, Electrotek Concepts, Knoxville, 1995.

Appendix A

EMTP models

In this appendix, the models of transformer, induction motor and transmission line are given as they used in the simulation presented in the thesis. These models are taken from [105].

Induction motor model

```
C Type 4 Induction Motor
C Rotor Mass Moment of Intertia
C
C <---Nodes--><---Refer--><-ohms<---mH<---uF
C <-Bus1<-Bus2<-Bus3<-Bus4<----R<----L<----C
  ROTOR1                              15.0E6
C
C Motor Losses (friction and windage)
C <---Nodes--><---Refer--><-ohms<---mH<---uF
C <-Bus1<-Bus2<-Bus3<-Bus4<----R<----L<----C
       ROTOR1              1.83
C
C Stub Line (Internal Adjustable Current Source and Rotor Mass)
C <---Nodes--><---Refer--><-ohms<---mH<---uF
C <-Bus1<-Bus2<-Bus3<-Bus4<----R<----L<----C
  ADJUSTROTOR1            1.0E-4
  LDTORQROTOR1            1.0E-4
C
C Motor Terminal Stray Capactiance
C <---Nodes--><---Refer--><-ohms<---mH<---uF
C <-Bus1<-Bus2<-Bus3<-Bus4<----R<----L<----C
  MOTORA                                0.10
  MOTORB                                0.10
  MOTORC                                0.10
C
C --Bus><><-----Ampl<-----Freq<----Phase<-------A1<------T1><---Tstart<----Tstop
14ADJUST-1 -0.000001   0.00001                                 -1.00E-3      9999
14LDTORQ-1  -2019.21   0.00001                               1500.0E-3      9999
C
C  Torque = (500HP * 746kW/HP) / [(1-0.02) * 188.5rad/sec] = 2019 N-M
C  3-phase, 4-pole, 60 Hz, 480 V (line-to-line)
C  Efficiency = 0.92, power factor = 0.90, full load slip = 2.0%
C  Xs=Xr = 0.08 pu, Xm = 3.0 pu, Rs=Rr = 0.03 pu
C
19
 1            0
C
BLANK END OF CLASS 1 DATA
C
C Class 2 U.M. Data Cards (Machine-Table)
 4    111ROTOR1       2
           0.0      0.004985
           0.0      0.004985
         100.0                    ADJUST
                                  MOTORA
       0.01534     0.000109 MOTORB
       0.01534     0.000109 MOTORC
C
C shorted equivalent rotor coils, B, C, A IN D-Axis, Q-Axis, and 0 sequence)
C -----RESIS--<----LLEAK----<
       0.01534     0.000109
       0.01534     0.000109

BLANK End of all UM Data
```

Transformer model

```
C Saturation (Hysteretic Reactor - (TYPE-96))
C <---Nodes--><----------><IST--<PHI--<PHIRS
96TRHA  NODE_A             8888.
C
C    CURRENT--->    FLUX------->
 -0.31125001E+01 -0.39058824E+02
 -0.20750000E+01 -0.38823529E+02
 -0.93375002E+00 -0.37999999E+02
 -0.41499998E+00 -0.37176471E+02
 -0.15562499E+00 -0.36470588E+02
  0.51874998E-01 -0.35058823E+02
  0.18156250E+00 -0.33411764E+02
  0.30087499E+00 -0.30588235E+02
  0.36312500E+00 -0.25882353E+02
  0.41499998E+00 -0.18823529E+02
  0.51875000E+00  0.12588235E+02
  0.57062499E+00  0.17411765E+02
  0.72624999E+00  0.23529412E+02
  0.93375002E+00  0.28235294E+02
  0.11308750E+01  0.30588235E+02
  0.14784375E+01  0.32941176E+02
  0.20231249E+01  0.35058823E+02
  0.27753126E+01  0.36705883E+02
  0.36312499E+01  0.37882354E+02
  0.51874999E+01  0.39058824E+02
  0.83000000E+01  0.40000000E+02
  0.11412500E+02  0.40235295E+02
            9999
96TRHB  NODE_BTRHA  NODE_A
96TRHC  NODE_CTRHA  NODE_A
C
C TRANSFORMER <--Ref<---><--Iss<--Phi<-Name<-Rmag
  TRANSFORMER                        TRSA
C <---CURRENT--><--FLUX-------->
            9999
C <---Nodes--><----------><-Ohms<---mH<---kV
C <-Bus1<-Bus2<----------><---Rk<---Lk<-Volt
01TRHA                    1.8061 54.79 14.40
02TRLA                    2.E-03 0.060  .480
  TRANSFORMER TRSA                   TRSB
01TRHB
02TRLB
  TRANSFORMER TRSA                   TRSC
01TRHC
02TRLC
C
C High Side Stray Capacitance of 10,000 pF
C and Core Losses (5 kW - 14.4 kV)
C <---Nodes--><---Refer--><-Ohms<---mH<---uF
C Bus1->Bus2->Bus3->Bus4-><----R<----L<----C
  TRHA                               0.0100
  TRHB                               0.0100
  TRHC                               0.0100
  TRHA                    41472.
  TRHB                    41472.
  TRHC                    41472.
```

Transmission line model

```
BEGIN NEW DATA CASE
JMARTI SETUP
$ERASE
BRANCH  LINSA LINRA LINSB LINRB LINSC LINRC
LINE CONSTANTS
C ENGLISH UNITS
C S<SKIN<--RESI->I<---REACT--<DIAM<---HORI<---VTOW<---VMID
  0  0.5  3.4468 4           0.349   -8.00   100.0   100.0
  0  0.5  3.4468 4           0.349    8.00   100.0   100.0
  1  0.5  0.0523 4           1.525    14.3    84.2    84.2
  2  0.5  0.0523 4           1.525    18.6    67.2    67.2
  3  0.5  0.0523 4           1.525    14.3    52.2    52.2
BLANK card ending conductor cards of imbedded  "LINE CONSTANTS"
C <--Rho<--Fmatrix<----------------------><-----Len<-Iseg
   250.0   10000.0         1                  100.00
   250.0      50.0         1                  100.00
   250.0       0.1         1                  100.00
BLANK card ending frequency cards of imbedded  "LINE CONSTANTS"
BLANK card ending  "LINE CONSTANTS"
C LECT        +1      -4
               1                  .48D-7
             .30      30       0       1       1       0       0
             .30      30       0       1       1       0       0      .0
$PUNCH
BLANK card ending  "JMARTI SETUP"  data cases
```